AN ANALYSIS OF CARRIER PHASE JITTER IN AN MPSK RECEIVER UTILIZING MAP ESTIMATION

Semi-Annual Status Report

Center for Space Telemetering and Telecommunications Systems Grant

Period Covered: July 1993 through January 1994

NASA Grant No. NAG 5-1491

Principal Investigator: Dr. William P. Osborne

New Mexico State University
Electrical and Computer Engineering
Box 30001 - Dept. 3-0
Las Cruces, NM 88003

AN ANALYSIS OF CARRIER PHASE JITTER IN AN MPSK RECEIVER UTILIZING MAP ESTIMATION

BY

BRIAN THOMAS KOPP, B.S., M.S.

A Dissertation submitted to the Graduate School
in partial fulfillment of the requirements
for the Degree
Doctor of Philosophy, Engineering

Specialization in: Electrical Engineering

New Mexico State University
Las Cruces, New Mexico
May 1994

ABSTRACT

AN ANALYSIS OF CARRIER PHASE JITTER IN AN MPSK RECEIVER UTILIZING MAP ESTIMATION

BY

BRIAN THOMAS KOPP, B.S., M.S.

Doctor of Philosophy, Engineering

Specialization in Electrical Engineering

New Mexico State University

Las Cruces, New Mexico, 1994

Dr. William P. Osborne, Chair

The use of 8 and 16 PSK TCM to support satellite communications in an effort to achieve more bandwidth efficiency in a power-limited channel has been proposed. This project addresses the problem of carrier phase jitter in an M-PSK receiver utilizing the high SNR approximation to the maximum aposteriori estimation of carrier phase. In particular, numerical solutions to the 8 and 16 PSK self-noise and phase detector gain in the carrier tracking loop are presented. The effect of changing SNR on the loop noise bandwidth is also discussed. These data are then used to compute variance of phase error as a function of SNR.

Simulation and hardware data are used to verify these calculations. The results show that there is a threshold in the variance of phase error versus SNR curves that is a strong function of SNR and a weak function of loop bandwidth. The M-PSK variance thresholds occur at SNR's in the range of practical interest for the use of 8 and 16-PSK TCM. This suggests that phase error variance is an important consideration in the design of these systems.

TABLE OF CONTENTS

List of Appendix Tables

List of Figures

List of Appendix Figures

Chapter 1

INTRODUCTION

"Observe due measure, for right timing is in all things the most important factor."

Hesiod,
poet & philosopher, 700 B.C.

The information age is moving forward at an impressive speed. In recent years, global telecommunications traffic has maintained a growth rate of no less than 15% compounded annually [1]. This, coupled with the increased demands for scientific data from space and atmospheric based remote sensing and experimentation, has created a strong interest in increasing the capacity and performance of available communication satellite resources. Toward this end, New Mexico State University's space telemetering and telecommunications research center has been pursuing research projects whose thrust is the investigation of more efficient methods of utilzing an existing satellite channel. One area of particular interest has been the study of spectrally efficient modulation formats.

A current modulation standard for satellite communications is phase shift keying. Specifically, binary phase shift keying (BPSK) and quadrature phase shift keying (QPSK) are used

extensively. For example, Intelsat earth station standards A, B, C, E, and F have provisions for the use of QPSK in single channel per carrier (SCPC) modes and time division multiple access (TDMA) burst communication modes [2]. Further, the National Aeronautics and Space Administration's (NASA) most extensive satellite communication system, the tracking and data relay satellite (TDRS) system, uses BPSK and QPSK for all of its user services and TDRS tracking, telemetry, and command links with the exception of one space shuttle service [3].

By modulating with BPSK it is possible to convey one bit of information in a given channel through the transmission of one of two phases of a sinusoidal carrier. With QPSK, four phases are used and thus two bits can be conveyed in that same channel. It is possible to extend this process through the use of eight phases to send three bits (8PSK) or, going even further, using sixteen phases to convey four bits (16PSK). Both extensions can utilize the same channel as the BPSK and QPSK signals. However, if the signal power level is maintained there will be a corresponding increase in bit error rate (BER) as the distance between adjacent constellation points drops with the conveyance of more phases. In satellite systems, where both available channel bandwidth and available power are usually at a premium it is desirable to consider the use of 8PSK and 16PSK. For example, if it is desired to increase the performance of a QPSK link without changing the signalling speed, 2/3 rate 8PSK trellis coded modulation (TCM)

could possibly be employed. TCM utilizes specific constellation signal set expansions and convolutional encoding to achieve a decrease in BER over uncoded QPSK. If a two-fold increase in data throughput is needed and loss in performance can be tolerated it may be possible to consider 16PSK. The economical key to making these extensions in an existing satellite channel is that the channel must be a relay or "bent pipe" channel. If the channel involves a regenerative transponder onboard the spacecraft this obviously won't work without modification to the satellite. It is much cheaper if the extensions involve engineering changes in the ground communications equipment only.

With that in mind much research is being conducted in the area of 8PSK and 16PSK [4] - [14]. Specifically the 8PSK and 16PSK TCM schemes have been paid particular attention in the literature [4] - [12]. The current available research examines higher order PSK systems, and specifically TCM systems, all chiefly in terms of bit error rate performance. One important area in the consideration of the use of these coherent schemes that has not been fully addressed in the literature is the synchronization performance of the receiver. Specifically, the quantity of carrier phase variance, or jitter, in the reference generated in the receiver for demodulation has not been calculated for popular receiver designs, at various signal to noise ratios (SNR), under tracking or "locked" conditions. This characteristic is an extremely important one since jitter in the carrier translates into uncertainty

of the location of the received PSK constellation points. If this jitter is large enough it can cause a degradation in BER performance. Further, it will set a minimum range of operational SNR below which the jitter will be so severe that phaselock in a feedback-type receiver will be unattainable and/or unmaintainable. This is of particular importance in 8PSK and 16PSK where the constellation points are much closer together than BPSK and QPSK. In the literature it is possible to find research that does analyze the impact of certain amounts of carrier phase jitter on the BER performance of 8PSK and 16PSK receivers [5]. However, a quantitative analysis of how much jitter is to be expected is generally unavailable.

Since the quantity of jitter depends on the type of receiver used, the first task of this project was to decide which receiver to analyze. The PSK signal being received is a double-sideband suppressed carrier (DSB-SC) signal. The lack of a discrete carrier component coupled with discrete phase transistions conveying the data makes coherent demodulation of PSK signals a challenging task. There are several receiver designs that were considered for use in this study and they can be grouped roughly into two major types: forward acting designs and feed-back designs. The decision of which receiver design to use was based on several factors. First, a practical receiver design was a criterion since it was intended from the start to build an M-ary PSK (MPSK) link to verify theoretical and simulation results for BPSK, QPSK, 8PSK, and

16PSK. Second, the results of this study would be of great value to NASA, the principal benefactor of the telemetering and telecommunication center, so choosing a type of receiver that they use and are familiar with, particularly at the TDRS White Sands ground terminal (WSGT) twenty-five miles northeast of NMSU, was also a consideration. At the WSGT a type of loop called a modified Costas loop is used for the demodulation of both BPSK and QPSK. This feedback loop design is based on the loop first proposed by Costas [15] for the demodulation of DSB-SC signals. The basic modified Costas loop is shown in Figure 1-1 and for comparison the original Costas design is included in Figure 1-2. The third consideration in the decision process was that the choosen design needs to be backwards comparable with published data, if possible, to ensure that the research data is accurate. In other words, a baseline study with BPSK and QPSK using the same design would allow for a comparison with published data on how much jitter should occur. When the calculated, simulated, or experimental data agrees closely with published data for BPSK and QPSK then there is verification that the design being used is accurate and extensions to 8PSK and 16PSK can be made. This third consideration inferred that a design that is flexible and can test BPSK through 16PSK with minimal modification is desirable and that the choosen design be popular enough to have already received attention in the literature in so far as BPSK and QPSK carrier phase jitter are concerned.

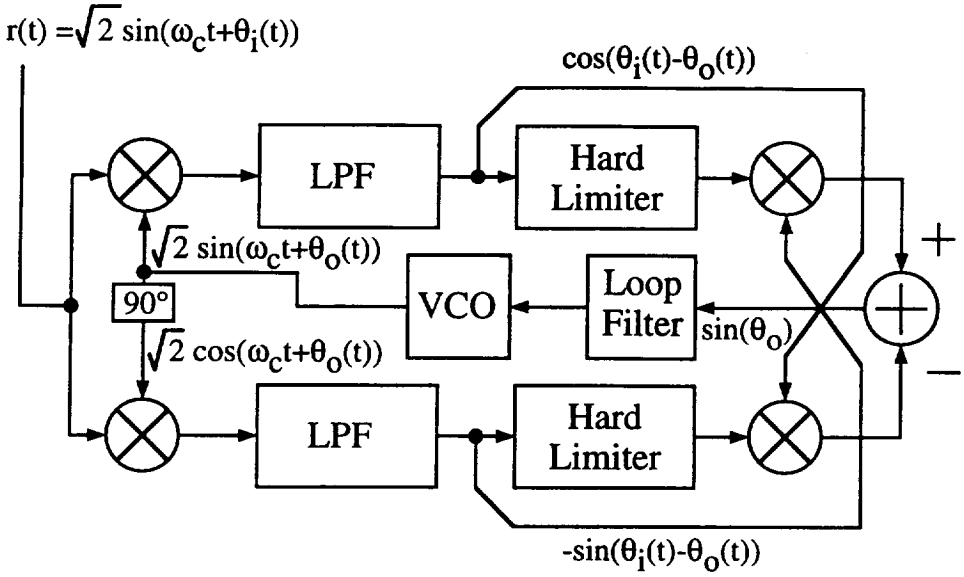

Figure 1-1. The modified Costas loop.

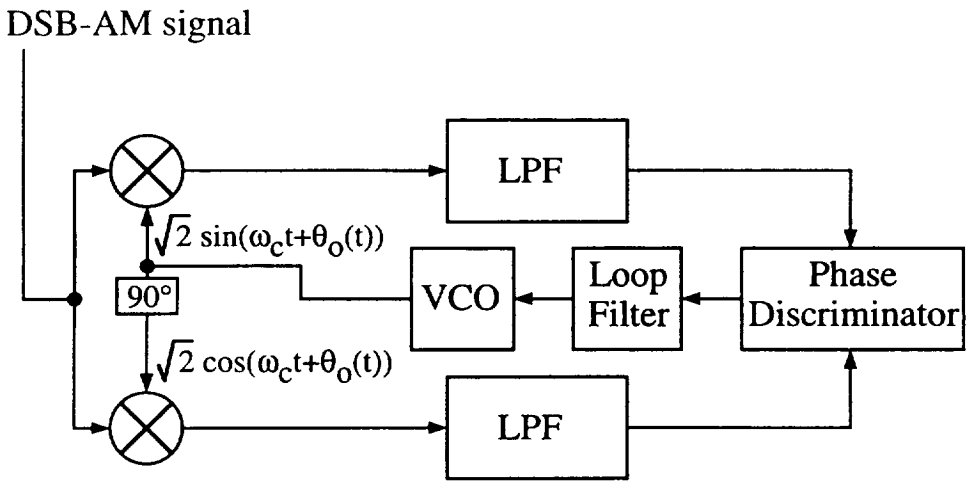

Figure 1-2. The Costas loop.

To facilitate making a choice, several receiver designs in each of the categories mentioned above were examined. Two forward-acting designs were examined. The times-N loop, shown in Figure 1-3, is a forward-acting type loop in which the received MPSK signal is multiplied by itself N times. The N in the loop's name refer's to the M in MPSK. By performing this multiplication the data is effectively multiplied out resulting in a spectral component at a frequency of N times the carrier that can then be tracked by a standard phaselock loop (or even filtered by a bandpass filter). Unfortunately, as N, i.e., M increases, the frequency at which the carrier phase tracking loop must operate increases. For example, a 370 mega-Hertz (MHz) 16PSK signal would require a "times 16" loop. The quiescent frequency of such a phaselock loop would be approximately 6 Gigahertz (Ghz).

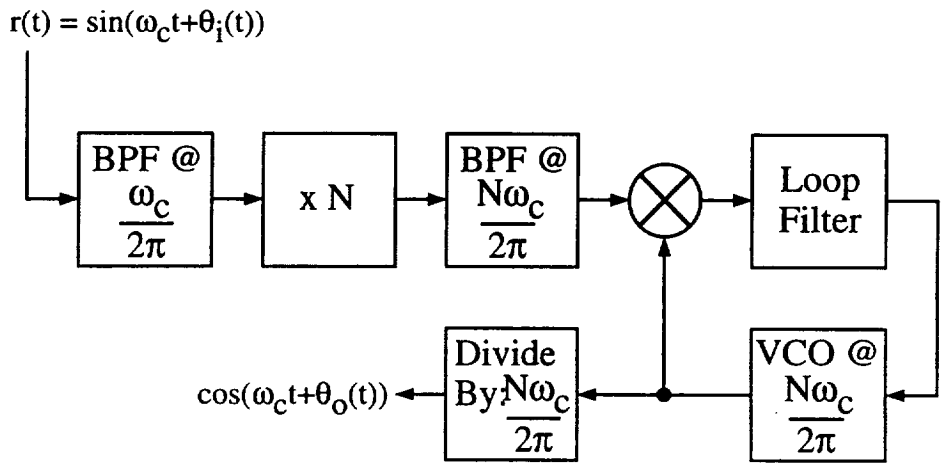

Figure 1-3. The "Times N" loop.

Implementing a carrier tracking loop at such a frequency in firmware or hardware can be prohibitory because of the difficulties involved with working at such a high frequency.

Another forward-acting design, the feed-forward carrier synchronization system, is an approach that contains no feedback loop [16]. The system estimates carrier phase by calculating its arctangent over 2N+1 samples where N is varied depending on the signal to noise ratio. The feed-forward system is shown in Figure 1-4. This system is used in burst communication applications since the possibility of hang-up during acquisition, while not eliminated, can be significantly reduced.[1] In evaluating this loop in terms of the decision criteria it is noted that there is a significant amount of digital hardware and 2 pairs of phase detectors present in the loop. While this alone is not a significant deterrent when compared to some of the other designs, and in particular the design finally chosen, it is noted that this design is substantially different from that used by NASA at the WSGT. It contains no feedback loop, as does the modified Costas loop, and its unique ability to acquire a received signal quickly is not of great importance at the WSGT where a particular communication link between the ground station and a user spacecraft, called a "sho",

[1]Hang-up is a term for a condition that can occur in PLL's. When the intial reference phase is 180° out from the lock point a phase error of zero will occur at the output of most phase detectors. However this point is an unstable equilibrium point for the PLL and thus noise will cause the phase to move toward the lock point. This process can be slow to start and the result is a long acquistion time or "hang-up" before the PLL locks.

may last many minutes and result in the transmission of many gigabits of data.

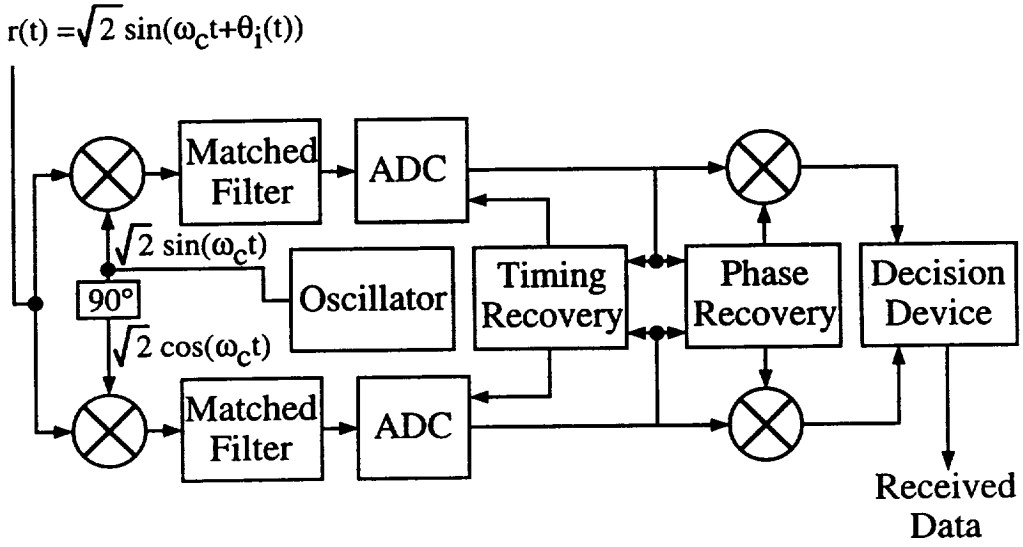

Figure 1-4. The feed-forward loop.

The second type of PSK DSB-SC receiver design that was considered is the feedback loop design. This loop has several variations. Costas loops, demodulation/remodulation loops, reverse modulation loops, and maximum aposteriori phase (MAP) estimation loops are all forms of feedback loops. All of these feedback loops involve the use of some form of PLL to provide a coherent reference for demodulation, except in the reverse modulation loop where a bandpass filter can be substituted [17, pg. 177]. There are several feedback designs that fall into a special category called decision-directed loops. A loop can be considered a

decision-directed loop if at some point in the receiver the transmitted baseband data is effectively recovered and used in the demodulation process. Examples of decision-directed loops are the QPSK Costas loop with hard limiters and the MPSK high-SNR approximation to the MAP estimation loop.

A feedback loop that is a type of Costas loop and that showed early promise as a possible candidate for the research into carrier phase jitter is a loop referred to as the Leclert and Vandamme variation [18]. It is shown in Figure 1-5. In this loop an error signal that drives a VCO is calculated from several hard-limiter processors, each related to the recovered data. The hard limiters provide the inputs to dual polar quantizers which estimate the transmitted phase. These estimates are then used along with the hard limiter outputs to calculate an error signal.

Two more types of feedback loops are the demodulation-remodulation loop [17, Fig. 6.6, pg. 176] and the reverse modulation loop [17, Fig. 6.7, pg.177]. In the former, the recovered data is modulated onto the VCO reference and then phase compared with the received signal. If good decisions are being made then the only phase difference between the two signals will be due to a carrier phase offset. In the reverse modulation loop recovered baseband data is "reverse" modulated on to the received signal. The resultant signal will have a spectral component at the carrier frequency that can be tracked. Further, in reverse modulation loops, like feed-forward systems, the

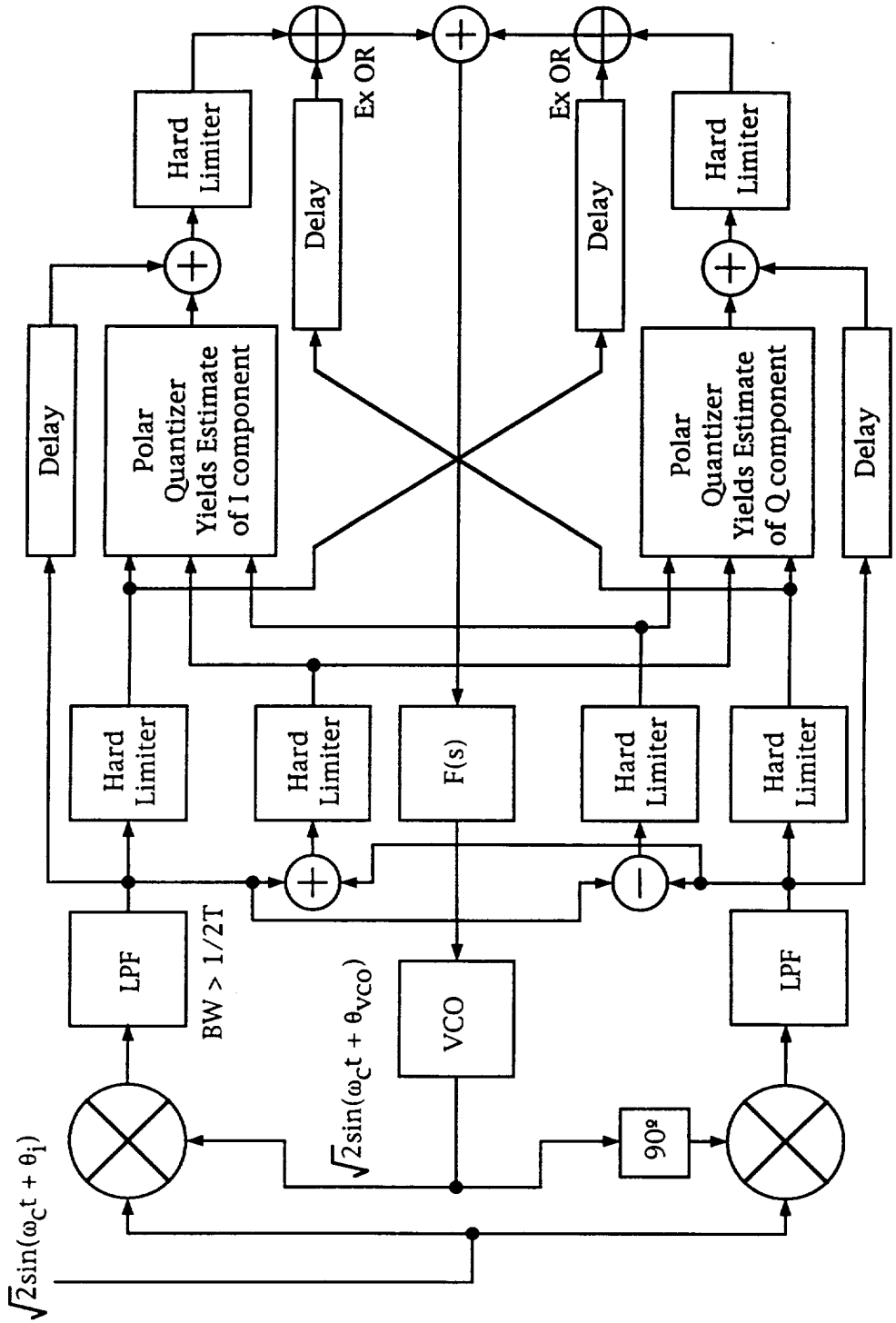

Figure 1-5. 8-PSK Leclert and Vandamme variation.

chance of hang-up during acquistion can be minimized by replacing the PLL with a bandpass filter.

The fourth type of feedback loop that was considered is the MAP estimation loop. This loop uses an optimum aposteriori phase estimation calculation, based on the recovered data, to determine what the most likely transmitted signal carrier phase was. This complex estimate is then used to calculate an error signal to drive a VCO which provides the coherent reference.

In the early stages of the receiver design selection process the feedback loops received the most consideration. All of the four feedback designs mentioned above are relatively adaptable for construction in an MPSK system. In contrast, the times-N loop is adaptable to MPSK environments for construction but only at a considerable cost. To support an M of 2, 4, 8, or 16 would, in effect, require that four receivers be constructed if the task were completed with analog circuitry. A digital implementation would require substantial circuitry as well, and some form of wide bandwidth numerically controlled oscillator to achieve the range of from twice-the-carrier-frequency to 16 times the carrier frequency. This lack of adaptability and the fact that times-N loops aren't employed at the WSGT were sufficient drawbacks to warrant withdrawal of this type of loop from consideration. Although easily adaptable to the MPSK environment, the feed-forward systems distinct variation from the feedback technique used at the WSGT coupled with significantly large overall

hardware requirements, compared to several of the feedback loops, effectively eliminated it from consideration as well. What remained at this point in the selection process was to decide which feedback loop to use for the research on carrier phase jitter.

Of the four feedback loops two stand out for their overall simplicity of implementation. These are the Leclert and Vandamme variation and the MAP estimation loop. The other two, the demodulation-remodulation loop and the reverse modulation loop, both require increased circuit complexity to implement when compared to the first two loops and thus were eliminated from consideration. Having narrowed the decision to the Leclert/Vandamme and MAP estimation loops, it was decided that simulations should be performed to compare the performance of the two loops. While the methodology for conducting these phaselock loop simulations will be discussed in detail later in this dissertation, it should be noted here that the simulation source code and results are presented in Appendix A. The results indicate that the performance of the Leclert and Vandamme variation was less satisfactory than that of the MAP estimation loop. This performance difference is attributable to the Leclert and Vandamme's discrete processing algorithm involving only hardlimiters which results in a loop that performs like a "bang-bang" servo control. It should be stressed that the difference in performance was minimal. It should also be noted that the Leclert and Vandamme variation requires a slight increase in digital

circuitry compared to the MAP estimation loop. Neither of these reasons was significant enough to dismiss the Leclert and Vandamme variation by themselves. However, this loop design is relatively new and little research has been published on it in the literature. In contrast, research into the use of MAP estimation for demodulation was first investigated in the early 1950's [19] and much has been written about it in the literature since [20]-[23], [24, chap. 5], [25]-[28], [29, chap 11], [30]-[36]. This interest in the literature for MAP estimation was the final reason that lead to the selection of the MAP estimation loop design over the Leclert and Vandamme variation. The MAP estimation loop is relatively easy to model and construct in an MPSK environment. It is very similar to the modified Costas loop employed at the WSGT (in fact at high-SNR's they are mathematically equivalent), and there is a large enough source of literature research to verify that the models developed and tested, and the hardware constructed, were done properly. Yuen, at The Jet Propulsion Laboratory, [37, chap 5] and Hinedi and Lindsey [35] have both published data related to the jitter that proved useful in verifying the results of this study for BPSK and QPSK and thus allowed the extensions to 8PSK and 16PSK to be considered valid.

One restriction was placed on the MAP estimation loop to simplify its modelling and to make the data from the study more useful to NASA at the WSGT. The MAP estimation technique uses an algorithm that provides an estimate of the phase of the

received signal. This algorithm is mathematically complicated and involves the use of hyperbolic trigonometric functions. Before the advent of digital signal processing, implementing this algorithm with analog circuitry would have required a prohibitive amount of electronics. However, if it is assumed the received signal exists in a high-SNR environment then the MAP estimation algorithm reduces to an equation that is easily implemented. Further the analysis of the loop is significantly simplified as well. A similar reduction in complexity occurs if a low SNR environment is assumed. However, it is the high-SNR approximation that was particularly attractive to this study. The modified Costas loop used at the WSGT is equivalent to the QPSK Costas loop with hard limiters and thus equivalent to the high-SNR approximation of the MAP estimation loop. Further the above mentioned published results on BPSK and QPSK carrier phase jitter are applicable to a comparison with the original MAP estimation loop only at high-SNR's. If a feedback loop that employs the high-SNR approximation to the MAP estimation loop is used, the results are completely comparable. Insofar as presenting these results to NASA was concerned it is possible to inform them what they should expect in terms of carrier phase jitter if they continue to use the same type of receiver design for 8PSK and 16PSK.

Having concluded the selection process and chosen a receiver design that utilizes the high-SNR approximation to the MAP estimation of carrier phase, it was possible to begin the

analysis of carrier phase jitter. The analysis begins with understanding jitter and what it is, specifically, in feedback loops. To accomplish this one of the most basic of feedback loops, the phaselock loop, can be used. The next chapter of this dissertation presents, as background, a brief discussion of the basic phaselock loop: how it works and how its jitter can be analyzed. Chapter 3 presents the MAP estimation loop as a phaselock loop for the carrier recovery of PSK DSB-SC signals. The approximation for high-SNR is described as well. In Chapter 4 the high-SNR MAP estimation loop is reduced to a baseband model to simplify analysis and simulation. It is here that the equation that describes carrier phase jitter in the high-SNR approximation loop is presented. Although this equation has been previously solved analytically for BPSK and QPSK it is shown that for 8PSK and 16PSK an analytical solution for several of the components of the jitter do not exist and another approach is necessary. In the next chapter (Chapter 4) numerical solutions are obtained for the components for 8PSK and 16PSK. The accuracy of the numerical techniques is verifyed using the BPSK and QPSK analytic solutions. The 8PSK and 16PSK data could then be tentatively assumed to be correct. Through the use of simulation techniques and a laboratory hardware design for the high-SNR approximation loop the numerical data could be verified more assuredly. All of the results for carrier phase jitter are presented together in Chapter 6.

As the reader progresses several other important factors and characteristics will come to light as well. For example the loop noise bandwidth exhibits some interesting phenomena that are not previously discussed in the literature and are of great value to the MPSK receiver designer. This bandwidth changes significantly with SNR, narrowing as the SNR drops. It is attributable to the dropping phase detector gain as the SNR decreases. Smaller design loop damping factors can minimize this effect. Further, as the SNR decreases, a threshold region is reached where the trade-off for carrier phase variance that exists between SNR and loop bandwidth is no longer linear. In this region, if it is desired to maintain a certain level of jitter while dropping the SNR by 3 decibels (dB), it is not possible to merely narrow the loop bandwidth by 3 dB. The loop bandwidth would require significantly more reduction to maintain the same level of jitter at half the SNR. This nonlinear exchange does not exist at higher SNR's where maintaining the same amount of jitter while dropping the SNR 3 dB can be achieved by narrowing the loop bandwidth 3 dB.

Another interesting, and alarming, characteristic that was revealed in the study of the 8PSK and 16PSK carrier tracking loops concerns the minimum SNR that will maintain carrier lock in the receiver. As will be shown, the carrier phase variance is large for 8PSK and 16PSK at low SNR's that would be considered operational for BPSK and QPSK. At these SNR's 8PSK and 16PSK

show difficulty in maintaining phaselock. While this data was not obtained through the mathematical use of acquistion models, it was observed in both the simulators and the hardware at similar SNR's.

All of these results will be presented in the subsequent chapters where appropriate and summarized with the jitter data in the results chapter (Chapter 6). Chapter 7 is the conclusions chapter in which results are discussed and suggestions offered for what to do next, now that the MSPK jitter has been quantified. Following the conclusions, there are several appendices. Appendix A presents the Leclert and Vandamme simulation comparison with the high-SNR approximation to the MAP estimation loop. Appendices B and C conain the optimum MAP estimator derivations for 8PSK and 16PSK. The data for two of the components of phase error variance are in the next two Appendices. Appendix D contains the equivalent noise variance data and Appendix E contains the phase detector gain data. The variance of the phase error data is tabulated in three Appendices. Appendix F has the theoretical results for BPSK and QPSK as well as the numerical results for 8PSK and 16PSK. The simulation results are in Appendix G and the hardware results are in Appendix H.

Chapter 2

THE PHASELOCK LOOP

"Here and elsewhere we shall not obtain the best insight into things until we actually see them growing from the beginning ..."

Aristotle
philosopher, 384 - 322 B. C.

2.1 The Basic Phaselock Loop

Investigating the MAP estimation loop carrier phase jitter requires a model of the loop's steady state operation. The jitter that it is desired to measure occurs when the loop has acquired and is locked. To build the mathematical model from which the jitter can be extracted, and to extract the jitter itself, several mathematical procedures must be performed. To understand these procedures and their significance it is prudent to discuss first their purpose in the most basic of feedback synchronizers: the phaselock loop.

The in-depth analysis of PLL's is available in many sources [24][29][38][39]. The discussion presented here is meant only to cover those procedures that are required to understand carrier phase jitter and how it can be evaluated. The basic PLL is used to

phaselock two sinusoidal signals that are 90° apart in phase. The quadrature relationship is necessary when a multiplier type phase detector (the most common for PLL's) is used. The first of the two sinusoidal signals, the received signal, has an unknown phase component and is denoted

$$r(t) = \sqrt{2P_r}\sin(\omega_c t + \theta_i(t)). \tag{2-1}$$

The second signal is the sinusoid generated in the receiver

$$v(t) = \sqrt{2}A_v\cos(\omega_c t + \theta_o(t)). \tag{2-2}$$

The constant amplitude coefficients are chosen for convenience. Note that the phase arguments, $\theta_i(t)$ and $\theta_o(t)$, are considered to have spectrums significantly below their common carrier frequency of ω_c, i.e., they are varying slowly [39, pg. 21]. For the locally generated signal to phaselock to, or track, the received signal, information regarding which signal is lagging and which signal is leading is required. An error signal which conveys this information and provides equal amounts of absolute error, whether a lead or lag condition exists, can be achieved with a device that yields an odd function of the phase difference between the signals. The device that provides the error signal in a PLL is called a phase detector. The multiplier-type phase detector multiplies the two sinusoids together and lowpass filters the

product to remove the double frequency term. The output from such a device with inputs (2-1) and (2-2) and a gain of K_d (which has dimensions of $volts^{-1}$) is the odd function error signal

$$e(t) = K_d \sqrt{P_r} A_v \sin\left(\theta_i(t) - \theta_o(t)\right). \tag{2-3}$$

Besides the phase detector, two other basic components are also part of the PLL. They are the linear loop filter and the voltage controlled oscillator (VCO). All three components are shown in the PLL of Figure 2-1. The function of the loop filter varys with the application of the PLL but in general its output can be represented by convolving its impulse response, $f(t)$, with its input (2-3) as

$$x(t) = \int_0^t f(t-\lambda) K_d \sqrt{P_r} A_v \sin\left(\theta_i(\lambda) - \theta_o(\lambda)\right) d\lambda . \tag{2-4}$$

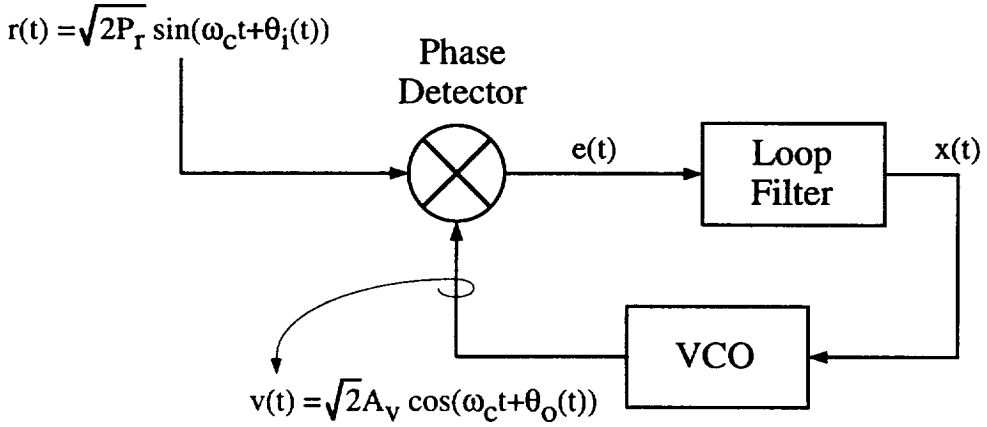

Figure 2-1. The phaselock loop.

The VCO is a unique device in that its output is a sinusoid whose frequency varies in proportion to the voltage of its input signal. When the VCO's input is zero its output has a constant frequency ω_c. When the VCO's input is $x(t)$, the output of the loop filter, its output frequency, will be

$$\omega'(t) = \omega_c + K_o x(t). \tag{2-5}$$

Note that $\omega'(t)$ is thus the instanteous frequency of the locally generated sinusoidal signal since it is the VCO's output that provides the reference sinusoid in Figure 2-1. Since the instantaneous frequency and overall phase of the reference sinusoid are related by the expression

$$\frac{d\Phi_o(t)}{dt} = \omega'(t) \tag{2-6}$$

and since the overall phase of the reference in (2-2) is

$$\Phi_o(t) = \omega_c t + \theta_o(t) \tag{2-7}$$

the deviation of the VCO from ω_c, namely $K_o x(t)$, can be expressed in terms of the phase component of the reference sinusoid, $\theta_o(t)$. Using (2-5)-(2-7), this relationship is

$$\frac{d\theta_o(t)}{dt} = K_o x(t). \tag{2-8}$$

Combining (2-3), (2-4), and (2-8) it is possible to state the integro-differential equation that describes the operation of the PLL as

$$\frac{d\theta_o(t)}{dt} = K_o K_d \sqrt{P_r} A_v \int_0^t f(t-\lambda)\sin\left(\theta_i(\lambda) - \theta_o(\lambda)\right)d\lambda . \qquad (2\text{-}9)$$

An extremely important quantity that has not been mathematically introduced yet and that is needed to further explore the integro-differential equation of (2-9) is the phase error

$$\theta_e(t) = \theta_i(t) - \theta_o(t). \qquad (2\text{-}10)$$

This term represents the phase difference between the received sinusoid and the locally generated sinusoid. Since it is the purpose of the PLL to track the received signal's phase and to do so does not necessarily require absolute knowledge of the signal's phase, it is equivalent to define the function of the PLL as that of maintaining as small a phase error as possible between the received and locally generated sinusoids. Introducing the phase error, $\theta_e(t)$ into (2-9) yields

$$\frac{d\theta_e(t)}{dt} = \frac{d\theta_i(t)}{dt} - K_o K_d \sqrt{P_r} A_v \int_0^t f(t-\lambda)\sin\left(\theta_e(\lambda)\right)d\lambda . \qquad (2\text{-}11)$$

Equation (2-9), or (2-11), lead directly to the baseband (low frequency) model of Figure 2-2. Note that the VCO is modeled as an integrator corresponding to the relationship between the VCO input frequency deviation and its output phase change. This model is useful for two reasons in particular. It provides direct access to the phase error and it has eliminated the need to keep track of the frequency, ω_c. While the latter reason may seem insignificant, if this frequency is included when the loop is simulated (as in a complete time simulation of the loop) valuable computing resources will be consumed in unnecessarily high sampling rates. This model demonstrates that it is not necessary to simulate the loop in such a manner. Rather, a baseband simulation will suffice.

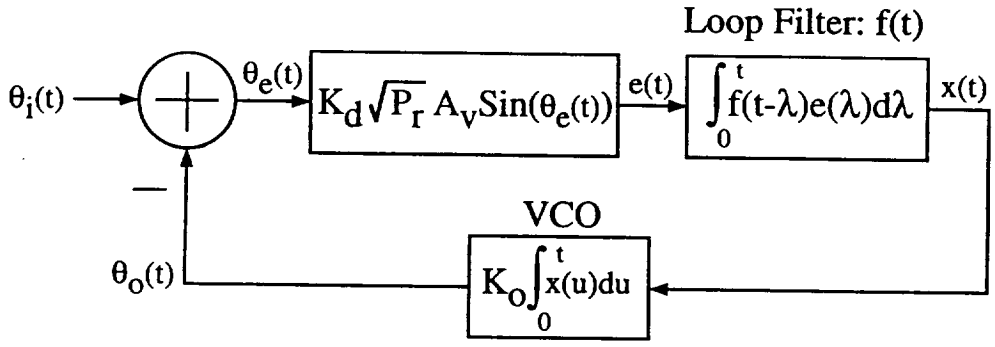

Figure 2-2. The nonlinear baseband model.

This nonlinear model is certainly useful for studying transient response behavior and acquistion phenomena but its nonlinear nature makes it unattractive for studying steady-state characteristics where a linear approximation will suffice and thus allow the use of some very powerful analysis tools. The carrier phase jitter we are interested in analyzing can be obtained through the use of a linear approximation to the model in Figure 2-2. The assumption that must be made to linearize the loop model is that the phase error is small. This assumption is predicated by the notion that the loop has acquired and is tracking the received signal. The loop is in steady state. If the phase error is small then

$$\sin(\theta_e(t)) \approx \theta_e(t). \tag{2-12}$$

This approximation provides the necessary change to convert the nonlinear model of Figure 2-2 into the linear model of Figure 2-3. Given that the model is now a linear one it is possible to describe its transfer function. To do so consider the further modified model of Figure 2-4 where now the Laplace transforms of the loop filter and the VCO have been introduced. Further, the assumption has been made that the Laplace transforms of the phase components of the received signal and the reference signal exist. It is now possible to construct the transfer function for the loop. While there are several transfer functions available in this control loop

the desired one for assisting in the calculation of the carrier phase jitter is the relationship between the received signal phase, $\theta_i(s)$, and the VCO output phase, $\theta_o(s)$, namely

$$H(s)=\frac{\theta_o(s)}{\theta_i(s)}. \qquad (2\text{-}13)$$

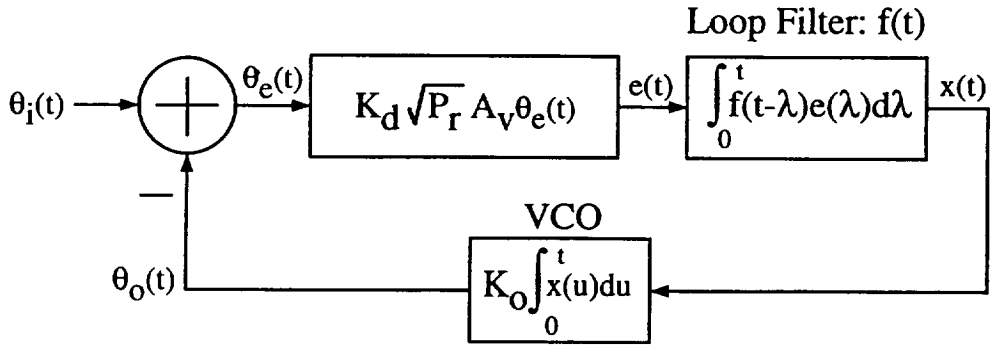

Figure 2-3. The linear baseband model.

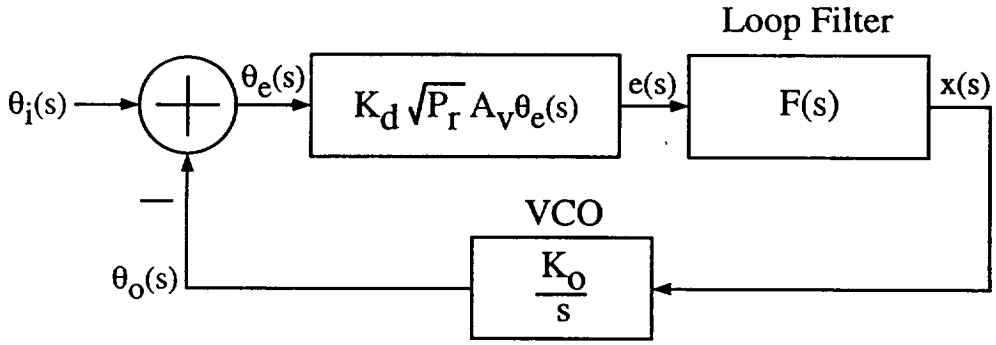

Figure 2-4. The Laplace transformed linear baseband model.

From Figure 2-4 it is clear that $\theta_o(s)$ can be expressed as

$$\theta_o(s) = \theta_e(s)\sqrt{P_r}A_v K_d F(s)\frac{K_o}{s}. \qquad (2\text{-}14)$$

Using (2-10) and (2-14) to construct the desired transfer function yields

$$H(s) = \frac{\theta_o(s)}{\theta_i(s)} = \frac{\sqrt{P_r}A_v K_d K_o \dfrac{F(s)}{s}}{1 + \sqrt{P_r}A_v K_d K_o \dfrac{F(s)}{s}} = \frac{\sqrt{P_r}A_v K_d K_o F(s)}{s + \sqrt{P_r}A_v K_d K_o F(s)}. \qquad (2\text{-}15)$$

To develop the transfer function further requires that the loop filter be selected. A commonly used loop filter is one that creates a second order control loop [38, pg. 9]. Such a loop is unconditionally stable (A third order loop is not). Further, if the loop filter is constructed using a perfect integrator the loop can track out static frequency differences between the received signal and the locally generated signal (a first order loop cannot). To achieve a second order control loop that can track out static frequency differences requires a loop filter transfer function of

$$F(s) = 1 + \frac{a}{s} \qquad (2\text{-}16)$$

where the constant a is the constant of integration for the loop filter integrator. Inserting (2-16) into the last part of (2-15) yields the transfer function

$$H(s) = \frac{s\sqrt{P_r}A_v K_d K_o + a\sqrt{P_r}A_v K_d K_o}{s^2 + s\sqrt{P_r}A_v K_d K_o + a\sqrt{P_r}A_v K_d K_o}. \tag{2-17}$$

If the phase detector gain, VCO gain, and VCO magnitude coefficient are combined to form a new constant K, the transfer function becomes

$$H(s) = \frac{s\sqrt{P_r}K + a\sqrt{P_r}K}{s^2 + s\sqrt{P_r}K + a\sqrt{P_r}K} \tag{2-18}$$

where $K = K_d K_o \sqrt{A_v}$. This transfer function now has the form of the classical second order control loop transfer function

$$H(s) = \frac{s2\zeta\omega_n + \omega_n^2}{s^2 + s2\zeta\omega_n + \omega_n^2} \tag{2-19}$$

where ζ is the damping factor of the loop and ω_n is the natural frequency of the loop. The relationships between these two classical loop design parameters and the gain terms, $\sqrt{P_r}K$ and a, are

$$\sqrt{P_r}K = 2\zeta\omega_n,$$

$$\sqrt{P_r}Ka = \omega_n^2, \tag{2-20}$$

or conversely

$$\zeta = \frac{1}{2}\sqrt{\frac{\sqrt{P_r}K}{a}},$$

and (2-21)

$$\omega_n = \sqrt{\sqrt{P_r}Ka}.$$

Note that throughout this analysis the signal power, P_r, has appeared. It is an important component of the gain of the loop. If the signal strength changes or fluctuates during operation, the loop performance will change.

One last characteristic of the PLL that will be introduced is its loop noise bandwidth. Practically speaking, the PLL is a bandpass filter [17, pg. 170]. Its input is a sinusoid in the presence of channel noise and therefore has a certain SNR associated with it (assuming some form of predetection filtering). Its output is (when tracking properly) a sinusoid of exactly the same frequency with significantly increased SNR. The baseband model from which the transfer function is derived has a lowpass characteristic, thus the name baseband. Its noise bandwidth reflects how wide this

lowpass characteristic is by equating an equivalent ideal "brickwall" lowpass bandwidth through the use of one of the integrals [38, pg.30] [39, pg. 124]

$$B_L = \frac{1}{2\pi|H(0)|^2}\int_{-\infty}^{\infty}|H(\omega)|^2 d\omega = \frac{1}{|H(0)|^2}\int_{-\infty}^{\infty}|H(f)|^2 df. \qquad (2\text{-}22)$$

It is important to note that the result of calculating the loop bandwidth with either part of (2-22) is a number expressed in Hertz. For the second order loop of interest this bandwidth is well known and is expressed as [38, pg. 31]

$$B_L = \omega_n\left(\zeta + \frac{1}{4\zeta}\right) \qquad (2\text{-}23)$$

using the classical design parameters or as Viterbi presents it [24, pg. 36]

$$B_L = \frac{\sqrt{P_r}K + a}{2} \qquad (2\text{-}24)$$

when the gain terms are used. It is important to note here that equations (2-22) - (2-24) all yield the same result, i.e., the double-sided loop noise bandwidth.

2.2 The Phaselock Loop With Noise: Calculating Jitter

Having analyzed the PLL and obtained a transfer function from its linearized model it is now useful to introduce noise into the PLL and examine how the loop models change. Introducing noise into the loop will also allow for calculation of the carrier phase jitter since it is, afterall, noise that causes jitter to occur. Before proceeding it is reiterated that this simple PLL presentation is readily available in the literature [24][29][38][39] and is a compilation of the information available there. Consider now the composite signal

$$r(t) = \sqrt{2P_r}\sin(\omega_c t + \theta_i(t)) + w(t) \qquad (2\text{-}25)$$

where the noise term, $w(t)$, is additive white Gaussian Noise with a two-sided power spectral density of $\frac{N_o}{2}$ watts/Hz. At the front end of the PLL there is a predetection bandpass filter, centered at $\frac{\omega_c}{2\pi}$ Hz and with a bandwidth of B_{IF} Hz. At the output of this filter the composite signal has become

$$r(t) = \sqrt{2P_r}\sin(\omega_c t + \theta_i(t)) + n(t) \qquad (2\text{-}26)$$

where

$$n(t) = \sqrt{2}n_1(t)\cos(\omega_c t) - \sqrt{2}n_2(t)\sin(\omega_c t) \qquad (2\text{-}27)$$

is a narrowband noise process whose power spectrum is shown in Figure 5a. The noise components of $n(t)$, namely, $n_1(t)$ and $n_2(t)$, are zero-mean, independent, white Gaussian noise processes [29, pg. 28]. Figure 5b shows the baseband power spectrum associated with both $n_1(t)$ and $n_2(t)$. The power in $n(t)$ is calculated

$$P_n = 2B_{IF}\frac{N_o}{2} = B_{IF}N_o. \tag{2-28}$$

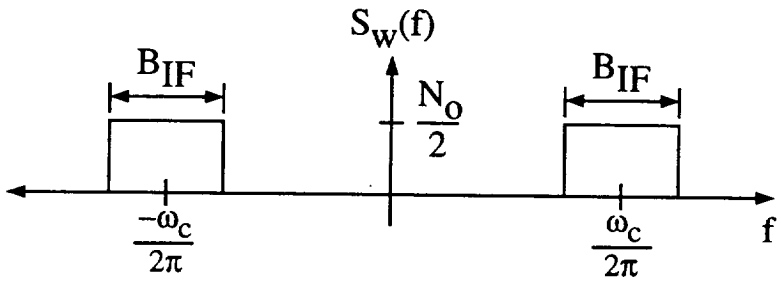

Figure 2-5a. The narrowband noise power spectrum.

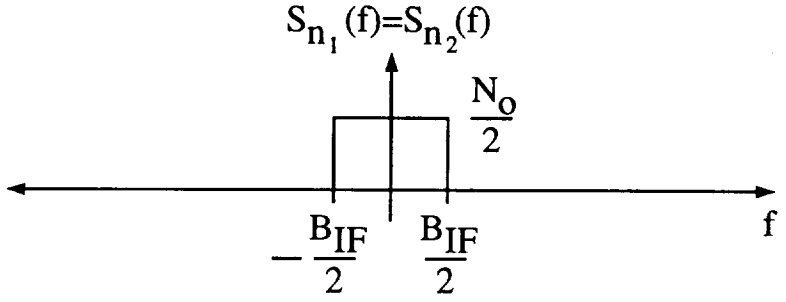

Figure 2-5b. The baseband noise power spectrum.

Since the power in the signal is P_r the SNR at the input to the PLL is

$$SNR_r = \frac{P_r}{N_o B_{IF}}. \tag{2-29}$$

The composite signal at the input to the PLL can now be expressed

$$r(t) = \sqrt{2P_r}\sin(\omega_c t + \theta_i(t)) + \sqrt{2}n_1(t)\cos(\omega_c t) - \sqrt{2}n_2(t)\sin(\omega_c t). \tag{2-30}$$

When this signal is applied to the phase detector along with (2-2), the VCO signal, the result is the noisey error signal

$$\begin{aligned} e(t) &= K_d\sqrt{P_r}A_v\sin(\theta_i(t) - \theta_o(t)) \\ &\quad + K_d A_v n_1(t)\cos(-\theta_o(t)) \\ &\quad - K_d A_v n_2(t)\sin(-\theta_o(t)) \end{aligned} \quad . \tag{2-31}$$

Noting that the cosine function is even and the sine is odd (2-31) becomes

$$\begin{aligned} e(t) &= K_d\sqrt{P_r}A_v\sin(\theta_i(t) - \theta_o(t)) \\ &\quad + K_d A_v n_1(t)\cos(\theta_o(t)) \\ &\quad + K_d A_v n_2(t)\sin(\theta_o(t)) \end{aligned} \quad . \tag{2-32}$$

The signal amplitude coefficient, $\sqrt{P_r}$, is sometimes incorporated in the noise components of (2-32) so that when the variance of the phase error is calculated it can be interpreted in terms of the

SNR at the input to the PLL [38, pp. 26-27][39, pp. 106-107]. This incorporation is accomplished by the manipulation

$$e(t) = K_d\sqrt{P_r}A_v\left[\sin(\theta_i(t)-\theta_o(t))+\frac{n_1(t)}{\sqrt{P_r}}\cos(\theta_o(t))+\frac{n_2(t)}{\sqrt{P_r}}\sin(\theta_o(t))\right]. \tag{2-33}$$

The noise components in the brackets of (2-33) are often referred to collectively as the equivalent noise of the loop, stated [39, pg. 106]

$$n_e(t) = \frac{n_1(t)}{\sqrt{P_r}}\cos(\theta_o(t))+\frac{n_2(t)}{\sqrt{P_r}}\sin(\theta_o(t)). \tag{2-34}$$

The error signal is thus

$$e(t) = K_d\sqrt{P_r}A_v\left[\sin(\theta_i(t)-\theta_o(t))+n_e(t)\right]. \tag{2-35}$$

The output from the loop filter will now be

$$x(t) = \int_0^t f(t-\lambda)K_d\sqrt{P_r}A_v\left[\sin(\theta_i(\lambda)-\theta_o(\lambda))+n_e(\lambda)\right]d\lambda\,. \tag{2-36}$$

Therefore, the integro-differential equation for the loop can be expressed as

$$\frac{d\theta_e(t)}{dt} = \frac{d\theta_i(t)}{dt} - K_o K_d \sqrt{P_r} A_v \int_0^t f(t-\lambda)\left[\sin\left(\theta_e(\lambda)\right) + n_e(\lambda)\right] d\lambda .$$

(2-37)

This equation leads to the nonlinear model of Figure 2-6.

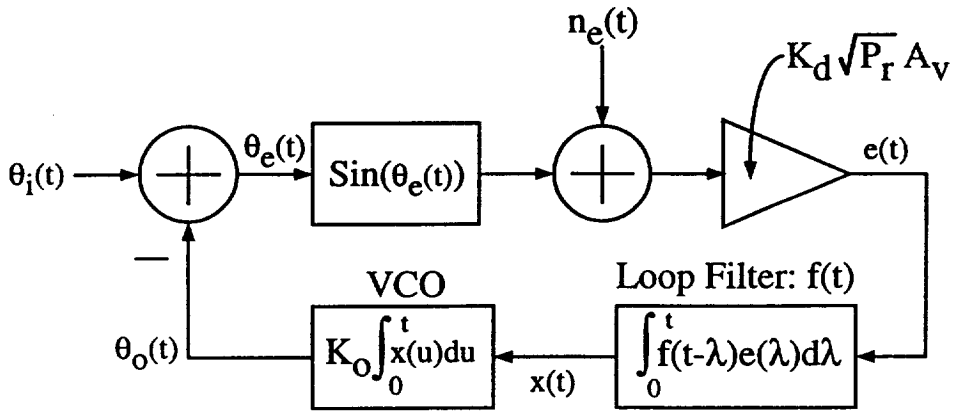

Figure 2-6. The nonlinear baseband model that incorporates noise.

The next step is to linearize the model and develop its transfer function. Once this is accomplished the jitter can be calculated as the variance of the phase error. To calculate the variance requires that the statistics of the equivalent noise be stationary. Therefore, before proceeding with the development of the linear model the statistics of the equivalent noise must be examined. In (2-34) the equivalent noise is seen to be strictly dependent on the VCO phase, $\theta_o(t)$. However, it is noted that the

loop bandwidth is, in general, much narrower than the bandwidth of the input noise for carrier tracking loops such as this [24, pg. 31]. Thus the main lobe of the sinc function that is the autocorrelation function of either of the noise components, $n_1(t)$ and $n_2(t)$, will be narrow, relative to the time $\tau = \frac{1}{B_L}$. In other words the loop, which has a lowpass-type response, responds slowly to changes in the input noise and while the VCO phase is dependent on noise that occurred on the order of $\frac{1}{B_L}$ seconds ago, it is not dependent on noise that occurred at the input in the range of $\frac{1}{B_{IF}}$ seconds ago. This makes esoteric sense too when it is considered that the function of the PLL is to filter out the noise at its input and thus produce a sinusoid that has less noise, i.e., jitter associated with it. As for the equivalent noise, it can now be stated that the VCO phase, in effect, does not vary during the small time intervals over which the noise is correlated. Then for the purpose of evaluating the statistics of the equivalent noise it can be written

$$n_e(t) = \frac{n_1(t)}{\sqrt{P_r}}\cos(\theta_o) + \frac{n_2(t)}{\sqrt{P_r}}\sin(\theta_o) \qquad (2\text{-}38)$$

where θ_o is a constant. The autocorrelation function of the equivalent noise is

$$E[n_e(t+\tau)n_e(t)] = E\begin{bmatrix} \frac{1}{P_r}n_1(t+\tau)n_1(t)\cos^2(\theta_o) \\ +\frac{1}{P_r}n_2(t+\tau)n_2(t)\sin^2(\theta_o) \\ +\frac{1}{P_r}n_1(t+\tau)n_2(t)\cos(\theta_o)\sin(\theta_o) \\ +\frac{1}{P_r}n_2(t+\tau)n_1(t)\sin(\theta_o)\cos(\theta_o) \end{bmatrix}. \qquad (2\text{-}39)$$

Combining like terms and using the linearity property of the expected value function results in

$$E[n_e(t+\tau)n_e(t)] = \frac{1}{P_r}\left\{E[n_1(t+\tau)n_1(t)]\cos^2(\theta_o) + E[n_2(t+\tau)n_2(t)]\sin^2(\theta_o)\right\} + \frac{1}{P_r}\cos(\theta_o)\sin(\theta_o)\left\{E[n_1(t+\tau)n_2(t)] + E[n_2(t+\tau)n_1(t)]\right\} \qquad (2\text{-}40)$$

However, since $n_1(t)$ and $n_2(t)$ are independent and have zero mean their crosscorrelation functions, $E[n_1(t+\tau)n_2(t)]$ or $E[n_2(t+\tau)n_1(t)]$ equate to zero as can be seen for the former crosscorrelation term

$$E[n_1(t+\tau)n_2(t)] = E[n_1(t+\tau)]E[n_2(t)] = 0. \qquad (2\text{-}41)$$

Having equated the crosscorrelation terms of $n_1(t)$ and $n_2(t)$ to zero the autocorrelation function of the equivalent noise becomes

$$E[n_e(t+\tau)n_e(t)] = \frac{1}{P_r}\left\{E[n_1(t+\tau)n_1(t)]\cos^2(\theta_o) + E[n_2(t+\tau)n_2(t)]\sin^2(\theta_o)\right\}.$$

(2-42)

Since $n_1(t)$ and $n_2(t)$ are identically distributed their autocorrelation functions are equivalent and thus (2-42) reduces to

$$E[n_e(t+\tau)n_e(t)] = \frac{1}{P_r}E[n_1(t+\tau)n_1(t)]\left\{\cos^2(\theta_o) + \sin^2(\theta_o)\right\} = \frac{1}{P_r}E[n_1(t+\tau)n_1(t)].$$

(2-43)

Noting that $n_1(t)$, like $n_2(t)$, is stationary, its autocorrelation is thus a function only of the time difference, τ. Therefore, it is possible to write the autocorrelation of the equivalent noise as

$$R_{n_e}(\tau) = \frac{R_{n_1}(\tau)}{P_r}. \qquad (2\text{-}44)$$

Since the autocorrelation function is the Fourier transform pair of the power spectral density of $n_e(t)$ it is possible to state

$$S_{n_e}(f) = \frac{S_{n_1}(f)}{P_r} = \frac{N_o}{2P_r} \text{ for } |f| \le \frac{B_{IF}}{2}. \qquad (2\text{-}45)$$

Having identified the equivalent noise as a stationary Gaussian process and having obtained its power spectral density, it is possible to obtain the variance of the phase error by analyzing the output power spectral density of the linear loop model in response to the equivalent noise.

Linearizing the model of Figure 2-6 leads to the model of Figure 2-7. If the input phase, $\theta_i(t)$, is held constant and equal to zero then the output of the linear system, i.e., the VCO phase, will be due only to the equivalent noise input. The transfer function from the equivalent noise input to the VCO phase output is seen in Figure 2-7 to be identical to that of (2-18). For a linear system the output power spectrum can be obtained using

$$S_{\theta_o}(f) = |H(f)|^2 S_{n_e}(f). \tag{2-46}$$

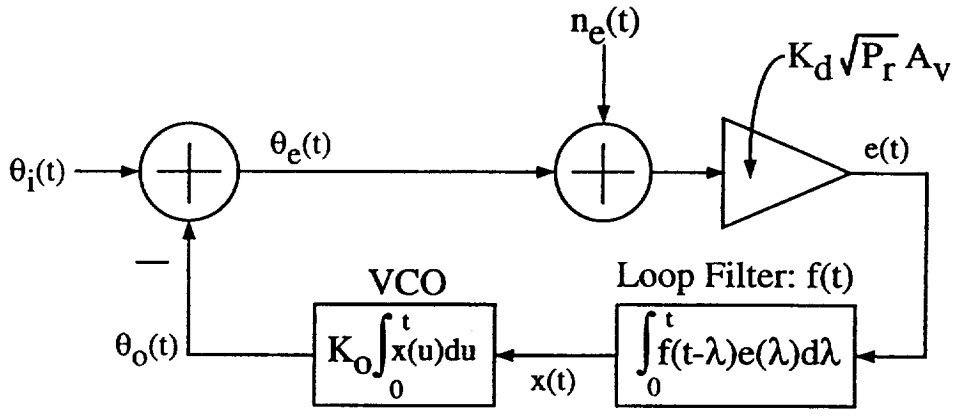

Figure 2-7. The linear baseband model that incorporates noise.

Noting that with $\theta_i(t)=0$ the phase error is the negative of the VCO phase and so the output power spectral density of the VCO phase is also that of the phase error. This is stated

$$S_{\theta_e}(f)=|H(f)|^2 S_{n_e}(f). \tag{2-47}$$

Since the equivalent noise has zero mean and therefore $\theta_e(t)$ does, too, the variance of $\theta_e(t)$ is its autocorrelation function evaluated at zero

$$\sigma_{\theta_e}^2 = R_{\theta_e}(\tau)\Big|_{\tau=0} = \int_{-\infty}^{\infty} S_{\theta_e}(f)e^{if\tau}df\Bigg|_{\tau=0} = \int_{-\infty}^{\infty} S_{\theta_e}(f)df = \int_{-\infty}^{\infty}|H(f)|^2 S_{n_e}(f)df. \tag{2-48}$$

Next, consider that since the power spectral density of the equivalent noise, as described by (2-45), has a constant value over the entire frequency range that $|H(s)|$ is essentially non-zero, it is possible to express (2-48) as

$$\sigma_{\theta_e}^2 = \frac{N_o}{2P_r}\int_{-\frac{B_{IF}}{2}}^{\frac{B_{IF}}{2}}|H(f)|^2 df \tag{2-49}$$

where (2-45) has been used for the power spectral density of the equivalent noise. Using the definition for the loop noise bandwidth given in (2-22), and noting that the loop noise bandwidth is much smaller than the IF bandwidth, the variance of the phase error can be expressed as

$$\sigma_{\theta_e}^2 = \frac{N_o B_L}{2P_r}|H(0)|^2. \tag{2-50}$$

Since the loop transfer function of (2-18) has unity DC gain the jitter becomes

$$\sigma_{\theta_e}^2 = \frac{N_o B_L}{2P_r}. \tag{2-51}$$

Using the input SNR to the PLL, described by (2-29), the variance of the phase error of the PLL becomes

$$\sigma_{\theta_e}^2 = \frac{1}{2SNR_r}\frac{B_L}{B_{IF}}. \tag{2-52}$$

A final, useful though intangible quantity that is often considered in understanding the performance of a PLL is the SNR in the loop. It is usually described in terms of the variance of the phase error as

$$SNR_L = \frac{1}{\sigma_{\theta_e}^2} = 2SNR_r\frac{B_{IF}}{B_L}. \tag{2-53}$$

The quantity is considered intangible because there is no signal that exists in the loop that exhibits this SNR. Its function is as a reference for measuring performance and it will be encountered again in the descriptions of the performance of the high-SNR MAP loop.

As has been demonstrated jitter in a PLL is represented by the variance of the phase of the VCO's signal due to noise at the PLL input. This jitter is dependent on the SNR of the received signal and on both the IF and loop bandwidth. All of these factors will appear again, in one form or another, when the jitter in the high-SNR MAP approximation loop is analyzed. The procedure will be very similar as well. The linear baseband model for the loop will be developed and its transfer function used to obtain the jitter of the VCO's phase due to a noisy input.

Chapter 3

MAP ESTIMATION DERIVATIONS FOR CARRIER PHASE JITTER

"It is truth very certain that when it is not in our power to determine what is true, we ought to follow what is most probable."

René Descartes
mathematician & philosopher, 1596 - 1650

3.1 Introduction

In a coherent MPSK system we have the transmitted signal

$$s(t) = \sqrt{\frac{2E}{T}} \cos(\omega_c t - \theta_m(t)) \qquad (3\text{-}1)$$

of duration T seconds and symbol energy E, where $\theta_m(t)$ is the phase shift key modulation. For $M = 2$, $\theta_m(t)$ can take on the values $(0, \pi)$. For $M > 2$ the modulation can take on the values $\frac{(2m+1)\pi}{M}$ for $m = 0,1...(M-1)$. The channel adds white Gaussian noise (AWGN) to the signal and shifts the carrier phase by an unknown amount, θ_i. It is considered here that the function of the coherent receiver is to detect the data in the received PSK signal in the presence of noise. The received signal (after predetection filtering) is denoted

$$r(t) = \sqrt{\frac{2E}{T}} \cos(\omega_c t - \theta_m(t) + \theta_i) + n(t). \qquad (3\text{-}2)$$

As was done with the PLL of Chapter 2, the noise component, $n(t)$, will be assumed to be narrowband noise having passed through the predetection bandpass filter[1] before entering the receiver. For MPSK, the optimum receiver can be achieved with the use of two correlators [40, pps. 257-259]. These correlators require a coherent reference. In order to obtain this reference it is necessary for the receiver to estimate what the unknown phase component, θ_i, is. There are several criteria that can be used to achieve the optimum estimate of θ_i [24, pg. 126]. However the estimation technique of interest here is the maximum aposteriori criterion. This approach involves selecting θ_i in such a manner that the aposteriori probabilty of θ_i, given that $r(t)$ was received, is maximized [26]. The a posteriori probability density of the phase θ_i, given received signal $r(t)$, is denoted $p(\theta_i|R)$.[2] It can be expressed in terms of the channel transition probability density and the received signal and carrier phase probability densities using Bayes theorem

$$p(\theta_i|R) = \frac{p(R|\theta_i)p(\theta_i)}{p(R)} \tag{3-3}$$

where $p(R|\theta_i)$ is the transitional probability density of receiving the signal R given a carrier signal with phase θ_i. We are

---

[1] Note that the bandwidth of the predetection filter is wide compared to the symbol rate.

[2] Note that time designator has been dropped for mathematical convenience.

interested in maximizing this quantity to obtain the best estimate of the carrier phase and will therefore be computing its derivative. However, before this is done the natural log function is introduced to separate the terms in (3-3). This will not affect the derivative since the natural log function is a monotonically increasing function. Applying the log function results in

$$\ln\left(p(\theta_i|R)\right) = \ln\left(p\left(R|\theta_i\right)\right) + \ln\left(p(\theta_i)\right) - \ln(p(R)) \qquad (3\text{-}4)$$

Now (3-4) can be maximized by taking its derivative with respect to the carrier phase and setting it equal to zero. We add the further constraint that the phase of the optimum receiver's coherent reference will equal θ_i when the maximum a posteriori phase estimate is obtained. This will help formulate the estimator into a control loop.

Noting that the probability of receiving R is not a function of the carrier phase (3-4) can be written as

$$\left.\frac{\partial \ln\left(p(\theta_i|R)\right)}{\partial \theta_i}\right|_{\theta_i=\theta_o} = \left.\frac{\partial \ln\left(p\left(R|\theta_i\right)\right)}{\partial \theta_i}\right|_{\theta_i=\theta_o} + \left.\frac{\partial \ln\left(p(\theta_i)\right)}{\partial \theta_i}\right|_{\theta_i=\theta_o} = 0. \qquad (3\text{-}5)$$

Since the carrier phase θ_i is uniformly distributed it is possible to state

$$\left.\frac{\partial \ln\left(p(\theta_i|R)\right)}{\partial \theta_i}\right|_{\theta_i=\theta_o} = \left.\frac{\partial \ln\left(p(R|\theta_i)\right)}{\partial \theta_i}\right|_{\theta_i=\theta_o} = 0. \qquad (3\text{-}6)$$

It is now possible to derive the maximum aposteriori phase (MAP) estimator by using $p(R|\theta_i)$, the likelihood function.

3.2 MAP Derivation For BPSK

To proceed with obtaining $p(R|\theta_i)$ the M=2 case (BPSK) signal set will be considered first. Once its MAP estimator is obtained the subsequent estimators for M=4,8, and 16 will be presented. To compute $p(R|\theta_i)$ begin with the received signal

$$r(t) = \sqrt{\frac{2E}{T}}\cos(\omega_c t - \theta_m + \theta_i) + n(t). \qquad (3\text{-}7)$$

The MPSK signal can be expressed in two dimensions using the orthonormal basis

$$\Psi_1(t) = \sqrt{\frac{2}{T}}\cos(w_c t)$$

$$\Psi_2(t) = \sqrt{\frac{2}{T}}\sin(w_c t) \qquad (3\text{-}8)$$

which results in $r(t) = r_1(t)\Psi_1(t) + r_2(t)\Psi_2(t)$ where

$$r_1 = \int_0^T r(t)\sqrt{\frac{2}{T}}\cos(\omega_c t)dt \tag{3-9}$$

and

$$r_2 = \int_0^T r(t)\sqrt{\frac{2}{T}}\sin(\omega_c t)dt\,.$$

Performing the integration for r_1 and r_2 yields

$$\begin{aligned} r_1 &= \sqrt{E}\cos(\theta_i - \theta_m) + n_1 = s_1 + n_1 \\ r_2 &= -\sqrt{E}\sin(\theta_i - \theta_m) + n_2 = s_2 + n_2\,. \end{aligned} \tag{3-10}$$

To continue, the likelihood function can be obtained from the conditional density of R given both the modulation angle θ_m and the carrier phase θ_i. Noting that this conditional density can be expressed in terms of the orthonormal basis components r_1 and r_2 it is expressed

$$p(R|\theta_i, \theta_m) = p(r_1|\theta_i, \theta_m)p(r_2|\theta_i, \theta_m) \tag{3-11}$$

The conditonal densities on the right of the equality in (3-11) are the noise probability densities of n_1 and n_2 expressed in the

received signal space with means s_1 and s_2 respectively. The conditional density of (3-11) can therefore be expressed[3]

$$p(R|\theta_i,\theta_m)=\frac{1}{\sqrt{2\pi\sigma^2}}e^{-\frac{(r_1-s_1)^2}{2\sigma^2}}\frac{1}{\sqrt{2\pi\sigma^2}}e^{-\frac{(r_2-s_2)^2}{2\sigma^2}}. \tag{3-12}$$

To obtain the likelihood function the modulation angle random variable is integrated out of the conditional density in (3-12) as follows

$$p(R|\theta_i)=\int_{-\infty}^{\infty}p(R|\theta_i,\theta_m)p(\theta_m)d\theta_m. \tag{3-13}$$

For BPSK the modulation angle probability density is

$$p(\theta_m)=\frac{1}{2}\delta(\theta_m)+\frac{1}{2}\delta(\theta_m-\pi). \tag{3-14}$$

Substituting (3-14) into (3-13) and applying the sifting property of the delta function the likelihood function becomes

$$p(R|\theta_i)=\frac{1}{2}p(R|\theta_i,\theta_m=0)+\frac{1}{2}p(R|\theta_i,\theta_m=\pi). \tag{3-15}$$

---

[3] Note that the noise samples out of the quardrature arm correlators will be Gaussian and have variance $\sigma^2=\frac{N_o}{2E}$.

To insert (3-12) into (3-15) the quantities $r_1 - s_1$ and $r_2 - s_2$ must first be analyzed for both values of θ_m. For $\theta_m = 0$

$$r_1 - s_1 = r_1 - \sqrt{E}\cos(\theta_i - 0) = r_1 - \sqrt{E}\cos(\theta_i) \tag{3-16a}$$

and

$$r_2 - s_2 = r_2 + \sqrt{E}\sin(\theta_i - 0) = r_2 + \sqrt{E}\sin(\theta_i). \tag{3-16b}$$

For $\theta_m = \pi$

$$r_1 - s_1 = r_1 - \sqrt{E}\cos(\theta_i - \pi) = r_1 + \sqrt{E}\cos(\theta_i) \tag{3-17a}$$

and

$$r_2 - s_2 = r_2 + \sqrt{E}\sin(\theta_i - \pi) = r_2 - \sqrt{E}\sin(\theta_i). \tag{3-17b}$$

Now using (3-16) and (3-17), it is possible to insert (3-12) into (3-15) and obtain the likelihood function

$$p(R|\theta_i)=\frac{1}{2\pi\sigma^2}\left\{\frac{e^{-\frac{(r_1-\sqrt{E}\cos(\theta_i))^2}{2\sigma^2}}e^{-\frac{(r_2+\sqrt{E}\sin(\theta_i))^2}{2\sigma^2}}}{2}+\frac{e^{-\frac{(r_1+\sqrt{E}\cos(\theta_i))^2}{2\sigma^2}}e^{-\frac{(r_2-\sqrt{E}\sin(\theta_i))^2}{2\sigma^2}}}{2}\right\}. \quad (3\text{-}18)$$

Completing the square and combining exponential terms yields

$$p(R|\theta_i)=\frac{1}{2\pi\sigma^2}\left\{\frac{e^{-\frac{\left(r_1^2-2r_1\sqrt{E}\cos(\theta_i)+E\cos^2(\theta_i)+r_2^2+2r_2\sqrt{E}\sin(\theta_i)+E\sin^2(\theta_i)\right)}{2\sigma^2}}}{2}+\frac{e^{-\frac{\left(r_1^2+2r_1\sqrt{E}\cos(\theta_i)+E\cos^2(\theta_i)+r_2^2-2r_2\sqrt{E}\sin(\theta_i)+E\sin^2(\theta_i)\right)}{2\sigma^2}}}{2}\right\}. \quad (3\text{-}19)$$

By reducing, the conditional density becomes

$$p(R|\theta_i)=\frac{1}{2\pi\sigma^2}\left\{\frac{e^{-\frac{\left(r_1^2+r_2^2+E\right)}{2\sigma^2}}e^{-\frac{\left(-2r_1\sqrt{E}\cos(\theta_i)+2r_2\sqrt{E}\sin(\theta_i)\right)}{2\sigma^2}}}{2}\right.$$

$$\left.+\frac{e^{-\frac{\left(r_1^2+r_2^2+E\right)}{2\sigma^2}}e^{-\frac{\left(2r_1\sqrt{E}\cos(\theta_i)-2r_2\sqrt{E}\sin(\theta_i)\right)}{2\sigma^2}}}{2}\right\}. \quad (3\text{-}20)$$

Rewriting the exponents in the form of the hyperbolic cosine produces

$$p(R|\theta_i)=\frac{1}{2\pi\sigma^2}\left\{e^{-\frac{\left(r_1^2+r_2^2+E\right)}{2\sigma^2}}\left[\frac{e^{\frac{\left(2r_1\sqrt{E}\cos(\theta_i)-2r_2\sqrt{E}\sin(\theta_i)\right)}{2\sigma^2}}}{2}\right.\right.$$

$$\left.\left.+\frac{e^{-\frac{\left(2r_1\sqrt{E}\cos(\theta_i)-2r_2\sqrt{E}\sin(\theta_i)\right)}{2\sigma^2}}}{2}\right]\right\} \quad . \quad (3\text{-}21)$$

Inserting the hyperbolic cosine function results in

$$p(R|\theta_i)=\frac{1}{2\pi\sigma^2}e^{-\frac{\left(r_1^2+r_2^2+E\right)}{2\sigma^2}}\cosh\left(\frac{\left(2r_1\sqrt{E}\cos(\theta_i)-2r_2\sqrt{E}\sin(\theta_i)\right)}{2\sigma^2}\right).$$

(3-22)

Substituing in r_1 and r_2 from (3-9) the conditional density becomes

$$p(R|\theta_i) = \frac{1}{2\pi\sigma^2} e^{-\frac{\left(r_1^2+r_2^2+E\right)}{2\sigma^2}} \cosh\left(\frac{\sqrt{E}\cos(\theta_i)\int_0^T r(t)\sqrt{\frac{2}{T}}\cos(\omega_c t)dt}{\sigma^2} - \frac{\sqrt{E}\sin(\theta_i)\int_0^T r(t)\sqrt{\frac{2}{T}}\sin(\omega_c t)dt}{\sigma^2} \right) \cdot$$

(3-23)

Combining the integrals yields

$$p(R|\theta_i) = \frac{1}{2\pi\sigma^2} e^{-\frac{\left(r_1^2+r_2^2+E\right)}{2\sigma^2}} \times \cosh\left(\frac{\sqrt{\frac{2E}{T}}}{\sigma^2} \int_0^T r(t)\left(\cos(\omega_c t)\cos(\theta_i) - \sin(\omega_c t)\sin(\theta_i)\right)dt \right) \cdot$$

(3-24)

Applying a trigonometric identity results in

$$p(R|\theta_i) = \frac{1}{2\pi\sigma^2} e^{-\frac{\left(r_1^2 + r_2^2 + E\right)}{2\sigma^2}} \cosh\left(\frac{\sqrt{\frac{2E}{T}}}{\sigma^2} \int_0^T r(t)\cos(\omega_c t + \theta_i)dt \right). \quad (3\text{-}25)$$

To continue with deriving the MAP estimator in (3-6) the log likelihood function,

$$\ln\left[p(R|\theta_i)\right] = \ln\left[\frac{1}{2\pi\sigma^2} e^{-\frac{\left(r_1^2 + r_2^2 + E\right)}{2\sigma^2}} \cosh\left(\frac{\sqrt{\frac{2E}{T}}}{\sigma^2} \int_0^T r(t)\cos(\omega_c t + \theta_i)dt \right) \right]$$

(3-26)

is used. The MAP estimator is obtained by taking the derivative of (3-26) with respect to θ_i. To compute this derivative we note the multiplicative property of the logarithm function and the following application of the chain rule

$$\frac{\partial\left\{\ln[\cosh(u)]\right\}}{\partial\theta_i} = \frac{1}{\cosh(u)} \frac{\partial[\cosh(u)]}{\partial\theta_i} = \frac{\sinh(u)}{\cosh(u)} \frac{\partial(u)}{\partial\theta_i} = \tanh(u) \frac{\partial(u)}{\partial\theta_i}.$$

(3-27)

Taking the derivative of (3-26) results in

$$\frac{\partial \ln\left(p\left(R|\theta_i\right)\right)}{\partial\theta_i} = \frac{\partial \ln\left[\frac{1}{2\pi\sigma^2} e^{-\frac{\left(r_1^2+r_2^2+E\right)}{2\sigma^2}}\right]}{\partial\theta_i}$$

$$-\tanh\left[\frac{\sqrt{\frac{2E}{T}}}{\sigma^2}\int_0^T r(t)\cos\left(\omega_c t+\theta_i\right)dt\right]\times\frac{\sqrt{\frac{2E}{T}}}{\sigma^2}\int_0^T r(t)\sin\left(\omega_c t+\theta_i\right)dt \qquad (3\text{-}28)$$

Next, note that the quantity $r_1^2+r_2^2$, the square of the magnitude of the received signal, is not a function of θ_i and therefore the first term of the sum in (3-28) equates to zero. To complete the MAP estimator derivation set the right side of (3-28) equal to zero and insert the necessary condition for the optimum estimator mentioned in (3-6) regarding the control of the receiver reference (i.e., $\theta_i = \theta_o$). The resulting MAP estimator can be used in a control loop where a loop filter and voltage controlled oscillator can be used to drive the MAP estimator equation, or more appropriately the error signal, to zero [26]. To conclude, the BPSK MAP estimator equation is [27]

$$-\tanh\left[\frac{\sqrt{\frac{2E}{T}}}{\sigma^2}\int_0^T r(t)\cos\left(\omega_c t+\theta_o\right)dt\right]\times\int_0^T r(t)\sin\left(\omega_c t+\theta_o\right)dt = 0. \qquad (3\text{-}29)$$

When it is employed in a control loop to drive an error signal to zero the result is the loop of Figure 3-1.

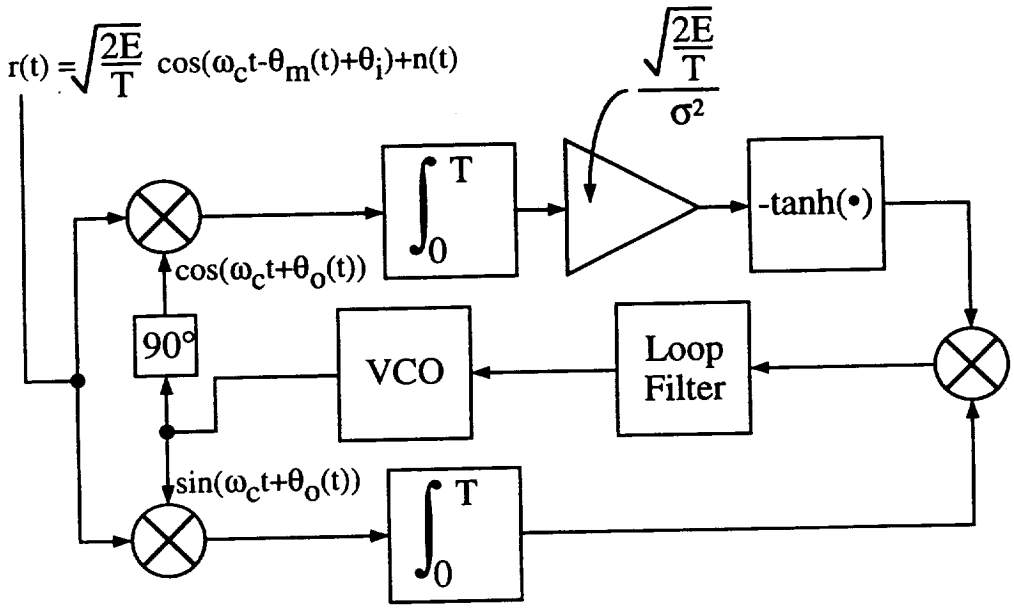

Figure 3-1. The optimum MAP estimator loop for BPSK carrier tracking.

Historically, the implementation of complicated functions like the hyperbolic tangent function was a costly procedure in terms of the large quantity of analog hardware it required. As a result alternative approximations were considered. In the case of the hyperbolic tangent function two approximations have been considered for implementation in the loop of Figure 3-1. The first is accurate when the function argument is large. In that case the hyperbolic tangent function may be replaced by a hard limiter.

This is known as the high-SNR approximation. When the function argument is small the hyperbolic tangent function can be replaced by a "through connection" since the function has a linear unity gain response to small arguments. The loop of interest in this study is the high-SNR approximation to the MAP estimation technique and it is shown in Figure 3-2 for BPSK.

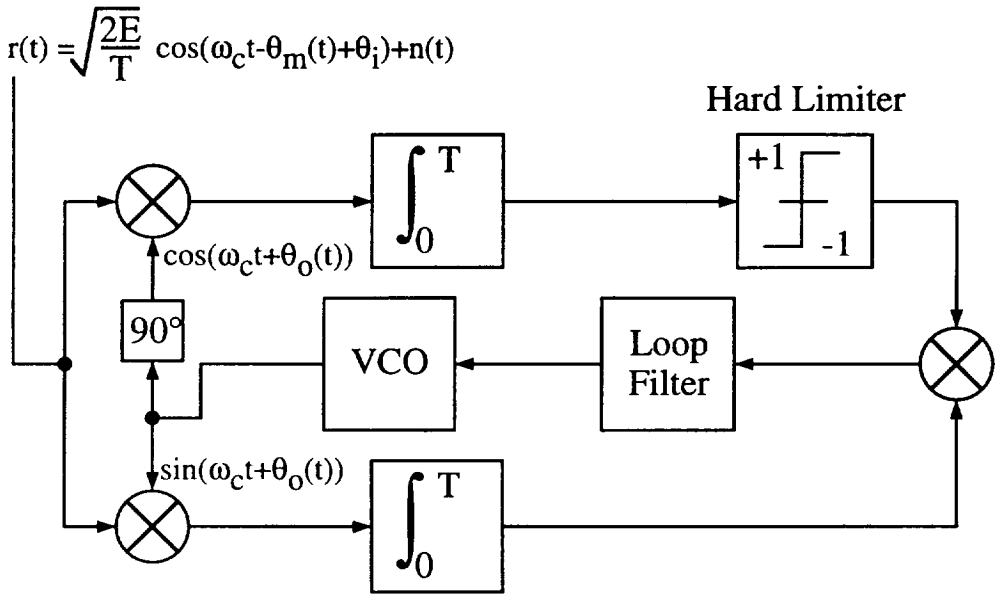

Figure 3-2. The high SNR approximation loop for BPSK carrier tracking.

3.3 MAP Derivation For QPSK

To obtain the optimum MAP estimator, and subsequently the high-SNR approximation for QPSK the derivation presented for

BPSK must be altered starting with the probability density function for the modulation angle,$p(\theta_m)$. Once this is done the likelihood function for QPSK can be used to arrive at the appropriate estimator. Therefore to begin, the QPSK modulation angle probability density function is

$$p(\theta_m)=\frac{1}{4}\delta\left(\theta_m-\frac{\pi}{4}\right)+\frac{1}{4}\delta\left(\theta_m-\frac{3\pi}{4}\right)+\frac{1}{4}\delta\left(\theta_m+\frac{\pi}{4}\right)+\frac{1}{4}\delta\left(\theta_m+\frac{3\pi}{4}\right). \tag{3-30}$$

Once again using the sifting property to integrate out the modulation from the conditional density of R given both the modulation angle θ_m and the carrier phase θ_i results in the likelihood function

$$\begin{aligned} p(R|\theta_i)=&\frac{1}{4}p\left(R\middle|\theta_i,\theta_m=\frac{\pi}{4}\right)+\frac{1}{4}p\left(R\middle|\theta_i,\theta_m=\frac{3\pi}{4}\right)\\ &+\frac{1}{4}p\left(R\middle|\theta_i,\theta_m=\frac{-\pi}{4}\right)+\frac{1}{4}p\left(R\middle|\theta_i,\theta_m=\frac{-3\pi}{4}\right). \end{aligned} \tag{3-31}$$

To proceed (3-12), the conditional noise probability density, is inserted into (3-31) for each of the four values of θ_m. To do this the two quantities r_1-s_1 and r_2-s_2 must first be analyzed for the four values of θ_m. For $\theta_m=\frac{\pi}{4}$

$$r_1-s_1=r_1-\sqrt{E}\cos\left(\theta_i-\frac{\pi}{4}\right) \tag{3-32a}$$

and

$$r_2 - s_2 = r_2 + \sqrt{E}\sin\left(\theta_i - \frac{\pi}{4}\right). \tag{3-32b}$$

For $\theta_m = \frac{3\pi}{4}$

$$r_1 - s_1 = r_1 - \sqrt{E}\cos\left(\theta_i - \frac{3\pi}{4}\right) \tag{3-33a}$$

and

$$r_2 - s_2 = r_2 + \sqrt{E}\sin\left(\theta_i - \frac{3\pi}{4}\right). \tag{3-33b}$$

For $\theta_m = -\frac{\pi}{4}$

$$r_1 - s_1 = r_1 - \sqrt{E}\cos\left(\theta_i + \frac{\pi}{4}\right) \tag{3-34a}$$

and

$$r_2 - s_2 = r_2 + \sqrt{E}\sin\left(\theta_i + \frac{\pi}{4}\right). \tag{3-34b}$$

For $\theta_m = -\frac{3\pi}{4}$

$$r_1 - s_1 = r_1 - \sqrt{E}\cos\left(\theta_i + \frac{3\pi}{4}\right) \tag{3-35a}$$

and

$$r_2 - s_2 = r_2 + \sqrt{E}\sin\left(\theta_i + \frac{3\pi}{4}\right). \tag{3-35b}$$

Now using (3-32) - (3-35) it is possible to substitute (3-12) into (3-31) and doing so yields

$$p(R|\theta_i) = \frac{1}{2\pi\sigma^2}\left\{\frac{e^{-\frac{\left(r_1-\sqrt{E}\cos\left(\theta_i+\frac{\pi}{4}\right)\right)^2}{2\sigma^2}} e^{-\frac{\left(r_2+\sqrt{E}\sin\left(\theta_i+\frac{\pi}{4}\right)\right)^2}{2\sigma^2}}}{4}\right.$$

$$+\frac{e^{-\frac{\left(r_1-\sqrt{E}\cos\left(\theta_i+\frac{3\pi}{4}\right)\right)^2}{2\sigma^2}} e^{-\frac{\left(r_2+\sqrt{E}\sin\left(\theta_i+\frac{3\pi}{4}\right)\right)^2}{2\sigma^2}}}{4}$$

$$+\frac{e^{-\frac{\left(r_1-\sqrt{E}\cos\left(\theta_i-\frac{\pi}{4}\right)\right)^2}{2\sigma^2}} e^{-\frac{\left(r_2+\sqrt{E}\sin\left(\theta_i-\frac{\pi}{4}\right)\right)^2}{2\sigma^2}}}{4}$$

$$\left.+\frac{e^{-\frac{\left(r_1-\sqrt{E}\cos\left(\theta_i-\frac{3\pi}{4}\right)\right)^2}{2\sigma^2}} e^{-\frac{\left(r_2+\sqrt{E}\sin\left(\theta_i-\frac{3\pi}{4}\right)\right)^2}{2\sigma^2}}}{4}\right\}. \tag{3-36}$$

To proceed with minimum confusion, each of the terms in (3-36) corresponding to a particular modulation angle will be considered separately. Thus,

$$\langle A\rangle = \frac{1}{8\pi\sigma^2} e^{-\frac{\left(r_1-\sqrt{E}\cos\left(\theta_i+\frac{\pi}{4}\right)\right)^2}{2\sigma^2}} e^{-\frac{\left(r_2+\sqrt{E}\sin\left(\theta_i+\frac{\pi}{4}\right)\right)^2}{2\sigma^2}} \tag{3-37}$$

corresponds to the first term in (3-36). Completing the square of the exponential arguments in (3-37) and then combining them results in

$$\langle A\rangle = \frac{1}{8\pi\sigma^2} e^{-\frac{\left[\begin{array}{l} r_1^2-2r_1\sqrt{E}\cos\left(\theta_i+\frac{\pi}{4}\right)+E\cos^2\left(\theta_i+\frac{\pi}{4}\right) \\ +r_2^2+2r_2\sqrt{E}\sin\left(\theta_i+\frac{\pi}{4}\right)+E\sin^2\left(\theta_i+\frac{\pi}{4}\right)\end{array}\right]}{2\sigma^2}}. \tag{3-38}$$

By combining and separating like terms (3-38) becomes

$$\langle A\rangle = \frac{1}{8\pi\sigma^2} e^{-\frac{r_1^2+r_2^2+E-2r_1\sqrt{E}\cos\left(\theta_i+\frac{\pi}{4}\right)+2r_2\sqrt{E}\sin\left(\theta_i+\frac{\pi}{4}\right)}{2\sigma^2}}. \tag{3-39}$$

Applying trigonometric identities to expand the sinusoidal terms forms

$$\langle A\rangle = \frac{1}{8\pi\sigma^2} e^{-\frac{r_1^2+r_2^2+E}{2\sigma^2}} \times e^{-\frac{-2r_1\sqrt{E}\left[\cos(\theta_i)\cos\left(\frac{\pi}{4}\right)-\sin(\theta_i)\sin\left(\frac{\pi}{4}\right)\right]}{2\sigma^2}} \times e^{-\frac{2r_2\sqrt{E}\left[\sin(\theta_i)\cos\left(\frac{\pi}{4}\right)+\cos(\theta_i)\sin\left(\frac{\pi}{4}\right)\right]}{2\sigma^2}}. \quad (3\text{-}40)$$

Noting that $\cos\left(\frac{\pi}{4}\right)=\sin\left(\frac{\pi}{4}\right)=\frac{\sqrt{2}}{2}$, (3-40) becomes

$$\langle A\rangle = \frac{1}{8\pi\sigma^2} e^{-\frac{r_1^2+r_2^2+E}{2\sigma^2}} e^{-\frac{-r_1\sqrt{2E}\left[\cos(\theta_i)-\sin(\theta_i)\right]}{2\sigma^2}} e^{-\frac{r_2\sqrt{2E}\left[\sin(\theta_i)+\cos(\theta_i)\right]}{2\sigma^2}}. \quad (3\text{-}41)$$

Inserting the equations for r_1 and r_2, given in (3-9) resolves (3-41) into

$$\langle A\rangle = \frac{1}{8\pi\sigma^2} e^{-\frac{r_1^2+r_2^2+E}{2\sigma^2}} \times e^{-\frac{-\left[\int_0^T r(t)\sqrt{\frac{2}{T}}\cos(\omega_c t)dt\right]\sqrt{2E}\left[\cos(\theta_i)-\sin(\theta_i)\right]}{2\sigma^2}} \times e^{-\frac{\left[\int_0^T r(t)\sqrt{\frac{2}{T}}\sin(\omega_c t)dt\right]\sqrt{2E}\left[\sin(\theta_i)+\cos(\theta_i)\right]}{2\sigma^2}}. \quad (3\text{-}42)$$

By combining the integrals and distributing the carrier components within the single integrand, (3-42) becomes

$$\langle A\rangle = \frac{1}{8\pi\sigma^2} e^{-\frac{r_1^2+r_2^2+E}{2\sigma^2}} \times e^{\frac{\left\{2\sqrt{\frac{E}{T}}\int_0^T r(t)\left[\cos(\omega_c t)\cos(\theta_i)-\cos(\omega_c t)\sin(\theta_i)-\sin(\omega_c t)\sin(\theta_i)-\sin(\omega_c t)\cos(\theta_i)\right]dt\right\}}{2\sigma^2}}.$$

(3-43)

Next, using the trigonometric identities

$$\cos(x)\cos(y)-\sin(x)\sin(y)=\cos(x+y)$$

and (3-44)

$$\cos(x)\sin(y)+\sin(x)\cos(y)=\sin(x+y)$$

the integral in (3-43) is separated into two new integrals. This new form is

$$\langle A\rangle = \frac{1}{8\pi\sigma^2} e^{-\frac{r_1^2+r_2^2+E}{2\sigma^2}} e^{\frac{\left[2\sqrt{\frac{E}{T}}\int_0^T r(t)\cos(\omega_c t+\theta_i)dt\right]}{2\sigma^2}} + \frac{\left[-2\sqrt{\frac{E}{T}}\int_0^T r(t)\sin(\omega_c t+\theta_i)dt\right]}{2\sigma^2}.$$

(3-45)

At this point the second term of (3-36), the term corresponding to a modulation angle of $\theta_m = \frac{3\pi}{4}$, is considered. From (3-36) this second term is

$$\langle B \rangle = \frac{1}{8\pi\sigma^2} e^{-\frac{\left(r_1 - \sqrt{E}\cos\left(\theta_i + \frac{3\pi}{4}\right)\right)^2}{2\sigma^2}} e^{-\frac{\left(r_2 + \sqrt{E}\sin\left(\theta_i + \frac{3\pi}{4}\right)\right)^2}{2\sigma^2}}. \qquad (3\text{-}46)$$

Using the same approach as was done for the first term, (3-46) is first resolved into

$$\langle B \rangle = \frac{1}{8\pi\sigma^2} e^{-\frac{r_1^2 + r_2^2 + E}{2\sigma^2}} \times e^{\frac{-2r_1\sqrt{E}\left[\cos(\theta_i)\cos\left(\frac{3\pi}{4}\right) - \sin(\theta_i)\sin\left(\frac{3\pi}{4}\right)\right]}{2\sigma^2}} \times e^{\frac{2r_2\sqrt{E}\left[\sin(\theta_i)\cos\left(\frac{3\pi}{4}\right) + \cos(\theta_i)\sin\left(\frac{3\pi}{4}\right)\right]}{2\sigma^2}}. \qquad (3\text{-}47)$$

Making use of the fact that $\cos\left(\frac{3\pi}{4}\right) = -\frac{\sqrt{2}}{2}$ and $\sin\left(\frac{3\pi}{4}\right) = \frac{\sqrt{2}}{2}$ the second term becomes

$$\langle B \rangle = \frac{1}{8\pi\sigma^2} e^{-\frac{r_1^2 + r_2^2 + E}{2\sigma^2}} e^{-\frac{-r_1\sqrt{2E}\left[-\cos(\theta_i) - \sin(\theta_i)\right]}{2\sigma^2}} e^{-\frac{r_2\sqrt{2E}\left[-\sin(\theta_i) + \cos(\theta_i)\right]}{2\sigma^2}}. \qquad (3\text{-}48)$$

Inserting the equations for r_1 and r_2, given in (3-9) converts (3-48) into

$$\langle B\rangle = \frac{1}{8\pi\sigma^2} e^{-\frac{r_1^2+r_2^2+E}{2\sigma^2}} \times e^{\frac{-\left[\int_0^T r(t)\sqrt{\frac{2}{T}}\cos(\omega_c t)dt\right]\sqrt{2E}\left[-\cos(\theta_i)-\sin(\theta_i)\right]}{2\sigma^2}} \times e^{\frac{-\left[\int_0^T r(t)\sqrt{\frac{2}{T}}\sin(\omega_c t)dt\right]\sqrt{2E}\left[-\sin(\theta_i)+\cos(\theta_i)\right]}{2\sigma^2}}. \quad (3\text{-}49)$$

Once again combining the integrals and distributing the carrier component inside the integrand yields

$$\langle B\rangle = \frac{1}{8\pi\sigma^2} e^{-\frac{r_1^2+r_2^2+E}{2\sigma^2}} \times e^{\frac{\left\{2\sqrt{\frac{E}{T}}\int_0^T r(t)\left[-\cos(\omega_c t)\cos(\theta_i)-\cos(\omega_c t)\sin(\theta_i)+\sin(\omega_c t)\sin(\theta_i)-\sin(\omega_c t)\cos(\theta_i)\right]dt\right\}}{2\sigma^2}}. \quad (3\text{-}50)$$

Using the same trigonometric identities as with the first term and separating the integral in the same manner yields

$$\langle B\rangle = \frac{1}{8\pi\sigma^2} e^{-\frac{r_1^2+r_2^2+E}{2\sigma^2}} e^{\frac{\left[-2\sqrt{\frac{E}{T}}\int_0^T r(t)\cos(\omega_c t+\theta_i)dt\right]}{2\sigma^2}} + \frac{\left[-2\sqrt{\frac{E}{T}}\int_0^T r(t)\sin(\omega_c t+\theta_i)dt\right]}{2\sigma^2}.$$

(3-51)

The third term of (3-36) is

$$\langle C\rangle = \frac{1}{8\pi\sigma^2} e^{-\frac{\left(r_1-\sqrt{E}\cos\left(\theta_i-\frac{\pi}{4}\right)\right)^2}{2\sigma^2}} e^{-\frac{\left(r_2+\sqrt{E}\sin\left(\theta_i-\frac{\pi}{4}\right)\right)^2}{2\sigma^2}}. \tag{3-52}$$

Following the procedure established for the first two terms

$$\begin{aligned}\langle C\rangle = \frac{1}{8\pi\sigma^2} & e^{-\frac{r_1^2+r_2^2+E}{2\sigma^2}} \\ & \times e^{-\frac{-2r_1\sqrt{E}\left[\cos(\theta_i)\cos\left(-\frac{\pi}{4}\right)-\sin(\theta_i)\sin\left(-\frac{\pi}{4}\right)\right]}{2\sigma^2}} \\ & \times e^{-\frac{2r_2\sqrt{E}\left[\sin(\theta_i)\cos\left(-\frac{\pi}{4}\right)+\cos(\theta_i)\sin\left(-\frac{\pi}{4}\right)\right]}{2\sigma^2}}\end{aligned}. \tag{3-53}$$

Here it is noted that $\cos\left(-\frac{\pi}{4}\right)=\frac{\sqrt{2}}{2}$ and that $\sin\left(-\frac{\pi}{4}\right)=-\frac{\sqrt{2}}{2}$.

Therefore (3-53) becomes

$$\langle C\rangle = \frac{1}{8\pi\sigma^2} e^{-\frac{r_1^2+r_2^2+E}{2\sigma^2}} e^{-\frac{-r_1\sqrt{2E}\left[\cos(\theta_i)+\sin(\theta_i)\right]}{2\sigma^2}} e^{-\frac{r_2\sqrt{2E}\left[\sin(\theta_i)-\cos(\theta_i)\right]}{2\sigma^2}}.$$

(3-54)

Once again inserting the equations for r_1 and r_2, given in (3-9) resolves (3-54) into

$$\langle C\rangle = \frac{1}{8\pi\sigma^2} e^{-\frac{r_1^2+r_2^2+E}{2\sigma^2}} \times e^{-\frac{-\left[\int_0^T r(t)\sqrt{\frac{2}{T}}\cos(\omega_c t)dt\right]\sqrt{2E}\left[\cos(\theta_i)+\sin(\theta_i)\right]}{2\sigma^2}} \times e^{-\frac{\left[\int_0^T r(t)\sqrt{\frac{2}{T}}\sin(\omega_c t)dt\right]\sqrt{2E}\left[\sin(\theta_i)-\cos(\theta_i)\right]}{2\sigma^2}} \quad (3\text{-}55)$$

Once again combining the integrals and distributing the carrier component inside the integrand yields

$$\langle C\rangle = \frac{1}{8\pi\sigma^2} e^{-\frac{r_1^2+r_2^2+E}{2\sigma^2}} \times e^{-\frac{\left\{2\sqrt{\frac{E}{T}}\int_0^T r(t)\left[\cos(\omega_c t)\cos(\theta_i)+\cos(\omega_c t)\sin(\theta_i)-\sin(\omega_c t)\sin(\theta_i)+\sin(\omega_c t)\cos(\theta_i)\right]dt\right\}}{2\sigma^2}} \quad (3\text{-}56)$$

Using the same trigonometric identities as with the first two term and separating the integral in the same manner yields

$$\langle C\rangle = \frac{1}{8\pi\sigma^2} e^{-\frac{r_1^2+r_2^2+E}{2\sigma^2}} e^{\frac{\left[2\sqrt{\frac{E}{T}}\int_0^T r(t)\cos(\omega_c t+\theta_i)dt\right]}{2\sigma^2}} e^{\frac{\left[2\sqrt{\frac{E}{T}}\int_0^T r(t)\sin(\omega_c t+\theta_i)dt\right]}{2\sigma^2}}.$$

(3-57)

The final term in (3-36)

$$\langle D\rangle = \frac{1}{8\pi\sigma^2} e^{-\frac{\left(r_1-\sqrt{E}\cos\left(\theta_i-\frac{3\pi}{4}\right)\right)^2}{2\sigma^2}} e^{-\frac{\left(r_2+\sqrt{E}\sin\left(\theta_i-\frac{3\pi}{4}\right)\right)^2}{2\sigma^2}} \tag{3-58}$$

resolves into

$$\langle D\rangle = \frac{1}{8\pi\sigma^2} e^{-\frac{r_1^2+r_2^2+E}{2\sigma^2}} \times e^{\frac{-2r_1\sqrt{E}\left[\cos(\theta_i)\cos\left(-\frac{3\pi}{4}\right)-\sin(\theta_i)\sin\left(-\frac{3\pi}{4}\right)\right]}{2\sigma^2}} \times e^{\frac{2r_2\sqrt{E}\left[\sin(\theta_i)\cos\left(-\frac{3\pi}{4}\right)+\cos(\theta_i)\sin\left(-\frac{3\pi}{4}\right)\right]}{2\sigma^2}}. \tag{3-59}$$

Noting that $\cos\left(-\frac{3\pi}{4}\right) = \sin\left(-\frac{3\pi}{4}\right) = -\frac{\sqrt{2}}{2}$, (3-59) becomes

$$\langle D\rangle = \frac{1}{8\pi\sigma^2} e^{-\frac{r_1^2+r_2^2+E}{2\sigma^2}} e^{\frac{-r_1\sqrt{2E}\left[-\cos(\theta_i)+\sin(\theta_i)\right]}{2\sigma^2}} e^{\frac{r_2\sqrt{2E}\left[-\sin(\theta_i)-\cos(\theta_i)\right]}{2\sigma^2}}.$$

(3-60)

Inserting the equations for r_1 and r_2, given in (3-9) resolves (3-60) into

$$\langle D\rangle = \frac{1}{8\pi\sigma^2} e^{-\frac{r_1^2+r_2^2+E}{2\sigma^2}} \times e^{\frac{-\left[\int_0^T r(t)\sqrt{\frac{2}{T}}\cos(\omega_c t)dt\right]\sqrt{2E}\left[-\cos(\theta_i)+\sin(\theta_i)\right]}{2\sigma^2}} \times e^{\frac{-\left[\int_0^T r(t)\sqrt{\frac{2}{T}}\sin(\omega_c t)dt\right]\sqrt{2E}\left[-\sin(\theta_i)-\cos(\theta_i)\right]}{2\sigma^2}}. \quad (3\text{-}61)$$

Once again by combining the integrals and distributing the carrier components within the integrand (3-61) becomes

$$\langle D\rangle = \frac{1}{8\pi\sigma^2} e^{-\frac{r_1^2+r_2^2+E}{2\sigma^2}} \times e^{\frac{\left\{2\sqrt{\frac{E}{T}}\int_0^T r(t)\left[-\cos(\omega_c t)\cos(\theta_i)+\cos(\omega_c t)\sin(\theta_i)+\sin(\omega_c t)\sin(\theta_i)+\sin(\omega_c t)\cos(\theta_i)\right]dt\right\}}{2\sigma^2}}. \quad (3\text{-}62)$$

As with the previous terms, trigonometric identities are used to separate the integral in (3-62) into two new integrals. This new form is

$$\langle D\rangle = \frac{1}{8\pi\sigma^2} e^{-\frac{r_1^2+r_2^2+E}{2\sigma^2}} e^{\frac{\left[-2\sqrt{\frac{E}{T}}\int_0^T r(t)\cos(\omega_c t+\theta_i)dt\right]}{2\sigma^2}+\frac{\left[+2\sqrt{\frac{E}{T}}\int_0^T r(t)\sin(\omega_c t+\theta_i)dt\right]}{2\sigma^2}}.$$

(3-63)

Having developed the four terms that make up (3-36), the likelihood function, we now state (3-36) as

$$p(R|\theta_i) = \frac{1}{8\pi\sigma^2} e^{-\frac{r_1^2+r_2^2+E}{2\sigma^2}} \times \left\{ e^{\frac{\left[2\sqrt{\frac{E}{T}}\int_0^T r(t)\cos(\omega_c t+\theta_i)dt\right]}{2\sigma^2}+\frac{\left[-2\sqrt{\frac{E}{T}}\int_0^T r(t)\sin(\omega_c t+\theta_i)dt\right]}{2\sigma^2}} \right.$$
$$+ e^{\frac{\left[-2\sqrt{\frac{E}{T}}\int_0^T r(t)\cos(\omega_c t+\theta_i)dt\right]}{2\sigma^2}+\frac{\left[-2\sqrt{\frac{E}{T}}\int_0^T r(t)\sin(\omega_c t+\theta_i)dt\right]}{2\sigma^2}}$$
$$+ e^{\frac{\left[2\sqrt{\frac{E}{T}}\int_0^T r(t)\cos(\omega_c t+\theta_i)dt\right]}{2\sigma^2}+\frac{\left[2\sqrt{\frac{E}{T}}\int_0^T r(t)\sin(\omega_c t+\theta_i)dt\right]}{2\sigma^2}}$$
$$\left. + e^{\frac{\left[-2\sqrt{\frac{E}{T}}\int_0^T r(t)\cos(\omega_c t+\theta_i)dt\right]}{2\sigma^2}+\frac{\left[2\sqrt{\frac{E}{T}}\int_0^T r(t)\sin(\omega_c t+\theta_i)dt\right]}{2\sigma^2}} \right\}. \quad (3\text{-}64)$$

The sum in (3-64) is of the exponential form

$$f(x,y) = e^{x}e^{-y} + e^{-x}e^{-y} + e^{x}e^{y} + e^{-x}e^{y} \tag{3-65}$$

where

$$x = \frac{1}{\sigma^2}\sqrt{\frac{E}{T}}\int_0^T r(t)\cos(\omega_c t + \theta_i)dt$$

and (3-66)

$$y = \frac{1}{\sigma^2}\sqrt{\frac{E}{T}}\int_0^T r(t)\sin(\omega_c t + \theta_i)dt\,.$$

This sum can be expressed as

$$f(x,y) = \left(e^{x} + e^{-x}\right)\left(e^{y} + e^{-y}\right) = 4\cosh(x)\cosh(y). \tag{3-67}$$

Applying this new form of the sum in (3-64) yields

$$\begin{aligned} p\left(R|\theta_i\right) = \frac{1}{2\pi\sigma^2}e^{-\frac{r_1^2 + r_2^2 + E}{2\sigma^2}} \\ \times\cosh\left[\frac{1}{\sigma^2}\sqrt{\frac{E}{T}}\int_0^T r(t)\cos(\omega_c t + \theta_i)dt\right]. \\ \times\cosh\left[\frac{1}{\sigma^2}\sqrt{\frac{E}{T}}\int_0^T r(t)\sin(\omega_c t + \theta_i)dt\right] \end{aligned} \tag{3-68}$$

Next the log likelihood function is obtained and can be stated

$$\ln\left[p\left(R|\theta_i\right)\right] = \ln\left[\frac{1}{2\pi\sigma^2}e^{-\frac{r_1^2+r_2^2+E}{2\sigma^2}}\right] + \ln\left\{\cosh\left[\frac{1}{\sigma^2}\sqrt{\frac{E}{T}}\int_0^T r(t)\cos\left(\omega_c t+\theta_i\right)dt\right]\right\}. + \ln\left\{\cosh\left[\frac{1}{\sigma^2}\sqrt{\frac{E}{T}}\int_0^T r(t)\sin\left(\omega_c t+\theta_i\right)dt\right]\right\} \tag{3-69}$$

As with BPSK, the next step is to take the derivative of (3-69) with respect to θ_i. Once again it is noted that the first term in the log likelihood function will equate to zero in the derivative. The derivative of the QPSK log likelihood function is stated

$$\frac{\partial \ln\left(p\left(R|\theta_i\right)\right)}{\partial\theta_i} = \tanh\left[\frac{\sqrt{\frac{2E}{T}}}{\sigma^2}\int_0^T r(t)\sin\left(\omega_c t+\theta_i\right)dt\right]\times\int_0^T r(t)\cos\left(\omega_c t+\theta_i\right)dt - \tanh\left[\frac{\sqrt{\frac{2E}{T}}}{\sigma^2}\int_0^T r(t)\cos\left(\omega_c t+\theta_i\right)dt\right]\times\int_0^T r(t)\sin\left(\omega_c t+\theta_i\right)dt \tag{3-70}$$

To complete the MAP estimator derivation for QPSK set the right side of (3-70) equal to zero and insert the necessary condition for the optimum estimator mentioned in (3-6) regarding the control of the receiver reference, i.e., $\theta_i = \theta_o$, just as was done for BPSK. The resulting MAP estimator is [32]

$$\tanh\left[\frac{\sqrt{\frac{2E}{T}}}{\sigma^2}\int_0^T r(t)\sin(\omega_c t+\theta_o)dt\right]\times\int_0^T r(t)\cos(\omega_c t+\theta_o)dt$$
$$-\tanh\left[\frac{\sqrt{\frac{2E}{T}}}{\sigma^2}\int_0^T r(t)\cos(\omega_c t+\theta_o)dt\right]\times\int_0^T r(t)\sin(\omega_c t+\theta_o)dt=0 \qquad (3\text{-}71)$$

When a loop filter and VCO are used in conjuction with the above control signal the result is the carrier tracking loop of Figure 3-3. To obtain the high-SNR approximation for QPSK the use of hardlimiters is once again employed in replacing the hyperbolic tangent functions. The resulting loop is shown in Figure 3-4.

3.4 MAP Derivation For 8PSK

The rigorous derivation for the MAP estimator for 8PSK is presented in Appendix B. The optimum MAP estimator for 8PSK is stated here as

$$\frac{s_1 x\tanh(s_1 y)-c_1 y\tanh(c_1 x)}{1+\dfrac{\cosh(c_2 x)\cosh(s_2 y)}{\cosh(c_1 x)\cosh(s_1 y)}}+\frac{s_2 x\tanh(s_2 y)-c_2 y\tanh(c_2 x)}{1+\dfrac{\cosh(c_1 x)\cosh(s_1 y)}{\cosh(c_2 x)\cosh(s_2 y)}}=0 \qquad (3\text{-}72)$$

where

$$c_1 = \cos\frac{\pi}{8}, \quad s_1 = \sin\frac{\pi}{8}, \quad c_2 = \cos\frac{3\pi}{8}, \quad s_2 = \sin\frac{3\pi}{8}, \tag{3-73}$$

$$x = \frac{1}{\sigma^2}\sqrt{\frac{E}{T}}\int_0^T r(t)\cos(\omega_c t + \theta_o)dt, \tag{3-74}$$

and

$$y = \frac{1}{\sigma^2}\sqrt{\frac{E}{T}}\int_0^T r(t)\sin(\omega_c t + \theta_o)dt. \tag{3-75}$$

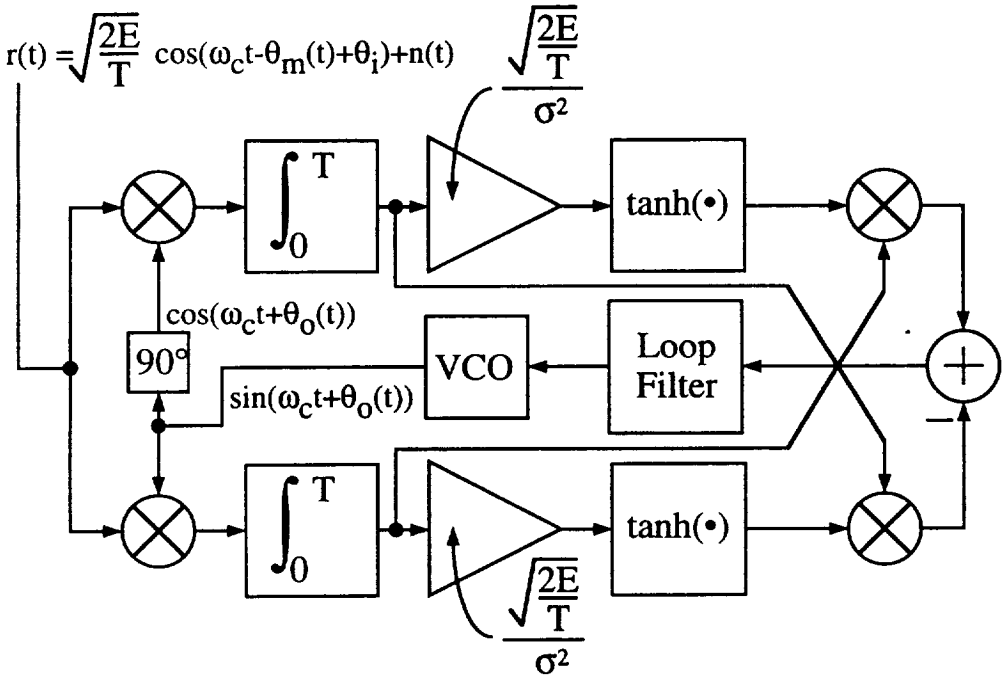

Figure 3-3. The optimum MAP estimator loop for QPSK carrier tracking.

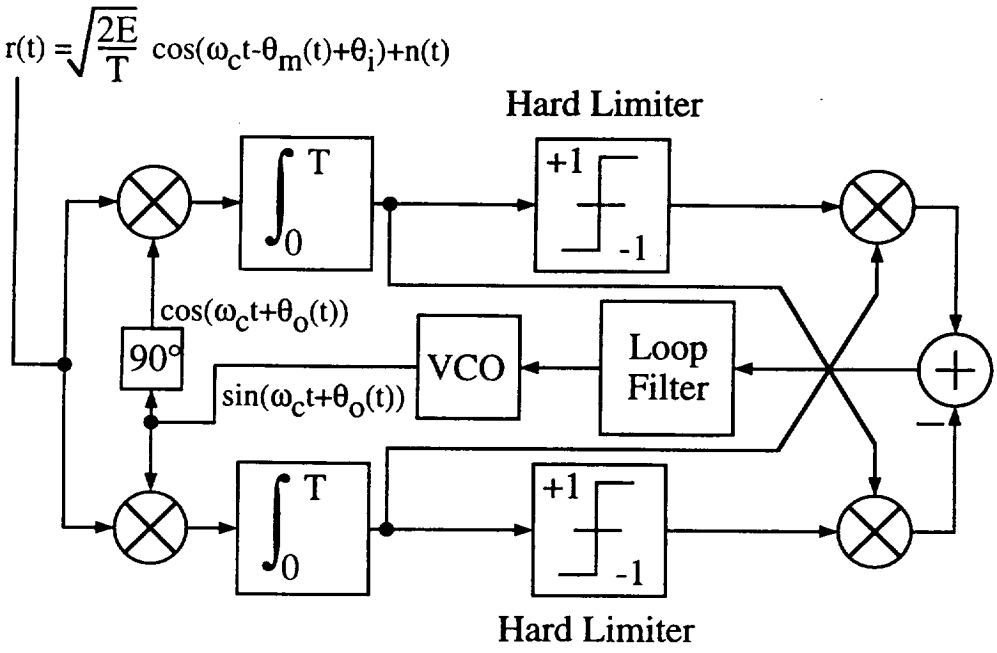

Figure 3-4. The high SNR approximation loop for QPSK carrier tracking.

The operation of this estimator uses the scaled outputs from quadrature arm correlators, as is done for BPSK and QPSK, i.e., (3-74) and (3-75). Once again the obvious obstacles to implementation that (3-72) possesses motivates a simplified solution, namely the high-SNR approximation. To obtain this approximation hardlimiters are used in place of the hyperbolic tangents for large arguments. Further, instead of hyperbolic cosines, the following approximation is used [31]

$$\cosh(\lambda) \approx \frac{1}{2} e^{|\lambda|}, \quad |\lambda| >> 0. \tag{3-76}$$

This follows since the SNR is incorporated in the calculation of x and y as a scale factor. The first step in proceeding with the evaluation of the high-SNR approximation is to examine the impact of using the hyperbolic cosine approximation of (3-76). Inserting (3-76) into (3-72) reduces the estimator equation to

$$\frac{s_1 x \tanh(s_1 y) - c_1 y \tanh(c_1 x)}{1 + \dfrac{e^{|c_2 x|} e^{|s_2 y|}}{e^{|c_1 x|} e^{|s_1 y|}}} + \frac{s_2 x \tanh(s_2 y) - c_2 y \tanh(c_2 x)}{1 + \dfrac{e^{|c_1 x|} e^{|s_1 y|}}{e^{|c_2 x|} e^{|s_2 y|}}} = 0. \quad (3\text{-}77)$$

To consider the impact of using hardlimiters in place of the hyperbolic tangents it is noted that the inputs to the hardlimiters are the scaled correlator output coordinates (scaled by the SNR) describing where the received 8PSK symbol was detected in the 2 dimensional constellation space. If the received symbol is detected in the first quadrant both hardlimiters will output a +1 and the estimator equation will then reduce to

$$\frac{s_1 x - c_1 y}{1 + \dfrac{e^{|c_2 x|} e^{|s_2 y|}}{e^{|c_1 x|} e^{|s_1 y|}}} + \frac{s_2 x - c_2 y}{1 + \dfrac{e^{|c_1 x|} e^{|s_1 y|}}{e^{|c_2 x|} e^{|s_2 y|}}} = 0,\ x > 0,\ y > 0. \quad (3\text{-}78)$$

Correspondingly, if the received symbol is in the second quadrant the hardlimiter corresponding to the inphase correlator will output a -1 while the quadrature correlator will output a +1. The resulting estimator is

$$\frac{s_1x+c_1y}{1+\frac{e^{|c_2x|}e^{|s_2y|}}{e^{|c_1x|}e^{|s_1y|}}}+\frac{s_2x+c_2y}{1+\frac{e^{|c_1x|}e^{|s_1y|}}{e^{|c_2x|}e^{|s_2y|}}}=0,\ x<0,\ y>0. \tag{3-79}$$

It follows that for the third quadrant where $x<0$ and $y<0$ the estimator will become

$$\frac{-s_1x+c_1y}{1+\frac{e^{|c_2x|}e^{|s_2y|}}{e^{|c_1x|}e^{|s_1y|}}}+\frac{-s_2x+c_2y}{1+\frac{e^{|c_1x|}e^{|s_1y|}}{e^{|c_2x|}e^{|s_2y|}}}=0,\ x<0,\ y<0 \tag{3-80}$$

and in the fourth quadrant where $x>0$ and $y<0$ the estimator is

$$\frac{-s_1x-c_1y}{1+\frac{e^{|c_2x|}e^{|s_2y|}}{e^{|c_1x|}e^{|s_1y|}}}+\frac{-s_2x-c_2y}{1+\frac{e^{|c_1x|}e^{|s_1y|}}{e^{|c_2x|}e^{|s_2y|}}}=0,\ x>0,\ y>0. \tag{3-81}$$

The four estimator equations of (3-78) to (3-81) correspond to using the high-SNR approximation for each of the four two-dimensional quadrants. To proceed further each 8PSK sector must be addressed individually in terms of the received 8PSK symbols. To accomplish this consider first the received 8PSK sector wherein $x>0$, $y>0$, and $x>y$. Since this sector is in the first quadrant, the reduced estimator equation of (3-78) is used. It can be reduced further to

$$\frac{s_1x-c_1y}{1+e^{(c_2x+s_2y-c_1x-s_1y)}}+\frac{s_2x-c_2y}{1+e^{(c_1x+s_1y-c_2x-s_2y)}}=0,\ x>0,\ y>0. \tag{3-82}$$

To reduce the denominators of (3-82) consider again that this is a high-SNR approximation and that the outputs from the correlators will be approximately the actual transmitted data scaled by a large factor that incorporates the SNR. For reception in the first sector this is stated

$$x \approx \mu \cos\left(\frac{\pi}{8}\right) = \mu c_1 \tag{3-83}$$

and

$$y \approx \mu \sin\left(\frac{\pi}{8}\right) = \mu s_1. \tag{3-84}$$

Inserting (3-83) and (3-84) into the denominators of (3-82) results in

$$\frac{s_1 x - c_1 y}{1 + e^{\mu(c_2 c_1 + s_2 s_1 - c_1 c_1 - s_1 s_1)}} + \frac{s_2 x - c_2 y}{1 + e^{\mu(c_1 c_1 + s_1 s_1 - c_2 c_1 - s_2 s_1)}} = 0,\ x > 0,\ y > 0,\ x > y. \tag{3-85}$$

This reduces to

$$\frac{s_1 x - c_1 y}{1 + e^{\mu(2c_2 c_1 - 1)}} + \frac{s_2 x - c_2 y}{1 + e^{\mu(1 - 2c_2 c_1)}} = 0,\ x > 0,\ y > 0,\ x > y. \tag{3-86}$$

Since $0 < 2c_2c_1 < 1$ and μ is a large number the denominator of the first term of the sum in (3-86) will reduce to unity and the denominator of the second term will become very large. The result will be that the estimator equation of (3-86) will reduce to

$$s_1 x - c_1 y = 0, x > 0, y > 0, x > y. \tag{3-87}$$

Cross multiplying off the large scale factor in x and y and noting that in the first sector $s_1 = \hat{Q}$ and $c_1 = \hat{I}$ are the data estimates of what were transmitted, the estimator equation can be considered as the error signal in the loop that is to be driven to zero and expressed as

$$e(t) = I\hat{Q} - Q\hat{I}, I > 0, Q > 0, I > Q \tag{3-88}$$

where I and Q are the outputs from actual correlators in the constructed carrier tracking loop and in the case of no noise at all represent vector coordinates to a point on the unit circle. Note that (3-88) has been obtained only for the case that the received symbol is detected in the first sector, i.e., $x > 0$, $y > 0$, and $x > y$. In fact, this error signal is the same for any received 8PSK symbol designated by quadrature correlator outputs I and Q and utilizing received sector locations to identify the data estimates. To show this is true the case for the second sector, namely when $x > 0$, $y > 0$, and $y > x$, is now considered.

Starting from (3-82) and using the the approximations

$$x \approx \mu \cos\left(\frac{3\pi}{8}\right) = \mu c_2 \tag{3-89}$$

and

$$y \approx \mu \sin\left(\frac{3\pi}{8}\right) = \mu s_2 \tag{3-90}$$

in the denominator forms the estimator

$$\frac{s_1 x - c_1 y}{1 + e^{\mu(c_2 c_2 + s_2 s_2 - c_1 c_2 - s_1 s_2)}} + \frac{s_2 x - c_2 y}{1 + e^{\mu(c_1 c_2 + s_1 s_2 - c_2 c_2 - s_2 s_2)}} = 0,\ x > 0,\ y > 0,\ y > x.$$

(3-90)

This reduces to

$$\frac{s_1 x - c_1 y}{1 + e^{\mu(1 - 2c_1 c_2)}} + \frac{s_2 x - c_2 y}{1 + e^{\mu(2c_1 c_2 - 1)}} = 0,\ x > 0,\ y > 0,\ y > x. \tag{3-91}$$

Once again since $0 < 2c_2 c_1 < 1$ and μ is a large number the estimator is reducable, in this case, to

$$s_2 x - c_2 y = 0,\ x > 0,\ y > 0,\ y > x. \tag{3-92}$$

A loop error signal is obtained from this estimator, as before, by cross multiplying off the large scale factor in x and y and noting that in the second sector $s_2 = \hat{Q}$ and $c_2 = \hat{I}$ are the data estimates of what was transmitted. This error signal is then

$$e(t) = I\hat{Q} - Q\hat{I}, I > 0, Q > 0, Q > I. \tag{3-99}$$

where I and Q are defined as for the first sector. Indeed it is possible to show that in all of the sectors the same error signal will result when the high-SNR approximations used above are assumed. This will now be demonstrated in an abridged fashion for the remaining six sectors rotating in a counter clockwise fashion as was started for the first two sectors.

In the third sector where the estimator of (3-79) is used and, $x < 0$, $y > 0$, and $|x| < y$, it is assumed that

$$x \approx \mu \cos\left(\frac{5\pi}{8}\right) = -\mu \cos\left(\frac{3\pi}{8}\right) = -\mu c_2 \tag{3-100}$$

and

$$y \approx \mu \sin\left(\frac{5\pi}{8}\right) = \mu \sin\left(\frac{3\pi}{8}\right) = \mu s_2. \tag{3-101}$$

The estimator of (3-79) then reduces to

$$\frac{s_1 x + c_1 y}{1 + e^{\mu(1-2c_1c_2)}} + \frac{s_2 x + c_2 y}{1 + e^{\mu(2c_1c_2-1)}} = 0,\ x < 0,\ y > 0, |x| < y \tag{3-102}$$

and finally to

$$s_2 x + c_2 y = 0,\ x < 0,\ y > 0, |x| < y. \tag{3-103}$$

In this sector $s_2 = \hat{Q}$ and $-c_2 = \hat{I}$ and so the error signal becomes

$$e(t) = I\hat{Q} - Q\hat{I},\ I < 0, Q > 0, |I| < Q. \tag{3-104}$$

In the fourth sector where the estimator of (3-79) is again used and, $x < 0$, $y > 0$, and $|x| > y$, it is assumed that

$$x \approx \mu \cos\left(\frac{7\pi}{8}\right) = -\mu \cos\left(\frac{\pi}{8}\right) = -\mu c_1 \tag{3-105}$$

and

$$y \approx \mu \sin\left(\frac{7\pi}{8}\right) = \mu \sin\left(\frac{\pi}{8}\right) = \mu s_1. \tag{3-106}$$

The estimator of (3-79) then reduces to

$$\frac{s_1 x + c_1 y}{1 + e^{\mu(2c_2c_1-1)}} + \frac{s_2 x + c_2 y}{1 + e^{\mu(1-2c_2c_1)}} = 0,\ x < 0,\ y > 0, |x| > 0 \tag{3-107}$$

and finally to

$$s_1 x + c_1 y = 0,\ x < 0,\ y > 0,\ |x| > y. \tag{3-108}$$

In this sector $s_1 = \hat{Q}$ and $-c_1 = \hat{I}$ and so the error signal becomes

$$e(t) = I\hat{Q} - Q\hat{I},\ I < 0,\ Q > 0,\ |I| > Q. \tag{3-109}$$

In the fifth sector where the estimator of (3-80) is used and, $x < 0$, $y < 0$, and $x < y$, it is assumed that

$$x \approx \mu \cos\left(\frac{9\pi}{8}\right) = -\mu \cos\left(\frac{\pi}{8}\right) = -\mu c_1 \tag{3-110}$$

and

$$y \approx \mu \sin\left(\frac{9\pi}{8}\right) = \mu \sin\left(\frac{-\pi}{8}\right) = -\mu s_1. \tag{3-111}$$

The estimator of (3-80) then reduces to

$$\frac{-s_1 x + c_1 y}{1 + e^{\mu(2c_2 c_1 - 1)}} + \frac{-s_2 x + c_2 y}{1 + e^{\mu(1 - 2c_2 c_1)}} = 0,\ x < 0,\ y < 0,\ x < y \tag{3-112}$$

and finally to

$$-s_1 x + c_1 y = 0,\ x < 0,\ y < 0,\ x < y. \tag{3-113}$$

In this sector $-s_1 = \hat{Q}$ and $-c_1 = \hat{I}$ and so the error signal becomes

$$e(t) = I\hat{Q} - Q\hat{I}, I < 0, Q < 0, I < Q. \tag{3-114}$$

In the sixth sector where the estimator of (3-80) is again used and, $x < 0$, $y < 0$, and $x > y$, it is assumed that

$$x \approx \mu \cos\left(\frac{11\pi}{8}\right) = -\mu \cos\left(\frac{3\pi}{8}\right) = -\mu c_2 \tag{3-115}$$

and

$$y \approx \mu \sin\left(\frac{11\pi}{8}\right) = \mu \sin\left(\frac{-3\pi}{8}\right) = -\mu s_2. \tag{3-116}$$

The estimator of (3-80) then reduces to

$$\frac{-s_1 x + c_1 y}{1 + e^{\mu(1-2c_2c_1)}} + \frac{-s_2 x + c_2 y}{1 + e^{\mu(2c_2c_1-1)}} = 0, x < 0, y < 0, x > y \tag{3-117}$$

and finally to

$$-s_2 x + c_2 y = 0, x < 0, y < 0, x > y. \tag{3-118}$$

In this sector $-s_2 = \hat{Q}$ and $-c_2 = \hat{I}$ and so the error signal becomes

$$e(t) = I\hat{Q} - Q\hat{I}, I < 0, Q < 0, I > Q. \tag{3-119}$$

Q-2.

In the seventh sector where the estimator of (3-81) is used and, $x>0$, $y<0$, and $x<|y|$, it is assumed that

$$x \approx \mu\cos\left(\frac{13\pi}{8}\right)=\mu\cos\left(\frac{3\pi}{8}\right)=\mu c_2 \tag{3-120}$$

and

$$y \approx \mu\sin\left(\frac{13\pi}{8}\right)=\mu\sin\left(\frac{-3\pi}{8}\right)=-\mu s_2. \tag{3-121}$$

The estimator of (3-81) then reduces to

$$\frac{-s_1x-c_1y}{1+e^{\mu(1-2c_1c_2)}}+\frac{-s_2x-c_2y}{1+e^{\mu(2c_1c_2-1)}}=0,\ x>0,\ y<0,\ x<|y| \tag{3-122}$$

and finally to

$$-s_2x-c_2y=0,\ x>0,\ y<0,\ x<|y|. \tag{3-123}$$

In this sector $-s_2=\hat{Q}$ and $c_2=\hat{I}$ and so the error signal becomes

$$e(t)=I\hat{Q}-Q\hat{I},\ I>0,\ Q<0,\ I<|Q|. \tag{3-124}$$

In the eighth sector where the estimator of (3-81) is again used and, $x>0$, $y<0$, and $x>|y|$, it is assumed that

$$x \approx \mu \cos\left(\frac{15\pi}{8}\right) = \mu \cos\left(\frac{\pi}{8}\right) = \mu c_1 \tag{3-125}$$

and

$$y \approx \mu \sin\left(\frac{15\pi}{8}\right) = \mu \sin\left(\frac{-\pi}{8}\right) = -\mu s_1 . \tag{3-126}$$

The estimator of (3-81) then reduces to

$$\frac{-s_1 x - c_1 y}{1 + e^{\mu(2c_1c_2 - 1)}} + \frac{-s_2 x - c_2 y}{1 + e^{\mu(1 - 2c_1c_2)}} = 0,\ x > 0,\ y < 0,\ x > |y| \tag{3-127}$$

and finally to

$$-s_1 x - c_1 y = 0,\ x > 0,\ y < 0,\ x > |y| . \tag{3-128}$$

In this sector $-s_1 = \hat{Q}$ and $c_1 = \hat{I}$ and so the error signal becomes

$$e(t) = I\hat{Q} - Q\hat{I},\ I > 0,\ Q < 0,\ I > |Q| . \tag{3-129}$$

Since all of the error signals for all eight sectors are identical the limitations on I and Q are dropped and the error signal becomes simply

$$e(t) = I\hat{Q} - Q\hat{I} . \tag{3-130}$$

This is the error signal that is required for implementing an 8PSK carrier tracking loop that utilizes the high-SNR approximation to MAP estimation of carrier phase.

3.5 MAP Derivation For 16PSK

The rigorous derivation for the MAP estimator for 16PSK is presented in Appendix C. It is stated here as

$$\frac{-c_1 y\tanh(c_1 x)+s_1 x\tanh(s_1 y)}{\left[1+\frac{\cosh(c_2 x)\cosh(s_2 y)}{\cosh(c_1 x)\cosh(s_1 y)}+\frac{\cosh(s_1 x)\cosh(c_1 y)}{\cosh(c_1 x)\cosh(s_1 y)}+\frac{\cosh(s_2 x)\cosh(c_2 y)}{\cosh(c_1 x)\cosh(s_1 y)}\right]}$$
$$+\frac{-c_2 y\tanh(c_2 x)+s_2 x\tanh(s_2 y)}{\left[\frac{\cosh(c_1 x)\cosh(s_1 y)}{\cosh(c_2 x)\cosh(s_2 y)}+1+\frac{\cosh(s_1 x)\cosh(c_1 y)}{\cosh(c_2 x)\cosh(s_2 y)}+\frac{\cosh(s_2 x)\cosh(c_2 y)}{\cosh(c_2 x)\cosh(s_2 y)}\right]}$$
$$+\frac{-s_1 y\tanh(s_1 x)+c_1 x\tanh(c_1 y)}{\left[\frac{\cosh(c_1 x)\cosh(s_1 y)}{\cosh(s_1 x)\cosh(c_1 y)}+\frac{\cosh(c_2 x)\cosh(s_2 y)}{\cosh(s_1 x)\cosh(c_1 y)}+1+\frac{\cosh(s_2 x)\cosh(c_2 y)}{\cosh(s_1 x)\cosh(c_1 y)}\right]}$$
$$+\frac{-s_2 y\tanh(s_2 x)+c_2 x\tanh(c_2 y)}{\left[\frac{\cosh(c_1 x)\cosh(s_1 y)}{\cosh(s_2 x)\cosh(c_2 y)}+\frac{\cosh(c_2 x)\cosh(s_2 y)}{\cosh(s_2 x)\cosh(c_2 y)}+\frac{\cosh(s_1 x)\cosh(c_1 y)}{\cosh(s_2 x)\cosh(c_2 y)}+1\right]}=0 \qquad (3\text{-}131)$$

This estimator equation has the same form as that of (3-72) for 8PSK. In fact the procedure for analyzing the high-SNR case is exactly the same. Each of the 16 sectors is considered individually and the error signals turn out to be identical. The result is that the

error signal that is required for implementing a 16PSK carrier tracking loop that utilizes the high-SNR approximation to MAP estimation of carrier phase is the same as that of 8PSK. In fact the error signal is exactly the same for any M-ary PSK signal set. In the case of QPSK a review of the high-SNR carrier tracking loop of Figure 3-4 shows the error signal of (3-130) is exactly what is present at the input to the loop filter. For BPSK consider that the high-SNR loop of Figure 3-2 has the error signal

$$e(t) = -Q\hat{I}. \tag{3-132}$$

Since the estimate of what was transmitted on the quadrature channel will always equal zero, i.e., $\hat{Q} = 0$, for BPSK the error signal of (3-132) may be generalized to that of (3-130). So it is therefore possible to conclude that for any M-ary PSK scheme the error signal in a carrier tracking loop utilizing the high-SNR approximation to MAP estimation has the error signal of equation (3-130). This general MPSK high-SNR loop is shown in Figure 3-5. Note that the decision device that generates the data estimates is based on determining which sector the received 2 dimensional symbol was detected in, just as the mathematical discussion of the high-SNR approximation used.

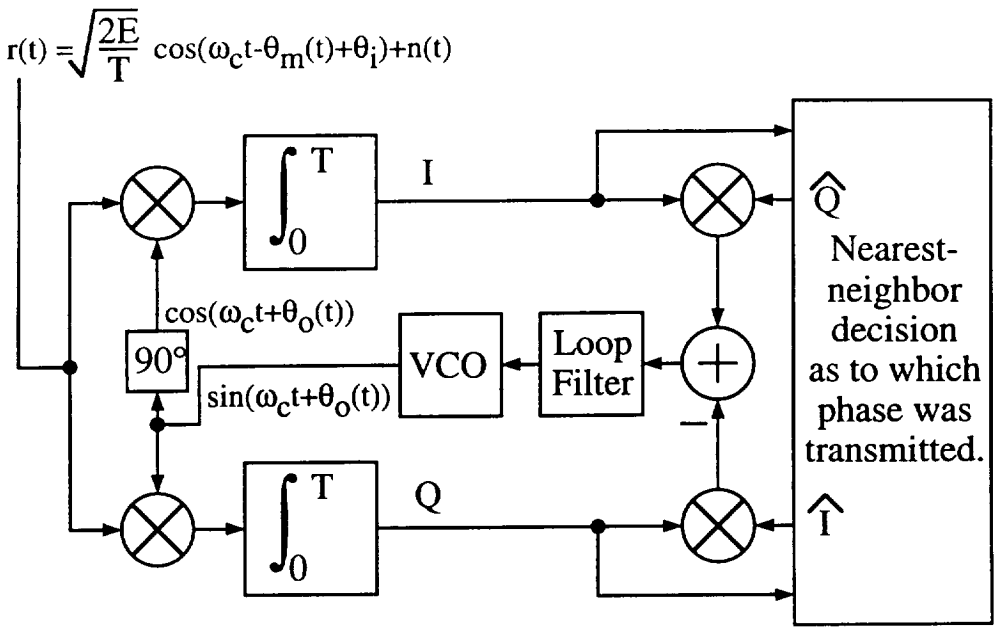

Figure 3-5. The high SNR approximation loop for MPSK carrier tracking.

Chapter 4

DERIVING THE VARIANCE OF THE PHASE ERROR FOR THE HIGH-SNR MSPK CARRIER TRACKING LOOP

"Mathematics is an experimental science and definitions do not come first, but later on."

Oliver Heaviside
physicist & electrician, 1850 - 1925

4.1 Introduction

In the first chapter the need for quantifying the variance of the phase error in the MPSK carrier tracking loop that uses the high-SNR approximation to MAP estimation was discussed. In Chapter 2 the mathematical derivation involved in calculating this variance, or jitter, for a basic PLL was presented. Further, before discussing the variance of the more complicated MPSK carrier tracking loop it was necessary to discuss the loop itself. This was the purpose of Chapter 3. Now having established a mathematical foundation of understanding for both the basic idea of jitter and the tracking loop of interest, it is possible to proceed with the subject of this chapter: obtaining an equation that describes the actual variance of the phase error in a high-SNR MPSK carrier tracking loop. The procedure is straight forward and follows that of Chapter 2. Starting with the integro-differential equation of the loop, a linear baseband model is constructed from which an

appropriate transfer function is obtained. This transfer function is then used to relate the noise in the loop to the jitter or carrier phase variance.

4.2 The Variance Of The Phase Error

To begin, consider the high-SNR MPSK carrier tracking loop presented in Figure 3-5 and shown here again in Figure 4-1 with one modification in particular. A gain term on the quadrature arm integrators has been introduced. This term allows for the normalization of the average energy associated with the I and Q components. It reflects the physical assumption that the receiver is utilizing perfect automatic gain control of the received signal. When the error signal in the loop is discussed shortly, the purpose of the gain term will become more clear.

The output of the loop filter in Figure 4-1, stated in terms of its error signal input, $e(t)$, is

$$x(t) = \int_0^t f(t-\lambda)e(\lambda)d\lambda . \tag{4-1}$$

Using (2-8), which describes the VCO output phase in terms of its input, we can form the expression

$$\frac{d\theta_o(t)}{dt} = K_o \int_0^t f(t-\lambda)e(\lambda)d\lambda . \tag{4-2}$$

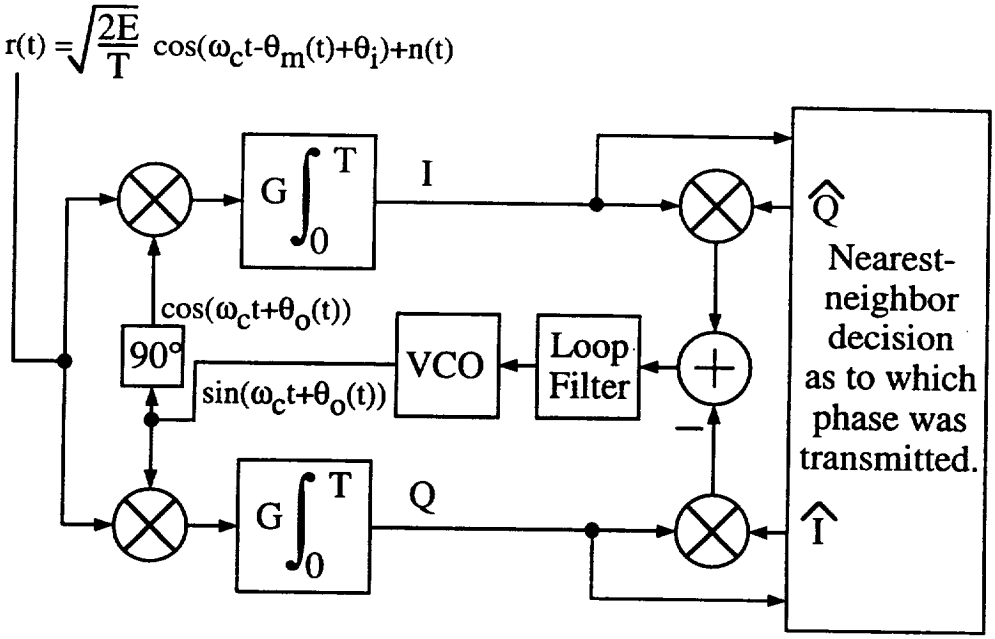

Figure 4-1. The high SNR approximation loop for MPSK carrier tracking, modified for error signal analysis.

Again describing the difference between the received signal carrier phase and the VCO phase as the phase error changes (4-2) into

$$\frac{d\theta_e(t)}{dt} = \frac{d\theta_i(t)}{dt} - K_o \int_0^t f(t-\lambda)e(\lambda)d\lambda . \qquad (4\text{-}3)$$

The integro-differential equation cannot be described further without exploring the error signal. So far the error signal has been presented as a function of the quadrature arm correlator outputs

and the data estimates. It must now be described in terms of the phase error.

First, note that the error signal, derived in Chapter 3, carries with it a time delay of one symbol period associated with the quadrature arm integrators. Strictly speaking this should be incorporated in the error signal [29, pg. 65] and doing so for this loop results in

$$e(t) = e^{-pT}\left[I\hat{Q} - Q\hat{I}\right] \tag{4-4}$$

where p is the Heaviside operator and T is the symbol period over which the integration takes place. Insofar as the loop bandwidth of this type of loop is much less than $\frac{1}{T}$, the delay component e^{-pT} is essentially unity over the frequencies of interest and can be disregarded [29, pg. 65]. It is of interest to note here that while this delay does introduce questions as to the performance of the loop in the nonlinear sense, (acquisition and mean-time between slip characteristics) it does not impact the steady state performance analysis of phase jitter when it is neglected.

To relate the quadrature arm outputs, I and Q, to the phase error consider first the output from each of the quadrature mixers

$$\begin{aligned} X(t) = &\frac{1}{2}\sqrt{\frac{2E}{T}}\cos(\theta_e - \theta_m) + n(t)\cos(\omega_c t + \theta_o) \\ &+ \frac{1}{2}\sqrt{\frac{2E}{T}}\cos(2\omega_c t + \theta_e - \theta_m) \end{aligned} \tag{4-5}$$

and

$$Y(t) = \frac{1}{2}\sqrt{\frac{2E}{T}}\left[-\sin(\theta_e - \theta_m)\right] + n(t)\sin(\omega_c t + \theta_o) + \frac{1}{2}\sqrt{\frac{2E}{T}}\sin(2\omega_c t + \theta_e - \theta_m) \tag{4-6}$$

where $\theta_e = \theta_i - \theta_o$ is the phase error and all the phase time designators have been dropped for convenience. At the output of each of the integrators the double frequency terms in $X(t)$ and $Y(t)$ will be effectively filtered out. If the gain term is

$$G = \sqrt{\frac{2}{TE}} \tag{4-7}$$

then the output from the integrators will be

$$I = \cos(\theta_e - \theta_m) + N_I \tag{4-8}$$

and

$$Q = -\sin(\theta_e - \theta_m) + N_Q \tag{4-9}$$

where the noise terms N_I and N_Q are zero mean Gaussian random variables. Because the narrowband noise $n(t)$ is necessarily wideband compared with the IF data bandwidth, $\frac{1}{T}$, it can be

considered as a white noise process in so far as the integrators are concerned. Doing so allows the following calculation of the noise variance at the output of either integrator

$$\sigma_{N_I}^2 = E\left[\int_0^T\int_0^T G^2 w(t)\cos(\omega_c t+\theta_o)w(u)\cos(\omega_c u+\theta_o)dtdu\right]. \qquad (4\text{-}10)$$

Bringing the expected value function inside the double integral to the noise processes results in

$$\sigma_{N_I}^2 = G^2\int_0^T\int_0^T E[w(t)w(u)]\cos(\omega_c t+\theta_o)\cos(\omega_c u+\theta_o)dtdu. \qquad (4\text{-}11)$$

Noting that for a white Gaussian process

$$E[w(t)w(u)] = R_{ww}(t,u) = \frac{N_o}{2}\delta(t-u) \qquad (4\text{-}12)$$

and then applying the sifting property to the outside integral converts (4-11) into

$$\sigma_{N_I}^2 = G^2\frac{N_o}{2}\int_0^T \cos(\omega_c t+\theta_o)\cos(\omega_c t+\theta_o)dt. \qquad (4\text{-}13)$$

Multiplying out the squared cosine term yields

$$\sigma_{N_I}^2 = G^2\frac{N_o}{2}\int_0^T \frac{1}{2}+\frac{1}{2}\cos(2\omega_c t+2\theta_o)dt \qquad (4\text{-}14)$$

and finally

$$\sigma_{N_I}^2 = G^2 \frac{N_o}{2}\frac{T}{2} = \frac{2}{ET}\frac{N_o}{2}\frac{T}{2} = \frac{N_o}{2E}. \qquad (4\text{-}15)$$

Thus the variance of the noise components out of the quadrature integrators is the reciprocal of twice the symbol energy-to-noise ratio in the channel. This calculation can be demonstrated spectrally by considering the response of the integrator to the narrowband noise in the frequency domain. The integrator's impulse response (truely, each is an integrate and dump function with a zero-order-hold designed to latch the dumped value over the next T second symbol interval) is a flat pulse of duration T seconds. It follows that the magnitude of its transfer function is a sinc function, centered at zero, and with first nulls at the symbol rate, $\frac{1}{T}$ Hz. The modulated narrowband noise, which, once again, is wide compared to the symbol rate, is flat over the significant frequencies of interest in the integrator transfer function. It is therefore possible to consider the noise output of the integrator as being due to its transfer function's effect on a white noise spectrum. This allows for accepting the above calculations resulting in the noise variance of (4-15).

Having identified the components of (4-8) and (4-9) they can now be considered when substituted into the error signal. The error signal is now stated as

$$e(t) = \cos(\theta_e - \theta_m)\hat{Q} + N_I\hat{Q} - \left(-\sin(\theta_e - \theta_m)\right)\hat{I} - N_Q\hat{I}. \qquad (4\text{-}16)$$

Writing the error signal as a control signal with an additive disturbance identifies this loop's equivalent noise term. Doing so yields

$$e(t) = \cos(\theta_e - \theta_m)\hat{Q} + \sin(\theta_e - \theta_m)\hat{I} + N_e(t) \qquad (4\text{-}17)$$

where

$$N_e(t) = N_I\hat{Q} - N_Q\hat{I} \qquad (4\text{-}18)$$

is the equivalent noise in this loop. That is, the IF noise appears inside the loop, in the error signal as noise weighted by the data decisions. The error signal of (4-17) can be reduced further by considering that for this loop, wherein the loop bandwidth is much smaller than the symbol rate, the phase error changes very slowly compared to a single symbol interval. Since it is essentially constant over several of these intervals it is appropriate to consider the average of the control function in analyzing the error signal. Therefore stating the error signal as its expected value (the expected value of the equivalent noise is zero) plus a disturbance results in

$$e(t) = E[e(t)] + N_e(t). \tag{4-19}$$

The expected value of the error signal is the effective phase detector characteristic of the loop [39, pg 116] and is denoted

$$PD(\theta_e) = E[e(t)] \tag{4-20}$$

Therefore the error signal itself can be stated as

$$e(t) = PD(\theta_e) + N_e(t). \tag{4-21}$$

Recall from Chapter 2 that the output from a multiplier type phase detector in the absense of noise is essentially the sine of the phase error. The error signal of (4-17) can be shown to reduce to exactly the sine of the phase error in the noiseless case if it is assumed that good data decisions are being made. Consider the noiseless error signal

$$e'(t) = \cos(\theta_e - \theta_m)\hat{Q} + \sin(\theta_e - \theta_m)\hat{I}. \tag{4-22}$$

The data estimates can be rewritten as $\hat{I} = \cos(\hat{\theta}_m)$ and $\hat{Q} = \sin(\hat{\theta}_m)$ where $\hat{\theta}_m$ is the estimate of the transmitted angle. With trigonometric manipulation (4-22) becomes

$$e'(t) = \cos(\theta_e)\left[\cos(\theta_m)\sin\left(\hat{\theta}_m\right) - \sin(\theta_m)\cos\left(\hat{\theta}_m\right)\right] + \sin(\theta_e)\left[\sin(\theta_m)\sin\left(\hat{\theta}_m\right) + \cos(\theta_m)\cos\left(\hat{\theta}_m\right)\right]. \quad (4\text{-}23)$$

Using the I and Q designators, (4-23) becomes

$$e'(t) = \cos(\theta_e)\left[I_m\hat{Q}_m - Q_m\hat{I}_m\right] + \sin(\theta_e)\left[Q_m\hat{Q}_m + I_m\hat{I}_m\right]. \quad (4\text{-}24)$$

Incorporating the assumption that good data decisions are being made reduces (4-24) to the expected phase detector characteristic, namely

$$e'(t) = \sin(\theta_e). \quad (4\text{-}25)$$

Returning now to the phase detector characteristic of (4-20), and again noting that the expected value of the additive equivalent noise is zero, it is possible to describe the phase detector characteristic as

$$PD(\theta_e) = E[e(t)] = E\left[\cos(\theta_e - \theta_m)\hat{Q} + \sin(\theta_e - \theta_m)\hat{I}\right]. \quad (4\text{-}26)$$

Again using trigonometric identities it is possible to manipulate (4-26) and reduce it to

$$PD(\theta_e) = E\left[\sin\left(\theta_e + \hat{\theta}_m - \theta_m\right)\right]. \quad (4\text{-}27)$$

This last form of the phase detector characteristic is exactly the form that will be needed in the next Chapter when the gain of the phase detector is calculated.

This analysis of the error signal was begun to obtain a form that included the phase error directly. The form of interest at this point is (4-21). Inserting it into (4-7) yields

$$\frac{d\theta_e(t)}{dt} = \frac{d\theta_i(t)}{dt} - K_o \int_0^t f(t-\lambda)\left\{PD\left[\theta_e(t)\right] + N_e(t)\right\} d\lambda \qquad (4\text{-}28)$$

where the time designator for the phase variables has been reinstated for uniformity. As in Chapter 2 this form of the integro-differential equation that describes the loops operation leads directly to a baseband model, in this case shown in Figure 4-2. To proceed with linearizing the baseband model of the loop it is first necessary to examine the phase detector characteristic more closely. It is convenient to express the phase detector characteristic in the form [39, pg. 269]

$$PD(\theta_e) = \alpha_{SNR} \sin(\theta_e) \qquad (4\text{-}29)$$

where α_{SNR} is the effective gain of the phase detector. It incorporates the impact of making poor data decisions in such a manner as to become smaller as more incorrect decisions are made, i.e., as the SNR goes down. Note that when the SNR is high and good data decisions are being made this gain term equates to

unity resulting in a phase detector characteristic that is once again the sine of the phase error. This gain term manifests itself as the slope of the phase detector characteristic measured at zero phase error. Mathematically it is expressed as [39, pg. 269]

$$\alpha_{SNR} = \left.\frac{\partial PD(\theta_e)}{\partial \theta_e}\right|_{\theta_e=0}. \tag{4-30}$$

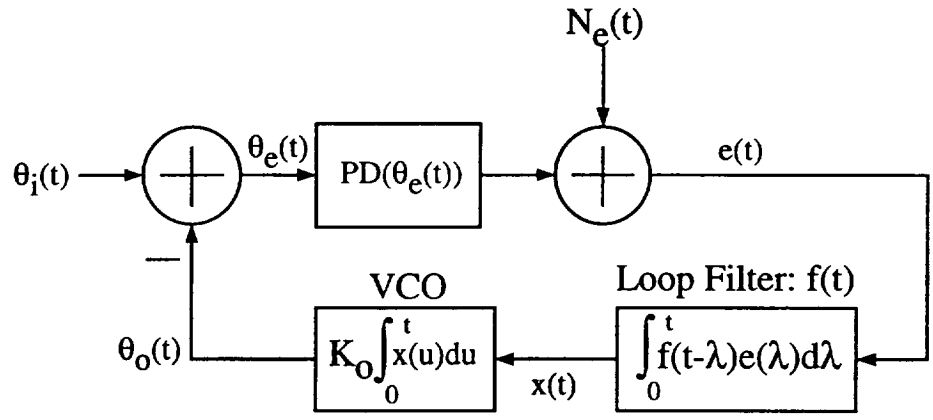

Figure 4-2. The nonlinear baseband model.

To linearize the loop it is assumed that the phase error is small and therefore (4-29) reduces to

$$PD(\theta_e) \approx \alpha_{SNR}\theta_e. \tag{4-31}$$

The linear baseband model of Figure 4-3 results. Note also that the employed loop filter is the same as before so that the loop will

be a second order control loop. From the linear model it is possible to develop the second order transfer function, just as was done in Chapter 2. For this loop the combined DC gain is $\alpha_{SNR}K_o$ and the transfer function that describes the relationship between the received signal phase and the VCO output phase is

$$H(s)=\frac{\alpha_{SNR}K_o(s+a)}{s^2+\alpha_{SNR}K_o(s+a)}. \tag{4-32}$$

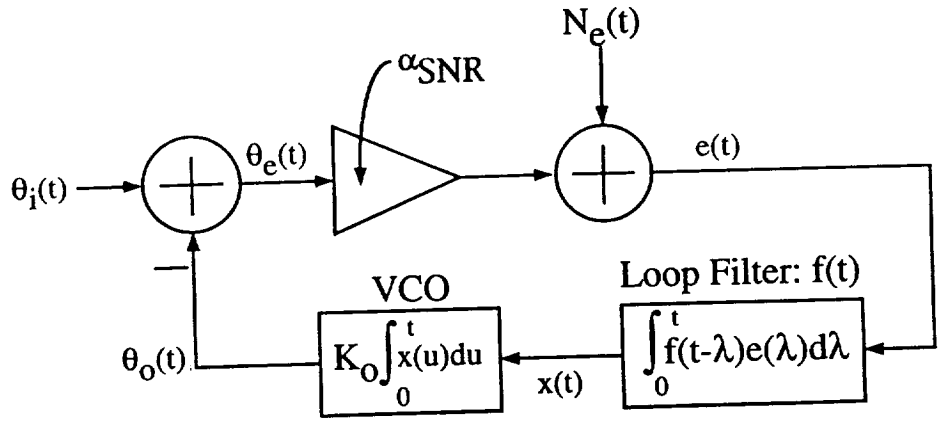

Figure 4-3. The linear baseband model.

The transfer function of equation (4-32) can be equated to the classical second order control loop transfer function and its design parameters through

$$H(s)=\frac{2\zeta'\omega_n's+\omega_n'^2}{s^2+2\zeta'\omega_n's+\omega_n'^2} \tag{4-33}$$

where

$$\omega_n' = \sqrt{\alpha_{SNR}}\sqrt{K_o a} = \sqrt{\alpha_{SNR}}\omega_n \tag{4-34}$$

and

$$\zeta' = \sqrt{\alpha_{SNR}}\frac{1}{2}\sqrt{\frac{K_o}{a}} = \sqrt{\alpha_{SNR}}\zeta. \tag{4-35}$$

To proceed with identifying the carrier phase jitter the transfer function that describes the relationship between the equivalent noise input and the VCO phase output is needed. From Figure 4-3 this relationship is

$$H_n(s) = \frac{K_o(s+a)}{s^2 + \alpha_{SNR}K_o(s+a)} = \frac{1}{\alpha_{SNR}}H(s). \tag{4-36}$$

To obtain the variance of the phase error the output power spectral density of the linear loop model is analysed in response to the equivalent noise. Doing so is once again preceeded by the notion that the equivalent noise is stationary. In fact, it is cyclostationary [35] with autocorrelation function

$$R_{N_e}(\tau) = \sigma_{N_e}^2\left[1 - \frac{|\tau|}{T}\right], \quad |\tau| < T. \tag{4-37}$$

To see that this is true consider that the equivalent noise itself can be represented as a pulse amplitude modulated waveform with period T. Further, its amplitude has zero mean and variance $\sigma_{N_e}^2$.

Recalling the approach used in Chapter 2 to describe the variance of the phase error, the output power spectral density for the phase error of the loop will be

$$S_{\theta_e}(f) = |H_n(f)|^2 S_{N_e}(f). \tag{4-38}$$

And it follows that the variance can be described as

$$\sigma_{\theta_e}^2 = \int_{-\infty}^{\infty} |H_n(f)|^2 S_{N_e}(f) df. \tag{4-39}$$

The power spectral density of the equivalent noise is obtained from its autocorrelation function (4-37) and is stated

$$S_{N_e}(f) = \sigma_{N_e}^2 T \operatorname{sinc}^2(fT). \tag{4-40}$$

In the case of the PLL of Chapter two the fact that the IF bandwidth was large compared to the loop bandwidth allowed for a simplification in the calculation of the variance, namely that the power spectral density of the equivalent noise is flat over the range of lowpass frequencies for which the square of the magnitude of the loop transfer function is essentially non zero. The same holds true here. The first null of the sinc-squared

function of (4-40) is at a much higher frequency than the highest significant frequency in the square of the magnitude of the loop transfer function. Therefore the variance of (4-39) can be reduced to

$$\sigma_{\theta_e}^2 = \sigma_{N_e}^2 T \int_{-f'}^{f'} |H_n(f)|^2 df \tag{4-41}$$

where f' is an arbitrary frequency slightly greater than the most significant frequency to be considered in the square of the magnitude of the loop transfer function. Using the transfer function relationship of (4-36), the variance becomes

$$\sigma_{\theta_e}^2 = \frac{\sigma_{N_e}^2 T}{\alpha_{SNR}^2} \int_{-f'}^{f'} |H(f)|^2 df . \tag{4-42}$$

Using the same reasoning as in Chapter 2 the integral in (4-42) is equated to the loop bandwidth, B_L, and the variance is therefore

$$\sigma_{\theta_e}^2 = \frac{\sigma_{N_e}^2 T B_L}{\alpha_{SNR}^2} . \tag{4-43}$$

And finally, since the symbol period, T, is the reciprocal of the symbol rate, SR, the variance of the phase error in an MPSK loop utilizing the high-SNR approximation to MAP estimation may be stated

$$\sigma^2_{\theta_e} = \frac{B_L}{SR}\frac{\sigma^2_{N_e}}{\alpha^2_{SNR}}. \qquad (4\text{-}44)$$

Making any comparisons between this equation and that of the variance for the basic PLL, namely, (2-52) will be withheld until after the components of (4-44) are further explored in the next Chapter.

With the exception of the symbol rate, all of the components that make up the variance equation of (4-44) vary with SNR. What is more, how they vary with SNR is dependent on which M-ary PSK scheme is being used. The first of these, the loop bandwidth, is directly dependent on the phase detector gain. As a result the loop bandwidth can become substantially narrower as the SNR decreases. The phase detector gain itself decreases with decreasing SNR. The amount it decreases at a particular SNR is greater as M goes up. The third component, the equivalent noise variance, increases with decreasing SNR. However, at a particular SNR , as M is increased, the variance of the equivalent noise can decrease (only at small SNR's). It never increases with M.

All of these changing components lead to a dynamic and complex relationship between SNR and the phase error variance. To proceed further with understanding the variance requires an indepth analysis of the above mentioned three components. This is the subject of the next chapter.

Chapter 5

THE COMPONENTS OF PHASE ERROR VARIANCE

"To talk sense is to talk quantities."

Alfred North Whitehead
mathematician & philosopher, 1861 - 1947

5.1 Introduction

In Chapter 4 the variance of the phase error in the MPSK carrier tracking loop that uses the high-SNR approximation to MAP estimation was derived. It is restated here for convenience as

$$\sigma_{\theta_e}^2 = \frac{B_L}{SR}\frac{\sigma_{N_e}^2}{\alpha_{SNR}^2}. \qquad (5\text{-}1)$$

The three components of this variance that change with SNR were also introduced. They are the loop bandwidth, B_L, the phase detector gain, α_{SNR}, and the variance of the equivalent noise, $\sigma_{N_e}^2$. It is the subject of this Chapter to discuss these three components in detail. As was mentioned at the end of Chapter 4, each of them has a dynamic response to changing SNR and to selected modulation type. Their combined effect on the variance of the phase error will be presented as results in Chapter 6.

5.2 The Equivalent Noise Variance

The first component of the phase error variance that will be discussed is the variance of the equivalent noise. This component consists of two characteristics as will be demonstrated. The first of these reflects the presence of channel noise in the IF receiver front-end. The second relates the impact of making bad data decisions on the noise in the loop itself. This second characteristic is particularly intriguing since it manifests itself in such a way as to slightly lessen the overall variance of the equivalent noise and therefore the variance of the phase error. To begin the analysis of the equivalent noise variance recall the equation for the equivalent noise given in (4-18) restated here as

$$N_e(t) = N_I\hat{Q} - N_Q\hat{I}. \tag{5-2}$$

In calculating the variance of the equivalent noise it is first noted that the mean of the equivalent noise is

$$E[N_e(t)] = E\left[N_I\hat{Q}\right] - E\left[N_Q\hat{I}\right] = 0, \tag{5-3}$$

since the statistics of $N_I\hat{Q}$ and of $N_Q\hat{I}$ are identical. The equivalent noise variance is therefore

$$\sigma_{N_e}^2 = E\left[N_e(t)^2\right] = E\left[N_Q^2\hat{I}^2 + N_I^2\hat{Q}^2 - 2N_IN_Q\hat{I}\hat{Q}\right]. \tag{5-4}$$

To proceed further, each modulation type is considered in turn. For BPSK, (5-4) can be reduced because the squared estimate on the I channel is always unity and the Q channel estimate is always zero. For BPSK the variance becomes

$$\sigma_{N_e}^2 = E\left[N_Q^2\right] = \sigma_{N_Q}^2 \tag{5-5}$$

which is simply the variance of the noise out of the quadrature arm integrator. Since noise out of each of the integrators has equivalent statistics, equation (5-5) can be equated to equation (4-15) and the result is

$$\sigma_{N_e}^2 = \frac{N_o}{2E}. \tag{5-6}$$

For BPSK the variance of the equivalent noise in the loop is exactly the variance of the noise out of the quadrature arm integrators. For QPSK the variance of (5-4) is expanded as

$$\sigma_{N_e}^2 = E\left[N_e(t)^2\right] = E\left[N_Q^2\hat{I}^2\right] + E\left[N_I^2\hat{Q}^2\right] - 2E\left[N_I N_Q \hat{I}\hat{Q}\right]. \tag{5-7}$$

In the case of QPSK the data estimates on either channel are independent of their orthogonal noise components. In other words, $\hat{I}$ is independent of N_Q and $\hat{Q}$ is independent of N_I. This permits the manipulation of (5-7) wherein

$$\sigma_{N_e}^2 = E\left[N_e(t)^2\right] = E\left[\hat{I}^2\right]E\left[N_Q^2\right] + E\left[\hat{Q}^2\right]E\left[N_I^2\right] - 2E\left[N_I\hat{I}\right]E\left[N_Q\hat{Q}\right].$$

(5-8)

Since the statitics of $N_I\hat{I}$ and $N_Q\hat{Q}$ are equivalent (5-8) becomes

$$\sigma_{N_e}^2 = E\left[N_e(t)^2\right] = E\left[\hat{I}^2\right]E\left[N_Q^2\right] + E\left[\hat{Q}^2\right]E\left[N_I^2\right] - 2\left\{E\left[N_I\hat{I}\right]\right\}^2. \qquad (5\text{-}9)$$

Note once again that the quadrature arm integrator output noise statistics are equivalent and the result is

$$\sigma_{N_e}^2 = E\left[N_e(t)^2\right] = E\left[N_I^2\right]\left\{E\left[\hat{I}^2\right] + E\left[\hat{Q}^2\right]\right\} - 2\left\{E\left[N_I\hat{I}\right]\right\}^2. \qquad (5\text{-}10)$$

This becomes

$$\sigma_{N_e}^2 = E\left[N_e(t)^2\right] = E\left[N_I^2\right]E\left[\hat{I}^2 + \hat{Q}^2\right] - 2\left\{E\left[N_I\hat{I}\right]\right\}^2. \qquad (5\text{-}11)$$

Using (4-15) and noting that the vector magnitude of the data estimates is always unity, the QPSK equivalent noise variance is

$$\sigma_{N_e}^2 = E\left[N_e(t)^2\right] = \frac{N_o}{2E} - 2\left\{E\left[N_I\hat{I}\right]\right\}^2. \qquad (5\text{-}12)$$

What remains is to calculate $E[N_I\hat{I}]$. This is accomplished by equating the expected value of a function of two random variables through

$$E[N_I\hat{I}] = \int_{-\infty}^{\infty}\int_{-\infty}^{\infty} N_I\hat{I}f(N_I)f(I_m)dN_I dI_m \tag{5-13}$$

where the two probability denisty functions are that of the noise,

$$f(N_I) = \frac{1}{\sqrt{2\pi}\sigma_{N_I}} e^{-\frac{N_I^2}{2\sigma_{N_I}^2}} \tag{5-14}$$

and that of the transmitted I channel data,

$$f(I_m) = \frac{1}{2}\delta\left(I_m - \frac{\sqrt{2}}{2}\right) + \frac{1}{2}\delta\left(I_m + \frac{\sqrt{2}}{2}\right). \tag{5-15}$$

To examine the integration of equation (5-13) it is noted that $\hat{I}$ can take on two values depending on which of the two possible I_m values were transmitted and depending on whether or not N_I caused an error to occur. The result is that there are four integrals corresponding to four combinations of possible transmitted data and possible estimated data that must be examined. This is expressed by integrating out the transmitted data from (5-13) resulting in

$$E\left[N_I\hat{I}\right]=\frac{1}{2}\frac{\sqrt{2}}{2}\left\{\int_{-\frac{\sqrt{2}}{2}}^{\infty}N_I f(N_I)dN_I\right\}+\frac{1}{2}\frac{-\sqrt{2}}{2}\left\{\int_{-\infty}^{-\frac{\sqrt{2}}{2}}N_I f(N_I)dN_I\right\}$$
$$+\frac{1}{2}\frac{-\sqrt{2}}{2}\left\{\int_{-\infty}^{\frac{\sqrt{2}}{2}}N_I f(N_I)dN_I\right\}+\frac{1}{2}\frac{\sqrt{2}}{2}\left\{\int_{\frac{\sqrt{2}}{2}}^{\infty}N_I f(N_I)dN_I\right\}. \quad (5\text{-}16)$$

The first and second integrals correspond to a transmission of $I_m=\frac{\sqrt{2}}{2}$ while the third and fourth integrals correspond to sending $I_m=-\frac{\sqrt{2}}{2}$. In the second integral the estimate has been made incorrectly because the noise is sufficiently large in the negative direction. In the fourth integral the estimate has been made incorrectly because the noise is sufficiently large in the positive direction. By inserting (5-14) into (5-16) and performing the integration the expected value of the product of the I channel noise and estimate becomes

$$E\left[N_I\hat{I}\right]=\frac{\sigma_{N_I}}{\sqrt{\pi}}e^{-\frac{1}{4\sigma_{N_I}^2}}. \quad (5\text{-}17)$$

Returning this result to (5-12), which describes the QPSK equivalent noise variance yields

$$\sigma_{N_e}^2 = \frac{N_o}{2E} - 2\left\{\frac{\sigma_{N_I}}{\sqrt{\pi}} e^{-\frac{1}{4\sigma_{N_I}^2}}\right\}^2 = \frac{N_o}{2E}\left(1 - \frac{2}{\pi} e^{-\frac{E}{N_o}}\right). \qquad (5\text{-}18)$$

Figure 5-1 shows the equivalent noise variance for BPSK and QPSK using (5-6) and (5-18). Note that at low SNR's the variance for QPSK is less than that of BPSK. This effect is known as "self noise" and in decision directed loops such as this it refers to the effect that making bad decisions (which occur more frequently at low SNR's) has on the noise inside the loop. This will be demonstrated graphically when 8 and 16PSK self noise are discussed. For QPSK though, the self noise is prevalent only at SNR's below about 5 dB. In fact, at higher SNR's the BPSK solution for equivalent noise variance can be used as an approximation.

To calculate the equivalent noise variance for 8 and 16PSK it is first determined that no reduction in the complexity of (5-4) is possible, as was done with BPSK and QPSK. The data estimates and corresponding orthogonal noise components are interdependent. For example, a noise sample on the I channel could move the received data point vector across a sector boundry and cause an error on the estimate of what was transmitted on the Q channel. This is shown for the 8PSK constellation in Figure 5-2. The hash marks on the vertical axis denote the possible transmitted quadrature channel data.

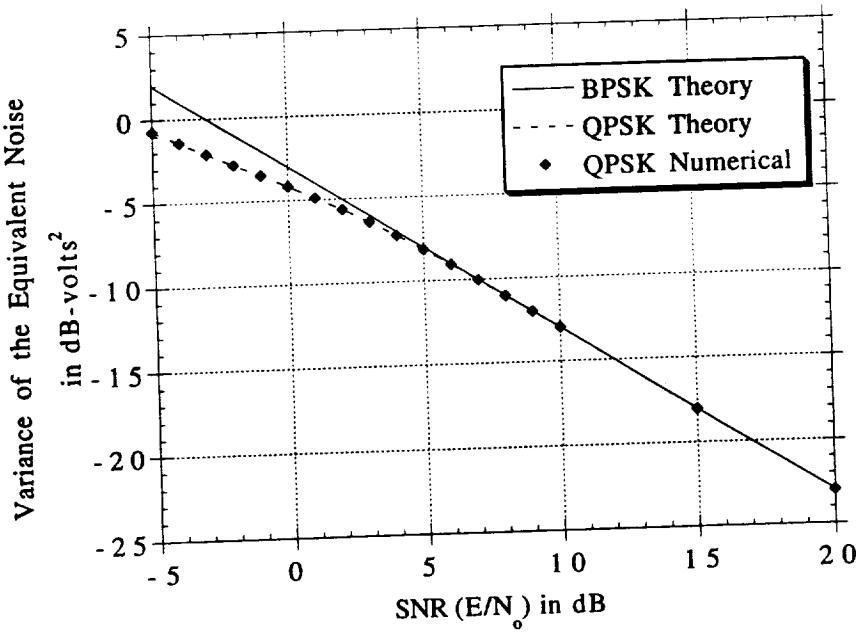

Figure 5-1. BPSK and QPSK equivalent noise variance.

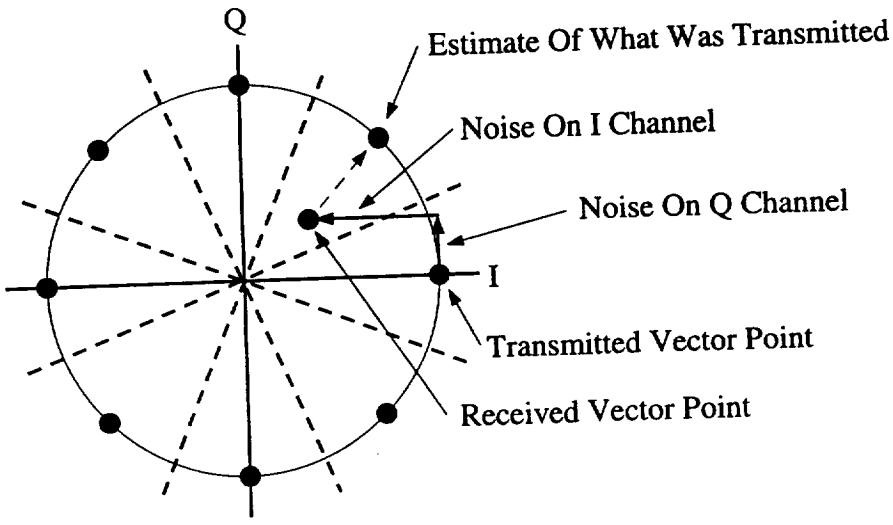

Figure 5-2. The 8PSK constellation with noisy received component.

Therefore to calculate the variance of the equivalent noise for 8PSK and 16PSK a direct approach was utilized. The variance was numerically calculated by evaluating the triple integral

$$\sigma_{N_e}^2 = E\left[N_e(t)^2\right] = \int_{-\infty}^{\infty}\int_{-\infty}^{\infty}\int_{-\infty}^{\infty} g\left(N_I, N_Q, \theta_m\right) f\left(N_I, N_Q, \theta_m\right) dN_I dN_Q d\theta_m \tag{5-19}$$

where

$$g\left(N_I, N_Q, \theta_m\right) = \left[N_I\hat{Q} - N_Q\hat{I}\right]^2 \tag{5-20}$$

is the square of the equivalent noise and $f\left(N_I, N_Q, \theta_m\right)$ is the joint density over the noise components and the discrete transmitted modulation angle. Each of the noise components and the transmitted modulation angle are all independent of each other and thus the joint density may be expressed as

$$f\left(N_I, N_Q, \theta_m\right) = f(N_I) f\left(N_Q\right) f(\theta_m). \tag{5-21}$$

If 8PSK modulation is assumed and it is assumed that there are equally likely transmitted symbols, then integrating out the modulation from (5-19) results in

$$\sigma_{N_e}^2 = \sum_{i=0}^{7} \frac{1}{8} \int_{-\infty}^{\infty} \int_{-\infty}^{\infty} g\left(N_I, N_Q, \theta_m = i\frac{\pi}{4}\right) f(N_I) f\left(N_Q\right) dN_I dN_Q \,. \qquad (5\text{-}22)$$

Since the double integral of (5-22) will yield the same result for each of the eight modulation points it is possible to reduce (5-22) to

$$\sigma_{N_e}^2 = \int_{-\infty}^{\infty} \int_{-\infty}^{\infty} g\left(N_I, N_Q, \theta_m = 0\right) f(N_I) f\left(N_Q\right) dN_I dN_Q \qquad (5\text{-}23)$$

where the zero-angle transmitted modulation point has been assumed for mathematical convenience. To proceed a change of variables is performed to move the joint Gaussian probability "mountain" out to the modulation point corresponding to $\theta_m = 0$. This allows the double integral to be performed over sectors that correspond to the decision regions for the data estimator.[1] The new double integral is

$$\sigma_{N_e}^2 = \sum_{j=0}^{7} \left\{ \int_{\beta_{1j}}^{\beta_{2j}} \int_{\alpha_{1j}}^{\alpha_{2j}} g(x-1, y, \theta_m = 0) f(y) f(x-1) dy dx \right\} \qquad (5\text{-}24)$$

where the point $(x = 1, y = 0)$ corresponds to the modulation point on the positive I axis. The limits of integration correspond to the values of x and y that are in each of the eight decision regions. To

[1]The thick dashed lines and the axes in Figure 5.2 form the boundries of the decision regions.

proceed with performing this numerical integration it is helpful to view the components of the integrand as 3-dimensional surfaces. Figure 5-3 shows the function $g(x-1, y, \theta_m = 0)$, the square of the equivalent noise, for 8PSK. For comparison, the same function is plotted for BPSK, QPSK, and 16PSK in Figures 5-4, 5-5, and 5-6, respectively. For an SNR of 10 dB the joint Gaussian probability mountain, centered at the $(x = 1, y = 0)$ modulation point, is shown in Figure 5-7. The entire integrand of the double integral is shown for 8PSK at an SNR of 10 dB in Figure 5-8. The variance of the equivalent noise is the volume under the integrand surface. What the 3-dimensional view contributes here is assistance in setting the limits of integration for the numerical calculation of (5-24). Before the use of surface analysis was employed it was not fully understood just how localized the surface prominences are. To test the technique the numerical approach was first applied to QPSK. This numerical data are shown in Figure 5-1. The source code for all M-ary PSK equivalent noise variance calculations and the data are given in Appendix D. Having verified the functionality of the approach for QPSK the technique was applied to 8PSK and 16PSK. The resulting data are shown in Figure 5-9 along with the closed form solutions to BPSK and QPSK. Note that at low SNR's the variance drops with increasing M. To understand how this is possible consider again the surface plots of the square of the equivalent noise. For BPSK this surface is a parabolic one, increasing with both positive and negative Y. For the other three,

the surface is discontinuous and, in particular, has channelized minima in regions that correspond to the increasing parabolic surface of BPSK. As M increases the number of minima increases and thus the volume under the square of the equivalent noise surface decreases. Correspondingly, the variance itself decreases. At high-SNR's, when the Gaussian probababilty mountain is very narrow, only the continuous, parabolic region (for all M) that contains the modulation point$(x=1, y=0)$ will provide significant contributions to the variance calculation. Thus, all of the MPSK equivalent noise variance calculations converge at high-SNR's.

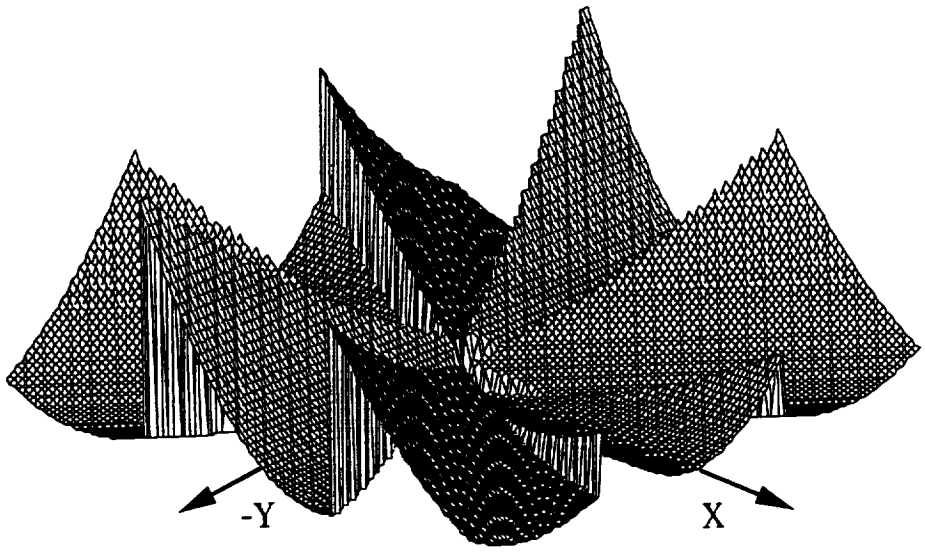

Figure 5-3. The 8PSK squared equivalent noise.

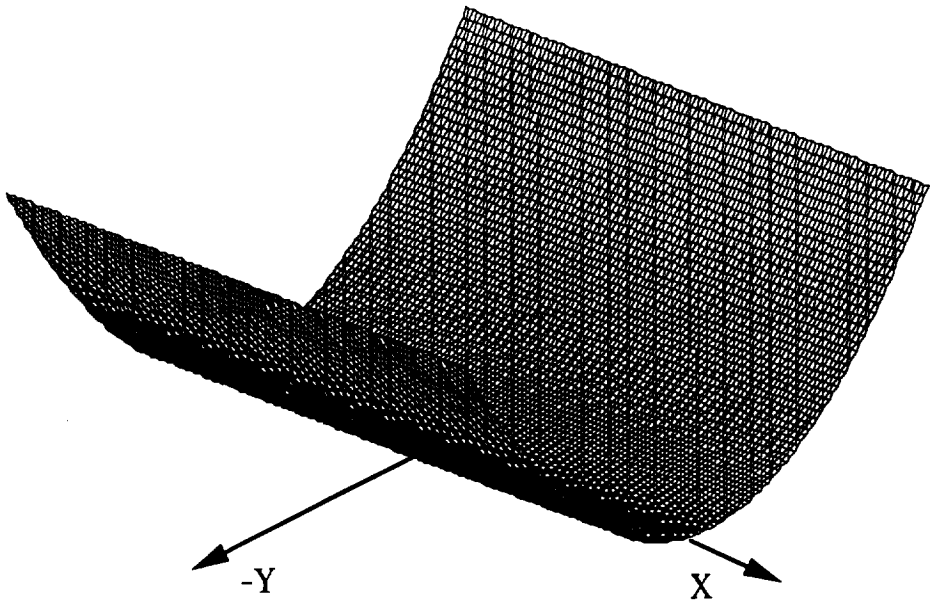

Figure 5-4. The BPSK squared equivalent noise.

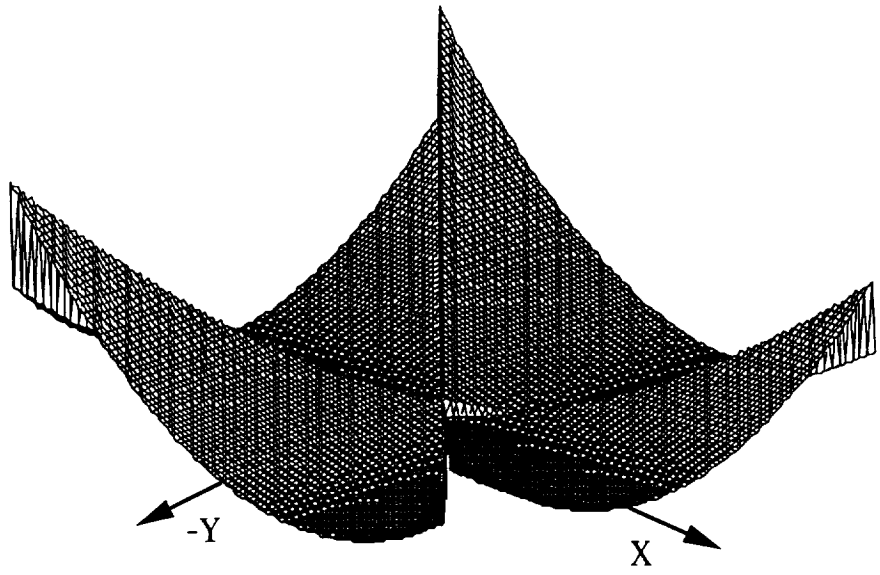

Figure 5-5. The QPSK squared equivalent noise.

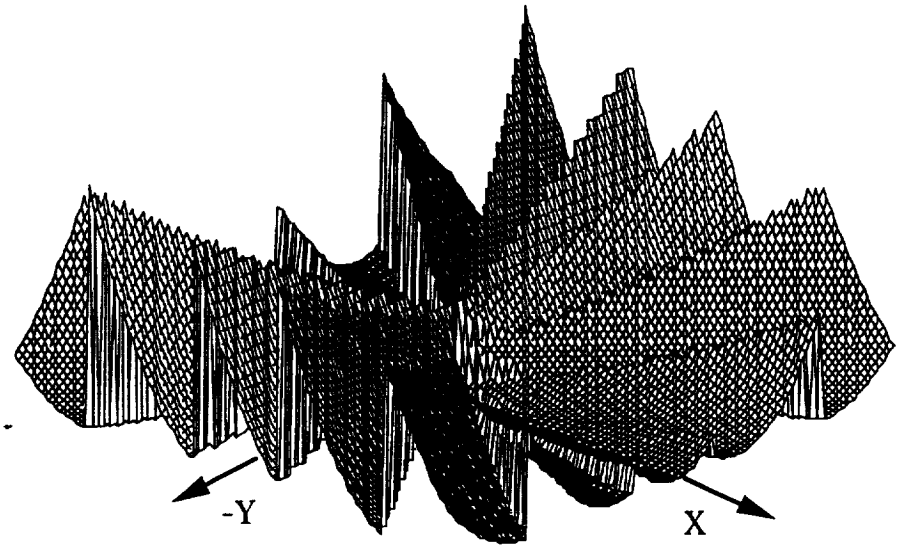

Figure 5-6. The 16PSK squared equivalent noise.

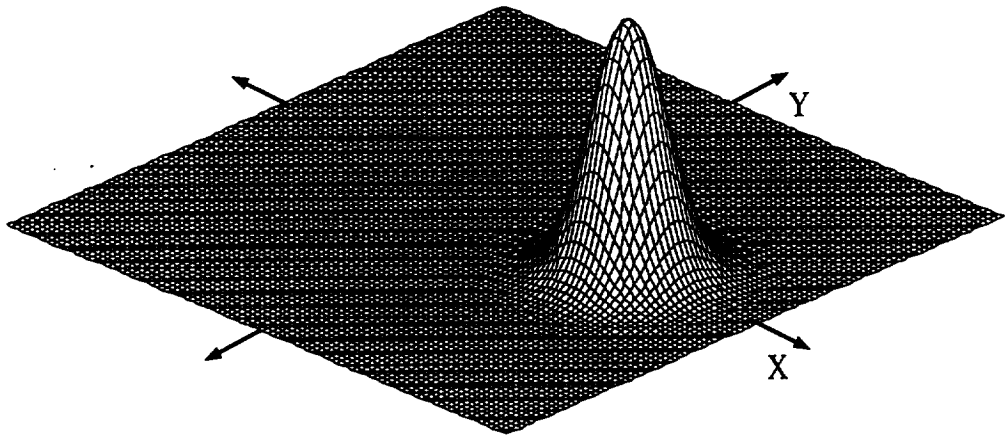

Figure 5-7. The joint Gaussian probability mountain at 10 dB SNR.

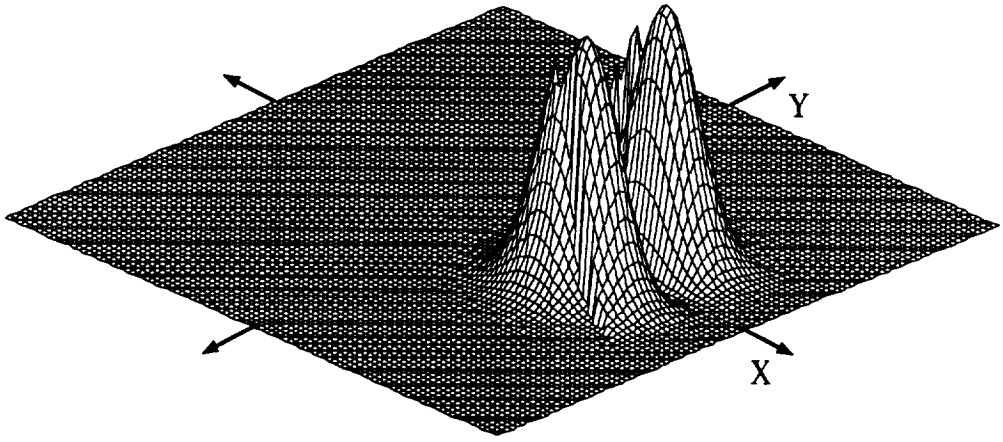

Figure 5-8. The 8PSK equivalent noise integrand at 10 dB SNR.

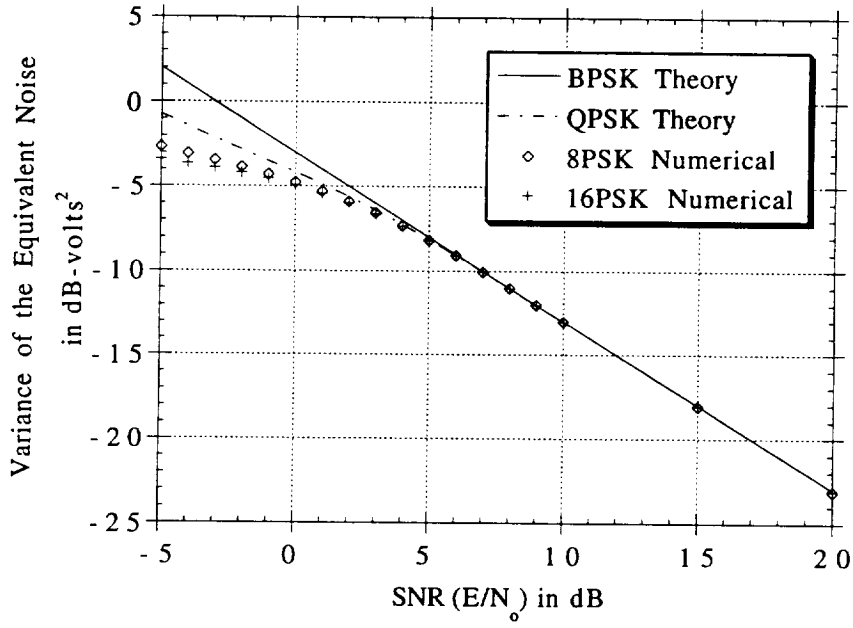

Figure 5-9. MPSK equivalent noise variance.

5.3 The Gain Of The Phase Detector

The next component of interest in the calculation of the variance of the phase error is the gain associated with the phase detector. In Chapter 4 the gain was shown to be a function of SNR through (4-27). Further, it was presented as the slope of the phase detector characteristic, measured at a phase error of zero, as shown in (4-30). Together these representations will allow the computation of the gain of the phase detector for 8PSK and 16PSK. As with the variance of the equivalent noise for 8PSK and 16PSK, the interdependence between the data estimate on the I channel with the noise on the Q channel and the interdependence between the data estimate on the Q channel with the noise on the I channel prohibit the closed form solution of the phase detector gain. Before discussing the solutions for 8PSK and 16PSK, the solutions for BPSK and QPSK will be presented.

Using (4-26) and (4-30) the phase detector gain is stated as

$$\alpha_{SNR} = \left.\frac{\partial E\left[\cos(\theta_e - \theta_m)\hat{Q} + \sin(\theta_e - \theta_m)\hat{I}\right]}{\partial \theta_e}\right|_{\theta_e = 0} . \qquad (5\text{-}25)$$

Expanding the trigonometric functions yields

$$\alpha_{SNR} = \frac{\partial E\begin{bmatrix}\{\cos(\theta_e)\cos(\theta_m)+\sin(\theta_e)\sin(\theta_m)\}\hat{Q} \\ +\{\sin(\theta_e)\cos(\theta_m)-\cos(\theta_e)\sin(\theta_m)\}\hat{I}\end{bmatrix}}{\partial\theta_e}\Bigg|_{\theta_e=0} . \qquad (5\text{-}26)$$

Writing the trigonometric functions of the transmitted modulation angle as I and Q data components and combining like terms forms

$$\alpha_{SNR} = \frac{\partial\{\cos(\theta_e)E[I_m\hat{Q}-\hat{I}Q_m]+\sin(\theta_e)E[Q_m\hat{Q}+I_m\hat{I}]\}}{\partial\theta_e}\Bigg|_{\theta_e=0} . \qquad (5\text{-}27)$$

Distributing the derivative and applying its multiplicative property results in

$$\alpha_{SNR} = E[I_m\hat{Q}-\hat{I}Q_m]\frac{\partial\cos(\theta_e)}{\partial\theta_e}\Bigg|_{\theta_e=0} + \cos(\theta_e)\frac{\partial E[I_m\hat{Q}-\hat{I}Q_m]}{\partial\theta_e}\Bigg|_{\theta_e=0}$$
$$+ E[Q_m\hat{Q}+I_m\hat{I}]\frac{\partial\sin(\theta_e)}{\partial\theta_e}\Bigg|_{\theta_e=0} + \sin(\theta_e)\frac{\partial E[Q_m\hat{Q}+I_m\hat{I}]}{\partial\theta_e}\Bigg|_{\theta_e=0} . \qquad (5\text{-}28)$$

The first and fourth terms of (5-28) equate to zero leaving

$$\alpha_{SNR} = \left.\frac{\partial E\left[I_m \hat{Q}\right]}{\partial \theta_e}\right|_{\theta_e=0} - \left.\frac{\partial E\left[\hat{I} Q_m\right]}{\partial \theta_e}\right|_{\theta_e=0} + E\left[Q_m \hat{Q}\right]_{\theta_e=0} + E\left[I_m \hat{I}\right]_{\theta_e=0}.$$

(5-29)

For BPSK, all but the last term of (5-29) equate to zero because the data sent on the Q channel and the estimate of what was sent on the Q channel are both always zero. The last term is the expected value of a function of random variables and is stated

$$E\left[I_m \hat{I}\right] = \int_{-\infty}^{\infty} \int_{-\infty}^{\infty} I_m \hat{I} f(I_m) f(N_I) dN_I dI_m. \qquad (5\text{-}30)$$

It is noted that the phase error has been set to zero before beginning the integration. Expressing the estimate of the I channel data as a function of the noise on the I channel and the particular transmitted data on the I channel makes it possible to integrate out the data and form

$$E\left[I_m \hat{I}\right] = \frac{1}{2} \int_{-\infty}^{\infty} g(N_I, I_m = 1) f(N_I) dN_I - \frac{1}{2} \int_{-\infty}^{\infty} g(N_I, I_m = -1) f(N_I) dN_I.$$

(5-31)

Now, considering the two possible values for the data estimate transforms (5-31) into

$$E\left[I_m\hat{I}\right]=\frac{1}{2}\int_{-1}^{\infty}f(N_I)dN_I-\frac{1}{2}\int_{-\infty}^{-1}f(N_I)dN_I+\frac{1}{2}\int_{-\infty}^{1}f(N_I)dN_I-\frac{1}{2}\int_{1}^{\infty}f(N_I)dN_I.$$

(5-32)

Using (5-14) and the "Q" function, which is related to the normal probability function and defined by

$$Q(y)=\int_{y}^{\infty}\frac{1}{\sqrt{2\pi}}e^{-\frac{x^2}{2}}dx, \qquad (5\text{-}33)$$

it is possible to express (5-32) as

$$E\left[I_m\hat{I}\right]=\frac{1}{2}Q\left(\frac{-1}{\sigma_{N_I}}\right)-\frac{1}{2}Q\left(\frac{1}{\sigma_{N_I}}\right)+\frac{1}{2}Q\left(\frac{-1}{\sigma_{N_I}}\right)-\frac{1}{2}Q\left(\frac{1}{\sigma_{N_I}}\right). \qquad (5\text{-}34)$$

This reduces to

$$E\left[I_m\hat{I}\right]=Q\left(\frac{-1}{\sigma_{N_I}}\right)-Q\left(\frac{1}{\sigma_{N_I}}\right)=1-2Q\left(\frac{1}{\sigma_{N_I}}\right). \qquad (5\text{-}35)$$

Again stating that for BPSK, (5-35) is the only non-zero term in the expanded equation for the phase detector gain, (5-29), and

noting the "Q" function's relationship to the standard "erf" function, namely

$$Q(y)=\frac{1}{2}\left[1-erf\left(\frac{y}{\sqrt{2}}\right)\right], \tag{5-36}$$

it is possible to state

$$\alpha_{SNR_{BPSK}}=erf\left(\frac{1}{\sqrt{2\sigma_{N_I}^2}}\right). \tag{5-37}$$

Inserting the expression for the variance of the I channel noise yields [37, pg. 91]

$$\alpha_{SNR_{BPSK}}=erf\left(\sqrt{\frac{E}{N_o}}\right). \tag{5-38}$$

For QPSK, all of the terms of (5-29) are non-zero, Further, the last two terms are equivalent and can be stated

$$E\left[Q_m\hat{Q}\right]=E\left[I_m\hat{I}\right]=\int_{-\infty}^{\infty}\int_{-\infty}^{\infty}I_m\hat{I}f(I_m)f(N_I)dN_I dI_m. \tag{5-39}$$

Following the same procedure as for BPSK, next the modulation is integrated out yielding

$$E\left[I_m\hat{I}\right]=\frac{1}{2}\frac{\sqrt{2}}{2}\int_{-\infty}^{\infty}g\left(N_I,I_m=\frac{\sqrt{2}}{2}\right)f(N_I)dN_I - \frac{1}{2}\frac{\sqrt{2}}{2}\int_{-\infty}^{\infty}g\left(N_I,I_m=\frac{\sqrt{2}}{2}\right)f(N_I)dN_I \quad (5\text{-}40)$$

Now, considering the two possible values for the data estimate transforms (5-40) into

$$E\left[I_m\hat{I}\right]=\frac{1}{2}\frac{\sqrt{2}}{2}\frac{\sqrt{2}}{2}\int_{-\frac{\sqrt{2}}{2}}^{\infty}f(N_I)dN_I+\frac{1}{2}\frac{\sqrt{2}}{2}\frac{-\sqrt{2}}{2}\int_{-\infty}^{-\frac{\sqrt{2}}{2}}f(N_I)dN_I + \frac{1}{2}\frac{-\sqrt{2}}{2}\frac{-\sqrt{2}}{2}\int_{-\infty}^{\frac{\sqrt{2}}{2}}f(N_I)dN_I+\frac{1}{2}\frac{-\sqrt{2}}{2}\frac{\sqrt{2}}{2}\int_{\frac{\sqrt{2}}{2}}^{\infty}f(N_I)dN_I \quad (5\text{-}41)$$

Once again applying the "Q" function, the result is

$$E\left[I_m\hat{I}\right]=\frac{1}{4}Q\left(\frac{-\sqrt{2}}{2\sigma_{N_I}}\right)-\frac{1}{4}Q\left(\frac{\sqrt{2}}{2\sigma_{N_I}}\right)+\frac{1}{4}Q\left(\frac{-\sqrt{2}}{2\sigma_{N_I}}\right)-\frac{1}{4}Q\left(\frac{\sqrt{2}}{2\sigma_{N_I}}\right). \quad (5\text{-}42)$$

This can be reduced to

$$E\left[I_m\hat{I}\right]=\frac{1}{2}-Q\left(\frac{\sqrt{2}}{2\sigma_{N_I}}\right) \quad (5\text{-}43)$$

or using the "erf" function with the I channel noise variance substituted in as

$$E\left[I_m\hat{I}\right]=\frac{1}{2}erf\left(\sqrt{\frac{E}{2N_o}}\right). \tag{5-44}$$

To complete the phase detector gain analysis for QPSK requires that the first two terms of (5-29) be examined. The procedure for calculating either one is similar. It is noted, however, that the phase error cannot be set to zero until after the derivative is evaluated. Therefore to proceed, consider the expected value function in the first term of (5-29), namely

$$E\left[I_m\hat{Q}\right]=\int_{-\infty}^{\infty}\int_{-\infty}^{\infty}\int_{-\infty}^{\infty}I_m\hat{Q}f(I_m)f(Q_m)f\left(N_Q\right)dN_Q dQ_m dI_m. \tag{5-45}$$

Next, integrate out the modulation and express the estimate of the Q channel data as a function of the noise and modulation data to form

$$\begin{aligned}E\left[I_m\hat{Q}\right]=&\frac{1}{2}\frac{1}{2}\frac{\sqrt{2}}{2}\int_{-\infty}^{\infty}g\left(N_Q,I_m=\frac{\sqrt{2}}{2},Q_m=\frac{\sqrt{2}}{2}\right)f\left(N_Q\right)dN_Q\\&+\frac{1}{2}\frac{1}{2}\frac{\sqrt{2}}{2}\int_{-\infty}^{\infty}g\left(N_Q,I_m=\frac{\sqrt{2}}{2},Q_m=\frac{-\sqrt{2}}{2}\right)f\left(N_Q\right)dN_Q\\&+\frac{1}{2}\frac{1}{2}\frac{-\sqrt{2}}{2}\int_{-\infty}^{\infty}g\left(N_Q,I_m=\frac{-\sqrt{2}}{2},Q_m=\frac{\sqrt{2}}{2}\right)f\left(N_Q\right)dN_Q\\&+\frac{1}{2}\frac{1}{2}\frac{-\sqrt{2}}{2}\int_{-\infty}^{\infty}g\left(N_Q,I_m=\frac{-\sqrt{2}}{2},Q_m=\frac{-\sqrt{2}}{2}\right)f\left(N_Q\right)dN_Q\end{aligned} \tag{5-46}$$

To continue the phase error, θ_e, must be considered. As was done previously, it is assumed that the phase error is small. Next consider that a phase error will rotate the received constellation in the decision space. Depending on whether the phase error is positive or negative and depending on what modulation data is transmitted the rotating effect can help or hinder the Q channel data decision process. When the rotation assists the Q channel decision, by moving the constellation point away from the I channel axis, it moves the point closer to the Q channel axis and thus hinders the I channel decision.

In terms of integrating N_Q, this phase error affects the boundry value in the decision space beyond which N_Q will cause an error. If the phase error has moved the constellation point away from the I channel axis, i.e., the Q channel decision boundry, a greater value of N_Q is required to cause an error in the Q channel estimate. A positive phase error will cause a transmitted symbol in the first or third quadrant to appear closer to the I channel axis in the decision space. This is shown in Figure 5-10. In the second and fourth quadrants a positive phase error will mean the symbol appears farther from the I channel axis.

Therefore, in the first quadrant the Q channel noise needs to be

$$N_Q < -\sin\left(\frac{\pi}{4} - \theta_e\right) \qquad (5\text{-}47)$$

to cause an error in choosing $\hat{Q}$. Correspondingly in the third quadrant an error will occur if

$$N_Q > -\sin\left(-\frac{3\pi}{4} - \theta_e\right) = \sin\left(\frac{\pi}{4} - \theta_e\right). \tag{5-48}$$

If in the second quadrant the noise is

$$N_Q < -\sin\left(\frac{3\pi}{4} - \theta_e\right) = -\sin\left(\frac{\pi}{4} + \theta_e\right) \tag{5-49}$$

or in the fourth quadrant

$$N_Q > -\sin\left(-\frac{\pi}{4} - \theta_e\right) = \sin\left(\frac{\pi}{4} + \theta_e\right) \tag{5-50}$$

an error will occur. These are the four noise boundries required to expand (5-46) taking into account the phase error. When they are applied to (5-46) the result is

$$E\left[I_m\hat{Q}\right]=\frac{1}{2}\frac{1}{2}\frac{\sqrt{2}}{2}\frac{\sqrt{2}}{2}\int_{-\sin\left(\frac{\pi}{4}-\theta_e\right)}^{\infty}f\left(N_Q\right)dN_Q+\frac{1}{2}\frac{1}{2}\frac{\sqrt{2}}{2}\frac{-\sqrt{2}}{2}\int_{-\infty}^{-\sin\left(\frac{\pi}{4}-\theta_e\right)}f\left(N_Q\right)dN_Q$$

$$+\frac{1}{2}\frac{1}{2}\frac{-\sqrt{2}}{2}\frac{\sqrt{2}}{2}\int_{-\sin\left(\frac{\pi}{4}+\theta_e\right)}^{\infty}f\left(N_Q\right)dN_Q+\frac{1}{2}\frac{1}{2}\frac{-\sqrt{2}}{2}\frac{-\sqrt{2}}{2}\int_{-\infty}^{-\sin\left(\frac{\pi}{4}+\theta_e\right)}f\left(N_Q\right)dN_Q$$

$$+\frac{1}{2}\frac{1}{2}\frac{-\sqrt{2}}{2}\frac{-\sqrt{2}}{2}\int_{-\infty}^{\sin\left(\frac{\pi}{4}-\theta_e\right)}f\left(N_Q\right)dN_Q+\frac{1}{2}\frac{1}{2}\frac{-\sqrt{2}}{2}\frac{\sqrt{2}}{2}\int_{\sin\left(\frac{\pi}{4}-\theta_e\right)}^{\infty}f\left(N_Q\right)dN_Q$$

$$+\frac{1}{2}\frac{1}{2}\frac{\sqrt{2}}{2}\frac{-\sqrt{2}}{2}\int_{-\infty}^{\sin\left(\frac{\pi}{4}+\theta_e\right)}f\left(N_Q\right)dN_Q+\frac{1}{2}\frac{1}{2}\frac{\sqrt{2}}{2}\frac{\sqrt{2}}{2}\int_{\sin\left(\frac{\pi}{4}+\theta_e\right)}^{\infty}f\left(N_Q\right)dN_Q$$

(5-51)

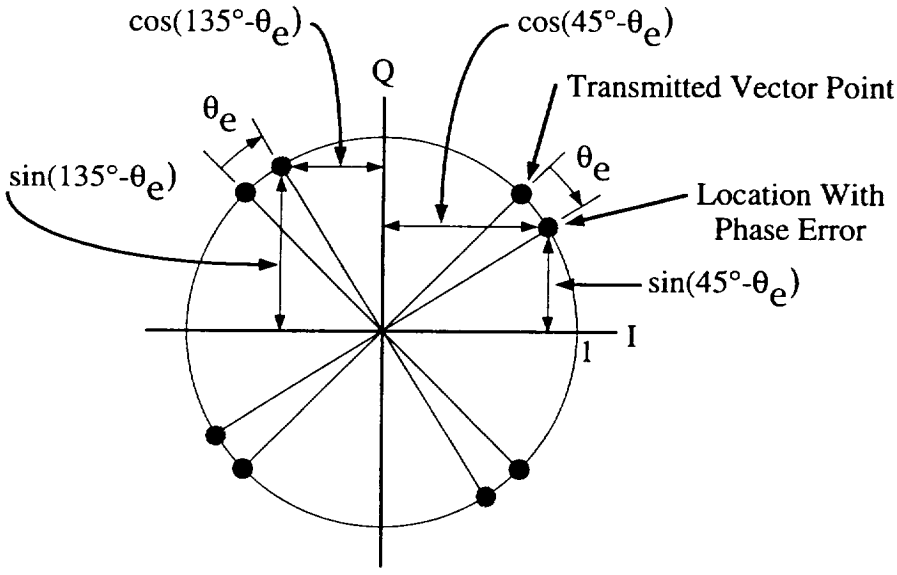

Figure 5-10. The QPSK constellation with and without phase error.

Applying the "Q" function yields

$$E\left[I_m\hat{Q}\right]=\frac{1}{8}Q\left[\frac{-\sin\left(\frac{\pi}{4}-\theta_e\right)}{\sigma_{N_I}}\right]-\frac{1}{8}Q\left[\frac{\sin\left(\frac{\pi}{4}-\theta_e\right)}{\sigma_{N_I}}\right]$$
$$-\frac{1}{8}Q\left[\frac{-\sin\left(\frac{\pi}{4}+\theta_e\right)}{\sigma_{N_I}}\right]+\frac{1}{8}Q\left[\frac{\sin\left(\frac{\pi}{4}+\theta_e\right)}{\sigma_{N_I}}\right]$$
$$+\frac{1}{8}Q\left[\frac{-\sin\left(\frac{\pi}{4}-\theta_e\right)}{\sigma_{N_I}}\right]-\frac{1}{8}Q\left[\frac{\sin\left(\frac{\pi}{4}-\theta_e\right)}{\sigma_{N_I}}\right]$$
$$-\frac{1}{8}Q\left[\frac{-\sin\left(\frac{\pi}{4}+\theta_e\right)}{\sigma_{N_I}}\right]+\frac{1}{8}Q\left[\frac{\sin\left(\frac{\pi}{4}+\theta_e\right)}{\sigma_{N_I}}\right] \quad (5\text{-}52)$$

Reducing yields

$$E\left[I_m\hat{Q}\right]=\frac{1}{4}Q\left[\frac{-\sin\left(\frac{\pi}{4}-\theta_e\right)}{\sigma_{N_I}}\right]-\frac{1}{4}Q\left[\frac{\sin\left(\frac{\pi}{4}-\theta_e\right)}{\sigma_{N_I}}\right]$$
$$-\frac{1}{4}Q\left[\frac{-\sin\left(\frac{\pi}{4}+\theta_e\right)}{\sigma_{N_I}}\right]+\frac{1}{4}Q\left[\frac{\sin\left(\frac{\pi}{4}+\theta_e\right)}{\sigma_{N_I}}\right] \quad (5\text{-}53)$$

After combining complementary "Q" functions (5-53) becomes

$$E\left[I_m\hat{Q}\right]=\frac{1}{4}-\frac{1}{2}Q\left[\frac{\sin\left(\frac{\pi}{4}-\theta_e\right)}{\sigma_{N_I}}\right]-\frac{1}{4}+\frac{1}{2}Q\left[\frac{\sin\left(\frac{\pi}{4}+\theta_e\right)}{\sigma_{N_I}}\right] \tag{5-54}$$

and finally

$$E\left[I_m\hat{Q}\right]=\frac{1}{2}Q\left[\frac{\sin\left(\frac{\pi}{4}+\theta_e\right)}{\sigma_{N_I}}\right]-\frac{1}{2}Q\left[\frac{\sin\left(\frac{\pi}{4}-\theta_e\right)}{\sigma_{N_I}}\right]. \tag{5-55}$$

By a similar approach for the second term of (5-29) its expected value function becomes

$$E\left[Q_m\hat{I}\right]=\frac{1}{2}Q\left[\frac{\sin\left(\frac{\pi}{4}-\theta_e\right)}{\sigma_{N_I}}\right]-\frac{1}{2}Q\left[\frac{\sin\left(\frac{\pi}{4}+\theta_e\right)}{\sigma_{N_I}}\right]. \tag{5-56}$$

Referring to (5-29) the QPSK phase detector gain is now stated

$$\alpha_{SNR_{QPSK}} = \left.\frac{\partial\left\{\frac{1}{2}Q\left[\frac{\sin\left(\frac{\pi}{4}+\theta_e\right)}{\sigma_{N_I}}\right]\right\}}{\partial\theta_e}\right|_{\theta_e=0} \left.- \frac{\partial\left\{\frac{1}{2}Q\left[\frac{\sin\left(\frac{\pi}{4}-\theta_e\right)}{\sigma_{N_I}}\right]\right\}}{\partial\theta_e}\right|_{\theta_e=0}$$

$$\left.- \frac{\partial\left\{\frac{1}{2}Q\left[\frac{\sin\left(\frac{\pi}{4}-\theta_e\right)}{\sigma_{N_I}}\right]\right\}}{\partial\theta_e}\right|_{\theta_e=0} \left.+ \frac{\partial\left\{\frac{1}{2}Q\left[\frac{\sin\left(\frac{\pi}{4}+\theta_e\right)}{\sigma_{N_I}}\right]\right\}}{\partial\theta_e}\right|_{\theta_e=0}$$

$$+1-2Q\left(\frac{\sqrt{2}}{2\sigma_{N_I}}\right) \qquad (5\text{-}57)$$

By reducing, (5-57) becomes

$$\alpha_{SNR_{QPSK}} = 2\frac{\partial\left\{\frac{1}{2}Q\left[\frac{\sin\left(\frac{\pi}{4}+\theta_e\right)}{\sigma_{N_I}}\right]\right\}}{\partial\theta_e}\Bigg|_{\theta_e=0} - 2\frac{\partial\left\{\frac{1}{2}Q\left[\frac{\sin\left(\frac{\pi}{4}-\theta_e\right)}{\sigma_{N_I}}\right]\right\}}{\partial\theta_e}\Bigg|_{\theta_e=0}$$

$$+1-2Q\left(\frac{\sqrt{2}}{2\sigma_{N_I}}\right) \qquad (5\text{-}58)$$

To further reduce the partial derivatives in (5-58) it is necessary to take the derivative of an integral through the use of the relation

$$\frac{\partial}{\partial y}\int_p^q f(x,y)dx = \int_p^q \frac{\partial}{\partial y}[f(x,y)]dx + f(q,y)\frac{\partial q}{\partial y} - f(p,y)\frac{\partial p}{\partial y}. \qquad (5\text{-}59)$$

Since the "Q" function integrand in (5-58) is not a function of the phase error, the first term in (5-59) will equate to zero. Further, since the upper limit on both "Q" function integrals is infinity, the second term of (5-59) will equate to zero. The result is that (5-58) becomes

$$\alpha_{SNR_{QPSK}} = \left\{ \left[-\frac{1}{\sqrt{2\pi}} e^{-\frac{\sin^2\left(\frac{\pi}{4}+\theta_e\right)}{2\sigma^2_{N_I}}} \right] \frac{\partial \left[\sin\left(\frac{\pi}{4}+\theta_e\right) \right]}{\partial \theta_e} \right\}_{\theta_e=0}$$

$$+ \left\{ \left[\frac{1}{\sqrt{2\pi}} e^{-\frac{\sin^2\left(\frac{\pi}{4}-\theta_e\right)}{2\sigma^2_{N_I}}} \right] \frac{\partial \left[\sin\left(\frac{\pi}{4}-\theta_e\right) \right]}{\partial \theta_e} \right\}_{\theta_e=0} . \qquad (5\text{-}60)$$

$$+1-2Q\left(\frac{\sqrt{2}}{2\sigma_{N_I}}\right)$$

This reduces to

$$\alpha_{SNR_{QPSK}} = \left\{\left[-\frac{1}{\sqrt{2\pi}}e^{-\frac{\sin^2\left(\frac{\pi}{4}+\theta_e\right)}{2\sigma^2_{N_I}}}\right]\frac{\cos\left(\frac{\pi}{4}+\theta_e\right)}{\sigma_{N_I}}\right\}\Bigg|_{\theta_e=0}$$

$$-\left\{\left[\frac{1}{\sqrt{2\pi}}e^{-\frac{\sin^2\left(\frac{\pi}{4}-\theta_e\right)}{2\sigma^2_{N_I}}}\right]\frac{\cos\left(\frac{\pi}{4}-\theta_e\right)}{\sigma_{N_I}}\right\}\Bigg|_{\theta_e=0} \quad . \qquad (5\text{-}61)$$

$$+1-2Q\left(\frac{\sqrt{2}}{2\sigma_{N_I}}\right)$$

Evaluating (5-61) at a phase error of zero yields

$$\alpha_{SNR_{QPSK}} = 1-2Q\left(\frac{\sqrt{2}}{2\sigma_{N_I}}\right)-\frac{1}{2\sqrt{\pi\sigma^2_{N_I}}}e^{-\frac{1}{4\sigma^2_{N_I}}}-\frac{1}{2\sqrt{\pi\sigma^2_{N_I}}}e^{-\frac{1}{4\sigma^2_{N_I}}} \qquad (5\text{-}62)$$

and finally

$$\alpha_{SNR_{QPSK}} = 1-2Q\left(\frac{\sqrt{2}}{2\sigma_{N_I}}\right)-\frac{1}{\sqrt{\pi\sigma^2_{N_I}}}e^{-\frac{1}{4\sigma^2_{N_I}}} \quad . \qquad (5\text{-}63)$$

Using the "erf" function and inserting the I channel noise variance (5-63) can also be stated [35]

$$\alpha_{SNR_{QPSK}} = erf\left(\sqrt{\frac{E}{2N_o}}\right) - \sqrt{\frac{2}{\pi}}\sqrt{\frac{E}{N_o}}e^{-\frac{E}{2N_o}}. \qquad (5\text{-}64)$$

This is the closed form solution of the phase detector gain for QPSK. The results for both the BPSK and QPSK closed form solutions are plotted in Figure 5-11. Note that the logarithm of the square of the gain is actually plotted. This will prove useful when the entire phase error variance equation is reconsidered in the next chapter.

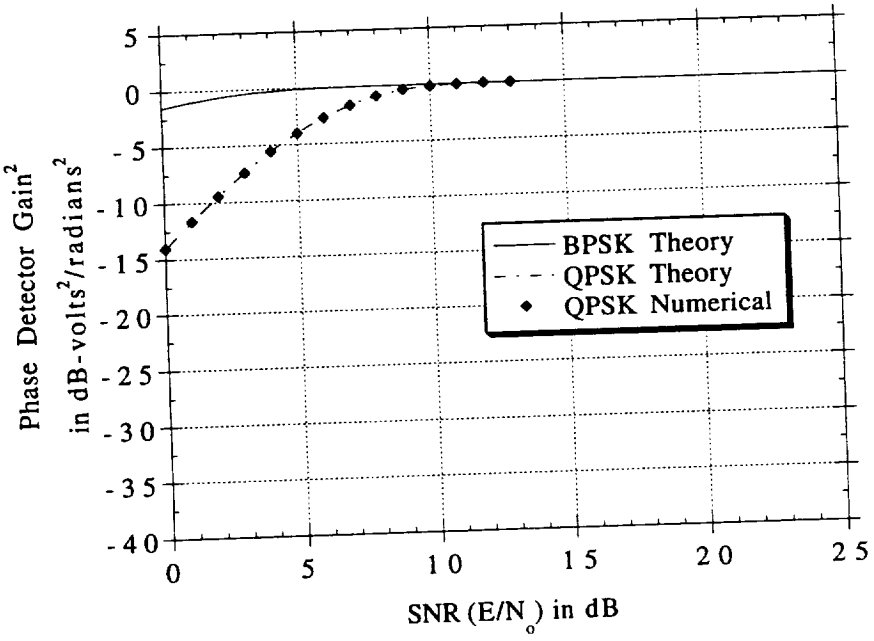

Figure 5-11. BPSK and QPSK phase detector gain.

For 8PSK and 16PSK a closed form solution is unobtainable. A review of the components in (5-29) will reveal this. The data estimates, both $\hat{I}$ and $\hat{Q}$, require that the expected value functions in each of the components of (5-29) be integrated over both N_I and N_Q because of the interdependence between each of the estimates and both noise channels. For each component a solution will arise involving the integration of a "Q" function. This cannot be solved in closed form.

To circumvent this problem the gain is calculated directly from the phase detector characteristic itself. By considering a small phase error, at a specific SNR, and calculating the phase detector characteristic output, the gain can be obtained. This process uses the approximation that for small phase errors the phase detector characteristic has a linear response. By so calculating the detector's response to a small phase error and dividing that response by the error, the slope, i.e., the gain, is computed.

To proceed, the phase detector characteristic of (4-27) is employed and restated here as

$$PD(\theta_e) = E\left[\sin\left(\theta_e + \hat{\theta}_m - \theta_m\right)\right]. \tag{5-65}$$

The first step is to express the expected value function as a summation over both discrete random variables, θ_m and $\hat{\theta}_m$, yielding

$$PD(\theta_e) = \sum_{i=0}^{M-1} \sum_{j=0}^{M-1} \sin\left(\theta_e + \hat{\theta}_{m_j} - \theta_{m_i}\right) P\left(\theta_{m_i}, \hat{\theta}_{m_j} | \theta_e\right). \qquad (5\text{-}66)$$

Next the mutual probability is decomposed resulting in

$$PD(\theta_e) = \sum_{i=0}^{M-1} \sum_{j=0}^{M-1} \sin\left(\theta_e + \hat{\theta}_{m_j} - \theta_{m_i}\right) P\left(\hat{\theta}_{m_j} | \theta_{m_i}, \theta_e\right) P\left(\theta_{m_i}\right). \qquad (5\text{-}67)$$

The expression of conditional probability in (5-67) describes the probability of receiving one of the M possible modulation angles when a particular modulation angle is transmitted. The apriori probability of the transmitted modulation angle in (5-67) equates to $\frac{1}{M}$ when the transmitted symbols are all equally likely thus producing

$$PD(\theta_e) = \frac{1}{M} \sum_{i=0}^{M-1} \sum_{j=0}^{M-1} \sin\left(\theta_e + \hat{\theta}_{m_j} - \theta_{m_i}\right) P\left(\hat{\theta}_{m_j} | \theta_{m_i}, \theta_e\right). \qquad (5\text{-}68)$$

Because the constellation is circularly symmetric each element of the sum over the transmitted modulation angles will be the same. Since there are M of these elements it is possible to reduce (5-68) by fixing the transmitted modulation angle, e.g., at $\theta_m = 0$, and then replacing the outer summation by multiplying through by M. In this way (5-68) becomes

$$PD(\theta_e) = \sum_{j=0}^{M-1} \sin\left(\theta_e + \hat{\theta}_{m_j}\right) P\left(\hat{\theta}_{m_j} | \theta_m = 0, \theta_e\right). \quad (5\text{-}69)$$

What remains is to describe the conditional probability of receiving a particular modulation angle estimate given that $\theta_m = 0$. This is accomplished by integrating the conditional density that describes the probability of receiving a particular phase, γ, given $\theta_m = 0$, over the decision region of phase that corresponds to the received modulation angle. The density is configured to account for a phase error, θ_e, and is expressed [41]

$$p(\gamma | \theta_m = 0, \theta_e) = \frac{e^{-\frac{E}{N_o}}}{2\pi} \left[\begin{array}{l} 1 + \sqrt{\frac{4E\pi}{N_o}} \cos(\gamma + \theta_e) e^{-\frac{E}{N_o}\cos^2(\gamma+\theta_e)} \\ \times Q\left(-\sqrt{\frac{2E}{N_o}} \cos(\gamma + \theta_e) \right) \end{array} \right]. \quad (5\text{-}70)$$

As was just mentioned, to compute each of the M conditional probabilities in (5-69) it is necessary to integrate the density of (5-70) over the decision region corresponding to each of the M possible received phases.

Through the use of (5-69) it is possible to examine the phase detector characteristic for any M. Figure 5-12 shows the phase detector characteristics, using this approach, for M=2,4,8 and 16 all at an SNR of 20 dB. For each M one detector cycle has been plotted. Note that all the characteristics have positive nearly equivalent slopes at zero phase error. This is because at 20 dB all

the PSK modes, with the exception of 16PSK, have a phase detector gain of unity. The gain for 16 PSK is slightly less than unity. Having equivalent gain follows when it is considered that at such a high-SNR the decision device in the loop is making near perfect decisions as to what was transmitted. As the SNR goes down the gain will go down. This is shown for each PSK mode in turn using Figures 5-13, 5-14, 5-15, and 5-16 for BPSK, QPSK, 8PSK, and 16PSK, respectively. In each of these plots a family of phase detector characteristics is presented wherein each characteristic is plotted at a different SNR. As the SNR drops the maximum magnitude and gain drop. Note also that the maximum magnitude of the phase error that can be tolerated before the phase detector output swings the opposite way and causes a cycle slip, also decreases with decreasing SNR. This is distinguished by the movement of the phase error location, of the maximum magnitude of the characteristic, inward toward the lock point as the SNR goes down. Evaluating any of the characteristics in Figures 5-13 through 5-16, at a very small phase error allows for the calculation of the gain of the phase detector characteristic, as mentioned before, simply by dividing the result by the phase error. For QPSK this data is plotted along with the closed form solutions in Figure 5-11. Once again this technique of comparing the numerical approach to the closed form solution was used for verification. In Figure 5-17 the 8PSK and 16PSK numerical results

are presented along with the BPSK and QPSK closed form solutions.

All of the numerical calculations were conducted using the source code in Appendix E. The raw data are presented there as well.

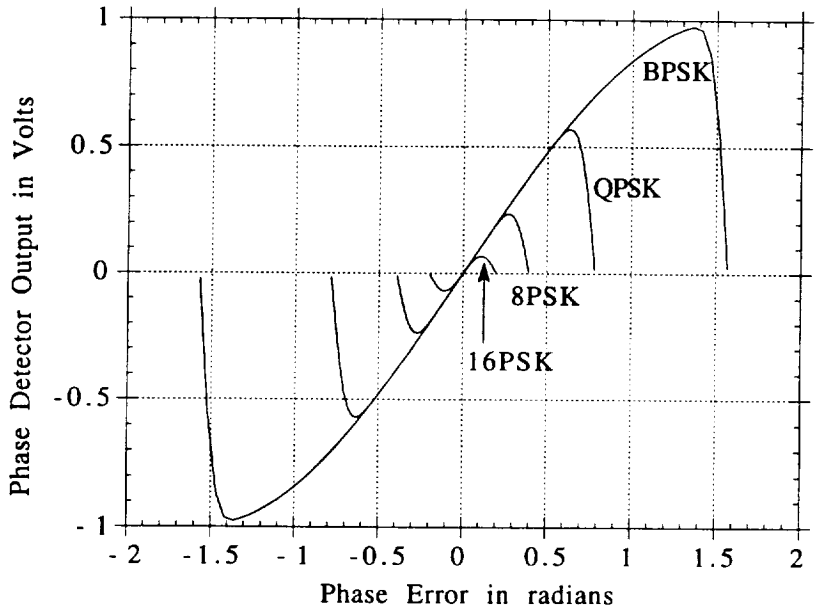

Figure 5-12. MPSK phase detector outputs at 20 dB SNR.

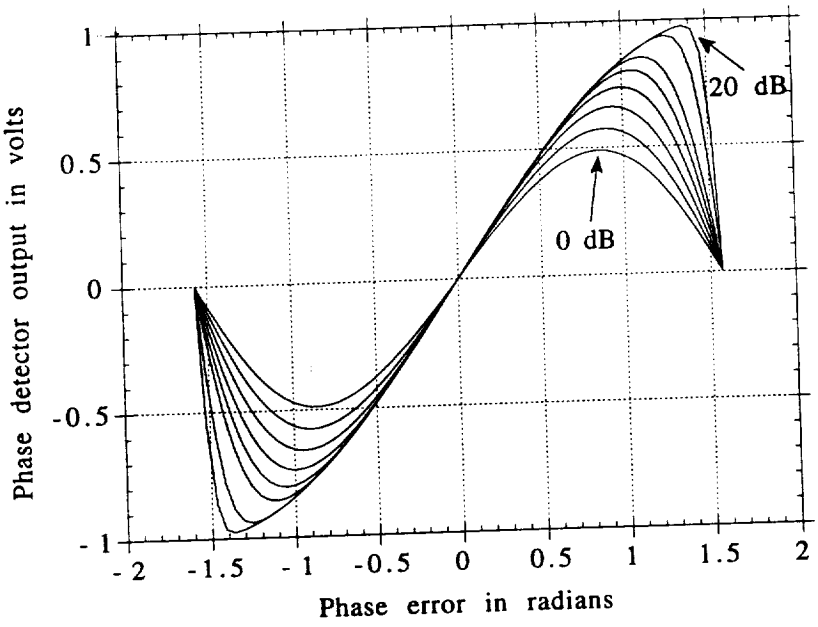

Figure 5-13. BPSK phase detector characteristics at SNR's of 0, 2, 4, 6, 8, 10, 15, and 20 dB.

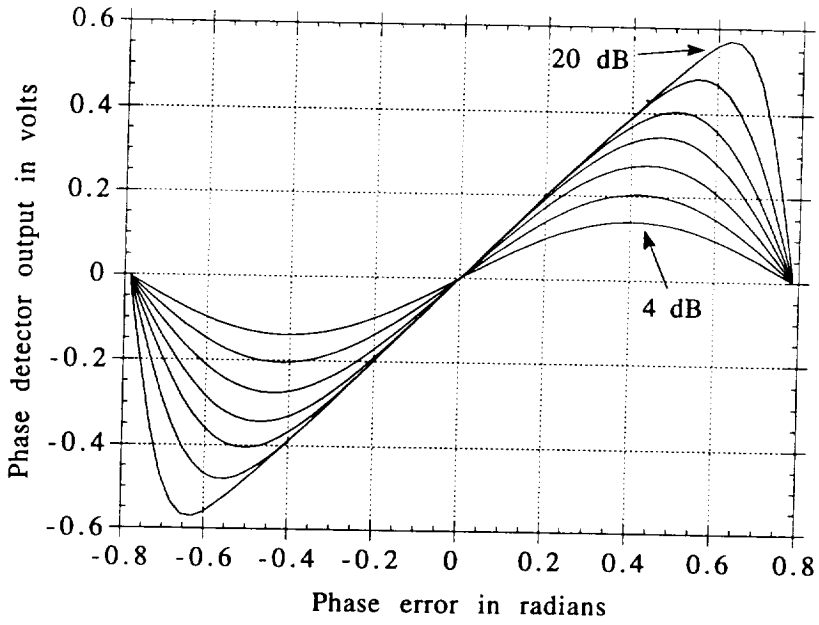

Figure 5-14. QPSK phase detector characteristics at SNR's of 4, 6, 8, 10, 12, 15, and 20 dB.

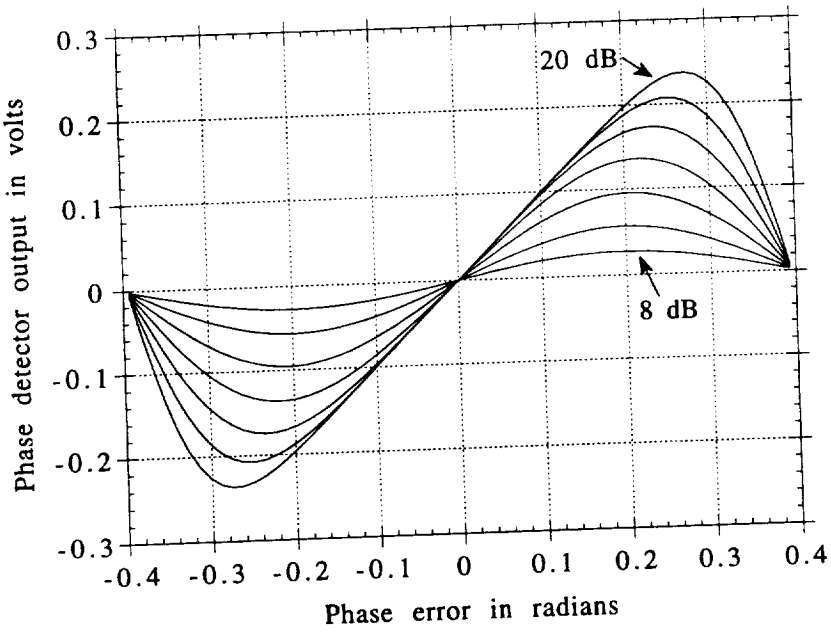

Figure 5-15. 8PSK phase detector characteristics at SNR's of 8, 10, 12, 14, 16, 18, and 20 dB.

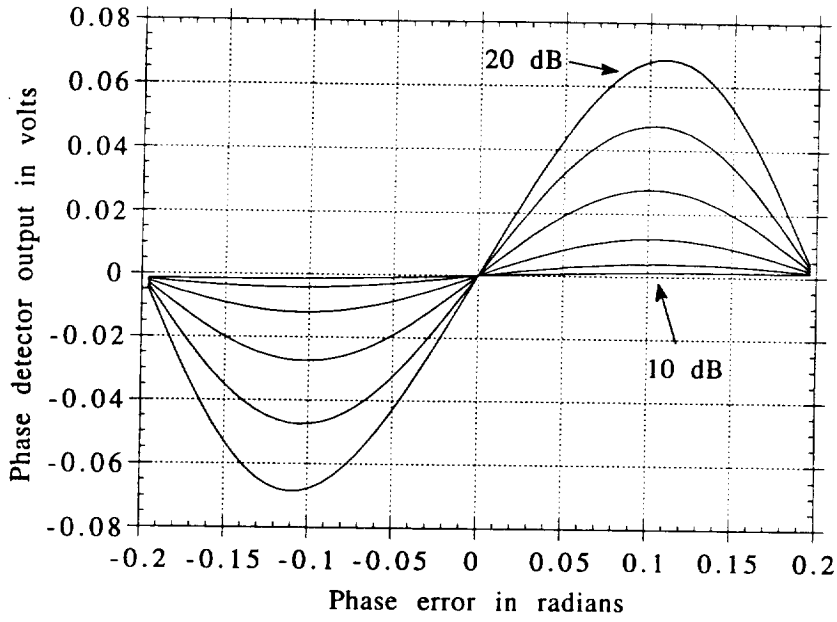

Figure 5-16. 16PSK phase detector characteristics at SNR's of 10, 12, 14, 16, 18, and 20 dB.

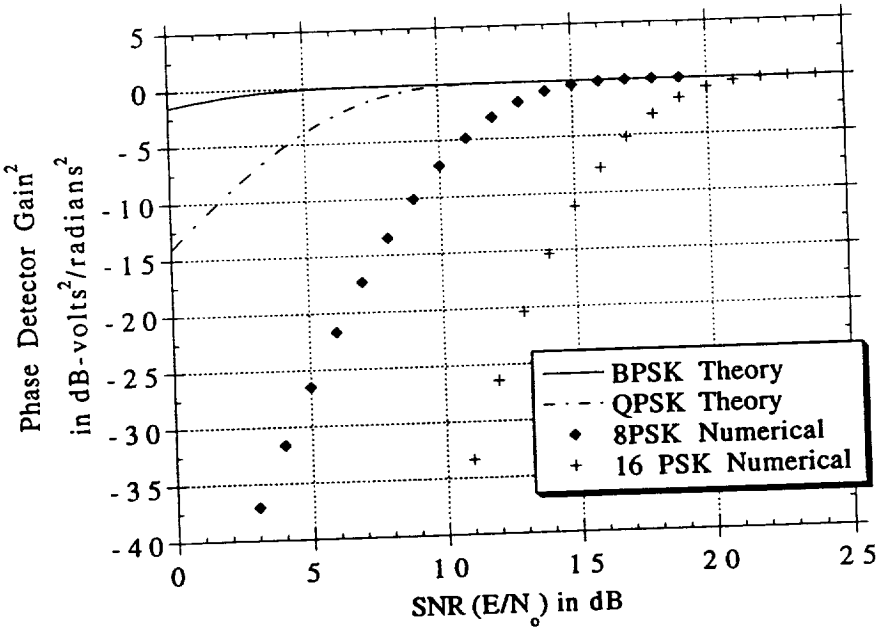

Figure 5-17. MPSK phase detector gain.

5.4 The Loop Bandwidth

The third component of the phase error variance equation that will be discussed is the loop bandwidth. As was shown in Chapter 2, the transfer function of a classical second order phaselock loop can be expressed by using the gain terms in the loop as

$$H(s)=\frac{s\sqrt{P_r}K+a\sqrt{P_r}K}{s^2+s\sqrt{P_r}K+a\sqrt{P_r}K} \tag{5-71}$$

or by using the classical design parameters as

$$H(s) = \frac{s2\zeta\omega_n + \omega_n^2}{s^2 + s2\zeta\omega_n + \omega_n^2}. \tag{5-72}$$

Further, its loop noise bandwidth can also be expressed in the same two ways. When the gain terms are used the double-sided loop noise bandwidth can be stated

$$B_L = \frac{\sqrt{P_r}K + a}{2}. \tag{5-73}$$

When the design parameters are used the result is

$$B_L = \omega_n\left(\zeta + \frac{1}{4\zeta}\right) \tag{5-74}$$

just as described in Chapter 2. In Chapter 4 the transfer function for the second order high-SNR loop was derived and is restated here as

$$H(s) = \frac{\alpha_{SNR}K_o(s+a)}{s^2 + \alpha_{SNR}K_o(s+a)}. \tag{5-75}$$

It was then equated to the design parameter version of the transfer function by stating

$$H(s) = \frac{2\zeta'\omega_n's + \omega_n'^2}{s^2 + 2\zeta'\omega_n's + \omega_n'^2} \tag{5-76}$$

where

$$\omega_n' = \sqrt{\alpha_{SNR}}\,\omega_n \tag{5-77}$$

and

$$\zeta' = \sqrt{\alpha_{SNR}}\,\zeta \tag{5-78}$$

are the "dynamic" design parameters. If the loop is designed assuming an SNR operating condition that is high enough to make the phase detector gain equate to unity, then the actual natural frequency and damping factor of the loop will be exactly those of the classical design. If operation is then conducted at lower SNR's, where the phase detector gain is less than unity, the actual natural frequency and damping factor will decrease from the original design values. Among other phenomena, this has the effect of narrowing the loop noise bandwidth. Substituting the design parameters of (5-77) and (5-78) into the loop noise bandwidth equation of (5-74) yields

$$B_L = \sqrt{\alpha_{SNR}}\,\omega_n\left(\sqrt{\alpha_{SNR}}\,\zeta + \frac{1}{4\sqrt{\alpha_{SNR}}\,\zeta}\right). \tag{5-79}$$

This reduces to

$$B_L = \omega_n\left(\alpha_{SNR}\zeta + \frac{1}{4\zeta}\right). \tag{5-80}$$

At high-SNR's, when $\alpha_{SNR} = 1$ the loop bandwidth of (5-80) will equate to (5-74) just as expected. However at low SNR's when $\alpha_{SNR} << 1$ equation (5-80) becomes

$$B_{L_{low\,SNR}} \approx \frac{\omega_n}{4\zeta}. \tag{5-81}$$

There is a transition from one loop bandwidth at high-SNR's to a narrower loop bandwidth at low SNR's. For all the PSK modes the transition occurs at higher SNR's as M increases. This is shown in Figures 5-18, 5-19, and 5-20 where the normalized bandwidth has been plotted for 3 different damping factors. Note that the damping factor plays a crucial role in determining the size of the transition. As ζ increases the loop bandwidth will have a much larger transition resulting in a much narrower relative bandwidth at low SNR's.

As has been shown, the loop bandwidth changes because the phase detector gain changes. Both the phase detector gain and the equivalent noise variance change because incorrect data decisions are being made. In the next Chapter the combined effects of all three of these components will be assimilated to calculate the variance of the phase error as a function of SNR.

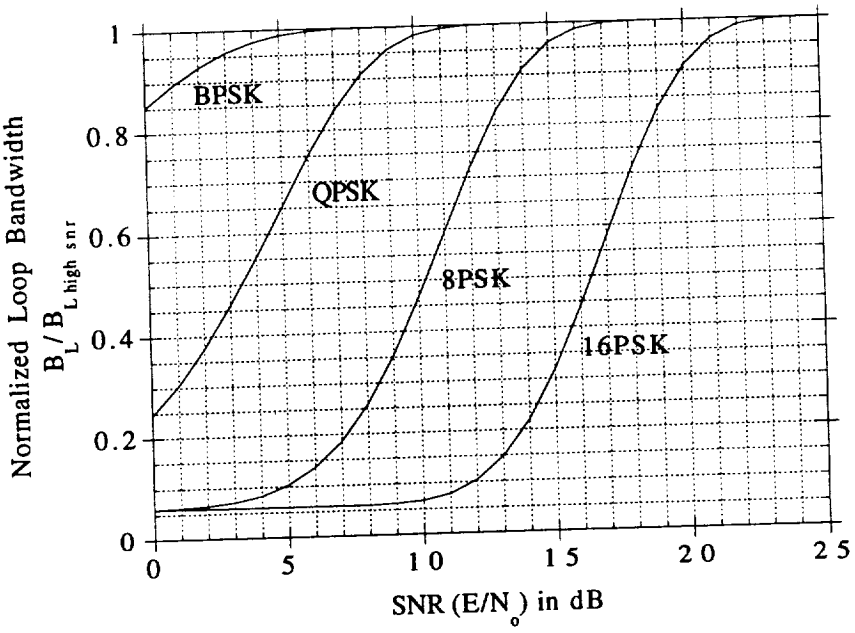

Figure 5-18. MPSK normalized loop noise bandwidth with ζ=2.0.

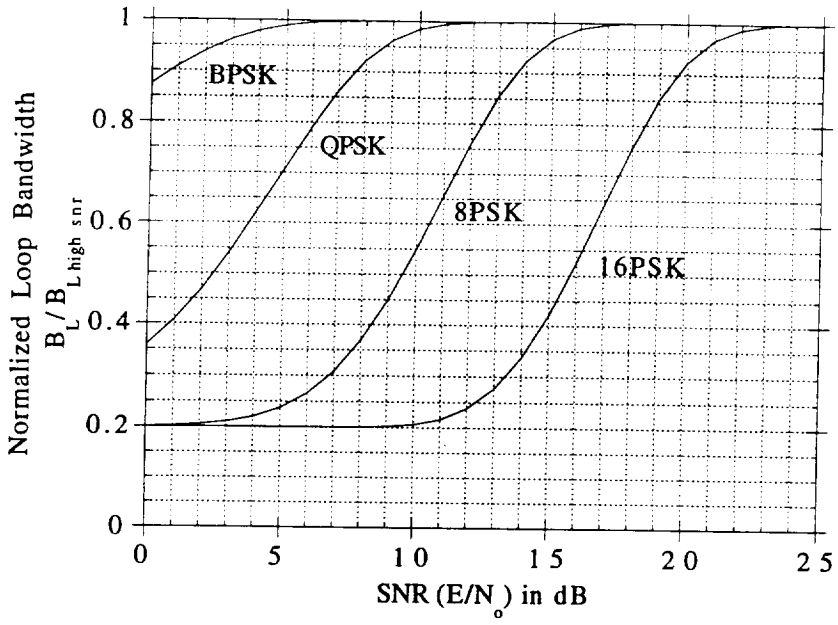

Figure 5-19. MPSK normalized loop noise bandwidth with ζ=1.0.

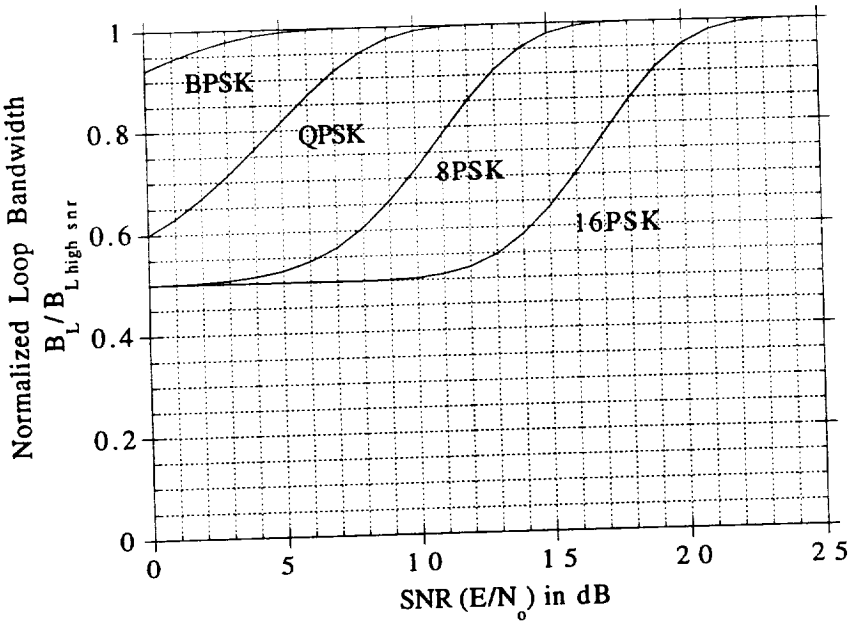

Figure 5-20. MPSK normalized loop noise bandwidth with ζ=0.5.

Chapter 6

PHASE ERROR VARIANCE RESULTS

"Why Think? Why not try the experiment?"

John Hunter
anatomist & surgeon, 1728 - 1793

6.1 Introduction

In Chapter 5 all of the complex components of the phase error were investigated individually. In this Chapter they will be combined in the equation for the phase error variance of the MPSK carrier tracking loop that uses the high-SNR approximation to MAP estimation. Once again this very important equation is restated for convenience as

$$\sigma_{\theta_e}^2 = \frac{B_L}{SR}\frac{\sigma_{N_e}^2}{\alpha_{SNR}^2}. \qquad (6\text{-}1)$$

6.2 N-Phase Loss

The first step in investigating the combined affect of each of the varying components of the right side of (6-1) is to reconsider the equivalent noise variance in light of the data obtained in Chapter 5. At high-SNR's the variance of the equivalent noise, for all M, can be approximated by the result for BPSK, namely, the

reciprocal of twice the signal-to-noise ratio. At low SNR's, for M>2, the self-noise in the receiver lessens the equivalent noise variance. It is possible to express the equivalent noise at any SNR and for all M, in terms of the BPSK approximation and the self noise, as

$$\sigma_{N_e}^2 = \frac{N_o}{2E}\xi \tag{6-2}$$

where ξ is the self noise and is a function of SNR. It follows that for BPSK the self noise term is unity for any SNR. As stated above, for M>2 at high-SNR's it will also equate to unity. At low SNR's, when the self noise is significant, it can be calculated using the equivalent noise variance data in Chapter 5 and equation 6-2.

Substituting this new expression for the equivalent noise variance into (6-1) yields

$$\sigma_{\theta_e}^2 = \frac{N_o}{2E}\frac{B_L}{SR}\frac{\xi}{\alpha_{SNR}^2}. \tag{6-3}$$

The reciprocal of the third fraction of (6-3) has a special designation. It is known as the N-phase loss.[1] Its effect is to increase the variance as the SNR goes down and is expressed as

[1]Classically this term has used the name "squaring loss". Its origin comes from the times-N loop employed for BPSK where N = 2. In that loop the received signal was squared to remove the modulation and provide a discrete spectral component at twice the carrier frequency for tracking purposes. The trade-off was an increase in the variance of the phase jitter known as squaring loss.

$$NL = \frac{\alpha_{SNR}^2}{\xi}. \tag{6-4}$$

The variance of (6-3) now becomes

$$\sigma_{\theta_e}^2 = \frac{N_o}{2E}\frac{B_L}{SR}\frac{1}{NL}. \tag{6-5}$$

Note that as NL gets smaller the variance goes up. This special term incorporates two competing effects for M>2. As the SNR goes down the self noise goes down. This should increase the N-phase loss and lessen the variance. However as the SNR goes down the phase detector gain goes down as well and this dominating effect lowers the N-phase loss overall, thus increasing the variance. In fact the N-phase loss has been approximated solely by the square of the phase detector gain for QPSK at reasonable SNR's of interest [35]. This approximation is valid for M>2 and is expressed as

$$NL \approx \alpha_{SNR}^2. \tag{6-6}$$

To see that this approximation is valid consider Figure 6-1 where both equations (6-4) and (6-6) have been plotted for M>2. Only for QPSK and 8PSK at low SNR's is the effect of self noise evident.

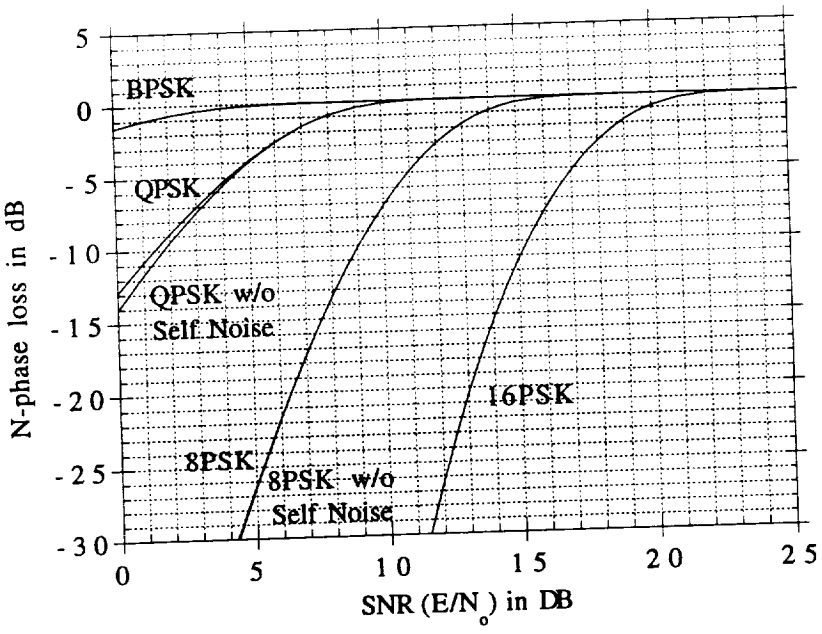

Figure 6-1. MPSK N-phase loss.

6.3 The Loop Bandwidth And The Symbol Rate

The second fraction of (6-5) is the ratio of the loop bandwidth to the symbol rate. As was mentioned in Chapter 4, for this type of loop this ratio is typically very small. To make the variance of the phase error data useful it is helpful to plot the data using the ratio of the high-SNR loop bandwidth to the symbol rate. That way loop designers can use the variance results at symbol rates of interest to them. This means that the variance can be expressed as

$$\sigma_{\theta_e}^2 = \frac{N_o}{2E}\mu_{SNR}\frac{B_{L_{HIGHSNR}}}{SR}\frac{1}{NL} \qquad (6\text{-}7)$$

where μ_{SNR} is the loop bandwidth compression factor. The normalized loop bandwidth data plotted in Figures 5-18 through 5-20 are actually plots of the loop bandwidth compression factor for various MPSK using 3 different damping factors. While the compression factor does decrease the variance of the phase error, its effect is limited. It causes a maximum amount of compression of the bandwidth, at low SNR's, that is a function of the damping factor. It is expressed, using (5-74) and (5-80), as

$$\mu_{SNR} = \frac{\left(\alpha_{SNR}4\zeta^2 + 1\right)}{\left(4\zeta^2 + 1\right)}. \qquad (6\text{-}8)$$

When the phase detector gain becomes very small μ_{SNR} reaches a minimum value, corresponding to the maximum amount of compression to the loop bandwidth. It is of interest to note that once again, in terms of variance of the phase error, there is a trade-off between the slight beneficial effect of the compressing bandwidth, which lessens the variance with decreasing SNR, and the decreasing phase detector gain, i.e., N-phase loss, which increases the variance with decreasing SNR. The N-phase loss dominates in this trade-off since it decreases as the square of the phase detector gain and since the compression factor reaches a minimum value while the N-phase loss continues to decrease.

6.4 The Variance Of The Phase Error

Having isolated and considered the combined effects of self noise and phase detector gain as one term, i.e., N-phase loss, and having discussed the changing loop bandwidth-to-symbol rate ratio, it is now prudent to evaluate the variance of the phase error. Referring to equation (6-7) the variance can be plotted using the data obtained in Chapter 5. The variance data is presented for BPSK, QPSK, 8PSK and 16PSK in Figures 6-2, 6-3, 6-4, and 6-5 respectively. The data are presented for various high-SNR loop bandwidth-to-symbol rate ratios all with a damping factor of $\zeta = 1$ and is tabulated in Appendix F.

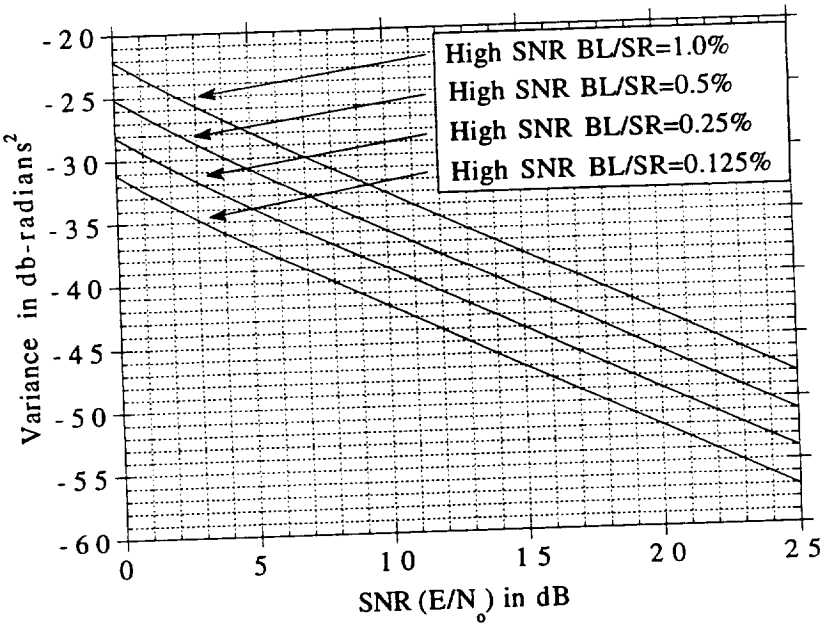

Figure 6-2. BPSK theoretical variance of phase error.

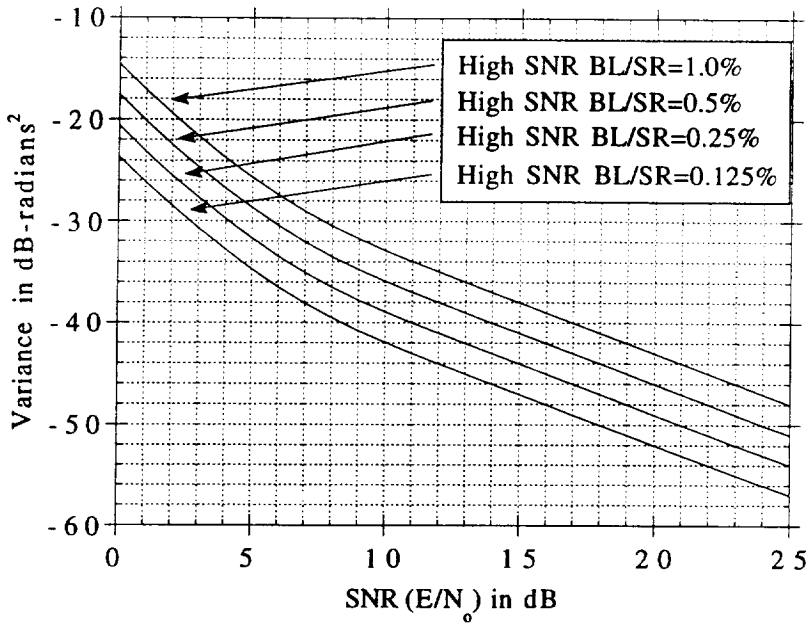

Figure 6-3. QPSK theoretical variance of phase error.

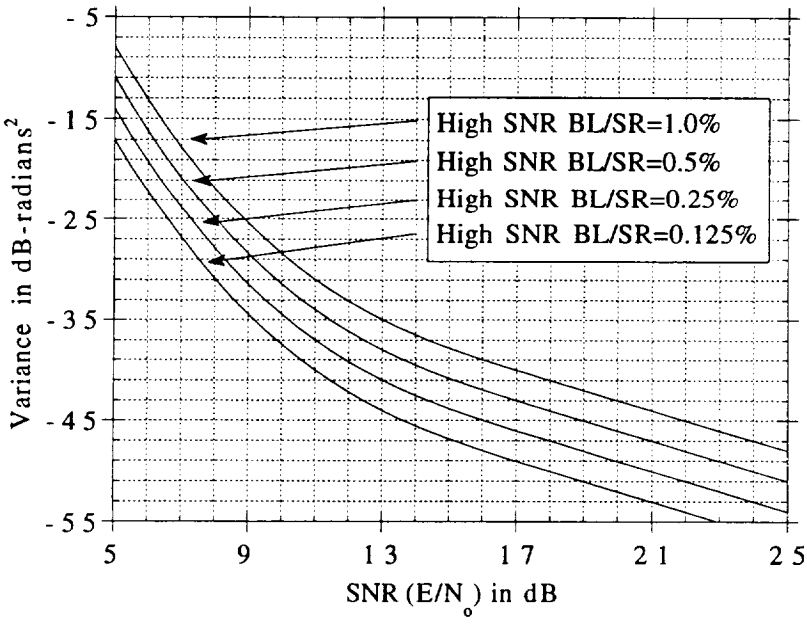

Figure 6-4. 8PSK numerical variance of phase error.

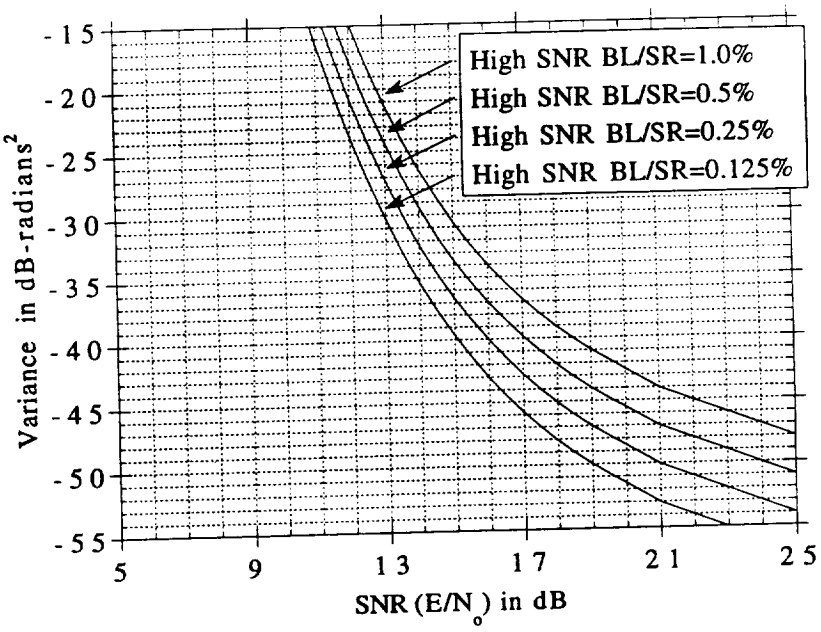

Figure 6-5. 16PSK numerical variance of phase error.

As expected the variance increases with diminishing SNR. At high-SNR's when the N-phase loss and loop compression factor are unity, the variance of the phase error can be approximated by

$$\sigma^2_{\theta_{e_{HIGHSNR}}} \approx \frac{N_o}{2E}\frac{B_{L_{HIGHSNR}}}{SR}. \qquad (6\text{-}9)$$

At low SNR's when the N-phase loss begins to decrease more rapidly the variance increases faster than the SNR decreases. This creates a thresholding effect where the variance curves begin to rise upward very quickly. There are several other characteristics of these curves that warrant disscussion as well.

Notice first that at high-SNR's there is a linear trade-off available to the loop designer in pursuit of maintaining a specific variance of phase error. The trade-off is between loop bandwidth and SNR. This trade-off is evident in equation (6-9) as well. If it is desired to lower the operating SNR by 3 dB, while still maintaining the same variance, the designer need only narrow the loop 3 dB (assuming other system constraints permit this option).

Unfortunately at low SNR's this trade-off is not linear. Narrowing the loop bandwidth 3 dB does not allow the designer to decrease the SNR 3 dB. This affect is demonstrated by considering the compression of the spacings between the variance curves in the thresholding region. Moving right from one variance curve to another along a fixed horizontal line of variance represents a 3 dB change in high-SNR loop bandwidth. As stated above, at high-SNR's this move also corresponds to a 3 dB drop in SNR. However, at low SNR's, specifically in the thresholding region, the move from one curve to another corresponds to less than a 3 dB decrease in SNR. The trade-off has diminished.

Another interesting characteristic of the thresholding effect is that it is a strong function of the SNR and a relatively weak function of the loop bandwidth. This is attributed to the reliance of the N-phase loss on SNR. It is noted graphically by first considering again that at any SNR a 3 dB change in loop bandwidth corresponds to a 3 dB change in variance (moving vertically from one curve to another). Next consider that, in the

threholding region, a 3 dB change in SNR can correspond to a change in variance of several orders of magnitude. Thus the variance is strongly dependent on the SNR.

A further, highly significant characteristic suggested by this data is that SNR's, where power-limited channel operation has been conducted for QPSK, may be too low to support 8PSK and especially 16PSK operation. This is the case because the SNR at which the thresholding region occurs increases with M. As was mentioned in Chapter 1, there is strong interest in using coded 8PSK and 16PSK systems to increase performance in limited channels. If the maximum available SNR is near or below the threshold region of the variance curves, then operation may not be possible because the variance does not meet operational specifications.[2] Further, as will be shown with the following simulation and hardware results, the loop may actually have trouble maintaining phaselock at SNR's in the threshold region.

6.5 Simulation Results

To verify that the numerical results for the 8PSK and 16PSK variance of the phase error were correct, simulations of the loop's operation were conducted. These simulations were conducted using the nonlinear baseband model of Figure 4-2. The code and raw data from the simulations are in Appendix G. The BPSK and

[2]A variance of -35 db-radians^2 represents an approximate RMS jitter of 1° while -25.6 db-radians^2 corresponds to about 3°.

QPSK simulation data match the theoretical results and thus confirm the simulation technique is accurate. The 8PSK and 16PSK simulation results are therefore assumed to be correct and indeed they confirm the numerical approach of calculating the variance is accurate when they are plotted together.

The simulation data are shown in the following 12 plots. The first three plots, Figures 6-6, 6-7, and 6-8, are for BPSK at three different high-SNR loop bandwidth-to-symbol rate ratios. Note, once again, that the reference here to high-SNR loop bandwidth corresponds to the case where the phase detector gain is unity. This loop bandwidth can also be referred to as the "design" loop bandwidth in that the classical loop design parameters are the operational parameters only at high-SNR's. The selected loop bandwidths were chosen to match the available hardware configurations. The simulation data are plotted with a 95% confidence interval.

Figures 6-9, 6-10, and 6-11 are for QPSK at the same design loop bandwidths as BPSK. Following these are Figures 6-12, 6-13, and 6-14 for 8PSK and Figures 6-15, 6-16, and 6-17 for 16PSK all reflecting the same bandwidths as that of BPSK and QPSK.

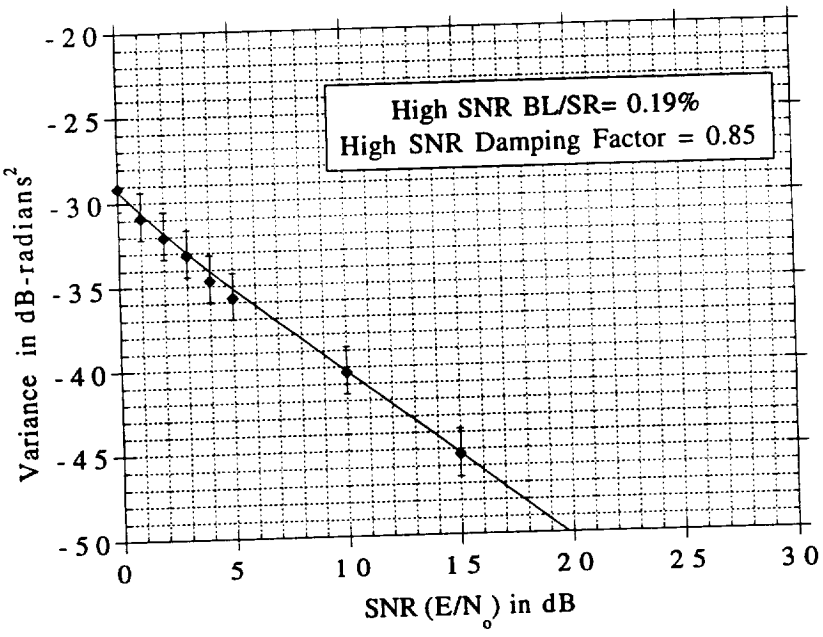

Figure 6-6 BPSK variance of phase error theoretical and simulation data.

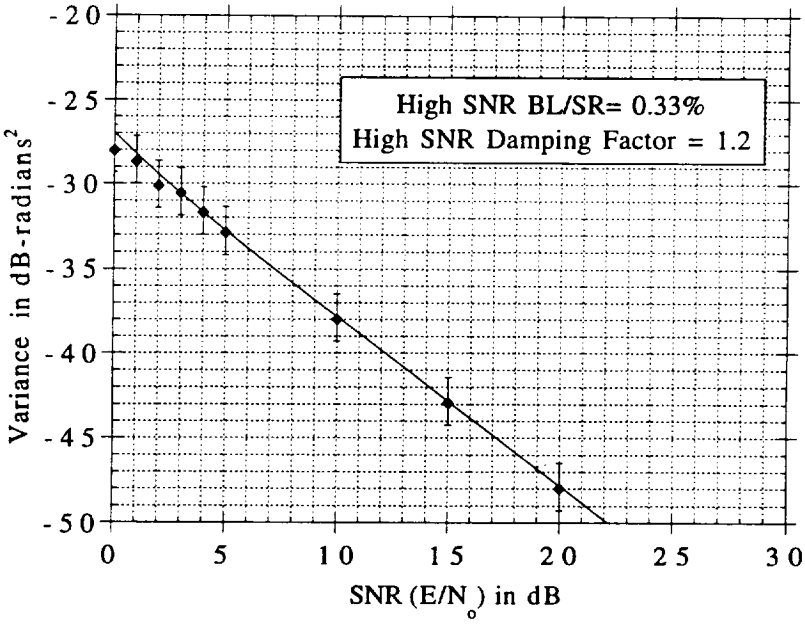

Figure 6-7 BPSK variance of phase error theoretical and simulation data.

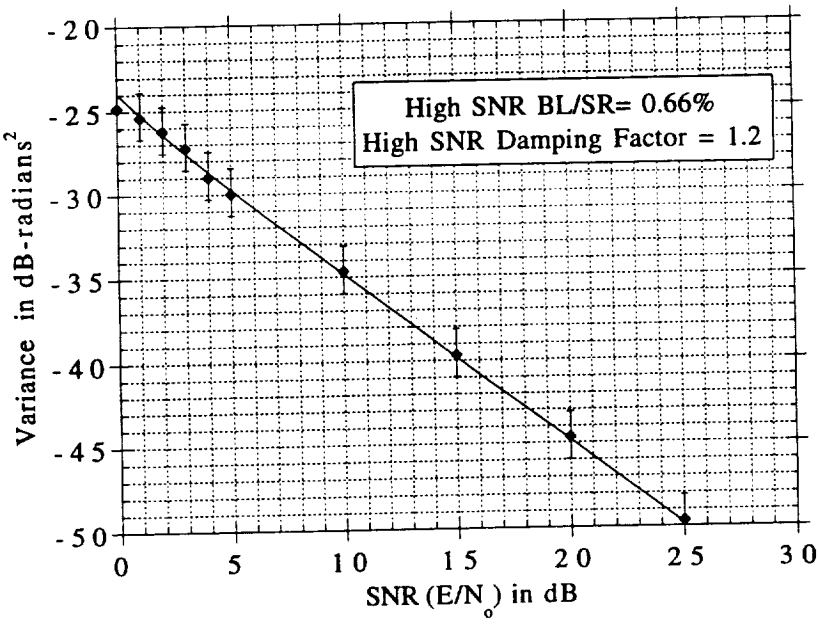

Figure 6-8 BPSK variance of phase error theoretical and simulation data.

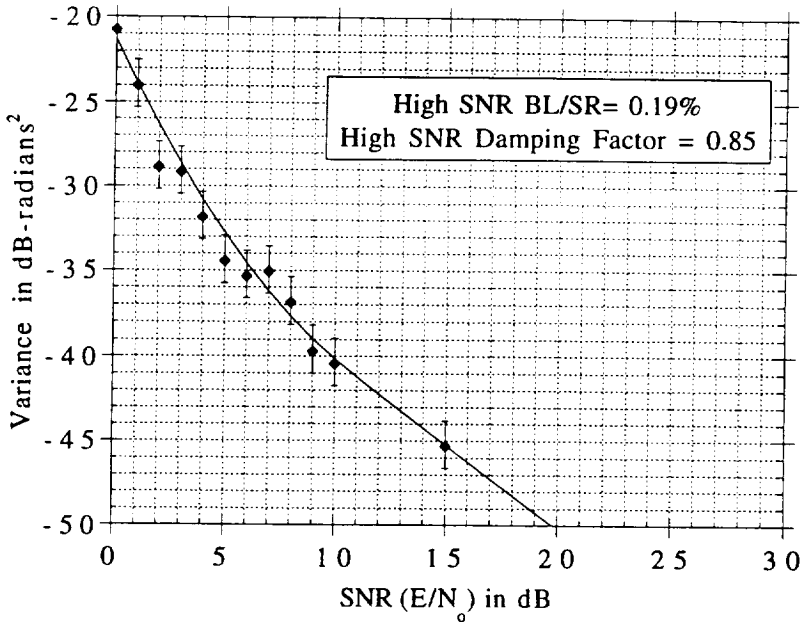

Figure 6-9 QPSK variance of phase error theoretical and simulation data.

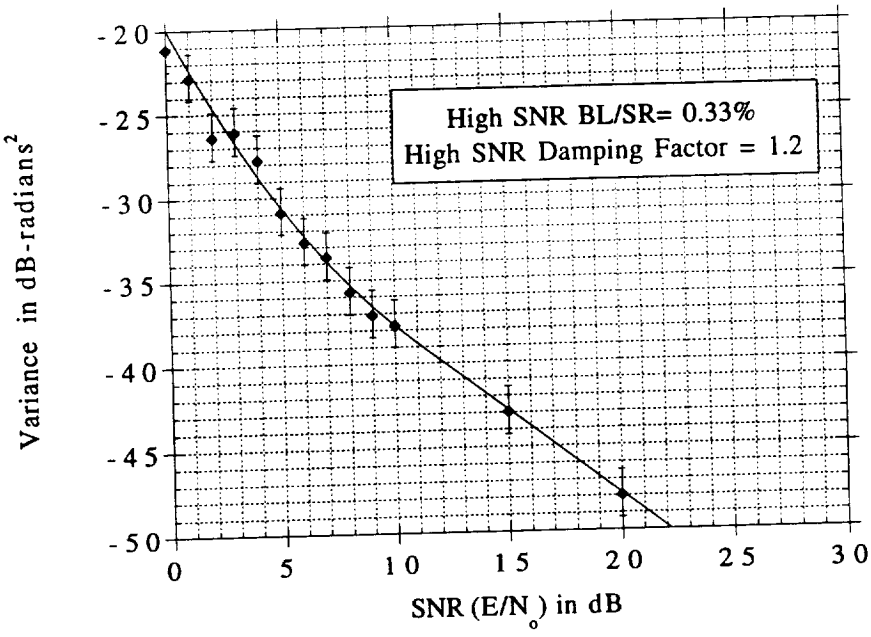

Figure 6-10 QPSK variance of phase error theoretical and simulation data.

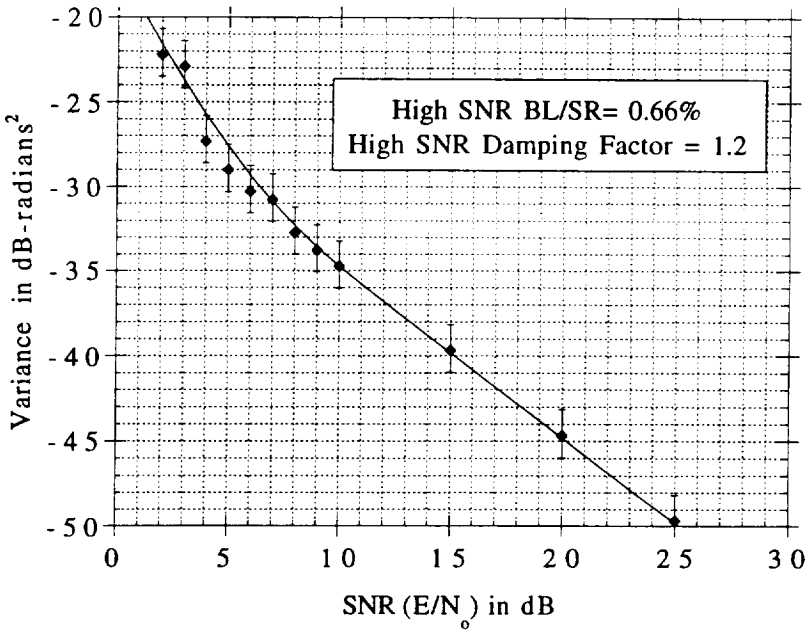

Figure 6-11 QPSK variance of phase error theoretical and simulation data.

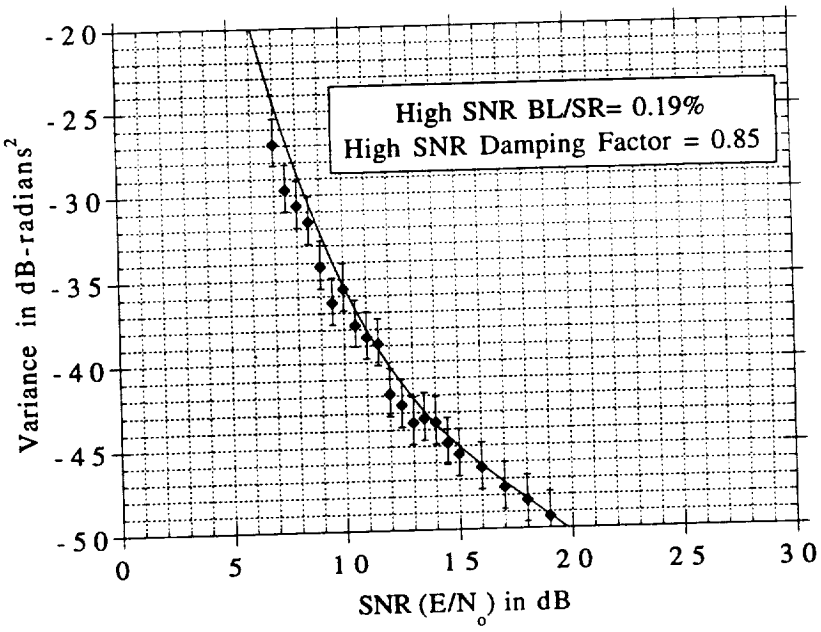

Figure 6-12 8PSK variance of phase error numerical and simulation data.

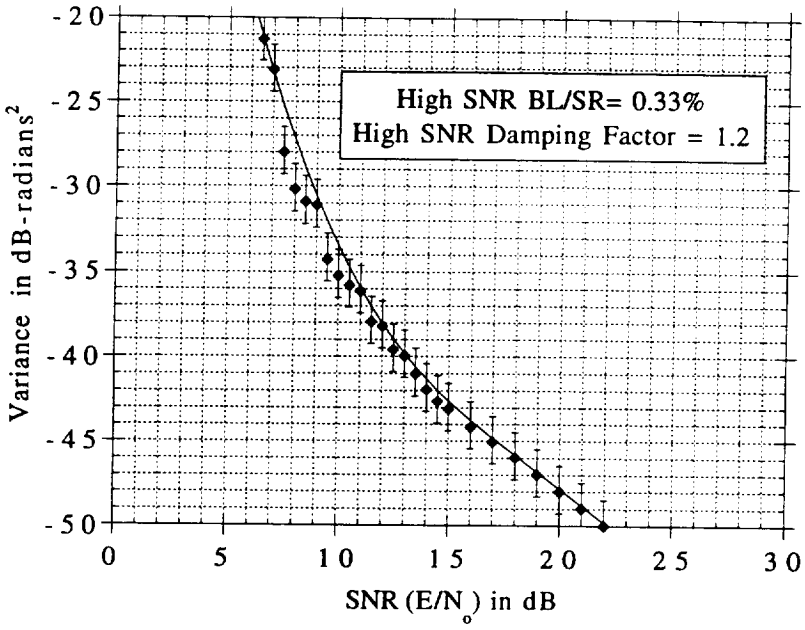

Figure 6-13 8PSK variance of phase error numerical and simulation data.

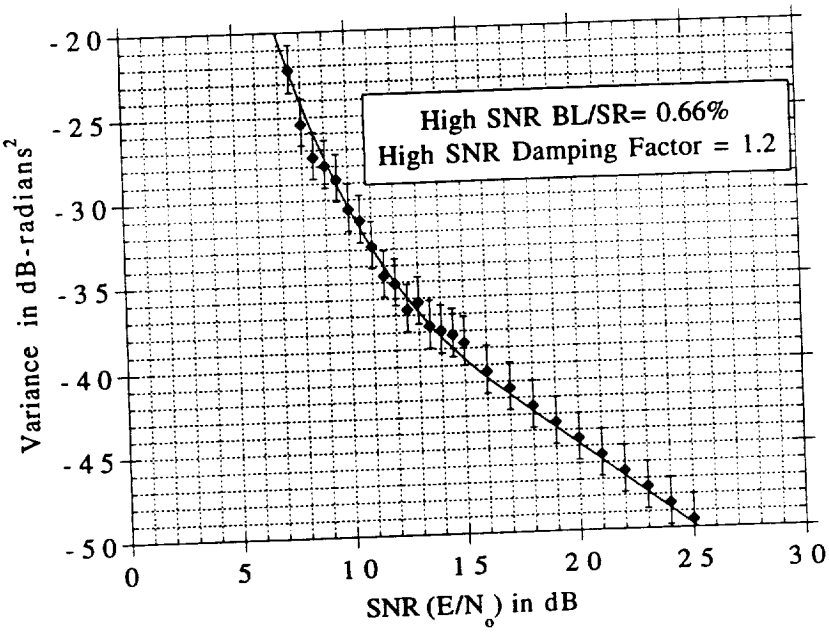

Figure 6-14 8PSK variance of phase error numerical and simulation data.

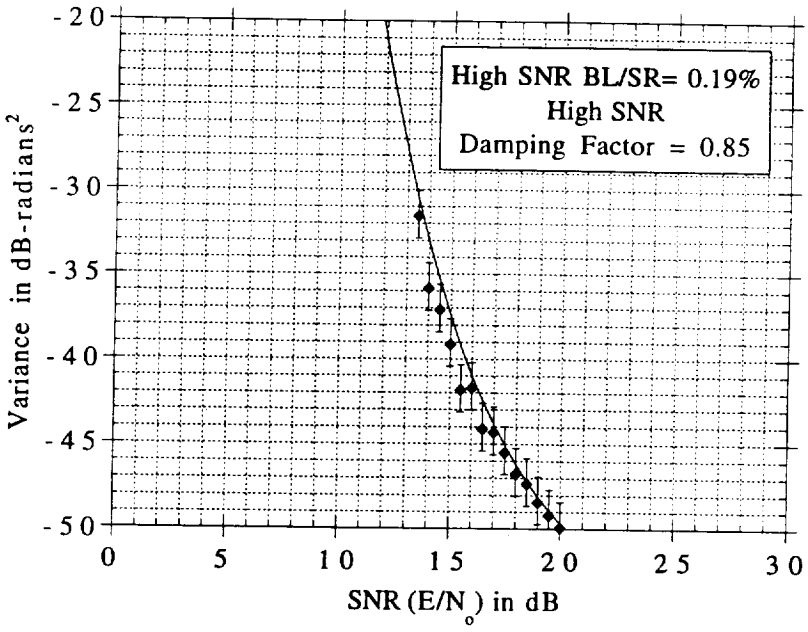

Figure 6-15 16PSK variance of phase error numerical and simulation data.

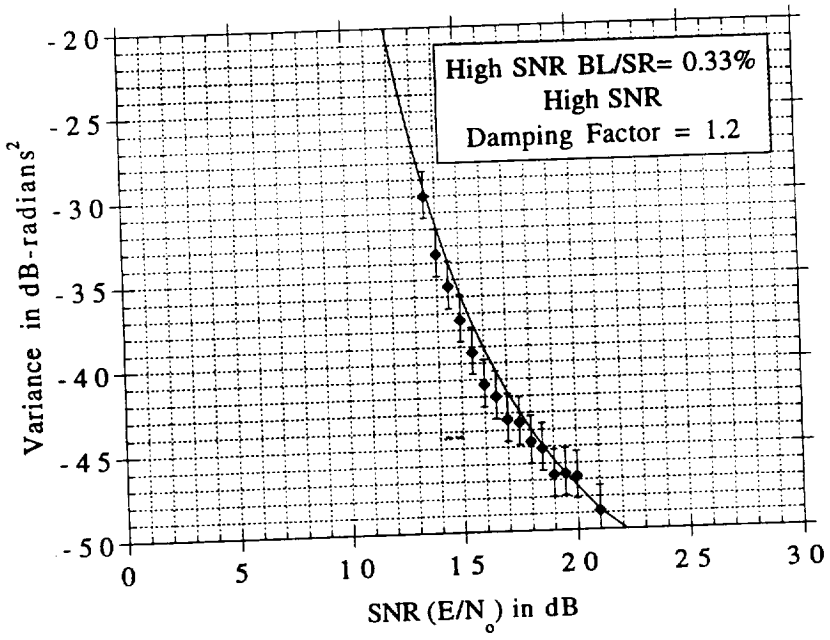

Figure 6-16 16PSK variance of phase error numerical and simulation data.

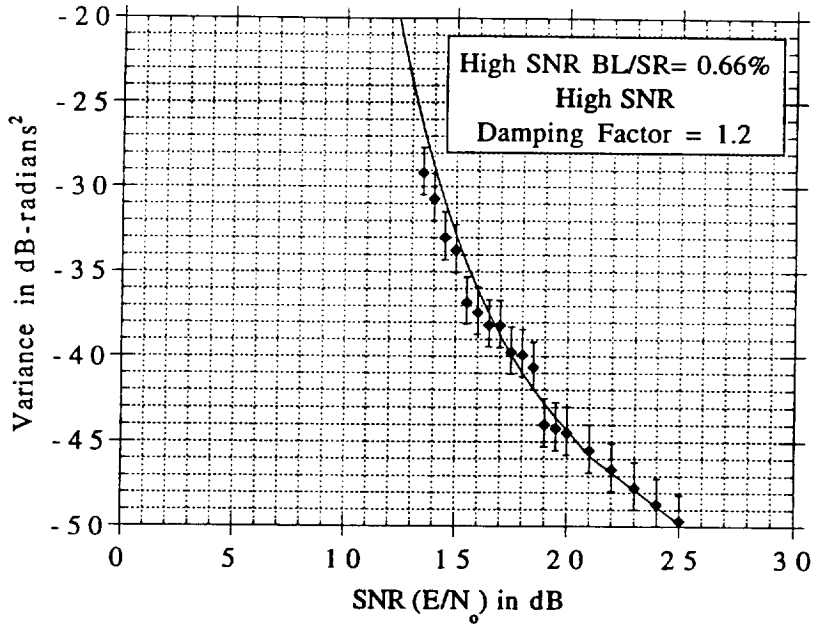

Figure 6-17 16PSK variance of phase error numerical and simulation data.

6.6 Hardware Results

As a third means of quantifying the variance of the phase error an MPSK high-SNR carrier tracking loop was constructed in hardware. The hardware has limits on the operational parameters it can support. It only has 64 loop bandwidth configurations. A specific loop bandwidth is selected by controlling the gains in the loop. Three of these bandwidths were selected over the range of operation of the hardware. They are the bandwidths used for the simulations mentioned in Section 6.5. The next 12 plots are the

hardware results for the variance of phase error. As with the simulations they are presented in sequence for each modulation scheme. The BPSK data are plotted in Figures 6-18, 6-19, and 6-20 and the QPSK data in Figures 6-21, 6-22, and 6-23. Figures 6-24, 6-25, and 6-26 are the 8PSK data and Figures 6-27, 6-28, and 6-29 are the 16PSK data. These data are tabulated in Appendix H along with a discussion of the hardware operation.

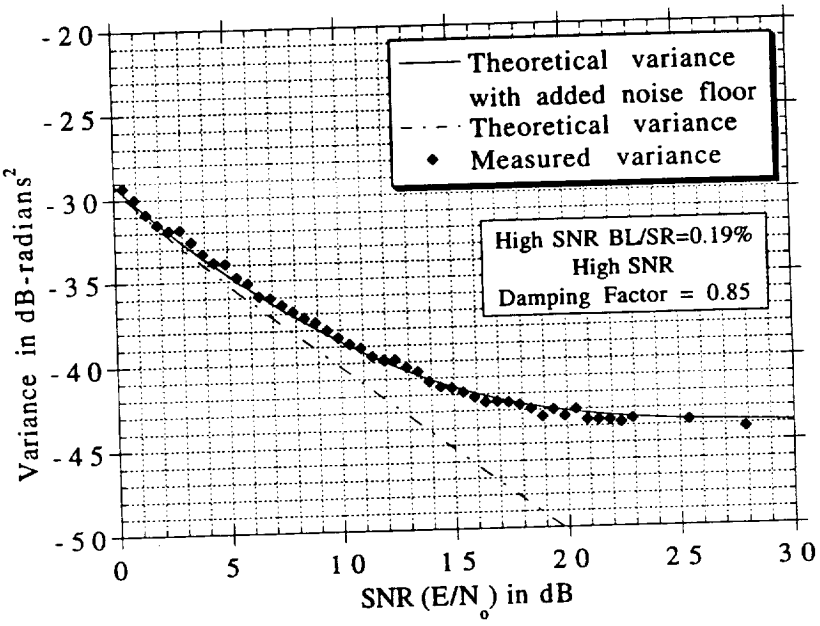

Figure 6-18 BPSK variance of phase error theoretical and measured data.

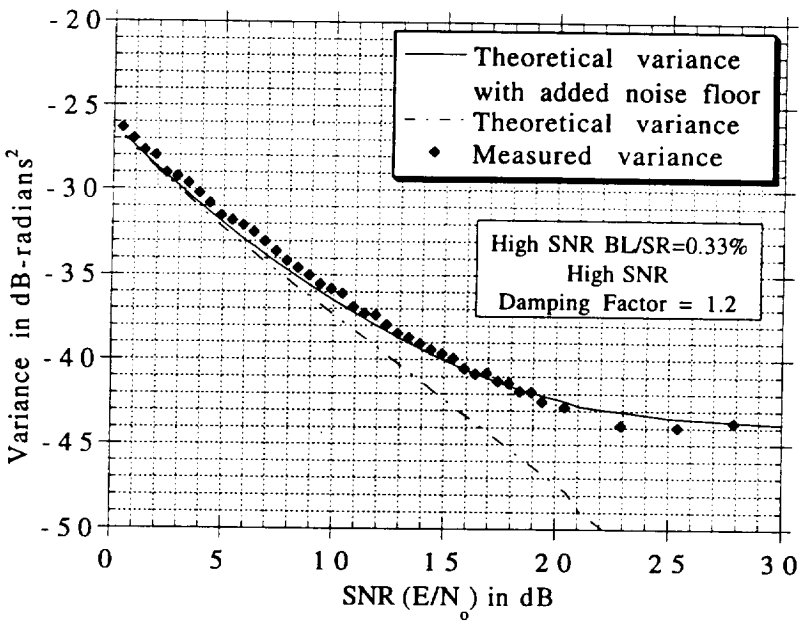

Figure 6-19 BPSK variance of phase error theoretical and measured data.

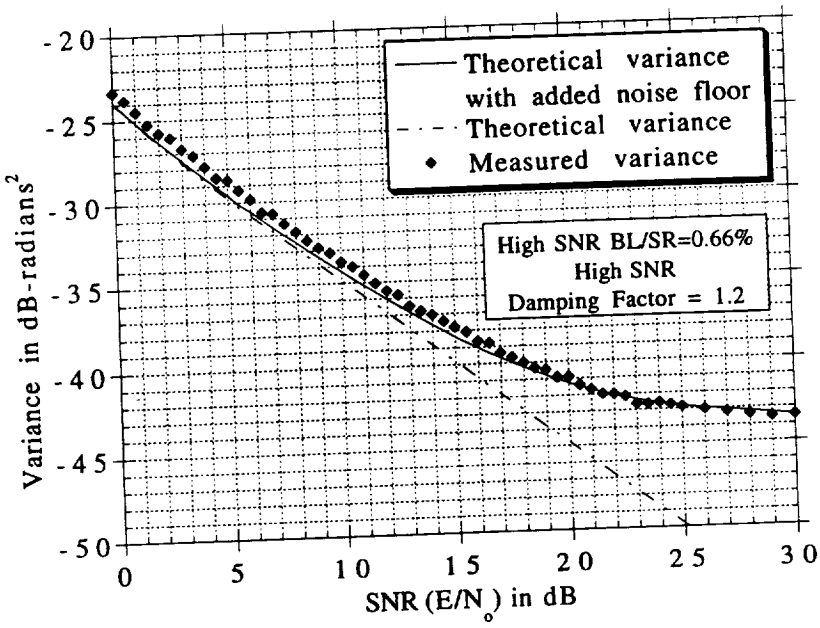

Figure 6-20 BPSK variance of phase error theoretical and measured data.

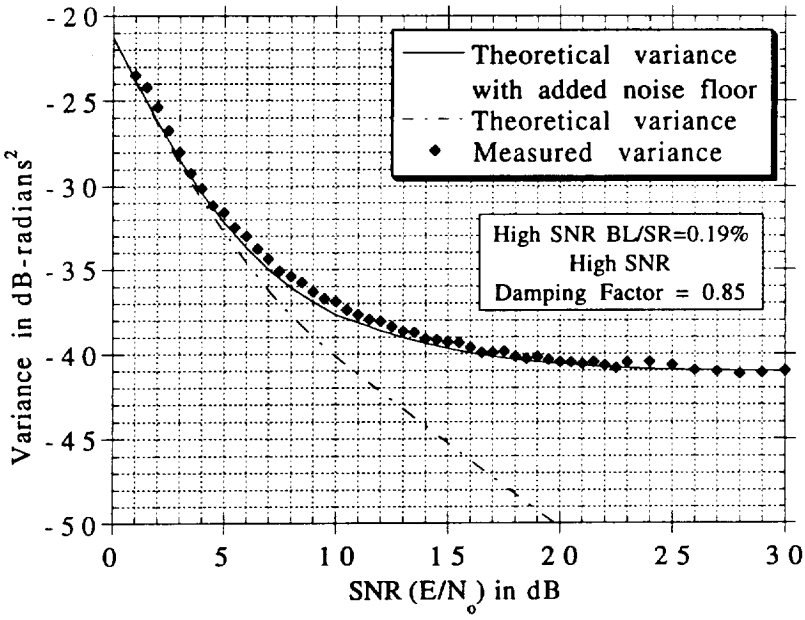

Figure 6-21 QPSK variance of phase error theoretical and measured data.

C-3.

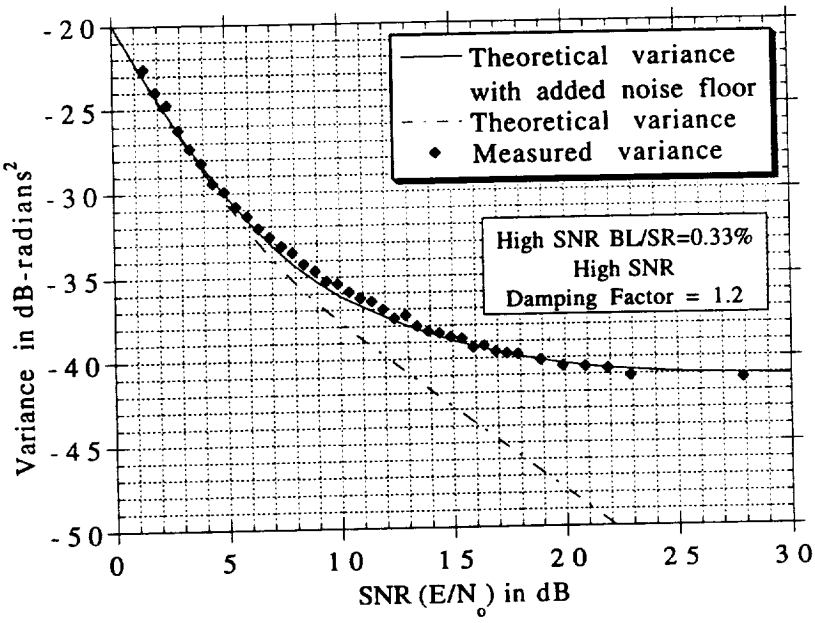

Figure 6-22 QPSK variance of phase error theoretical and measured data.

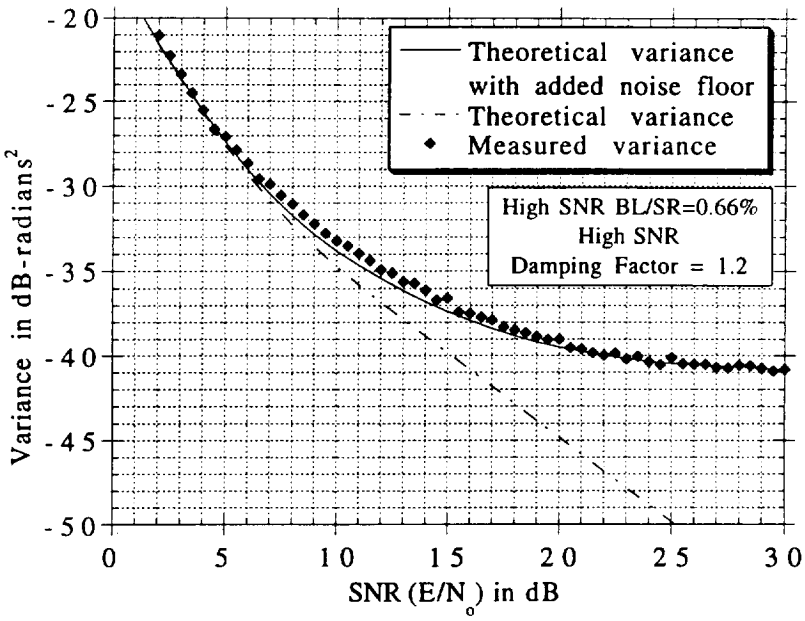

Figure 6-23 QPSK variance of phase error theoretical and measured data.

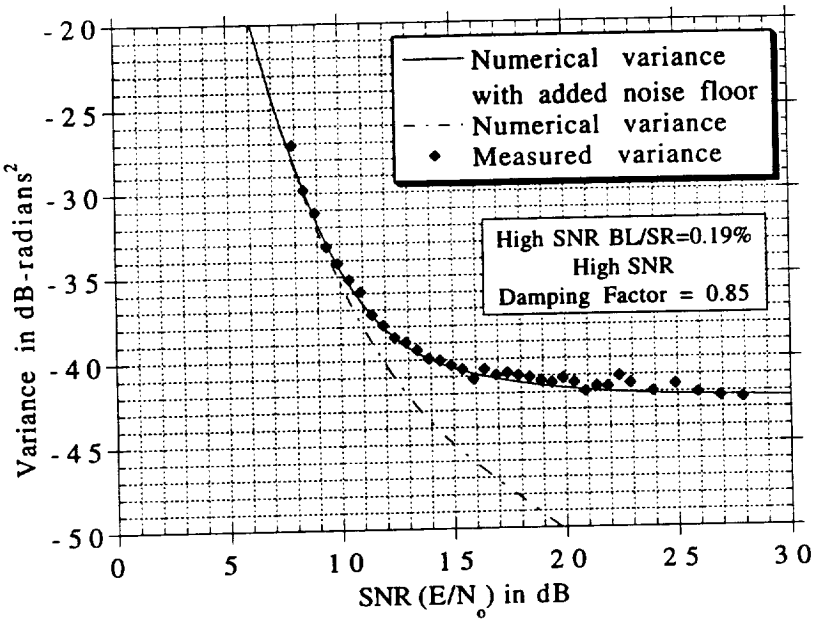

Figure 6-24 8PSK variance of phase error numerical and measured data.

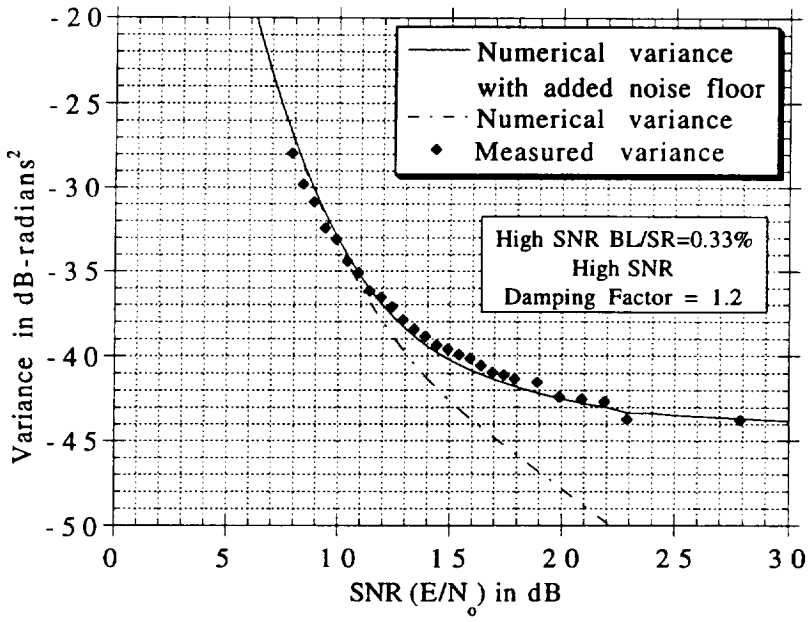

Figure 6-25 8PSK variance of phase error numerical and measured data.

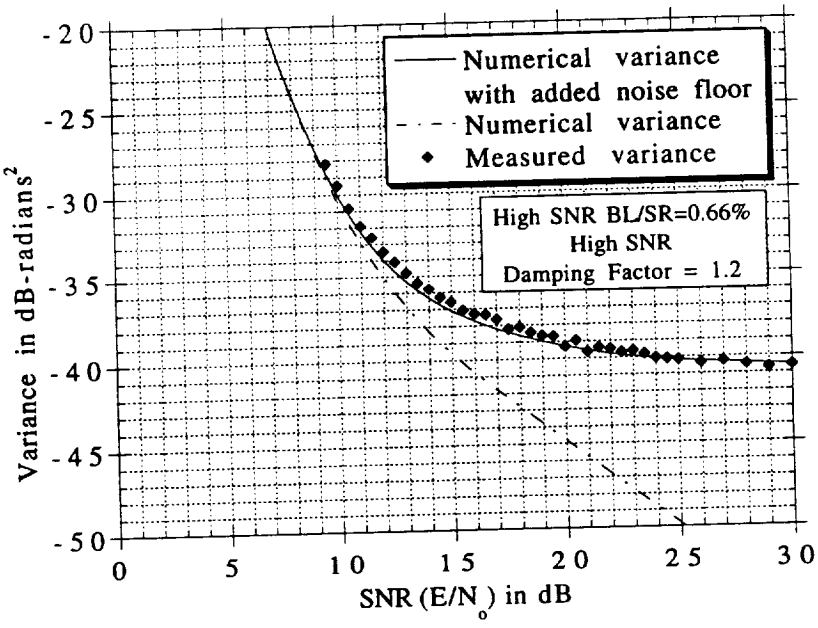

Figure 6-26 8PSK variance of phase error numerical and measured data.

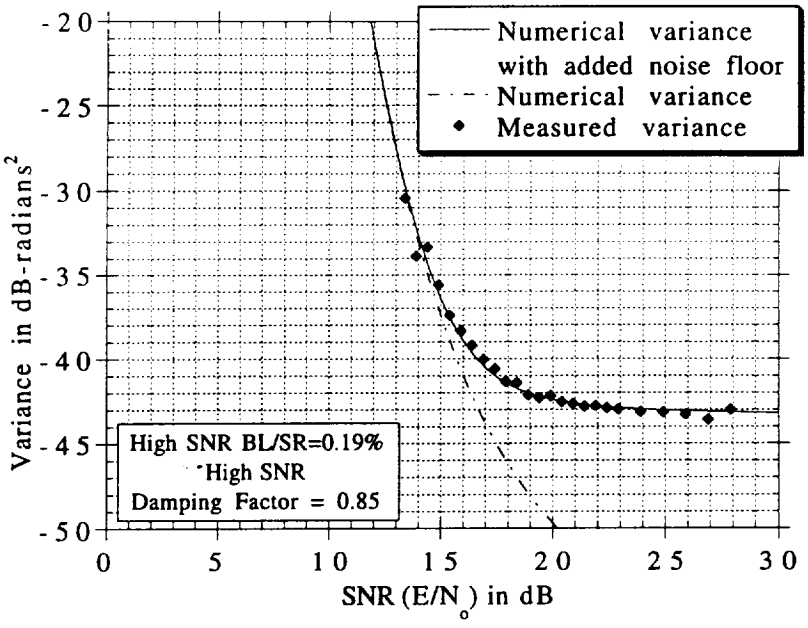

Figure 6-27 16PSK variance of phase error numerical and measured data.

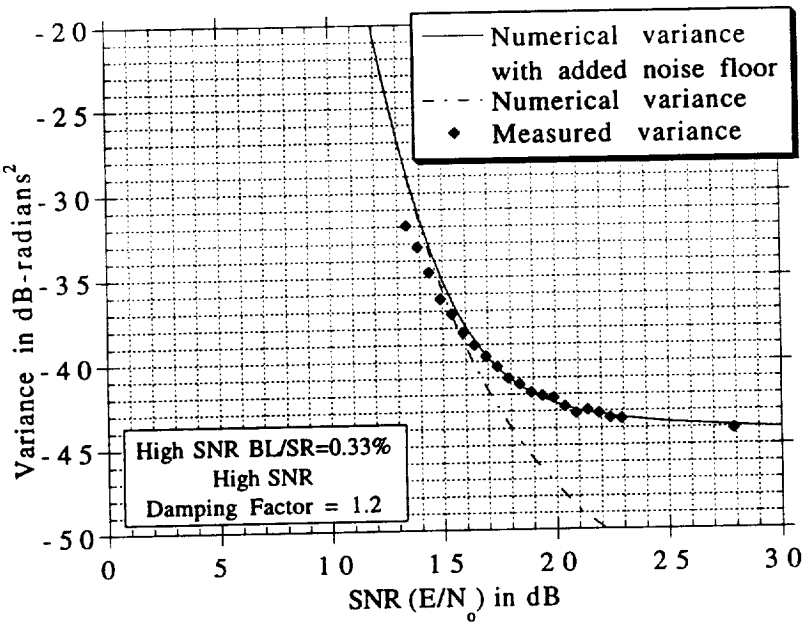

Figure 6-28 16PSK variance of phase error numerical and measured data.

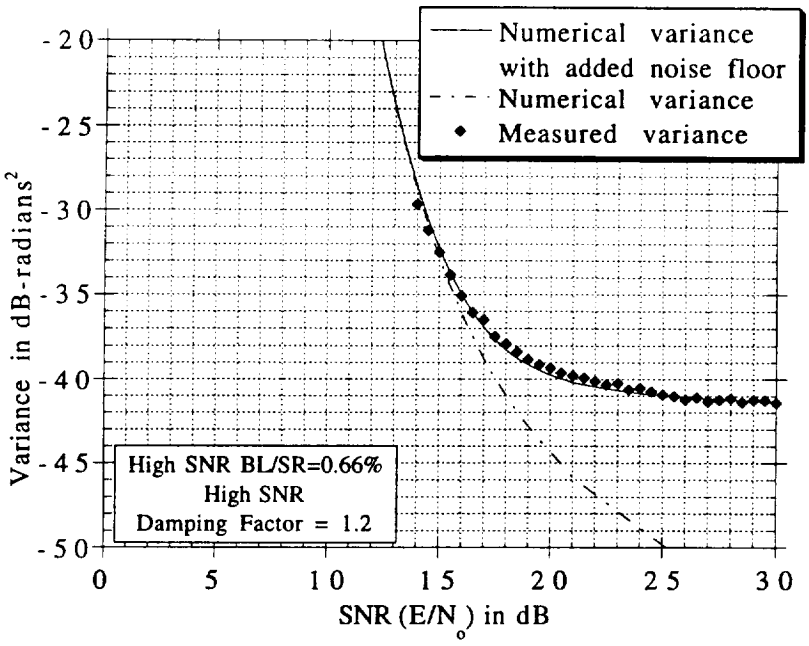

Figure 6-29 16PSK variance of phase error numerical and measured data.

6.7. Discussion Of The Simulation And Hardware Results

As the simulation and hardware data plotted in Figures 6-6 through 6-29 indicate there is substantial verification of the numerical approach used to calculate the variance of the phase error. With the exception of a few samples, all of the simulation data is within a 95% confidence interval of the theoretical and numerical solutions of the phase error variance. Before the validity of the hardware results can be discussed, an interesting phenomena in that data must be addressed. This phenomena is the minimum measured phase jitter that is represented by the flair in the hardware variance curves.

The presence of a phase jitter floor makes sense when it is considered that the hardware cannot obtain infinitely small variance of phase error data. There are several causes for this. First, the NCO uses direct digital synthesis to create its sinusoid outputs. As such it cannot exactly recreate the desired frequency. Related to this is the minimum phase error that will cause the minimum possible error signal to be created at the output of the EPROM's. This minimum error is approximately 0.5° measured along the constellation circle from the I or Q axis. There is the added affect of the variance measuring device, i.e., the modulation analyzer. This device digitizes the I and Q analog baseband data to creates samples that are then used to calculate the variance.

This variance noise floor in the hardware data dominates the results at high-SNR's only. At low SNR's the variance in the phase error data is accurately reflecting the mechanism of interest, i.e., the overall loss in performance due to making incorrect data decisions in the carrier tracking loop. When the MPSK theoretical and numerical data are "corrected" to account for the phase noise floor present in the hardware the results are accurate at all SNR's.

One last noted characteristic that is present in the 8PSK and 16PSK data from both the simulation and the hardware results is a minimum SNR below which phaselock cannot be maintained. While quantifying this phenomenon analytically requires an in-depth study of non-linear loop operation, some conclusions can be drawn from the simulation and hardware results since they are not affected by the constraints of linear analysis.

In the plots of simulation data and hardware data for 8PSK and 16PSK, the lowest SNR at which a data point is plotted represents the minimum SNR for which phaselock can be maintained. The striking result in this data is that the SNR where phaselock terminates seems to be a weak function of loop bandwidth and a strong function of SNR. For both 8PSK and 16PSK the simulation and hardware data cover a 5.4 dB range of high-SNR loop bandwidth-to-symbol rate ratios (from 0.19% to 0.66%). However, the phaselock threshold moves at most 1.6 dB for the

8PSK hardware results and not at all for the 16 PSK simulation results.

Chapter 7

CONCLUSIONS

"Thinking makes it so."

William Shakespeare
dramatist and poet, 1564-1616

7.1. Discussion

Quantifying the phase error variance of the carrier reference in an 8PSK or 16PSK receiver utilizing the high-SNR approximation to MAP estimation in a carrier tracking feedback loop was the motivating problem behind this research effort. This was accomplished by three different methods, including theoretical and numerical analysis, simulation, and laboratory hardware testing. All of these methods first required an understanding of the phase error variance and its origins. Chapter 2 is a discussion of what phase error variance is in a simple phaselock loop. This information alone is insufficient to understand the phase error variance in the phaselock loop of interest since it is a loop that tracks a DSB-SC MPSK signal as opposed to a CW carrier. The mechanism utilized to track the DSB-SC MPSK signal is an approximation to the optimum solution in the MAP sense. This approximation, i.e., the high SNR approximation, is a commonly employed and studied technique as outlined in Chapter 1. Chapter 3 provides a discussion of the MAP estimator approach and the

high-SNR approximation approach to estimating carrier phase. Riter and Hon [26] have previously discussed the optimum MAP estimator for BPSK while Simon [32] discussed the optimum MAP estimator for QPSK and 8PSK. Simon also presented the high-SNR loop structure for MPSK. The 16PSK MAP estimator solution is presented here in this research effort following the approach of Simon. Using the integro-differential equation for the high-SNR loop, the MPSK variance of phase error was derived in Chapter 4. The technique utilized for this follows the classical approach (see Chapter 2) and was verified by the QPSK variance of phase error derivations of Lindsey and Hinedi [35].

Quantifying the variance of phase error for the BPSK and QPSK high SNR loop has been accomplished [37, pg. 91][35] using the independence of the quadrature data estimates on their respective orthogonal noise components. Because of only recent increased interest in 8PSK and 16PSK and because the above-mentioned independence does not exist for these M>4 PSK schemes, the variance of phase error had not previously been quantified for M>4 in the high-SNR loop. The exact problem concerned the calculation of two components of the phase error variance, namely, the variance of the equivalent noise in the loop and the phase detector gain. A third previously uncalculated component of the phase error variance, the loop bandwidth, is a function of the phase detector gain. In Chapter 5 the calculation of all three of these components is accomplished. The approach is

verified using the previously published BPSK and QPSK results mentioned above. This theoretical analysis and set of numerical solutions represented the first method used to obtain the variance of phase error for 8PSK and 16PSK. The resultant data are shown in Chapter 6.

Simulations of the high-SNR loop were conducted to verify the results of the numerical solutions for 8PSK and 16PSK. The nonlinear baseband model of the loop was utilized in these simulations and the method verified by first simulating BPSK and QPSK. This second method of obtaining the variance data confirms that the numerical solutions for the components of the phase error variance and the variance itself are accurate.

The third method of obtaining variance of phase error data is in some ways the most important. An MPSK carrier tracking loop was constructed in hardware and used to obtain laboratory measurements of the variance of phase error. This is actual performance data as opposed to either analysis or simulation data. The hardware environment was designed so that the variance measurements reflected, as closely as possible, only the effects studied in this research. This was accomplished by removing other unknowns from the test configuration that would influence the variance such as symbol timing jitter, intersymbol interference, and received signal automatic gain control jitter. As the results of Chapter 6 and the discussion of Appendix H indicate, the hardware data verified both the numerical and simulation results.

Having quantified and verified the phase error variance for 8PSK and 16PSK and having plotted it as a function of both SNR and loop bandwidth it was possible to draw certain conclusions. Chapter 6 contains a discussion of these observations and so they are only summarized here.

The data show that at high SNR's the variance is directly related to both the SNR and loop bandwidth and can be obtained by the use of the approximation in (6-9). It should be noted that this form of the equation for variance closely follows the equation for variance of the basic PLL, namely (2-52). In fact equating the IF bandwidth to the symbol rate yields an exact match. This follows esoterically, too, when it is considered that at high SNR's the high-SNR MPSK loop makes good data decisions and produces an error signal that exactly matches that of the basic PLL. It is at low SNR's that the variance performance of the high-SNR MPSK loop is poorer than that of the basic PLL.

At low SNR's the variance begins to increase more rapidly than the SNR decreases. Further the high-SNR trade-off between loop bandwidth and SNR is degraded. Another interesting phenomenon is that the SNR location at which the variance begins to increase rapidly, the threshold region, cannot be moved appreciablely by a judicious narrowing of the high-SNR design loop bandwidth. The data also demonstrate that the location of the thresholding region may cause difficultly in systems attempting to use M>4 PSK schemes if operation is power limited. For 8PSK this

threshold occurs at an SNR of about 8dB and for 16PSK it occurs at about 15dB. A case in point is that of NASA's TDRSS BPSK/QPSK links. Typically they operate with SNR's on the order of 10 dB. If 8PSK is employed, as is being considered at this time, and the high-SNR loop structure is utilized, not only may the variance be excessive but the simulation and hardware data suggest that phaselock performance may be marginable. Further, this data suggests successful 16PSK operation would be unobtainable at 10 dB SNR.

Having considered some of these unique characteristics of the 8PSK and 16PSK variance of phase error data, quantified in this study, it is clear that coherent receiver design for these schemes must include a thorough analysis of the carrier tracking loop to be implemented. The high-SNR approximation is a popular choice, however, operation may not be possible if relatively high SNR conditions are not available. Designs involving the use of coded M-ary PSK schemes to increase performance in limited channels are a prime example.

7.2. Where To Next?

The use of the high-SNR approximation is just that: an approximation. The first obvious solution to improving the variance performance is to study the use of the optimum MAP estimator itself. It may yield superior performance at the SNR's of

interest and push the threshold region to the left, i.e., to a lower SNR. Further, the barrier to implemention, namely analog hardware construction of hyperbolic operators, no longer exists, since digital receivers are now commonplace. In point of fact, this is exactly the research avenue being pursued by the telecommunications department at NMSU. Early results suggest that there is a small performance increase in using the optimum MAP estimator for 8PSK [42].

Another option for possibly increasing the performance of the M>4 PSK receiver is to use coding to increase the performance of the data estimators. This was suggested for 8PSK by Ungerboeck [43]. Since the location of the threshold region is indirectly traceable to making bad data decisions, if the data decision process can be improved by coding gain, then the threshold region should move to the left. This idea is particularly attractive for systems where coding is already being employed, e.g., 8PSK and 16PSK TCM. Care must be exercised in utilizing this option to ensure that loop stability is not compromised by the required delay inherent in making estimates with such schemes.

Another area of interest in these loops that warrants study is the acquisition process. Several factors make the M>4 loops particularly attractive for study in this regard. First, the number of stable phaselock points in the constellation increases with M. In fact, there are M phaselock points in an MPSK carrier tracking feedback loop. It is also true that there are M unstable points that

generate zero phase error. It follows that the maximum phase error that can be tolerated drops with increasing M.

Another important factor in the acquistion process is the loop bandwidth. It has a strong relationship to acquistion parameters such as mean-time-between-cycle slips and, as was demonstrated, the loop bandwidth is narrowed as the SNR drops. Other factors, such as lock-in range and hold-in range, would also be affected since the loop bandwidth is changing.

REFERENCES

[1] Davis, John H., Dinn, Neil F., and Falconer, Warren E., "Technologies for Global Communications," *IEEE Comm. Mag.*, Vol. 30 No. 10, Oct. 1992.

[2] "The INTELSAT Global Satellite System," *Progress in Astronautics and Aeronautics,* Vol. 93, 1984, pps. 135-164.

[3] Osborne, Jack, Second NASA TDRS ground station, *Personal Communication,* Jan. 7, 1994.

[4] Carden, F., and Kopp, B., "A Quantized Euclidean Soft-Decision Maximum Likelihood Sequence Decoder for TCM," presented at MILCOM 1988.

[5] Fung, A., and McLane, P., "Phase Jitter Sensitivity of Rotationally Invariant 8 and 16 Point Trellis Codes," presented at IEEE GLOBECOM 1988.

[6] Deng, R. H., and Costello, D. J., "High Rate Concatenated Coding Systems Using Multidimensional Bandwidth-Efficient Trellis Inner Codes," *IEEE Trans. Commun.*, vol. COM-37, October 1989.

[7] Pietrobon, S. S., Deng, R. H., Lafanechere, A., Ungerboeck, G., and Costello, D. J., "Trellis-Coded Multidimensional Phase Modulation," *IEEE Trans. Inform Theory.*, vol. IT-36, January 1990.

[8] Dehesh, H., Kerr, R., and Viterbi, A. J., "Practical Applications of TCM," presented at IEEE MILCOM 1990.

[9] Ross, M., Carden, F., Osborne, W., "Pragmatic Trellis Coded Modulation: A Simulation Using 24-Sector Quantized 8-PSK," presented at IPCCC 1991.

[10] Fines, P., and Aghvami, A. H., "Performance Evaluation of High Level Coded Modulation Techniques over Satellite Channels," presented at IEEE GLOBECOM 1992.

[11] Ross, M., Osborne, W., Carden, F., and Stolarczyk, J. L., "Pragmatic Trellis Coded Modulation: A Hardware Implementation Using 24-Sector 8-PSK," presented at SUPERCOMM/ICC 1992.

[12] Carden, F., Ross, M., Osborne, W., and Kopp, W., "Fast TCM Decoding: Phase Quantizing and Integer Weighing," *IEEE Trans. Commun.*, Publication date TBD.

[13] Irshid, M. L., and Salous, I. S., "Bit Error Probability for Coherent M-ary PSK Systems," *IEEE Trans. Commun.*, vol. COM-39, March 1991.

[14] Yung, W., "Probability of Bit Error for MPSK Modulation with Diversity Reception in Rayleigh Fading and Log-Normal Shadowing Channel," *IEEE Trans. Commun.*, vol. COM-38, July 1990.

[15] Costas, J. P.,"Synchronous Communications," *Proc. of the IRE,* vol. 44, December 1956.

[16] Cowley, W. G., "Synchronization Algorithms for Digital Modems," presented at the 1989 Australian Symp. on signal processing and applications,Adelaide, Australia.

[17] Bingham, J. A. C., The Theory and Practice of Modem Design, John Wiley & Sons, New York, 1988.

[18] Leclert, A., and Vandamme, P., "Universal Carrier Recovery Loop for QASK and PSK Signal Sets," *IEEE Trans. Commun.,* vol. COM-31, January 1983.

[19] Lehan, F. W., and Parks, R. J., "Optimum Demodulation," presented at the IRE Convention, 1953.

[20] Thomas, J. B., and Wong, E., "On the Statistical Theory of Optimum Demodulation," *IRE Trans. Inform Theory.,* vol. IT-6, September 1960.

[21] Van Trees, H. L., "The Structure of Efficient Demodulators for Multidimensional Phase Modulated Signals," *IEEE Trans. Commun.,* vol. CS-11, September 1963.

[22] Viterbi, A. J., "Optimum Detection And Signal Selection For Partially Coherent Binary Communication," presented at WESCON 1964.

[23] Van Trees, H. L., "Analog Communication over Randomly-Time-Varying Channels," presented at WESCON 1964.

[24] Viterbi, A. J., *Principles of Coherent Communication,* McGraw-Hill, New York, 1966.

[25] Snyder, D. L., "The State-Variable Approach to Analog Communications Theory," *IEEE Trans. Inform Theory.*, vol. IT-14, January 1968.

[26] Riter, S., and Hon., W., "Practical Phase Reference Detectors For Fully Modulated PSK Signals," presented at EASCON, 1968.

[27] Riter, S., "An Optimum Phase Reference Detector for Fully Modulated Phase-Shift Keyed Signals," *IEEE Trans. Aerosp. Electron. Syst.*, vol. AES-5, July 1969.

[28] Lindsey, W. C., "Data-Aided Carrier Tracking Loops," *IEEE Trans. Commun.*, vol. COM-19, April 1971.

[29] Lindsey, W. C., and Simon, M. K., *Telecommunication Systems Engineering,* Prentice-Hall, Englewood Cliffs, NJ, 1972.

[30] Simon, M. K., and Lindsey, W. C., "Optimum Performance of Suppressed Carrier Receivers with Costas Loop Tracking," *IEEE Trans. Commun.*, vol. COM-25, February 1977.

[31] Simon, M. K., "Optimum Receiver Structures for Phase-Multiplexed Modulations," *IEEE Trans. Commun.*, vol. COM-26, June 1978.

[32] Simon, M. K., "Further Results on Optimum Receiver structures for Digital Phase and Amplitude Modulated Signals," presented at ICC 1978.

[33] Booth, R. W., "An Illustration of the MAP Estimation Method for Deriving Closed-Loop Phase Tracking Topologies: The MSK Signal Structure," *IEEE Trans. Commun.*, vol. COM-28, August 1980.

[34] Franks, L. E., "Carrier and Bit Synchronization in Data Communication - A Tutorial Review," *IEEE Trans. Commun.*, vol. COM-28, August 1980.

[35] Hinedi, S., and Lindsey, W., "On the Self-Noise in QASK Decision-Feedback Carrier Tracking Loops," *IEEE Trans. Commun.*, vol. COM-37, April 1989.

[36] Hinedi, S., and Lindsey, W., "Intersymbol Interference Effects on BPSK and QPSK Carrier Tracking Loops," *IEEE Trans. Commun.*, vol. COM-38, October, 1990.

[37] Yuen, J. H., *Deep Space Telecommunications Systems Engineering,* Plenum Press, New York, 1983.

[38] Gardner, F. M., *Phaselock Techniques,* John Wiley & Sons, New York, 1979.

[39] Meyr, H., and Ascheid, G., *Synchronization in Digital Communications,* John Wiley & Sons, New York, 1990.

[40] Van Trees, H. L., *Detection, Estimation, and Modulation Theory,* John Wiley & Sons, New York, 1968.

[41] Parsons, R. D., and Wilson, S. G., "Polar Quantizing for Coded PSK Transmission," *IEEE Trans. Commun.,* vol. COM-38, September 1990.

[42] Paz, Robert, Electrical Engineering Dept., New Mexico State University, *Personal Communication,* February, 1994.

[43] Ungerboeck, G., "Channel Coding With Multilevel/Phase Signals," *IEEE Trans. Inform Theory.,* vol. IT-28, January 1982.

Appendix A

SIMULATION COMPARISON BETWEEN HIGH SNR MAP LOOP AND LECLERT & VANDAMME VARIATION

To assist in making the decision as to which type of tracking loop to consider for the study of phase error variance two loop designs were compared using 8PSK simulations of each. To compare the two loops they were simulated at the same loop bandwidth over a range of SNR's. A static loop bandwidth was maintained in each loop by varying the phase detector gain. These early simulations were written in C. The source code for the Leclert & Vandamme simulation is:

```
/*Leclert & Vandamme 8PSK simulation of carrier recovery
with fixed loop bandwidth-to-symbol rate ratio*/


#include <stdio.h>
#include <stdlib.h>
#include <math.h>

main()
{

/*declare system parameters*/

int k;                          /*discrete time variable*/
int m;                          /*discrete time variable*/
int j;                          /*discrete time variable*/
int s;                          /*discrete time variable*/
int n;                          /*discrete time variable*/
int i;                          /*discrete time variable*/
int uncore;                     /*discrete time variable*/
double errk;                    /*error signal out of phase
                                detector at time k*/

double phsk;                    /*received signal phase at time k*/
double refk1;                   /*phase of VCO at time k+1*/
double pdifk;                   /*phase difference between
```

```
                                received signal & VCO at time k*/
double ik;                      /*received value for I sample at
                                time k*/
double imk;                     /*generated I sample at time k*/
double qk;                      /*received value for Q sample at
                                time k*/
double qmk;                     /*generated Q sample at time k*/
double i1k;                     /*initial condition of filter
                                integrator at time k*/
double i2k;                     /*initial condition of VCO
                                integrator at time k*/
double a;                       /*inverse of the one pole filter
                                time constant, 3dB break point*/
double t;                       /*symbol period*/
double k0;                      /*the VCO slope in Hertz per Volt*/
double i1k1;                    /*hold variable for intial
                                condition, I1, at time k+1*/
double sum;                     /*averaging of phase detector
                                error*/
double wn;                      /*user entered natural freq.
                                of loop*/
double damp;                    /*damping factor*/
double bw;                      /*loop bandwidth*/
char dptr[10];                  /*string pointer for entering
                                floating point numbers*/
char pdgains[10];               /*string pointer for entering
                                floating point numbers*/
double endb;                    /*E(s)/N(o) in dB*/
double pdgain;                  /*phase detector gain*/
double phsfix;                  /*fixed initial phase*/
double sqrerr;                  /*running sum of squared phase
                                error refk1*/
double sumerr;                  /*running sum of phase error
                                refk1*/
double meanphs;                 /*mean of phase error*/
double varphs;                  /*variance of phase error*/

 static double pdgmx[8] = {1.5425, 2.5, 4.0, 5.7, 7.3, 8.1, 9.0, 10.0};

/*declare data generation parameters*/

int d;
double testd;

/*declare QPSK test parameters*/

double x1;
double x2;

/*declare phase detector variables. These will be moved into a
subroutine eventually*/
```

```
double rcvdp;          /*the phase of the received vector
                       whose components are ik and qk*/
double ihatk;          /*for this phase detector this is the
                       output from the circular
                       quantizer*/
double qhatk;          /*for this phase detector this is the
                       output from the circular
                       quantizer*/

double errkhold;
int count;

/*declare noise model parameters. sigma is the WGN standard
deviation. nik and nqk are the gaussian noise samples at time
k with mean zero and standard deviation sigma.*/

double sigma;
long xcon1;
long xcon2;
long x;
long y;
double sample1;
double sample2;
double nik;
double nqk;

/*declare  output file parameters*/

FILE *outfile;
char *modehold;
char *namehold1;

/*initialize file output parameters*/

modehold = "w";
namehold1 = "Vandam";
outfile = fopen(namehold1,modehold);

/*initialize  uniform RV seed for repeated tests*/

srand(2546);
y = 47; /*seed*/

/*initialize phase step*/

phsfix = 0.0;

/*input natural frequency, damping factor, and Es/No for
loop*/
```

```
printf("This is a second order carrier loop synchronizer
simulator\n");

printf("\n");

printf("Please enter the natural frequency of the loop
transfer function:\n");

printf("\n");

scanf("%s",dptr);

wn = strtod(dptr,NULL);

printf("\n");

printf("Now please enter the loop damping factor:\n");

printf("\n");

scanf("%s",dptr);

printf("\n");

damp = strtod(dptr,NULL);

printf("\n");

bw = wn*(damp + 1.0/(4.0*damp));

a = wn/(2*damp);

/*determine sample interval that is required to uncorrelate
phase error variance calculation*/

uncore = floor(3.1415927/wn/4.0);

/*initialize phase detector gain counter*/

i = -1;

printf("\n");
printf("The loop noise bandwidth is:  %f  Hz\n",bw);
printf("\n");
printf("The loop filter time constant is:  %f  sec\n",a);
printf("\n");
fprintf(outfile,"8-PSK reconstruction loop results\n");
fprintf(outfile,"\n");
fprintf(outfile,"Initial phase step = %f\n",phsfix);
fprintf(outfile,"\n");
fprintf(outfile,"Noise random seed = %ld\n",y);
```

```
fprintf(outfile,"\n");
fprintf(outfile,"wn = %f\n",wn);
fprintf(outfile,"\n");
fprintf(outfile,"damping factor = %f\n",damp);
fprintf(outfile,"\n");
fprintf(outfile,"The loop noise bandwidth is:  %f  Hz\n",bw);
fprintf(outfile,"\n");
fprintf(outfile,"The loop filter time constant is:  %f  sec\n",a);
fprintf(outfile,"\n");
fprintf(outfile,"The number of skipped samples for
correlation is:  %d \n",uncore);
fprintf(outfile,"\n");

/*begin simulation*/

for(j=10;j<=24;j=j+2)
{
i = i+1;
endb = j;
sigma = 1.0/sqrt(2.0*pow(10.0,endb/10.0));

/*initialize system parameters*/

i1k = 0.0;
i2k = phsfix;
refk1 = i2k;
t = 1.0;
errkhold = 0.0;
phsk = 0.0;
errk = 0.0;
xcon2 = 16807;              /*for RV generation*/
xcon1 = 2147483647;         /*for RV generation*/
sqrerr = 0.0;
sumerr = 0.0;
s = 0;
pdgain = pdgmx[i];
k0 = 2*damp*wn/pdgain;


for(k=0;k<40;++k)
{
for(m = 0;m<500;++m)
{
/*construct received phase, noise, and transmitted data*/
/*running variance calculation*/

        if (k > 19)
        {
                if (fabs(refk1) < 0.392699)
                {
                s =s + 1;
```

```
                sqrerr = sqrerr + refk1*refk1;
                sumerr = sumerr + refk1;
                }
        }

for(n=0;n<uncore;++n)
{

/*received phase*/

/*phsk = 0.001*k;*/

/*noise*/

/*      x = rand();
        y = rand();
        sample1 = (x/32767.0)*0.999999;
        sample2 = (y/32767.0)*0.999999;
*/
        x =ldiv(y,xcon1).rem;
        x=labs(x*xcon2);

        y =ldiv(x,xcon1).rem;
        y=labs(y*xcon2);

        sample1 = (x/2147483647.0)*0.999999;
        sample2 = (y/2147483647.0)*0.999999;

        nik = sigma*sqrt(-2.0*log(1.0-sample1))
*cos(2.0*3.14159265*sample2);
        nqk = sigma*sqrt(-2.0*log(1.0-sample1))
*sin(2.0*3.14159265*sample2);

        /*transmitted data*/

        d = rand();     /*d is now divided into 8 regions each
                        representing a possible xmitted symbol*/

        if(d  < 4096)
                {
                imk = 0.923879;
                qmk = 0.382683;
                }
        else if((d  >= 4096) && (d < 8192))
                {
                imk = 0.382683;
                qmk = 0.923879;
                }
        else if((d  >= 8192) && (d < 12288))
                {
                imk = -0.382683;
```

```
            qmk = 0.923879;
            }
        else if((d  >= 12288) && (d < 16384))
            {
            imk = -0.923879;
            qmk = 0.382683;
            }
        else if((d  >= 16384) && (d < 20480))
            {
            imk = -0.923879;
            qmk = -0.382683;
            }
        else if((d  >= 20480) && (d < 24576))
            {
            imk = -0.382683;
            qmk = -0.923879;
            }
        else if((d  >= 24576) && (d < 28672))
            {
            imk = 0.382683;
            qmk = -0.923879;
            }
        else
            {
            imk = 0.923879;
            qmk = -0.382683;
            }

/*end generation part of the simulation. this generated
information will be used for this value of the simulation
counter only*/

/*subtract the reference phase from the received phase*/

        pdifk = phsk - refk1;

/*calculate the received symbol values for I and Q based on
the generated data and noise and the phase difference pdifk*/

        ik = imk*cos(pdifk) - qmk*sin(pdifk) + nik;
        qk = imk*sin(pdifk) + qmk*cos(pdifk) + nqk;

/*Now implement a phase detector to generate a phase error
signal errk. This implementation performs a circular
quantization on I and Q followed by some algebra to develop
the error signal.*/

/*calculate the phase of the received vector. The atan2
function adjusts for the appropriate quadrant.*/

        rcvdp = atan2(qk,ik);
```

```
/*quantize rcvdp into ihatk and qhatk*/

        if ((rcvdp >= 0.0) && (rcvdp < 0.785398))

/* 0 <= rcvdp < Pi/4 */

                {
                ihatk = 0.923879;
                qhatk = 0.382683;
                }
        else if ((rcvdp >= 0.785398) && (rcvdp < 1.570796))

/* Pi/4 <= rcvdp < Pi/2 */

                {
                ihatk = 0.382683;
                qhatk = 0.923879;
                }
        else if ((rcvdp >= 1.570796) && (rcvdp < 2.356194))

/* Pi/2 <= rcvdp < 3Pi/4 */

                {
                ihatk = -0.382683;
                qhatk = 0.923879;
                }
        else if ((rcvdp >= 2.356194) && (rcvdp < 3.141593))

/* 3Pi/4 <= rcvdp < Pi */

                {
                ihatk = -0.923879;
                qhatk = 0.382683;
                }
        else if ((rcvdp < -2.356194) && (rcvdp >= -3.141593))

/* -3Pi/4 < rcvdp >= -Pi */

                {
                ihatk = -0.923879;
                qhatk = -0.382683;
                }
        else if ((rcvdp >=  -2.356194) && (rcvdp < -1.570796))

/* -Pi/2 > rcvdp >= -3Pi/4 */

                {
                ihatk = -0.382683;
                qhatk = -0.923879;
                }
```

```
        else if ((rcvdp >= -1.570796) && (rcvdp < -0.785398))

/* -Pi/4 > rcvdp >= -Pi/2 */

                {
                ihatk = 0.382683;
                qhatk = -0.923879;
                }
        else if ((rcvdp >= -0.785398) && (rcvdp < 0.0))

/* 0 > rcvdp >= -Pi/4 */

                {
                ihatk = 0.923879;
                qhatk = -0.382683;
                }

/*calculate the phase error errk as a function of ik, qk, ihatk,
and qhatk.*/

        errk = ((qk-qhatk)/fabs(qk-qhatk))*(ik/fabs(ik)) -
((ik-ihatk)/fabs(ik-ihatk))*(qk/fabs(qk));

/*This is the end of the phase detector*/

/*The next step considers the loop filter and VCO in one
transfer function, as a difference equation. It calculates the
phase of the VCO, refk1, for the next simulation iteration.
refk1 is based not only on the error signal, errk, but also on
the state of the integrators that make up the one pole low-pass
filter and the VCO. The filter can be represented by the
function, 1 + a/s. a is one-over-the time constant, RC, of the
filter. The VCO xfer function can be considered as k0/s. k0 is
the ratio describing the output frequency of the VCO in terms
of the input error voltage from the loop filter. The filter
integrator initial condition at time k is i1k. The VCO integrator
initial condition at time k is i2k. The integration period is t. In
discrete time these transfer funcitons can be implemented as
follows*/

        refk1 = i2k + k0*t*errk + i1k*k0*t + a*k0*t*t*errk/2.0;

/*now reset the integrator intial conditions for the next
iteration*/

        i2k = refk1;
        i1k1 = i1k + a*t*errk;
        i1k = i1k1;

}
}
```

```
}
meanphs = (sumerr/s);

varphs = sqrerr/s - meanphs*meanphs;

fprintf(outfile,"\n");

fprintf(outfile,"E(s)/N(o) = %4.1f, mean of error = %10.7f,
variance of error = %10.7f\n",endb,meanphs,varphs);

fprintf(outfile,"The phase detector gain used was:
%f\n",pdgain);

fprintf(outfile,"The number of samples used in the previous
statistical analysis is: %d\n",s);

fprintf(outfile,"\n");

printf("Es/No = %4.1f, mean = %f, variance = %f, samples =
%d\n",endb,meanphs,varphs,s);

}
fclose(outfile);
}
```

The source code for the high-SNR loop simulation is:

```
/*high SNR 8PSK simulation of carrier recovery with fixed
loop bandwidth-to-symbol rate ratio*/

#include <stdio.h>
#include <stdlib.h>
#include <math.h>

main()
{

/*declare system parameters*/

int k;                  /*discrete time variable*/
int m;                  /*discrete time variable*/
int j;                  /*discrete time variable*/
int n;                  /*counter*/
int s;                  /*number of samples used in
                        variance calculation*/
int uncore;             /*number of samples to skip over
                        for variance calculation*/
```

```
double errk;            /*error signal out of phase detector
                        at time k*/
double phsk;            /*received signal phase at time k*/
double refk1;           /*phase of VCO at time k+1*/
double pdifk;           /*phase difference between
                        received signal and VCO at time k*/
double ik;              /*received value for I sample at
                        time k*/
double imk;             /*generated I sample at time k*/
double qk;              /*received value for Q sample at
                        time k*/
double qmk;             /*generated Q sample at time k*/
double i1k;             /*initial condition of filter
                        integrator at time k*/
double i2k;             /*initial condition of VCO
                        integrator at time k*/
double a;               /*inverse of the one pole filter time
                        constant (the 3dB break point)*/
double t;               /*symbol period*/
double k0;              /*the VCO slope in Hertz per Volt*/
double i1k1;            /*hold variable for intial condition,
                        I1, at time k+1*/
double sum;             /*averaging of phase detector
                        error*/
double wn;              /*user entered natural frequency
                        of loop*/
double damp;            /*damping factor*/
double bw;              /*loop bandwidth*/
char dptr[10];          /*string pointer for entering
                        floating point numbers*/
char pdgains[10];       /*string pointer for entering
                        floating point numbers*/
double endb;            /*E(s)/N(o) in dB*/
double pdgain;          /*phase detector gain*/
double phsfix;          /*fixed initial phase*/
double sqrerr;          /*running sum of squared phase
                        error refk1*/
double sumerr;          /*running sum of phase error
                        refk1*/
double meanphs;         /*mean of phase error*/
double varphs;          /*variance of phase error*/

/*declare data generation parameters*/

int d;
double testd;

/*declare QPSK test parameters*/

double x1;
double x2;
```

```
/*declare phase detector variables. These will be moved into a
subroutine eventually*/

double rcvdp;          /*the phase of the received vectort
                         whose components are ik and qk*/
double ihatk;          /*for this phase detector this is the
                         output from the circular
                         quantizer*/
double qhatk;          /*for this phase detector this is the
                         output from the circular
                         quantizer*/

double errkhold;
int count;

/*declare noise model parameters. sigma is the WGN standard
deviation. nik and nqk are the gaussian noise samples at time
k with mean zero and standard deviation sigma.*/

double sigma;
long xcon1;
long xcon2;
long x;
long y;
double sample1;
double sample2;
double nik;
double nqk;

/*declare  output file parameters*/

FILE *outfile;
char *modehold;
char *namehold1;

/*initialize file output parameters*/

modehold = "w";
namehold1 = "kghigh";
outfile = fopen(namehold1,modehold);

/*initialize  uniform RV seeds for repeated tests*/

srand(2546);
y = 47; /*seed*/

/*initialize phase step*/

phsfix = 0.0;
```

```
/*input natural frequency, damping factor for loop*/

printf("This is a second order carrier loop synchronizer
simulator\n");
printf("\n");
printf("Please enter the natural frequency of the loop
transfer function:\n");
printf("\n");
scanf("%s",dptr);
wn = strtod(dptr,NULL);
printf("\n");
printf("Now please enter the loop damping factor:\n");
printf("\n");
scanf("%s",dptr);
printf("\n");
damp = strtod(dptr,NULL);
printf("\n");
printf("And finally, please enter the phase detector gain:\n");
printf("\n");
scanf("%s",pdgains);
printf("\n");
pdgain = strtod(pdgains,NULL);
printf("\n");
printf("\n");
printf("\n");
printf("wn = %f,   damp = %f\n",wn,damp);
printf("\n");
printf("phase detector gain = %f\n",pdgain);

bw = wn*(damp + 1.0/(4.0*damp));

k0 = 2*damp*wn/pdgain;

a = wn/(2*damp);

/*determine sample interval that is required to uncorrelate
phase error variance calculation*/

uncore = floor(3.1415927/wn/4.0);

printf("\n");
printf("The loop noise bandwidth is:  %13.10f  Hz\n",bw);
printf("\n");
printf("The gain is:  %f  rad/sec/Volt\n",k0);
printf("\n");
printf("The loop filter time constant is:  %f  sec\n",a);
printf("\n");
printf("The number of skipped samples for correlation is:  %d
\n",uncore);
printf("\n");
```

```
fprintf(outfile,"8-PSK High SNR MAP estimator loop
results\n");
fprintf(outfile,"\n");
fprintf(outfile,"Initial phase step = %f\n",phsfix);
fprintf(outfile,"\n");
fprintf(outfile,"Noise random seed = %ld\n",y);
fprintf(outfile,"\n");
fprintf(outfile,"wn = %f\n",wn);
fprintf(outfile,"\n");
fprintf(outfile,"damping factor = %f\n",damp);
fprintf(outfile,"\n");
fprintf(outfile,"The loop noise bandwidth is:  %f  Hz\n",bw);
fprintf(outfile,"\n");
fprintf(outfile,"The gain is:  %f  rad/sec/Volt\n",k0);
fprintf(outfile,"\n");
fprintf(outfile,"The loop filter time constant is:  %f  sec\n",a);
fprintf(outfile,"\n");
fprintf(outfile,"phase detector gain = %f\n",pdgain);
fprintf(outfile,"\n");
fprintf(outfile,"The number of skipped samples for
correlation is:  %d \n",uncore);
fprintf(outfile,"\n");

/*begin simulation*/

for(j=30;j<=50;j=j+5)
{
endb = j;
sigma = 1.0/sqrt(2.0*pow(10.0,endb/10.0));

/*initialize system parameters*/

i1k = 0.0;
i2k = phsfix;
refk1 = i2k;
t = 1.0;
errkhold = 0.0;
phsk = 0.0;
errk = 0.0;
xcon2 = 16807; /*for RV generation*/
xcon1 = 2147483647; /*for RV generation*/
sqrerr = 0.0;
sumerr = 0.0;
s = 0;

for(k=0;k<=120;++k)
{

/*construct received phase, noise, and transmitted data*/

/*received phase*/
```

```
/*running variance calculation*/

        if (k >20)
        {
                if (fabs(refk1) < 0.392699)
                {
                s =s + 1;
                sqrerr = sqrerr + refk1*refk1;
                sumerr = sumerr + refk1;
                }
        }

for(n=0;n<uncore;++n)
{

/*      phsk = 0.001*k;*/

/*noise*/

/*      x = rand();
        y = rand();
        sample1 = (x/32767.0)*0.999999;
        sample2 = (y/32767.0)*0.999999;
*/
        x =ldiv(y,xcon1).rem;
        x=labs(x*xcon2);

        y =ldiv(x,xcon1).rem;
        y=labs(y*xcon2);

        sample1 = (x/2147483647.0)*0.999999;
        sample2 = (y/2147483647.0)*0.999999;

        nik = sigma*sqrt(-2.0*log(1.0-sample1))
*cos(2.0*3.14159265*sample2);
        nqk = sigma*sqrt(-2.0*log(1.0-sample1))
*sin(2.0*3.14159265*sample2);

        /*transmitted data*/

        d = rand();     /*d is now divided into 8 regions each
                        representing a possible xmitted symbol*/

        if(d  < 4096)
                {
                imk = 0.923879;
                qmk = 0.382683;
                }
        else if((d  >= 4096) && (d < 8192))
                {
```

```
                imk = 0.382683;
                qmk = 0.923879;
                }
        else if((d  >= 8192) && (d < 12288))
                {
                imk = -0.382683;
                qmk = 0.923879;
                }
        else if((d  >= 12288) && (d < 16384))
                {
                imk = -0.923879;
                qmk = 0.382683;
                }
        else if((d  >= 16384) && (d < 20480))
                {
                imk = -0.923879;
                qmk = -0.382683;
                }
        else if((d  >= 20480) && (d < 24576))
                {
                imk = -0.382683;
                qmk = -0.923879;
                }
        else if((d  >= 24576) && (d < 28672))
                {
                imk = 0.382683;
                qmk = -0.923879;
                }
        else
                {
                imk = 0.923879;
                qmk = -0.382683;
                }

/*end generation part of the simulation. this generated
information will be used for this value of the simulation
counter only*/

/*subtract the reference phase from the received phase*/

        pdifk = phsk - refk1;

/*calculate the received symbol values for I and Q based on
the generated data and noise and the phase difference pdifk*/

        ik = imk*cos(pdifk) - qmk*sin(pdifk) + nik;
        qk = imk*sin(pdifk) + qmk*cos(pdifk) + nqk;

/*Now implement a phase detector to generate a phase error
signal errk. This implementation performs a circular
```

```
quantization on I and Q followed by some algebra to develop
the error signal.*/

/*calculate the phase of the received vector. The atan2
function adjusts for the appropriate quadrant.*/

        rcvdp = atan2(qk,ik);

/*quantize rcvdp into ihatk and qhatk*/

        if ((rcvdp >= 0.0) && (rcvdp < 0.785398))

/* 0 <= rcvdp < Pi/4 */

                {
                ihatk = 0.923879;
                qhatk = 0.382683;
                }
        else if ((rcvdp >= 0.785398) && (rcvdp < 1.570796))

/* Pi/4 <= rcvdp < Pi/2 */

                {
                ihatk = 0.382683;
                qhatk = 0.923879;
                }
        else if ((rcvdp >= 1.570796) && (rcvdp < 2.356194))

/* Pi/2 <= rcvdp < 3Pi/4 */

                {
                ihatk = -0.382683;
                qhatk = 0.923879;
                }
        else if ((rcvdp >= 2.356194) && (rcvdp < 3.141593))

/* 3Pi/4 <= rcvdp < Pi */

                {
                ihatk = -0.923879;
                qhatk = 0.382683;
                }
        else if ((rcvdp < -2.356194) && (rcvdp >= -3.141593))

/* -3Pi/4 < rcvdp >= -Pi */

                {
                ihatk = -0.923879;
                qhatk = -0.382683;
                }
```

```
        else if ((rcvdp >=  -2.356194) && (rcvdp < -1.570796))

/* -Pi/2 > rcvdp >= -3Pi/4 */

                {
                ihatk = -0.382683;
                qhatk = -0.923879;
                }
        else if ((rcvdp >= -1.570796) && (rcvdp < -0.785398))

/* -Pi/4 > rcvdp >= -Pi/2 */

                {
                ihatk = 0.382683;
                qhatk = -0.923879;
                }
        else if ((rcvdp >= -0.785398) && (rcvdp < 0.0))

/* 0 > rcvdp >= -Pi/4 */

                {
                ihatk = 0.923879;
                qhatk = -0.382683;
                }

/*calculate the phase error errk as a function of ik, qk, ihatk,
and qhatk.*/

        errk = -ik*qhatk + qk*ihatk;

/*This is the end of the phase detector*/

/*The next step considers the loop filter and VCO in one
transfer function, as a difference equation. It calculates the
phase of the VCO, refk1, for the next simulation iteration.
refk1 is based not only on the error signal, errk, but also on
the state of the integrators that make up the one pole low-pass
filter and the VCO. The filter can be represented by the
function, 1 + a/s. a is one-over-the time constant, RC, of the
filter. The VCO xfer function can be considered as k0/s. k0 is
the ratio describing the output frequency of the VCO in terms
of the input error voltage from the loop filter. The filter
integrator initial condition at time k is i1k. The VCO integrator
initial condition at time k is i2k. The integration period is t. In
discrete time these transfer funcitons can be implemented as
follows*/

        refk1 = i2k + k0*t*errk + i1k*k0*t + a*k0*t*t*errk/2.0;

/*now reset the integrator intial conditions for the next
iteration*/
```

```
        i2k = refk1;
        i1k1 = i1k + a*t*errk;
        i1k = i1k1;

}

/*printf(" k = %d\n",k);*/

}

meanphs = (sumerr/s);

varphs = sqrerr/s - meanphs*meanphs;

fprintf(outfile,"\n");

fprintf(outfile,"E(s)/N(o) = %4.1f\n",endb);

fprintf(outfile,"Mean of error = %10.7f, variance of error =
%13.10f\n",meanphs,varphs);

fprintf(outfile,"\n");

fprintf(outfile,"The number of samples used in the previous
statistical analysis is: %d\n",s);

fprintf(outfile,"\n");

printf("\n");

printf("Es/No = %4.1f, mean = %f, variance = %f, samples =
%d\n",endb,meanphs,varphs,s);

}
fclose(outfile);
}
```

Both simulations were run with a loop bandwidth-to-symbol rate ratio of 0.53% and damping factor of 0.7071. The data plotted, in dB, in Table A-1 indicates the high-SNR loop performs better than the Leclert & variation in terms of variance of phase error.

Table A-1. The simulation data for comparing loop designs.

SNR (dB)	Leclert & Vandamme (variance)	High SNR (variance)
24	-44.271	-49.002
22	-42.652	-48.365
20	-41.244	-45.642
18	-39.642	-42.529
16	-37.535	-40.471
14	-34.825	-39.095
12	-30.965	-32.0768
10	-25.655	-26.655

Appendix B

THE 8PSK MAP ESTIMATOR DERIVATION

Extending the MAP estimator result for 8PSK (M=8) is a simple process. Equations (3-1) through (3-13) are applicable for any M. The modulation probability density in (3-14) is different for 8PSK and is stated as

$$p(\theta_m)=\frac{1}{8}\delta\left(\theta_m+\frac{\pi}{8}\right)+\frac{1}{8}\delta\left(\theta_m+\frac{3\pi}{8}\right)+\frac{1}{8}\delta\left(\theta_m+\frac{5\pi}{8}\right)+\frac{1}{8}\delta\left(\theta_m+\frac{7\pi}{8}\right)$$
$$+\frac{1}{8}\delta\left(\theta_m-\frac{\pi}{8}\right)+\frac{1}{8}\delta\left(\theta_m-\frac{3\pi}{8}\right)+\frac{1}{8}\delta\left(\theta_m-\frac{5\pi}{8}\right)+\frac{1}{8}\delta\left(\theta_m-\frac{7\pi}{8}\right)$$

(B-1)

The 8PSK likelihood function is

$$p(R|\theta_i)=\frac{1}{8}p\left(R\middle|\theta_i,\theta_m=\frac{-\pi}{8}\right)+\frac{1}{8}p\left(R\middle|\theta_i,\theta_m=\frac{-3\pi}{8}\right)+\frac{1}{8}p\left(R\middle|\theta_i,\theta_m=\frac{-5\pi}{8}\right)$$
$$+\frac{1}{8}p\left(R\middle|\theta_i,\theta_m=\frac{-7\pi}{8}\right)+\frac{1}{8}p\left(R\middle|\theta_i,\theta_m=\frac{\pi}{8}\right)+\frac{1}{8}p\left(R\middle|\theta_i,\theta_m=\frac{3\pi}{8}\right)$$
$$+\frac{1}{8}p\left(R\middle|\theta_i,\theta_m=\frac{5\pi}{8}\right)+\frac{1}{8}p\left(R\middle|\theta_i,\theta_m=\frac{7\pi}{8}\right)$$

(B-2)

We proceed by inserting (3-12) into (B-2) for all values of θ_m. To do this the two quantities $r_1 - s_1$ and $r_2 - s_2$ must first be analyzed for the 8 values of θ_m. Table B-1 contains this analysis.

Table B-1. Two dimensional noise component analysis.

θ_m	$r_1 - s_1$	$r_2 - s_2$
$\frac{-\pi}{8}$	$r_1 - \sqrt{E}\cos\left(\theta_i + \frac{\pi}{8}\right)$	$r_2 + \sqrt{E}\sin\left(\theta_i + \frac{\pi}{8}\right)$
$\frac{-3\pi}{8}$	$r_1 - \sqrt{E}\cos\left(\theta_i + \frac{3\pi}{8}\right)$	$r_2 + \sqrt{E}\sin\left(\theta_i + \frac{3\pi}{8}\right)$
$\frac{-5\pi}{8}$	$r_1 - \sqrt{E}\cos\left(\theta_i + \frac{5\pi}{8}\right)$	$r_2 + \sqrt{E}\sin\left(\theta_i + \frac{5\pi}{8}\right)$
$\frac{-7\pi}{8}$	$r_1 - \sqrt{E}\cos\left(\theta_i + \frac{7\pi}{8}\right)$	$r_2 + \sqrt{E}\sin\left(\theta_i + \frac{7\pi}{8}\right)$
$\frac{\pi}{8}$	$r_1 - \sqrt{E}\cos\left(\theta_i - \frac{\pi}{8}\right)$	$r_2 + \sqrt{E}\sin\left(\theta_i - \frac{\pi}{8}\right)$
$\frac{3\pi}{8}$	$r_1 - \sqrt{E}\cos\left(\theta_i - \frac{3\pi}{8}\right)$	$r_2 + \sqrt{E}\sin\left(\theta_i - \frac{3\pi}{8}\right)$
$\frac{5\pi}{8}$	$r_1 - \sqrt{E}\cos\left(\theta_i - \frac{5\pi}{8}\right)$	$r_2 + \sqrt{E}\sin\left(\theta_i - \frac{5\pi}{8}\right)$
$\frac{7\pi}{8}$	$r_1 - \sqrt{E}\cos\left(\theta_i - \frac{7\pi}{8}\right)$	$r_2 + \sqrt{E}\sin\left(\theta_i - \frac{7\pi}{8}\right)$

Now using Table B-1 it is possible to insert (3-12) into (B-2) and obtain the likelihood function. The process of obtaining the 8 PSK likelihood function will only be conducted for the first term of (B-2). The procedure is the same for all the terms in (B-2).

Inserting the data from Table B-1 for the first modulation phase, namely when $\theta_m = -\frac{\pi}{8}$, the first term in (B-2) can be stated as

$$\langle A \rangle = \frac{1}{8} p\left(R \middle| \theta_i, \theta_m = \frac{-\pi}{8} \right) = \frac{1}{16\pi\sigma^2} \left[\begin{array}{l} e^{-\frac{\left(r_1 - \sqrt{E}\cos\left(\theta_i + \frac{\pi}{8}\right)\right)^2}{2\sigma^2}} \\ \times e^{-\frac{\left(r_2 + \sqrt{E}\sin\left(\theta_i + \frac{\pi}{8}\right)\right)^2}{2\sigma^2}} \end{array} \right]. \qquad \text{(B-3)}$$

Completing the square of the exponential arguements in (B-3) and then combining, results in

$$\langle A \rangle = \frac{1}{16\pi\sigma^2} e^{-\frac{\left[\begin{array}{l} r_1^2 - 2r_1\sqrt{E}\cos\left(\theta_i + \frac{\pi}{8}\right) + E\cos^2\left(\theta_i + \frac{\pi}{8}\right) \\ + r_2^2 + 2r_2\sqrt{E}\sin\left(\theta_i + \frac{\pi}{8}\right) + E\sin^2\left(\theta_i + \frac{\pi}{8}\right) \end{array} \right]}{2\sigma^2}}. \qquad \text{(B-4)}$$

By combining and separating like terms (B-4) becomes

$$\langle A \rangle = \frac{1}{16\pi\sigma^2} e^{-\frac{r_1^2 + r_2^2 + E - 2r_1\sqrt{E}\cos\left(\theta_i + \frac{\pi}{8}\right) + 2r_2\sqrt{E}\sin\left(\theta_i + \frac{\pi}{8}\right)}{2\sigma^2}}. \qquad \text{(B-5)}$$

Applying the appropriate trigonometric identities to expand the sinusoidal terms forms

$$\langle A\rangle = \frac{1}{16\pi\sigma^2} e^{-\frac{r_1^2+r_2^2+E}{2\sigma^2}} \times e^{\frac{-2r_1\sqrt{E}\left[\cos(\theta_i)\cos\left(\frac{\pi}{8}\right)-\sin(\theta_i)\sin\left(\frac{\pi}{8}\right)\right]}{2\sigma^2}} \times e^{\frac{2r_2\sqrt{E}\left[\sin(\theta_i)\cos\left(\frac{\pi}{8}\right)+\cos(\theta_i)\sin\left(\frac{\pi}{8}\right)\right]}{2\sigma^2}} . \quad \text{(B-6)}$$

Inserting the equations for r_1 and r_2, given in (3-9) resolves (B-6) into

$$\langle A\rangle = \frac{1}{16\pi\sigma^2} e^{-\frac{r_1^2+r_2^2+E}{2\sigma^2}} \times e^{\frac{-\left[\int_0^T r(t)\sqrt{\frac{2}{T}}\cos(\omega_c t)dt\right]\sqrt{2E}\left[\cos(\theta_i)\cos\left(\frac{\pi}{8}\right)-\sin(\theta_i)\sin\left(\frac{\pi}{8}\right)\right]}{2\sigma^2}} \times e^{\frac{-\left[\int_0^T r(t)\sqrt{\frac{2}{T}}\sin(\omega_c t)dt\right]\sqrt{2E}\left[\sin(\theta_i)\cos\left(\frac{\pi}{8}\right)+\cos(\theta_i)\sin\left(\frac{\pi}{8}\right)\right]}{2\sigma^2}} . \quad \text{(B-7)}$$

By combining the integrals and distributing the carrier components within the integrand (B-7) becomes

$$\langle A\rangle = \frac{1}{8\pi\sigma^2} e^{-\frac{r_1^2+r_2^2+E}{2\sigma^2}} \times e^{\frac{\left\{2\sqrt{\frac{E}{T}}\int_0^T r(t)\left[\begin{array}{l}\cos(\omega_c t)\cos(\theta_i)\cos\left(\frac{\pi}{8}\right)-\cos(\omega_c t)\sin(\theta_i)\sin\left(\frac{\pi}{8}\right)\\ -\sin(\omega_c t)\sin(\theta_i)\cos\left(\frac{\pi}{8}\right)-\sin(\omega_c t)\cos(\theta_i)\sin\left(\frac{\pi}{8}\right)\end{array}\right]dt\right\}}{2\sigma^2}} . \quad \text{(B-8)}$$

Next the trigonometric identities

$$\cos(x)\cos(y)-\sin(x)\sin(y)=\cos(x+y)$$

and

$$\cos(x)\sin(y)+\sin(x)\cos(y)=\sin(x+y) \tag{B-9}$$

are used to separate the integral in (B-8) into two new integrals. This new form is

$$\langle A\rangle=\frac{1}{16\pi\sigma^2}e^{-\frac{r_1^2+r_2^2+E}{2\sigma^2}}e^{\left\{\frac{\left[2\cos\left(\frac{\pi}{8}\right)\sqrt{\frac{E}{T}}\int_0^T r(t)\cos(\omega_c t+\theta_i)dt\right]}{2\sigma^2}+\frac{\left[-2\sin\left(\frac{\pi}{8}\right)\sqrt{\frac{E}{T}}\int_0^T r(t)\sin(\omega_c t+\theta_i)dt\right]}{2\sigma^2}\right\}}. \tag{B-10}$$

Using the substitution adopted for QPSK, namely

$$x=\frac{1}{\sigma^2}\sqrt{\frac{E}{T}}\int_0^T r(t)\cos(\omega_c t+\theta_i)dt$$

and

$$y=\frac{1}{\sigma^2}\sqrt{\frac{E}{T}}\int_0^T r(t)\sin(\omega_c t+\theta_i)dt \tag{B-11}$$

reduces (B-10) to

$$\langle A\rangle = \frac{1}{16\pi\sigma^2} e^{-\frac{r_1^2+r_2^2+E}{2\sigma^2}} e^{\cos\left(\frac{\pi}{8}\right)x-\sin\left(\frac{\pi}{8}\right)y}. \tag{B-12}$$

Repeating the process for each of the seven remaining terms in the 8PSK likelihood function is accomplished by changing the trigonometric coefficients in (B-10) to accomodate the modulation angle corresponding to each term. Therefore the second term becomes

$$\langle B\rangle = \frac{1}{16\pi\sigma^2} e^{-\frac{r_1^2+r_2^2+E}{2\sigma^2}} e^{\cos\left(\frac{3\pi}{8}\right)x-\sin\left(\frac{3\pi}{8}\right)y}. \tag{B-13}$$

Similarly the other six terms are

$$\langle C\rangle = \frac{1}{16\pi\sigma^2} e^{-\frac{r_1^2+r_2^2+E}{2\sigma^2}} e^{\cos\left(\frac{5\pi}{8}\right)x-\sin\left(\frac{5\pi}{8}\right)y}, \tag{B-14}$$

$$\langle D\rangle = \frac{1}{16\pi\sigma^2} e^{-\frac{r_1^2+r_2^2+E}{2\sigma^2}} e^{\cos\left(\frac{7\pi}{8}\right)x-\sin\left(\frac{7\pi}{8}\right)y}, \tag{B-15}$$

$$\langle E\rangle = \frac{1}{16\pi\sigma^2} e^{-\frac{r_1^2+r_2^2+E}{2\sigma^2}} e^{\cos\left(\frac{-\pi}{8}\right)x-\sin\left(\frac{-\pi}{8}\right)y}, \tag{B-16}$$

$$\langle F\rangle = \frac{1}{16\pi\sigma^2} e^{-\frac{r_1^2+r_2^2+E}{2\sigma^2}} e^{\cos\left(\frac{-3\pi}{8}\right)x - \sin\left(\frac{-3\pi}{8}\right)y}, \tag{B-17}$$

$$\langle G\rangle = \frac{1}{16\pi\sigma^2} e^{-\frac{r_1^2+r_2^2+E}{2\sigma^2}} e^{\cos\left(\frac{-5\pi}{8}\right)x - \sin\left(\frac{-5\pi}{8}\right)y}, \tag{B-18}$$

$$\langle H\rangle = \frac{1}{16\pi\sigma^2} e^{-\frac{r_1^2+r_2^2+E}{2\sigma^2}} e^{\cos\left(\frac{-7\pi}{8}\right)x - \sin\left(\frac{-7\pi}{8}\right)y}. \tag{B-19}$$

All of the trigonometric coefficients in $\langle C\rangle$ through $\langle H\rangle$ can be written in terms of $\cos\left(\frac{\pi}{8}\right)$, $\sin\left(\frac{\pi}{8}\right)$, $\cos\left(\frac{3\pi}{8}\right)$, and $\sin\left(\frac{3\pi}{8}\right)$.

Performing the necessary conversions yields

$$\langle C\rangle = \frac{1}{16\pi\sigma^2} e^{-\frac{r_1^2+r_2^2+E}{2\sigma^2}} e^{-\cos\left(\frac{3\pi}{8}\right)x - \sin\left(\frac{3\pi}{8}\right)y}, \tag{B-20}$$

$$\langle D\rangle = \frac{1}{16\pi\sigma^2} e^{-\frac{r_1^2+r_2^2+E}{2\sigma^2}} e^{-\cos\left(\frac{\pi}{8}\right)x - \sin\left(\frac{\pi}{8}\right)y}, \tag{B-21}$$

$$\langle E\rangle = \frac{1}{16\pi\sigma^2} e^{-\frac{r_1^2+r_2^2+E}{2\sigma^2}} e^{\cos\left(\frac{\pi}{8}\right)x + \sin\left(\frac{\pi}{8}\right)y}, \tag{B-22}$$

$$\langle F\rangle = \frac{1}{16\pi\sigma^2} e^{-\frac{r_1^2+r_2^2+E}{2\sigma^2}} e^{\cos\left(\frac{3\pi}{8}\right)x + \sin\left(\frac{3\pi}{8}\right)y}, \tag{B-23}$$

$$\langle G\rangle = \frac{1}{16\pi\sigma^2} e^{-\frac{r_1^2+r_2^2+E}{2\sigma^2}} e^{-\cos\left(\frac{3\pi}{8}\right)x + \sin\left(\frac{3\pi}{8}\right)y}, \tag{B-24}$$

$$\langle H\rangle = \frac{1}{16\pi\sigma^2} e^{-\frac{r_1^2+r_2^2+E}{2\sigma^2}} e^{-\cos\left(\frac{\pi}{8}\right)x+\sin\left(\frac{\pi}{8}\right)y}. \tag{B-25}$$

Now making the assignments

$$c_1 = \cos\frac{\pi}{8}, \quad s_1 = \sin\frac{\pi}{8}$$

and (B-26)

$$c_2 = \cos\frac{3\pi}{8}, \quad s_2 = \sin\frac{3\pi}{8},$$

the 8PSK likelihood function can be expressed as

$$p\left(R|\theta_i\right) = \frac{1}{16\pi\sigma^2} e^{-\frac{r_1^2+r_2^2+E}{2\sigma^2}} \left[\begin{array}{l} e^{c_1x-s_1y} + e^{c_2x-s_2y} + e^{-c_2x-s_2y} + e^{-c_1x-s_1y} \\ +e^{c_1x+s_1y} + e^{c_2x+s_2y} + e^{-c_2x+s_2y} + e^{-c_1x+s_1y} \end{array}\right]. \tag{B-27}$$

Expanding the exponents and rearranging results in

$$p\left(R|\theta_i\right) = \frac{1}{16\pi\sigma^2} e^{-\frac{r_1^2+r_2^2+E}{2\sigma^2}} \left[\begin{array}{l} e^{c_1x}e^{s_1y} + e^{c_1x}e^{-s_1y} + e^{-c_1x}e^{s_1y} + e^{-c_1x}e^{-s_1y} \\ +e^{c_2x}e^{s_2y} + e^{c_2x}e^{-s_2y} + e^{-c_2x}e^{s_2y} + e^{-c_2x}e^{-s_2y} \end{array}\right]. \tag{B-28}$$

This reduces to

$$p(R|\theta_i)=\frac{1}{16\pi\sigma^2}e^{-\frac{r_1^2+r_2^2+E}{2\sigma^2}}\left[\begin{matrix}\left(e^{c_1x}+e^{-c_1x}\right)\left(e^{s_1y}+e^{-s_1y}\right)\\+\left(e^{c_2x}+e^{-c_2x}\right)\left(e^{s_2y}+e^{-s_2y}\right)\end{matrix}\right]. \qquad \text{(B-29)}$$

Using the definition of the hyperbolic cosine function, the 8PSK likelihood function becomes

$$p(R|\theta_i)=\frac{1}{16\pi\sigma^2}e^{-\frac{r_1^2+r_2^2+E}{2\sigma^2}}\left[\cosh(c_1x)\cosh(s_1y)+\cosh(c_2x)\cosh(s_2y)\right]. \qquad \text{(B-30)}$$

Next the log likelihood function is obtained and can be stated

$$\ln\left[p(R|\theta_i)\right]=\ln\left[\frac{1}{16\pi\sigma^2}e^{-\frac{r_1^2+r_2^2+E}{2\sigma^2}}\right]+\ln\left[\cosh(c_1x)\cosh(s_1y)+\cosh(c_2x)\cosh(s_2y)\right] \qquad \text{(B-31)}$$

Taking the derivative of (B-31) with respect to θ_i and noting that the first term in the log likelihood function will equate to zero in the derivative, the MAP estimator equation is found. The first step in computing the derivative is to apply the chain rule yielding

$$\frac{\partial\left\{\ln\left[p\left(R|\theta_i\right)\right]\right\}}{\partial\theta_i}=\frac{\dfrac{\partial\left[\cosh(c_1x)\cosh(s_1y)+\cosh(c_2x)\cosh(s_2y)\right]}{\partial\theta_i}}{\cosh(c_1x)\cosh(s_1y)+\cosh(c_2x)\cosh(s_2y)}. \quad \text{(B-32)}$$

Now taking the derivative of the products results in

$$\frac{\partial\left\{\ln\left[p\left(R|\theta_i\right)\right]\right\}}{\partial\theta_i}=\frac{\left\{\begin{array}{l}\cosh(s_1y)\dfrac{\partial\left[\cosh(c_1x)\right]}{\partial\theta_i}+\cosh(c_1x)\dfrac{\partial\left[\cosh(s_1y)\right]}{\partial\theta_i}\\ +\cosh(s_2y)\dfrac{\partial\left[\cosh(c_2x)\right]}{\partial\theta_i}+\cosh(c_2x)\dfrac{\partial\left[\cosh(s_2y)\right]}{\partial\theta_i}\end{array}\right\}}{\cosh(c_1x)\cosh(s_1y)+\cosh(c_2x)\cosh(s_2y)}. \quad \text{(B-33)}$$

Applying the chain rule to each of the derivatives on the right side of (B-33) forms

$$\frac{\partial\left\{\ln\left[p\left(R|\theta_i\right)\right]\right\}}{\partial\theta_i}=\frac{\left\{\begin{array}{l}c_1\cosh(s_1y)\sinh(c_1x)\dfrac{\partial[x]}{\partial\theta_i}\\ +s_1\cosh(c_1x)\sinh(s_1y)\dfrac{\partial[y]}{\partial\theta_i}\\ +c_2\cosh(s_2y)\sinh(c_2x)\dfrac{\partial[x]}{\partial\theta_i}\\ +s_2\cosh(c_2x)\sinh(s_2y)\dfrac{\partial[y]}{\partial\theta_i}\end{array}\right\}}{\cosh(c_1x)\cosh(s_1y)+\cosh(c_2x)\cosh(s_2y)}. \quad \text{(B-34)}$$

Using (B-11) it is noted that

$$\frac{\partial[x]}{\partial\theta_i} = -y$$

and (B-35)

$$\frac{\partial[y]}{\partial\theta_i} = x.$$

Substituting (B-35) into (B-34) yields

$$\frac{\partial\left\{\ln\left[p\left(R|\theta_i\right)\right]\right\}}{\partial\theta_i} = \frac{\left\{\begin{matrix}-c_1 y\cosh(s_1 y)\sinh(c_1 x) + s_1 x\cosh(c_1 x)\sinh(s_1 y) \\ -c_2 y\cosh(s_2 y)\sinh(c_2 x) + s_2 x\cosh(c_2 x)\sinh(s_2 y)\end{matrix}\right\}}{\cosh(c_1 x)\cosh(s_1 y) + \cosh(c_2 x)\cosh(s_2 y)}.$$

(B-36)

Writing (B-36) as a sum of two fractions yields

$$\frac{\partial\left\{\ln\left[p\left(R|\theta_i\right)\right]\right\}}{\partial\theta_i} = \frac{-c_1 y\cosh(s_1 y)\sinh(c_1 x) + s_1 x\cosh(c_1 x)\sinh(s_1 y)}{\cosh(c_1 x)\cosh(s_1 y) + \cosh(c_2 x)\cosh(s_2 y)} + \frac{-c_2 y\cosh(s_2 y)\sinh(c_2 x) + s_2 x\cosh(c_2 x)\sinh(s_2 y)}{\cosh(c_1 x)\cosh(s_1 y) + \cosh(c_2 x)\cosh(s_2 y)}.$$

(B-37)

Multiplying the first fraction by $\frac{\cosh(c_1x)\cosh(s_1y)}{\cosh(c_1x)\cosh(s_1y)}$ and the second fraction by $\frac{\cosh(c_2x)\cosh(s_2y)}{\cosh(c_2x)\cosh(s_2y)}$ forms the sum

$$\frac{\partial\left\{\ln\left[p\left(R|\theta_i\right)\right]\right\}}{\partial\theta_i}=\left[\frac{\frac{-c_1y\cosh(s_1y)\sinh(c_1x)+s_1x\cosh(c_1x)\sinh(s_1y)}{\cosh(c_1x)\cosh(s_1y)}}{\frac{\cosh(c_1x)\cosh(s_1y)+\cosh(c_2x)\cosh(s_2y)}{\cosh(c_1x)\cosh(s_1y)}}\right]+\left[\frac{\frac{-c_2y\cosh(s_2y)\sinh(c_2x)+s_2x\cosh(c_2x)\sinh(s_2y)}{\cosh(c_2x)\cosh(s_2y)}}{\frac{\cosh(c_1x)\cosh(s_1y)+\cosh(c_2x)\cosh(s_2y)}{\cosh(c_2x)\cosh(s_2y)}}\right]\cdot$$

(B-38)

This reduces to

$$\frac{\partial\left\{\ln\left[p\left(R|\theta_i\right)\right]\right\}}{\partial\theta_i}=\frac{s_1x\tanh(s_1y)-c_1y\tanh(c_1x)}{1+\frac{\cosh(c_2x)\cosh(s_2y)}{\cosh(c_1x)\cosh(s_1y)}}+\frac{s_2x\tanh(s_2y)-c_2y\tanh(c_2x)}{1+\frac{\cosh(c_2x)\cosh(s_2y)}{\cosh(c_2x)\cosh(s_2y)}}\cdot$$

(B-39)

Using the same approach for completing the MAP estimator as was done for BPSK and QPSK, the right side of (B-39) is equated to zero yielding

$$\frac{s_1 x \tanh(s_1 y) - c_1 y \tanh(c_1 x)}{1 + \dfrac{\cosh(c_2 x)\cosh(s_2 y)}{\cosh(c_1 x)\cosh(s_1 y)}} + \frac{s_2 x \tanh(s_2 y) - c_2 y \tanh(c_2 x)}{1 + \dfrac{\cosh(c_1 x)\cosh(s_1 y)}{\cosh(c_2 x)\cosh(s_2 y)}} = 0. \quad \text{(B-40)}$$

Appendix C

THE 16PSK MAP ESTIMATOR DERIVATION

Extending the MAP estimator result for 16PSK (M=16) is a simple process. Equations (3-1) through (3-13) are applicable for any M. The modulation probability density in (3-14) is different for 16PSK. Writing $p(\theta_m)$ for 16PSK as a summation while preserving the positive and negative references for the modulation points, as was done for the previous PSK modulations formats, results in

$$p(\theta_m) = \sum_{n=-8}^{7} \frac{1}{16} \delta\left(\theta_m - \frac{(2n+1)\pi}{16}\right). \tag{C-1}$$

The 16PSK likelihood function can be expressed in the same manner, namely,

$$p(R|\theta_i) = \sum_{n=-8}^{n=7} \frac{1}{16} p\left(R \middle| \theta_i, \theta_m = \frac{(2n+1)\pi}{16}\right). \tag{C-2}$$

We proceed by inserting (3-12) into (C-2) for all values of θ_m. To do this the two quantities $r_1 - s_1$ and $r_2 - s_2$ must first be analyzed for the 16 values of θ_m. Table C-1 contains this analysis.

Table C-1. Two dimensional noise component analysis.

θ_m	$r_1 - s_1$	$r_2 - s_2$
$-\frac{\pi}{16}$	$r_1 - \sqrt{E}\cos\left(\theta_i + \frac{\pi}{16}\right)$	$r_2 + \sqrt{E}\sin\left(\theta_i + \frac{\pi}{16}\right)$
$-\frac{3\pi}{16}$	$r_1 - \sqrt{E}\cos\left(\theta_i + \frac{3\pi}{16}\right)$	$r_2 + \sqrt{E}\sin\left(\theta_i + \frac{3\pi}{16}\right)$
$-\frac{5\pi}{16}$	$r_1 - \sqrt{E}\cos\left(\theta_i + \frac{5\pi}{16}\right)$	$r_2 + \sqrt{E}\sin\left(\theta_i + \frac{5\pi}{16}\right)$
$-\frac{7\pi}{16}$	$r_1 - \sqrt{E}\cos\left(\theta_i + \frac{7\pi}{16}\right)$	$r_2 + \sqrt{E}\sin\left(\theta_i + \frac{7\pi}{16}\right)$
$-\frac{9\pi}{16}$	$r_1 - \sqrt{E}\cos\left(\theta_i + \frac{9\pi}{16}\right)$	$r_2 + \sqrt{E}\sin\left(\theta_i + \frac{9\pi}{16}\right)$
$-\frac{11\pi}{16}$	$r_1 - \sqrt{E}\cos\left(\theta_i + \frac{11\pi}{16}\right)$	$r_2 + \sqrt{E}\sin\left(\theta_i + \frac{11\pi}{16}\right)$
$-\frac{13\pi}{16}$	$r_1 - \sqrt{E}\cos\left(\theta_i + \frac{13\pi}{16}\right)$	$r_2 + \sqrt{E}\sin\left(\theta_i + \frac{13\pi}{16}\right)$
$-\frac{15\pi}{16}$	$r_1 - \sqrt{E}\cos\left(\theta_i + \frac{15\pi}{16}\right)$	$r_2 + \sqrt{E}\sin\left(\theta_i + \frac{15\pi}{16}\right)$
$\frac{\pi}{16}$	$r_1 - \sqrt{E}\cos\left(\theta_i - \frac{\pi}{16}\right)$	$r_2 + \sqrt{E}\sin\left(\theta_i - \frac{\pi}{16}\right)$
$\frac{3\pi}{16}$	$r_1 - \sqrt{E}\cos\left(\theta_i - \frac{3\pi}{16}\right)$	$r_2 + \sqrt{E}\sin\left(\theta_i - \frac{3\pi}{16}\right)$
$\frac{5\pi}{16}$	$r_1 - \sqrt{E}\cos\left(\theta_i - \frac{5\pi}{16}\right)$	$r_2 + \sqrt{E}\sin\left(\theta_i - \frac{5\pi}{16}\right)$
$\frac{7\pi}{16}$	$r_1 - \sqrt{E}\cos\left(\theta_i - \frac{7\pi}{16}\right)$	$r_2 + \sqrt{E}\sin\left(\theta_i - \frac{7\pi}{16}\right)$
$\frac{9\pi}{16}$	$r_1 - \sqrt{E}\cos\left(\theta_i - \frac{9\pi}{16}\right)$	$r_2 + \sqrt{E}\sin\left(\theta_i - \frac{9\pi}{16}\right)$
$\frac{11\pi}{16}$	$r_1 - \sqrt{E}\cos\left(\theta_i - \frac{11\pi}{16}\right)$	$r_2 + \sqrt{E}\sin\left(\theta_i - \frac{11\pi}{16}\right)$
$\frac{13\pi}{16}$	$r_1 - \sqrt{E}\cos\left(\theta_i - \frac{13\pi}{16}\right)$	$r_2 + \sqrt{E}\sin\left(\theta_i - \frac{13\pi}{16}\right)$
$\frac{15\pi}{16}$	$r_1 - \sqrt{E}\cos\left(\theta_i - \frac{15\pi}{16}\right)$	$r_2 + \sqrt{E}\sin\left(\theta_i - \frac{15\pi}{16}\right)$

Now using Table C-1 it is possible to insert (3-12) into (C-2) and obtain the likelihood function. The process of obtaining the 16 PSK likelihood function will only be conducted for one term of (C-2). The procedure is the same for all the terms in (C-2) and the results will be presented after the derivation for this first term. Inserting the data from Table C-1 for the modulation phase corresponding to $\theta_m = -\frac{\pi}{16}$, the related term in (C-2) can be stated as

$$\langle A \rangle = \frac{1}{16} p\left(R \middle| \theta_i, \theta_m = \frac{-\pi}{16} \right) = \frac{1}{32\pi\sigma^2} \left[\begin{array}{l} e^{-\frac{\left(r_1 - \sqrt{E}\cos\left(\theta_i + \frac{\pi}{16} \right) \right)^2}{2\sigma^2}} \\ \times e^{-\frac{\left(r_2 + \sqrt{E}\sin\left(\theta_i + \frac{\pi}{16} \right) \right)^2}{2\sigma^2}} \end{array} \right]. \qquad \text{(C-3)}$$

Completing the square of the exponential arguments in (C-3) and then combining, results in

$$\langle A \rangle = \frac{1}{32\pi\sigma^2} e^{-\frac{\left[\begin{array}{l} r_1^2 - 2r_1\sqrt{E}\cos\left(\theta_i + \frac{\pi}{16} \right) + E\cos^2\left(\theta_i + \frac{\pi}{16} \right) \\ + r_2^2 + 2r_2\sqrt{E}\sin\left(\theta_i + \frac{\pi}{16} \right) + E\sin^2\left(\theta_i + \frac{\pi}{16} \right) \end{array} \right]}{2\sigma^2}}. \qquad \text{(C-4)}$$

By combining like terms (C-4) becomes

$$\langle A \rangle = \frac{1}{32\pi\sigma^2} e^{-\frac{r_1^2 + r_2^2 + E - 2r_1\sqrt{E}\cos\left(\theta_i + \frac{\pi}{16} \right) + 2r_2\sqrt{E}\sin\left(\theta_i + \frac{\pi}{16} \right)}{2\sigma^2}}. \qquad \text{(C-5)}$$

Applying appropriate trigonometric identities to expand the sinusoidal terms forms

$$\langle A\rangle = \frac{1}{32\pi\sigma^2} e^{-\frac{r_1^2+r_2^2+E}{2\sigma^2}} \times e^{\frac{-2r_1\sqrt{E}\left[\cos(\theta_i)\cos\left(\frac{\pi}{16}\right)-\sin(\theta_i)\sin\left(\frac{\pi}{16}\right)\right]}{2\sigma^2}} \times e^{\frac{2r_2\sqrt{E}\left[\sin(\theta_i)\cos\left(\frac{\pi}{16}\right)+\cos(\theta_i)\sin\left(\frac{\pi}{16}\right)\right]}{2\sigma^2}} . \quad \text{(C-6)}$$

Inserting the equations for r_1 and r_2, given in (3-9) resolves (C-6) into

$$\langle A\rangle = \frac{1}{32\pi\sigma^2} e^{-\frac{r_1^2+r_2^2+E}{2\sigma^2}} \times e^{\frac{-\left[\int_0^T r(t)\sqrt{\frac{2}{T}}\cos(\omega_c t)dt\right]\sqrt{2E}\left[\cos(\theta_i)\cos\left(\frac{\pi}{16}\right)-\sin(\theta_i)\sin\left(\frac{\pi}{16}\right)\right]}{2\sigma^2}} \times e^{\frac{\left[\int_0^T r(t)\sqrt{\frac{2}{T}}\sin(\omega_c t)dt\right]\sqrt{2E}\left[\sin(\theta_i)\cos\left(\frac{\pi}{16}\right)+\cos(\theta_i)\sin\left(\frac{\pi}{16}\right)\right]}{2\sigma^2}} . \quad \text{(C-7)}$$

By combining the integrals and distributing the carrier components within the integrand (C-7) becomes

$$\langle A\rangle = \frac{1}{32\pi\sigma^2} e^{-\frac{r_1^2+r_2^2+E}{2\sigma^2}} \times e^{\frac{\left\{2\sqrt{\frac{E}{T}}\int_0^T r(t)\left[\begin{array}{l}\cos(\omega_c t)\cos(\theta_i)\cos\left(\frac{\pi}{16}\right)-\cos(\omega_c t)\sin(\theta_i)\sin\left(\frac{\pi}{16}\right)\\ -\sin(\omega_c t)\sin(\theta_i)\cos\left(\frac{\pi}{16}\right)-\sin(\omega_c t)\cos(\theta_i)\sin\left(\frac{\pi}{16}\right)\end{array}\right]dt\right\}}{2\sigma^2}}. \quad \text{(C-8)}$$

Next the trigonometric identities

$$\cos(x)\cos(y)-\sin(x)\sin(y)=\cos(x+y)$$

and (C-9)

$$\cos(x)\sin(y)+\sin(x)\cos(y)=\sin(x+y)$$

are used to separate the integral in (C-8) into two new integrals. This new form is

$$\langle A\rangle = \frac{1}{32\pi\sigma^2} e^{-\frac{r_1^2+r_2^2+E}{2\sigma^2}} e^{\left\{\frac{\left[2\cos\left(\frac{\pi}{16}\right)\sqrt{\frac{E}{T}}\int_0^T r(t)\cos(\omega_c t+\theta_i)dt\right]}{2\sigma^2} + \frac{\left[-2\sin\left(\frac{\pi}{16}\right)\sqrt{\frac{E}{T}}\int_0^T r(t)\sin(\omega_c t+\theta_i)dt\right]}{2\sigma^2}\right\}}. \quad \text{(C-10)}$$

Using the substitution adopted for QPSK, namely

$$x = \frac{1}{\sigma^2}\sqrt{\frac{E}{T}}\int_0^T r(t)\cos(\omega_c t + \theta_i)dt$$

(C-11)

and

$$y = \frac{1}{\sigma^2}\sqrt{\frac{E}{T}}\int_0^T r(t)\sin(\omega_c t + \theta_i)dt$$

reduces (C-10) to

$$\langle A\rangle = \frac{1}{32\pi\sigma^2} e^{-\frac{r_1^2+r_2^2+E}{2\sigma^2}} e^{\cos\left(\frac{\pi}{16}\right)x - \sin\left(\frac{\pi}{16}\right)y}. \qquad \text{(C-12)}$$

Repeating the process for each of the fifteen remaining terms in the likelihood function is accomplished by changing the trigonometric coefficients in (C-10) to correspond to the modulation angle for that term. Therefore the second term becomes

$$\langle B\rangle = \frac{1}{32\pi\sigma^2} e^{-\frac{r_1^2+r_2^2+E}{2\sigma^2}} e^{\cos\left(\frac{3\pi}{16}\right)x - \sin\left(\frac{3\pi}{16}\right)y}. \qquad \text{(C-13)}$$

Similarly the other fourteen terms are

$$\langle C\rangle = \frac{1}{32\pi\sigma^2} e^{-\frac{r_1^2+r_2^2+E}{2\sigma^2}} e^{\cos\left(\frac{5\pi}{16}\right)x - \sin\left(\frac{5\pi}{16}\right)y}, \qquad \text{(C-14)}$$

$$\langle D\rangle = \frac{1}{32\pi\sigma^2} e^{-\frac{r_1^2+r_2^2+E}{2\sigma^2}} e^{\cos\left(\frac{7\pi}{16}\right)x - \sin\left(\frac{7\pi}{16}\right)y}, \tag{C-15}$$

$$\langle E\rangle = \frac{1}{32\pi\sigma^2} e^{-\frac{r_1^2+r_2^2+E}{2\sigma^2}} e^{\cos\left(\frac{9\pi}{16}\right)x - \sin\left(\frac{9\pi}{16}\right)y}, \tag{C-16}$$

$$\langle F\rangle = \frac{1}{32\pi\sigma^2} e^{-\frac{r_1^2+r_2^2+E}{2\sigma^2}} e^{\cos\left(\frac{11\pi}{16}\right)x - \sin\left(\frac{11\pi}{16}\right)y}, \tag{C-17}$$

$$\langle G\rangle = \frac{1}{32\pi\sigma^2} e^{-\frac{r_1^2+r_2^2+E}{2\sigma^2}} e^{\cos\left(\frac{13\pi}{16}\right)x - \sin\left(\frac{13\pi}{16}\right)y}, \tag{C-18}$$

$$\langle H\rangle = \frac{1}{32\pi\sigma^2} e^{-\frac{r_1^2+r_2^2+E}{2\sigma^2}} e^{\cos\left(\frac{15\pi}{16}\right)x - \sin\left(\frac{15\pi}{16}\right)y}, \tag{C-19}$$

$$\langle I\rangle = \frac{1}{32\pi\sigma^2} e^{-\frac{r_1^2+r_2^2+E}{2\sigma^2}} e^{\cos\left(-\frac{\pi}{16}\right)x - \sin\left(-\frac{\pi}{16}\right)y}, \tag{C-20}$$

$$\langle J\rangle = \frac{1}{32\pi\sigma^2} e^{-\frac{r_1^2+r_2^2+E}{2\sigma^2}} e^{\cos\left(-\frac{3\pi}{16}\right)x - \sin\left(-\frac{3\pi}{16}\right)y}, \tag{C-21}$$

$$\langle K\rangle = \frac{1}{32\pi\sigma^2} e^{-\frac{r_1^2+r_2^2+E}{2\sigma^2}} e^{\cos\left(-\frac{5\pi}{16}\right)x - \sin\left(-\frac{5\pi}{16}\right)y}, \tag{C-22}$$

$$\langle L\rangle = \frac{1}{32\pi\sigma^2} e^{-\frac{r_1^2+r_2^2+E}{2\sigma^2}} e^{\cos\left(-\frac{7\pi}{16}\right)x - \sin\left(-\frac{7\pi}{16}\right)y}, \tag{C-23}$$

$$\langle M\rangle = \frac{1}{32\pi\sigma^2} e^{-\frac{r_1^2+r_2^2+E}{2\sigma^2}} e^{\cos\left(-\frac{9\pi}{16}\right)x-\sin\left(-\frac{9\pi}{16}\right)y}, \tag{C-24}$$

$$\langle N\rangle = \frac{1}{32\pi\sigma^2} e^{-\frac{r_1^2+r_2^2+E}{2\sigma^2}} e^{\cos\left(-\frac{11\pi}{16}\right)x-\sin\left(-\frac{11\pi}{16}\right)y}, \tag{C-25}$$

$$\langle O\rangle = \frac{1}{32\pi\sigma^2} e^{-\frac{r_1^2+r_2^2+E}{2\sigma^2}} e^{\cos\left(-\frac{13\pi}{16}\right)x-\sin\left(-\frac{13\pi}{16}\right)y}, \tag{C-26}$$

$$\langle P\rangle = \frac{1}{32\pi\sigma^2} e^{-\frac{r_1^2+r_2^2+E}{2\sigma^2}} e^{\cos\left(-\frac{15\pi}{16}\right)x-\sin\left(-\frac{15\pi}{16}\right)y}. \tag{C-27}$$

All of the trigonometric coefficients in $\langle C\rangle$ through $\langle P\rangle$ can be written in terms of $\cos\left(\frac{\pi}{16}\right)$, $\sin\left(\frac{\pi}{16}\right)$, $\cos\left(\frac{3\pi}{16}\right)$, and $\sin\left(\frac{3\pi}{16}\right)$.

Performing the necessary conversions yields

$$\langle C\rangle = \frac{1}{32\pi\sigma^2} e^{-\frac{r_1^2+r_2^2+E}{2\sigma^2}} e^{\sin\left(\frac{3\pi}{16}\right)x-\cos\left(\frac{3\pi}{16}\right)y}, \tag{C-28}$$

$$\langle D\rangle = \frac{1}{32\pi\sigma^2} e^{-\frac{r_1^2+r_2^2+E}{2\sigma^2}} e^{\sin\left(\frac{\pi}{16}\right)x-\cos\left(\frac{\pi}{16}\right)y}, \tag{C-29}$$

$$\langle E\rangle = \frac{1}{32\pi\sigma^2} e^{-\frac{r_1^2+r_2^2+E}{2\sigma^2}} e^{-\sin\left(\frac{\pi}{16}\right)x-\cos\left(\frac{\pi}{16}\right)y}, \tag{C-30}$$

$$\langle F\rangle = \frac{1}{32\pi\sigma^2} e^{-\frac{r_1^2+r_2^2+E}{2\sigma^2}} e^{-\sin\left(\frac{3\pi}{16}\right)x-\cos\left(\frac{3\pi}{16}\right)y}, \tag{C-31}$$

$$\langle G\rangle = \frac{1}{32\pi\sigma^2} e^{-\frac{r_1^2+r_2^2+E}{2\sigma^2}} e^{-\cos\left(\frac{3\pi}{16}\right)x-\sin\left(\frac{3\pi}{16}\right)y}, \tag{C-32}$$

$$\langle H\rangle = \frac{1}{32\pi\sigma^2} e^{-\frac{r_1^2+r_2^2+E}{2\sigma^2}} e^{-\cos\left(\frac{\pi}{16}\right)x-\sin\left(\frac{\pi}{16}\right)y}, \tag{C-33}$$

$$\langle I\rangle = \frac{1}{32\pi\sigma^2} e^{-\frac{r_1^2+r_2^2+E}{2\sigma^2}} e^{\cos\left(\frac{\pi}{16}\right)x+\sin\left(\frac{\pi}{16}\right)y}, \tag{C-34}$$

$$\langle J\rangle = \frac{1}{32\pi\sigma^2} e^{-\frac{r_1^2+r_2^2+E}{2\sigma^2}} e^{\cos\left(\frac{3\pi}{16}\right)x+\sin\left(\frac{3\pi}{16}\right)y}, \tag{C-35}$$

$$\langle K\rangle = \frac{1}{32\pi\sigma^2} e^{-\frac{r_1^2+r_2^2+E}{2\sigma^2}} e^{\sin\left(\frac{3\pi}{16}\right)x+\cos\left(\frac{3\pi}{16}\right)y}, \tag{C-36}$$

$$\langle L\rangle = \frac{1}{32\pi\sigma^2} e^{-\frac{r_1^2+r_2^2+E}{2\sigma^2}} e^{\sin\left(\frac{\pi}{16}\right)x+\cos\left(\frac{\pi}{16}\right)y}, \tag{C-37}$$

$$\langle M\rangle = \frac{1}{32\pi\sigma^2} e^{-\frac{r_1^2+r_2^2+E}{2\sigma^2}} e^{-\sin\left(\frac{\pi}{16}\right)x+\cos\left(\frac{\pi}{16}\right)y}, \tag{C-38}$$

$$\langle N\rangle = \frac{1}{32\pi\sigma^2} e^{-\frac{r_1^2+r_2^2+E}{2\sigma^2}} e^{-\sin\left(\frac{3\pi}{16}\right)x+\cos\left(\frac{3\pi}{16}\right)y}, \tag{C-39}$$

$$\langle O\rangle = \frac{1}{32\pi\sigma^2} e^{-\frac{r_1^2+r_2^2+E}{2\sigma^2}} e^{-\cos\left(\frac{3\pi}{16}\right)x+\sin\left(\frac{3\pi}{16}\right)y}, \tag{C-40}$$

$$\langle P\rangle = \frac{1}{32\pi\sigma^2} e^{-\frac{r_1^2+r_2^2+E}{2\sigma^2}} e^{-\cos\left(\frac{\pi}{16}\right)x+\sin\left(\frac{\pi}{16}\right)y}. \qquad \text{(C-41)}$$

Now making the assignments

$$c_1 = \cos\frac{\pi}{16}, \quad s_1 = \sin\frac{\pi}{16}$$

and (C-42)

$$c_2 = \cos\frac{3\pi}{16}, \quad s_2 = \sin\frac{3\pi}{16},$$

the 16PSK likelihood function can be expressed as

$$p\left(R|\theta_i\right) = \frac{1}{32\pi\sigma^2} e^{-\frac{r_1^2+r_2^2+E}{2\sigma^2}} \begin{bmatrix} e^{c_1x-s_1y} + e^{c_2x-s_2y} + e^{s_2x-c_2y} + e^{s_1x-c_1y} \\ +e^{-s_1x-c_1y} + e^{-s_2x-c_2y} + e^{-c_2x-s_2y} + e^{-c_1x-s_1y} \\ +e^{c_1x+s_1y} + e^{c_2x+s_2y} + e^{s_2x+c_2y} + e^{s_1x+c_1y} \\ +e^{-s_1x+c_1y} + e^{-s_2x+c_2y} + e^{-c_2x+s_2y} + e^{-c_1x+s_1y} \end{bmatrix}. \qquad \text{(C-43)}$$

Expanding the exponents and rearranging, yields

$$p\left(R|\theta_i\right) = \frac{1}{32\pi\sigma^2} e^{-\frac{r_1^2+r_2^2+E}{2\sigma^2}} \begin{bmatrix} e^{c_1x}e^{s_1y} + e^{c_1x}e^{-s_1y} + e^{-c_1x}e^{s_1y} + e^{-c_1x}e^{-s_1y} \\ +e^{c_2x}e^{s_2y} + e^{c_2x}e^{-s_2y} + e^{-c_2x}e^{s_2y} + e^{-c_2x}e^{-s_2y} \\ +e^{s_1x}e^{c_1y} + e^{s_1x}e^{-c_1y} + e^{-s_1x}e^{c_1y} + e^{-s_1x}e^{-c_1y} \\ +e^{s_2x}e^{c_2y} + e^{s_2x}e^{-c_2y} + e^{-s_2x}e^{c_2y} + e^{-s_2x}e^{-c_2y} \end{bmatrix}.$$

(C-44)

This reduces to

$$p(R|\theta_i)=\frac{1}{32\pi\sigma^2}e^{-\frac{r_1^2+r_2^2+E}{2\sigma^2}}\begin{bmatrix}\left(e^{c_1x}+e^{-c_1x}\right)\left(e^{s_1y}+e^{-s_1y}\right)\\+\left(e^{c_2x}+e^{-c_2x}\right)\left(e^{s_2y}+e^{-s_2y}\right)\\+\left(e^{s_1x}+e^{-s_1x}\right)\left(e^{c_1y}+e^{-c_1y}\right)\\+\left(e^{s_2x}+e^{-s_2x}\right)\left(e^{c_2y}+e^{-c_2y}\right)\end{bmatrix}. \quad \text{(C-45)}$$

Using the definition of the hyperbolic cosine function, the 16PSK likelihood function becomes

$$p(R|\theta_i)=\frac{1}{32\pi\sigma^2}e^{-\frac{r_1^2+r_2^2+E}{2\sigma^2}}\begin{bmatrix}\cosh(c_1x)\cosh(s_1y)+\cosh(c_2x)\cosh(s_2y)\\+\cosh(s_1x)\cosh(c_1y)+\cosh(s_2x)\cosh(c_2y)\end{bmatrix}.$$

(C-46)

Next the log likelihood function is obtained and can be stated

$$\ln\left[p(R|\theta_i)\right]=\ln\left[\frac{1}{32\pi\sigma^2}e^{-\frac{r_1^2+r_2^2+E}{2\sigma^2}}\right]+\ln\begin{bmatrix}\cosh(c_1x)\cosh(s_1y)\\+\cosh(c_2x)\cosh(s_2y)\\+\cosh(s_1x)\cosh(c_1y)\\+\cosh(s_2x)\cosh(c_2y)\end{bmatrix}. \quad \text{(C-47)}$$

Taking the derivative of (C-47) with respect to θ_i and noting that the first term in the log likelihood function will equate to zero in the derivative, the MAP estimator equation is found. The first step in computing the derivative is to apply the chain rule yielding

$$\frac{\partial\left\{\ln\left[p\left(R|\theta_i\right)\right]\right\}}{\partial\theta_i}=\frac{\partial\begin{bmatrix}\cosh(c_1x)\cosh(s_1y)+\cosh(c_2x)\cosh(s_2y)\\+\cosh(s_1x)\cosh(c_1y)+\cosh(s_2x)\cosh(c_2y)\end{bmatrix}}{\partial\theta_i}}{\begin{matrix}\cosh(c_1x)\cosh(s_1y)+\cosh(c_2x)\cosh(s_2y)\\+\cosh(s_1x)\cosh(c_1y)+\cosh(s_2x)\cosh(c_2y)\end{matrix}}. \quad \text{(C-48)}$$

Now using the rule for the derivative of a product results in

$$\frac{\partial\left\{\ln\left[p\left(R|\theta_i\right)\right]\right\}}{\partial\theta_i}=\frac{\left\{\begin{matrix}\cosh(s_1y)\frac{\partial[\cosh(c_1x)]}{\partial\theta_i}+\cosh(c_1x)\frac{\partial[\cosh(s_1y)]}{\partial\theta_i}\\+\cosh(s_2y)\frac{\partial[\cosh(c_2x)]}{\partial\theta_i}+\cosh(c_2x)\frac{\partial[\cosh(s_2y)]}{\partial\theta_i}\\+\cosh(c_1y)\frac{\partial[\cosh(s_1x)]}{\partial\theta_i}+\cosh(s_1x)\frac{\partial[\cosh(c_1y)]}{\partial\theta_i}\\+\cosh(c_2y)\frac{\partial[\cosh(s_2x)]}{\partial\theta_i}+\cosh(s_2x)\frac{\partial[\cosh(c_2y)]}{\partial\theta_i}\end{matrix}\right\}}{\begin{matrix}\cosh(c_1x)\cosh(s_1y)+\cosh(c_2x)\cosh(s_2y)\\+\cosh(s_1x)\cosh(c_1y)+\cosh(s_2x)\cosh(c_2y)\end{matrix}}.$$

(C-49)

Applying the chain rule to each of the derivatives on the right side of (C-49) forms

$$\frac{\partial\left\{\ln\left[p(R|\theta_i)\right]\right\}}{\partial\theta_i} = \frac{\left\{\begin{array}{l} c_1\cosh(s_1y)\sinh(c_1x)\dfrac{\partial[x]}{\partial\theta_i} \\ +s_1\cosh(c_1x)\sinh(s_1y)\dfrac{\partial[y]}{\partial\theta_i} \\ +c_2\cosh(s_2y)\sinh(c_2x)\dfrac{\partial[x]}{\partial\theta_i} \\ +s_2\cosh(c_2x)\sinh(s_2y)\dfrac{\partial[y]}{\partial\theta_i} \\ +s_1\cosh(c_1y)\sinh(s_1x)\dfrac{\partial[x]}{\partial\theta_i} \\ +c_1\cosh(s_1x)\sinh(c_1y)\dfrac{\partial[y]}{\partial\theta_i} \\ +s_2\cosh(c_2y)\sinh(s_2x)\dfrac{\partial[x]}{\partial\theta_i} \\ +c_2\cosh(s_2x)\sinh(c_2y)\dfrac{\partial[y]}{\partial\theta_i} \end{array}\right\}}{\begin{array}{l}\cosh(c_1x)\cosh(s_1y)+\cosh(c_2x)\cosh(s_2y) \\ +\cosh(s_1x)\cosh(c_1y)+\cosh(s_2x)\cosh(c_2y)\end{array}}. \qquad \text{(C-50)}$$

Using (C-11) it is noted that

$$\frac{\partial[x]}{\partial\theta_i} = -y$$

and (C-51)

$$\frac{\partial[y]}{\partial\theta_i} = x.$$

Substituting (C-51) into (C-50) yields

$$\frac{\partial\left\{\ln\left[p\left(R|\theta_i\right)\right]\right\}}{\partial\theta_i}=\frac{\begin{Bmatrix}-c_1y\cosh(s_1y)\sinh(c_1x)+s_1x\cosh(c_1x)\sinh(s_1y)\\-c_2y\cosh(s_2y)\sinh(c_2x)+s_2x\cosh(c_2x)\sinh(s_2y)\\-s_1y\cosh(c_1y)\sinh(s_1x)+c_1x\cosh(s_1x)\sinh(c_1y)\\-s_2y\cosh(c_2y)\sinh(s_2x)+c_2x\cosh(s_2x)\sinh(c_2y)\end{Bmatrix}}{\begin{matrix}\cosh(c_1x)\cosh(s_1y)+\cosh(c_2x)\cosh(s_2y)\\+\cosh(s_1x)\cosh(c_1y)+\cosh(s_2x)\cosh(c_2y)\end{matrix}}.$$

(C-52)

Writing (C-52) as a sum of four fractions yields

$$\begin{aligned}\frac{\partial\left\{\ln\left[p\left(R|\theta_i\right)\right]\right\}}{\partial\theta_i}=&\frac{-c_1y\cosh(s_1y)\sinh(c_1x)+s_1x\cosh(c_1x)\sinh(s_1y)}{\begin{bmatrix}\cosh(c_1x)\cosh(s_1y)+\cosh(c_2x)\cosh(s_2y)\\+\cosh(s_1x)\cosh(c_1y)+\cosh(s_2x)\cosh(c_2y)\end{bmatrix}}\\&+\frac{-c_2y\cosh(s_2y)\sinh(c_2x)+s_2x\cosh(c_2x)\sinh(s_2y)}{\begin{bmatrix}\cosh(c_1x)\cosh(s_1y)+\cosh(c_2x)\cosh(s_2y)\\+\cosh(s_1x)\cosh(c_1y)+\cosh(s_2x)\cosh(c_2y)\end{bmatrix}}\\&+\frac{-s_1y\cosh(c_1y)\sinh(s_1x)+c_1x\cosh(s_1x)\sinh(c_1y)}{\begin{bmatrix}\cosh(c_1x)\cosh(s_1y)+\cosh(c_2x)\cosh(s_2y)\\+\cosh(s_1x)\cosh(c_1y)+\cosh(s_2x)\cosh(c_2y)\end{bmatrix}}\\&+\frac{-s_2y\cosh(c_2y)\sinh(s_2x)+c_2x\cosh(s_2x)\sinh(c_2y)}{\begin{bmatrix}\cosh(c_1x)\cosh(s_1y)+\cosh(c_2x)\cosh(s_2y)\\+\cosh(s_1x)\cosh(c_1y)+\cosh(s_2x)\cosh(c_2y)\end{bmatrix}}.\end{aligned}$$

(C-53)

Multiplying the first fraction by $\frac{\cosh(c_1x)\cosh(s_1y)}{\cosh(c_1x)\cosh(s_1y)}$, the second fraction by $\frac{\cosh(c_2x)\cosh(s_2y)}{\cosh(c_2x)\cosh(s_2y)}$, the third fraction by $\frac{\cosh(s_1x)\cosh(c_1y)}{\cosh(s_1x)\cosh(c_1y)}$, and the fourth fraction by $\frac{\cosh(s_2x)\cosh(c_2y)}{\cosh(s_2x)\cosh(c_2y)}$ forms the reduced sum

$$\frac{\partial\left\{\ln\left[p\left(R|\theta_i\right)\right]\right\}}{\partial\theta_i} = \frac{-c_1y\tanh(c_1x)+s_1x\tanh(s_1y)}{\left[1+\frac{\cosh(c_2x)\cosh(s_2y)}{\cosh(c_1x)\cosh(s_1y)}+\frac{\cosh(s_1x)\cosh(c_1y)}{\cosh(c_1x)\cosh(s_1y)}+\frac{\cosh(s_2x)\cosh(c_2y)}{\cosh(c_1x)\cosh(s_1y)}\right]}$$
$$+\frac{-c_2y\tanh(c_2x)+s_2x\tanh(s_2y)}{\left[\frac{\cosh(c_1x)\cosh(s_1y)}{\cosh(c_2x)\cosh(s_2y)}+1+\frac{\cosh(s_1x)\cosh(c_1y)}{\cosh(c_2x)\cosh(s_2y)}+\frac{\cosh(s_2x)\cosh(c_2y)}{\cosh(c_2x)\cosh(s_2y)}\right]}$$
$$+\frac{-s_1y\tanh(s_1x)+c_1x\tanh(c_1y)}{\left[\frac{\cosh(c_1x)\cosh(s_1y)}{\cosh(s_1x)\cosh(c_1y)}+\frac{\cosh(c_2x)\cosh(s_2y)}{\cosh(s_1x)\cosh(c_1y)}+1+\frac{\cosh(s_2x)\cosh(c_2y)}{\cosh(s_1x)\cosh(c_1y)}\right]}$$
$$+\frac{-s_2y\tanh(s_2x)+c_2x\tanh(c_2y)}{\left[\frac{\cosh(c_1x)\cosh(s_1y)}{\cosh(s_2x)\cosh(c_2y)}+\frac{\cosh(c_2x)\cosh(s_2y)}{\cosh(s_2x)\cosh(c_2y)}+\frac{\cosh(s_1x)\cosh(c_1y)}{\cosh(s_2x)\cosh(c_2y)}+1\right]} \quad . \quad \text{(C-54)}$$

Using the same approach for completing the MAP estimator as was done before for BPSK, QPSK, and 8PSK, the right side of (C-54) is equated to zero

$$\frac{-c_1 y\tanh(c_1 x)+s_1 x\tanh(s_1 y)}{\left[1+\frac{\cosh(c_2 x)\cosh(s_2 y)}{\cosh(c_1 x)\cosh(s_1 y)}+\frac{\cosh(s_1 x)\cosh(c_1 y)}{\cosh(c_1 x)\cosh(s_1 y)}+\frac{\cosh(s_2 x)\cosh(c_2 y)}{\cosh(c_1 x)\cosh(s_1 y)}\right]}$$
$$+\frac{-c_2 y\tanh(c_2 x)+s_2 x\tanh(s_2 y)}{\left[\frac{\cosh(c_1 x)\cosh(s_1 y)}{\cosh(c_2 x)\cosh(s_2 y)}+1+\frac{\cosh(s_1 x)\cosh(c_1 y)}{\cosh(c_2 x)\cosh(s_2 y)}+\frac{\cosh(s_2 x)\cosh(c_2 y)}{\cosh(c_2 x)\cosh(s_2 y)}\right]}$$
$$+\frac{-s_1 y\tanh(s_1 x)+c_1 x\tanh(c_1 y)}{\left[\frac{\cosh(c_1 x)\cosh(s_1 y)}{\cosh(s_1 x)\cosh(c_1 y)}+\frac{\cosh(c_2 x)\cosh(s_2 y)}{\cosh(s_1 x)\cosh(c_1 y)}+1+\frac{\cosh(s_2 x)\cosh(c_2 y)}{\cosh(s_1 x)\cosh(c_1 y)}\right]}$$
$$+\frac{-s_2 y\tanh(s_2 x)+c_2 x\tanh(c_2 y)}{\left[\frac{\cosh(c_1 x)\cosh(s_1 y)}{\cosh(s_2 x)\cosh(c_2 y)}+\frac{\cosh(c_2 x)\cosh(s_2 y)}{\cosh(s_2 x)\cosh(c_2 y)}+\frac{\cosh(s_1 x)\cosh(c_1 y)}{\cosh(s_2 x)\cosh(c_2 y)}+1\right]}=0 \qquad \text{(C-55)}$$

and it is noted that

$$x=\frac{1}{\sigma^2}\sqrt{\frac{E}{T}}\int_0^T r(t)\cos(\omega_c t+\theta_o)dt$$

and (C-56)

$$y=\frac{1}{\sigma^2}\sqrt{\frac{E}{T}}\int_0^T r(t)\sin(\omega_c t+\theta_o)dt\,.$$

Appendix D

EQUIVALENT NOISE DATA AND SIMULATION SOURCE CODE

In Chapter 5 the equivalent noise in the high-SNR loop was discussed. To verify the derived numerical approach, it was compared to the theoretical result for QPSK (5-18). It was then applied to 8PSK and 16PSK. The numerical calculations were executed with the use of MATLAB source code. The 8PSK source code is presented here for review:

```
%This program calculates the variance of the %equivalent
noise term in the error signal of the 8PSK %HIGH-SNR MAP
loop.

clear
format long

%Test EsNo

EsNo=10;

%sigma2 is the I or Q channel noise variance out
%of either of the integrators

sigma2=1/(2*10^(EsNo/10));

%k is the constant out in front of the exponents in the
%double integral for the equivalent noise calculation.

k=1/(2*3.14159*sigma2);

%ke is the constant in the exponent

ke=1/(2*sigma2);

%Clear the variable that tallies up the volume

volume = 0;

%To minimize computation time special measures were
%taken to ensure that the resolution of the integration
```

```
%was "fine" enough but not more than was necessary.
%Basically, the calculation was repeated, increasing the
%resolution each time, until the change in volume
%dropped below 0.1 percent.

%Set the length of one side of a pixel in the integration
%grid. This is the integration resolution

delta = .05;

%Begin the double loop that integrates across the grid

for i=1:281,
for j=1:281,

%Convert the matrix indices to bilateral coordinates
%that are designed to minimize the computation time
%needed. This minimization was done prior to this
%code being run. The size of the grid is designed so as
%to contain 99.9 percent of the volume of the Gaussian
%probability mountain. The size of the grid is
%therefore dependent on the SNR. Note that the
%Gaussian probability mountain is centered at the zero
%phase, modulation point. The ranges over which x
%and y are varied are the results of this minimization
%process.

%x range from -6 to 8

x=(j-121)*delta;

%y range from 7 to -7

y=(141-i)*delta;

%As the double loop sequences through each of the
%locations in the x,y plane (the grid) the following if-
%thens assign the data estimates for calculating the
%equivalent noise. Actually the square of I and of Q
%are needed as is the inner product

if (y>=-0.41421*x)&(y<0.41421*x),
        ihat2=1.0;
        qhat2=0.0;
        ihatqhat=0.0;
elseif (y>=0.41421*x)&(y<2.41421*x),
        ihat2=0.5;
        qhat2=0.5;
        ihatqhat=0.5;
elseif (y>=2.41421*x)&(y>-2.41421*x),
        ihat2=0.0;
```

```
        qhat2=1.0;
        ihatqhat=0.0;
elseif (y<=-2.41421*x)&(y>-0.41421*x),
        ihat2=0.5;
        qhat2=0.5;
        ihatqhat=-0.5;
elseif (y<=-0.41421*x)&(y>0.41421*x),
        ihat2=1.0;
        qhat2=0.0;
        ihatqhat=0.0;
elseif (y<=0.41421*x)&(y>2.41421*x),
        ihat2=0.5;
        qhat2=0.5;
        ihatqhat=0.5;
elseif (y<=2.41421*x)&(y<-2.41421*x),
        ihat2=0.0;
        qhat2=1.0;
        ihatqhat=0.0;
else,
        ihat2=0.5;
        qhat2=0.5;
        ihatqhat=-0.5;
end

%At location x,y calculate the joint noise density %function

c=exp(-ke*(y)^2)*exp(-ke*(x-1.0)^2);

%Calculate the square of the equivalent noise term

da(i,j) = ((y)^2*ihat2)+((x-1.0)^2*qhat2)
da(i,j) = da(i,j)-(2*(y)*(x-1.0)*ihatqhat);

%Multiply the two together and then by the constant k

d = da(i,j)*k*c;

%"d" is the magnitude at any point in the grid. It needs
%to be mulitiplied by the area of pixel to represent a
%volume element. However, to save computation this
%final step is withheld until the end

%Accumulate the "volume" for the variance calculation

volume = volume + d;

end
end

%Multply by the pixel area and calculate the variance
```

```
var=10*log10(delta*delta*volume);
%Save data
save dataout
```

The theoretical and numerical data, plotted in Figure 5-1 and Figure 5-9 is presented here, in dB, in Table D-1 and Table D-2.

Table D-1. The first set of MPSK equivalent noise variance data.

	BPSK	QPSK	QPSK	8PSK	16PSK
	Theoretical	Theoretical	Numerical	Numerical	Numerical
SNR	Data	Data	Data	Data	Data
(dB)	(variance)	(variance)	(variance)	(variance)	(variance)
-5.000	2.000	-0.719	-0.716	-2.648	-3.391
-4.500	1.500	-1.079			
-4.000	1.000	-1.433	-1.430	-3.041	-3.626
-3.500	0.500	-1.782			
-3.000	0.000	-2.126	-2.123	-3.434	-3.887
-2.500	-0.500	-2.468			
-2.000	-1.000	-2.807	-2.803	-3.843	-4.185
-1.500	-1.500	-3.145			
-1.000	-2.000	-3.484	-3.479	-4.279	-4.532
-0.500	-2.500	-3.825			
0.000	-3.000	-4.169	-4.165	-4.758	-4.939
0.500	-3.500	-4.519			
1.000	-4.000	-4.876	-4.876	-5.303	-5.425
1.500	-4.500	-5.242			
2.000	-5.000	-5.618	-5.618	-5.898	-5.98
2.500	-5.500	-6.004			
3.000	-6.000	-6.404	-6.404	-6.578	-6.628
3.500	-6.500	-6.816			
4.000	-7.000	-7.241	-7.241	-7.34	-7.368
4.500	-7.500	-7.679			
5.000	-8.000	-8.129	-8.129	-8.179	-8.193
5.500	-8.500	-8.591			
6.000	-9.000	-9.062	-9.062	-9.084	-9.09
6.500	-9.500	-9.542			
7.000	-10.000	-10.029	-10.029	-10.036	-10.038
7.500	-10.500	-10.520			
8.000	-11.000	-11.015	-11.015	-11.017	-11.017
8.500	-11.500	-11.513			
9.000	-12.000	-12.011	-12.011	-12.011	-12.011
9.500	-12.500	-12.511			

Table D-2. The second set of MPSK equivalent noise variance data.

	BPSK	QPSK	QPSK	8PSK	16PSK
	Theoretical	Theoretical	Numerical	Numerical	Numerical
SNR	Data	Data	Data	Data	Data
(dB)	(variance)	(variance)	(variance)	(variance)	(variance)
10.000	-13.000	-13.010	-13.010	-13.01	-13.01
10.500	-13.500	-13.510			
11.000	-14.000	-14.010			
11.500	-14.500	-14.510			
12.000	-15.000	-15.010			
12.500	-15.500	-15.510			
13.000	-16.000	-16.010			
13.500	-16.500	-16.510			
14.000	-17.000	-17.010			
14.500	-17.500	-17.510			
15.000	-18.000		-18.012	-18.078	-18.087
15.500	-18.500				
16.000	-19.000				
16.500	-19.500				
17.000	-20.000				
17.500	-20.500				
18.000	-21.000				
18.500	-21.500				
19.000	-22.000				
19.500	-22.500				
20.000	-23.000		-23.012	-23.11	-23.097

Appendix E

PHASE DETECTOR GAIN DATA AND SIMULATION SOURCE CODE

In Chapter 5 the phase detector gain in the high-SNR loop was discussed. To verify the derived numerical approach, it was compared to the theoretical result for QPSK (5-64). It was then applied to 8PSK and 16PSK. The numerical calculations were executed with the use of MATLAB source code. The 8PSK source code is presented here for review:

```
%This code generates the 8PSK phase detector gains
%for a high-SNR MAP loop

clear

%Set the number of points to integrate the entire
%phase probability over

k=20000;

snrdb 10.0;
snr=10^(snrdb/10);

%Select Phase error that the phase detector is
%evaluated at

psi=0.001;

%Clear storage variables

popsk=[0 0 0 0 0 0 0 0];

%Start counter that integrates across the density

for thetao=-k:1:k;

%Create phase variable from counter (+/- pi)

theta=thetao*pi/k;

%The next three equation all combine to represent the
```

```
%density of the phase

p1=2*sqrt(snr*pi)*cos(theta+psi)*exp(snr*cos(theta+psi)*cos
(theta+psi));

p2=.5*(1-erf(-sqrt(snr)*cos(theta+psi)));

p=(1/2/pi)*exp(-snr)*(1+p1*p2);

%Now decide which decision region to accumulate the
%density component in

if (theta<0.392699082)&(theta>=-0.392699082),
        popsk(1)=popsk(1)+p;
elseif (theta>=0.392699082)&(theta<1.178097245),
                popsk(2)=popsk(2)+p;
elseif (theta>=1.178097245)&(theta<1.963495409),
                popsk(3)=popsk(3)+p;
elseif (theta>=1.963495409)&(theta<2.748893572),
                popsk(4)=popsk(4)+p;
elseif (theta>=2.748893572)|(theta<-2.748893572),
                popsk(5)=popsk(5)+p;
elseif (theta>=-2.748893572)&(theta<-1.963495409),
                popsk(6)=popsk(6)+p;
elseif (theta>=-1.963495409)&(theta<-1.178097245),
                popsk(7)=popsk(7)+p;
else,
                popsk(8)=popsk(8)+p;
end

end

%Having accumulated the probabilities for each of the
%decision regions  they must be scaled so that their
%total equals unity

po1=pi/k*popsk(1);
po2=pi/k*popsk(2);
po3=pi/k*popsk(3);
po4=pi/k*popsk(4);
po5=pi/k*popsk(5);
po6=pi/k*popsk(6);
po7=pi/k*popsk(7);
po8=pi/k*popsk(8);

%These probabilities are now used to compute the
%phase detector characteristic output

pdo2=sin(psi)*po1+sin(psi+pi/4)*po2;
pdo2=pdo2+sin(psi+pi/2)*po3+sin(psi+3*pi/4)*po4;
pdo2=pdo2+sin(psi+pi)*po5+sin(psi+5*pi/4)*po6;
```

```
pdo2=pdo2+sin(psi+3*pi/2)*po7+sin(psi+7*pi/4)*po8;

%The gain is the phase detector characteristic output
%divided by the phase error. Also note that the square
%of the gain is what is desired

alpha2=20*log10(pdo2/psi);

%Save the data

save 8pskdata;
```

The theoretical and numerical data, plotted in Figure 5-11 and Figure 5-17 is presented here, in dB, in Table E-1 and Table E-2.

Table E-1. The first set of MPSK phase detector gain data.

	BPSK	QPSK	QPSK	8PSK	16PSK
	Theoretical	Theoretical	Numerical	Numerical	Numerical
SNR	Data	Data	Data	Data	Data
(dB)	(variance)	(variance)	(variance)	(variance)	(variance)
0.000	-1.486	-14.033	-14.029		
0.500	-1.251	-12.832			
1.000	-1.037	-11.663	-11.660		
1.500	-0.846	-10.533			
2.000	-0.677	-9.442	-9.440	-42.790	
2.500	-0.531	-8.396			
3.000	-0.407	-7.399	-7.397	-37.067	
3.500	-0.304	-6.454			
4.000	-0.220	-5.566	-5.564	-31.609	
4.500	-0.154	-4.739			
5.000	-0.104	-3.976	-3.974	-26.469	
5.500	-0.068	-3.281			
6.000	-0.042	-2.657	-2.656	-21.699	
6.500	-0.024	-2.106			
7.000	-0.014	-1.628	-1.627	-17.350	
7.500	-0.007	-1.224			
8.000	-0.003	-0.891	-0.890	-13.465	
8.500	-0.002	-0.625			
9.000	-0.001	-0.420	-0.420	-10.080	
9.500	0.000	-0.269			
10.000	0.000	-0.163	-0.163	-7.214	-41.304
10.500	0.000	-0.093			
11.000	0.000	-0.049	-0.049	-4.877	-33.383
11.500	0.000	-0.024			
12.000	0.000	-0.011	0.011	-3.061	-26.388
12.500	0.000	-0.004			
13.000	0.000	-0.002	0.002	-1.741	-20.376
13.500	0.000	-0.001			
14.000	0.000	0.000		-0.868	-15.324
14.500	0.000	0.000			

Table E-2. The second set of MPSK phase detector gain data.

	BPSK	QPSK	QPSK	8PSK	16PSK
	Theoretical	Theoretical	Numerical	Numerical	Numerical
SNR	Data	Data	Data	Data	Data
(dB)	(variance)	(variance)	(variance)	(variance)	(variance)
15.000	0.000	0.000		-0.364	-11.162
15.500	0.000	0.000			
16.000	0.000	0.000		-0.121	-7.803
16.500	0.000	0.000			
17.000	0.000	0.000		-0.030	-5.166
17.500	0.000	0.000			
18.000	0.000	0.000		-0.005	-3.177
18.500	0.000	0.000			
19.000	0.000	0.000		0.000	-1.769
19.500	0.000	0.000			
20.000	0.000	0.000			-0.861
20.500	0.000	0.000			
21.000	0.000	0.000			-0.350
21.500	0.000	0.000			
22.000	0.000	0.000			-0.112
22.500	0.000	0.000			
23.000	0.000	0.000			-0.026
23.500	0.000	0.000			
24.000	0.000	0.000			-0.004
24.500	0.000	0.000			
25.000	0.000	0.000			0.000

Appendix F

MPSK VARIANCE OF PHASE ERROR RESULTS

In Chapter 6 the equation that describes the variance of the phase error was discussed. Results were presented graphically. The components of the equation and the variance itself are tabulated here. Equation (6-7) is the equation used for computing the variance. Tables F-1 and F-2 contain the BPSK data for the 4 selected high-SNR loop bandwidth-to-symbol rate ratios. Table F-3 contains the QPSK variance data. The 8PSK numerical variance data is tabulated in Table F-4 and Table F-5 and the 16PSK numerical data is tabulated in F-6. All of the data are plotted in dB.

Table F-1. The first set of BPSK variance data.

SNR (dB)	High SNR BL/SR=1% (variance)	High SNR BL/SR=0.5% (variance)	High SNR BL/SR=0.25% (variance)	High SNR BL/SR=0.125% (variance)
40	-63.01	-66.021	-69.031	-72.041
30	-53.01	-56.021	-59.031	-62.041
25	-48.01	-51.021	-54.031	-57.041
24	-47.01	-50.021	-53.031	-56.041
23	-46.01	-49.021	-52.031	-55.041
22	-45.01	-48.021	-51.031	-54.041
21	-44.01	-47.021	-50.031	-53.041
20	-43.01	-46.021	-49.031	-52.041
19	-42.01	-45.021	-48.031	-51.041
18	-41.01	-44.021	-47.031	-50.041
17	-40.01	-43.021	-46.031	-49.041
16	-39.01	-42.021	-45.031	-48.041
15	-38.01	-41.021	-44.031	-47.041
14.5	-37.51	-40.521	-43.531	-46.541
14	-37.01	-40.021	-43.031	-46.041
13.5	-36.51	-39.521	-42.531	-45.541
13	-36.01	-39.021	-42.031	-45.041
12.5	-35.51	-38.521	-41.531	-44.541
12	-35.01	-38.021	-41.031	-44.041
11.5	-34.51	-37.521	-40.531	-43.541
11	-34.01	-37.021	-40.031	-43.041
10.5	-33.51	-36.521	-39.531	-42.541

Table F-2. The second set of BPSK variance data.

SNR (dB)	High SNR BL/SR=1% (variance)	High SNR BL/SR=0.5% (variance)	High SNR BL/SR=0.25% (variance)	High SNR BL/SR=0.125% (variance)
10	-33.01	-36.021	-39.031	-42.041
9.5	-32.51	-35.521	-38.531	-41.541
9	-32.01	-35.02	-38.03	-41.041
8	-31.008	-34.019	-37.029	-40.039
7	-30.002	-33.013	-36.023	-39.033
6	-28.986	-31.996	-35.006	-38.017
5	-27.948	-30.958	-33.968	-36.979
4	-26.878	-29.888	-32.899	-35.909
3	-25.765	-28.776	-31.786	-34.796
2	-24.602	-27.612	-30.623	-33.633
1	-23.383	-26.393	-29.404	-32.414
0	-22.108	-25.118	-28.129	-31.139

Table F-3. The QPSK variance data.

SNR (dB)	High SNR BL/SR=1% (variance)	High SNR BL/SR=0.5% (variance)	High SNR BL/SR=0.25% (variance)	High SNR BL/SR=0.125% (variance)
40	-63.01	-66.021	-69.031	-72.041
30	-53.01	-56.021	-59.031	-62.041
25	-48.01	-51.021	-54.031	-57.041
24	-47.01	-50.021	-53.031	-56.041
23	-46.01	-49.021	-52.031	-55.041
22	-45.01	-48.021	-51.031	-54.041
21	-44.01	-47.021	-50.031	-53.041
20	-43.01	-46.021	-49.031	-52.041
19	-42.01	-45.021	-48.031	-51.041
18	-41.01	-44.021	-47.031	-50.041
17	-40.01	-43.021	-46.031	-49.041
16	-39.01	-42.021	-45.031	-48.041
15	-38.01	-41.021	-44.031	-47.041
14	-37.01	-40.021	-43.031	-46.041
13	-36.009	-39.019	-42.03	-45.04
12	-35.004	-38.014	-41.024	-44.035
11	-33.981	-36.991	-40.001	-43.012
10	-32.912	-35.923	-38.933	-41.943
9	-31.758	-34.769	-37.779	-40.789
8	-30.478	-33.488	-36.498	-39.508
7	-29.039	-32.05	-35.06	-38.07
6	-27.434	-30.445	-33.455	-36.465
5	-25.666	-28.676	-31.686	-34.696
4	-23.741	-26.752	-29.762	-32.772
3	-21.671	-24.682	-27.692	-30.702
2	-19.458	-22.468	-25.478	-28.489
1	-17.099	-20.11	-23.12	-26.13
0	-14.588	-17.598	-20.608	-23.618

Table F-4. The first set of 8PSK variance data.

SNR (dB)	High SNR BL/SR=1% (variance)	High SNR BL/SR=0.5% (variance)	High SNR BL/SR=0.25% (variance)	High SNR BL/SR=0.125% (variance)
40	-63.01	-66.021	-69.031	-72.041
30	-53.01	-56.021	-59.031	-62.041
25	-48.01	-51.021	-54.031	-57.041
24	-47.01	-50.021	-53.031	-56.041
23	-46.01	-49.021	-52.031	-55.041
22	-45.01	-48.021	-51.031	-54.041
21	-44.01	-47.021	-50.031	-53.041
20	-43.01	-46.021	-49.031	-52.041
19	-42.01	-45.021	-48.031	-51.041
18	-41.007	-44.018	-47.028	-50.038
17	-39.992	-43.003	-46.013	-49.023
16	-38.938	-41.948	-44.958	-47.969
15	-37.791	-40.802	-43.812	-46.822
14.5	-37.163	-40.173	-43.184	-46.194
14	-36.486	-39.496	-42.507	-45.517
13.5	-35.751	-38.761	-41.772	-44.782
13	-34.951	-37.961	-40.972	-43.982
12.5	-34.079	-37.089	-40.1	-43.11
12	-33.128	-36.138	-39.148	-42.158
11.5	-32.091	-35.101	-38.112	-41.122
11	-30.962	-33.973	-36.983	-39.993
10.5	-29.735	-32.746	-35.756	-38.766

Table F-5. The second set of 8PSK variance data.

SNR (dB)	High SNR BL/SR=1% (variance)	High SNR BL/SR=0.5% (variance)	High SNR BL/SR=0.25% (variance)	High SNR BL/SR=0.125% (variance)
10	-28.403	-31.414	-34.424	-37.434
9.5	-26.959	-29.969	-32.979	-35.989
9	-25.393	-28.403	-31.413	-34.424
8.5	-23.7	-26.71	-29.72	-32.731
8	-21.873	-24.883	-27.894	-30.904
7.5	-19.905	-22.915	-25.926	-28.936
7	-17.793	-20.803	-23.814	-26.824
6.5	-15.537	-18.548	-21.558	-24.568
6	-13.139	-16.149	-19.16	-22.17
5.5	-10.606	-13.616	-16.626	-19.637
5	-7.9448	-10.955	-13.965	-16.976
4	-2.286	-5.2963	-8.3066	-11.317
3	3.7369	0.72662	-2.2837	-5.294
2	10.026	7.0159	4.0056	0.9953

Table F-6. The 16PSK variance data.

SNR (dB)	High SNR BL/SR=1% (variance)	High SNR BL/SR=0.5% (variance)	High SNR BL/SR=0.25% (variance)	High SNR BL/SR=0.125% (variance)
40	-63.01	-66.021	-69.031	-72.041
30	-53.01	-56.021	-59.031	-62.041
25	-48.01	-51.021	-54.031	-57.041
24	-47.01	-50.021	-53.031	-56.041
23	-46.01	-49.021	-52.031	-55.041
22	-45.01	-48.021	-51.031	-54.041
21	-44.01	-47.021	-50.031	-53.041
20	-42.491	-45.501	-48.511	-51.522
19.5	-41.749	-44.759	-47.769	-50.78
19	-40.935	-43.945	-46.956	-49.966
18.5	-40.04	-43.051	-46.061	-49.071
18	-39.056	-42.066	-45.076	-48.087
17.5	-37.971	-40.981	-43.991	-47.002
17	-36.775	-39.786	-42.796	-45.806
16.5	-35.457	-38.467	-41.478	-44.488
16	-34.001	-37.011	-40.022	-43.032
15.5	-32.39	-35.401	-38.411	-41.421
15	-30.605	-33.615	-36.625	-39.635
14.5	-28.62	-31.63	-34.641	-37.651
14	-26.411	-29.422	-32.432	-35.442
13.5	-23.952	-26.962	-29.973	-32.983
13	-21.218	-24.228	-27.239	-30.249
12.5	-18.19	-21.2	-24.211	-27.221
12	-14.857	-17.868	-20.878	-23.888
11.5	-11.219	-14.229	-17.24	-20.25
11	-7.2854	-10.296	-13.306	-16.316
10.5	-3.0789	-6.0892	-9.0995	-12.11

Appendix G

MPSK HIGH-SNR MAP CARRIER TRACKING SIMULATION RESULTS

In Chapter 6 the simulation results were presented. Simulations were conducted to verify that the numerical results for the 8PSK and 16PSK variance of the phase error were correct. These simulations were conducted using the nonlinear baseband model of Figure 4-2. All of the baseband simulations assume phaselock at the modulation point corresponding to the zero-phase angle modulation symbol and assume that only the zero-angle modulation symbol is being transmitted. This is exactly what was done for the variance of the phase error component calculations of Chapter 5. Further, it speeds up the simulation time since random data is not required.

One sample per symbol period is used in these time-simulations where the output at the end of a simulation run is the statistical variance of 35 samples of the VCO phase in the baseband loop. Since the "received" signal phase is held at a constant zero radians, the VCO output phase is indeed the phase error. Only 35 samples were used to save computational time.

Each simulation actually executes several thousand iterations to obtain the 35 statistical samples. This is required because adjacent samples in time are highly correlated with each other. It is the nature of the phaselock loop to average out the effects of noise and thus vary the phase slowly in response. To

obtain statisically uncorrelated samples required analysis of the transfer function of the loop.

The tracking loop is a filter whose transfer function, translated down to baseband, is $H(s)$. The response of this filter to white Gaussian noise is a noise process whose normalized power spectral density magnitude response is $|H(s)|^2$. The inverse Fourier transform of this response yields the normalized autocorrelation function of the process. What is of interest in this autocorrelation function are the points at which the function equates to zero. These points correspond to the time difference required between noise samples so that they have zero correlation with each other. The response, $|H(s)|^2$, is a lowpass function and its inverse Fourier transform yields a function that has a damped oscillation in both directions as the time difference increases. The first zero crossing represents the shortest amount of time required between uncorrelated samples. Therefore for all 4 PSK schemes, at 3 different loop bandwidths, and for all the desired SNR's, the first zero crossing was obtained. This minimized the required run time of the simulations.

The source code for the simulation of the 8PSK baseband carrier tracking loop is:

```
%8PSK high-SNR MAP carrier tracking simulator

clear
t1=clock;
format long
```

```
%Initialization parameters: natural freq, damping
%factor,symbol rate

wn=1171.88;
zeta=1.2;
sr=5e5;

%Calculate filter integrator gain: a, integrator parmeter
%c=a*T, high-SNR gain: k,vco integrator parameter;

a=wn/(2*zeta);
c=a/sr;
k=2*wn*zeta;
k2=k/sr;

%Initialize carrier phase, vco initial phase, and loop
%filter integrator

sigphs=0;
vcophs=0;
fltint=0;

%set random number distribution

rand('normal');

%Set statcnt size for snrs. This is the number of
%samples used to compute the variance of the phase
%error. It sets up the size of the outer loop. The size of
%the inner loop is found from the auto correlation
%function associated with white noise that has passed
%through a lowpass function that has the same
%transfer function as the loop, namely H(s).

stattot=35;

% For snr's from 5.5 to 15 dB in .5 dB steps and then
%16 to 25 in 1 db steps the zero crossings occur at the
%following simulation time sample increments

statsize=[6280
5495
4867
4239
3768
3454
3140
2826
2512
2355
2198
```

```
2041
1884
1727
1727
1570
1570
1570
1570
1413
1413
1413
1413
1413
1413
1413
1413
1413
1413];

%The snr's that the simulations will be run at

snrv=[5.5
6
6.5
7
7.5
8
8.5
9
9.5
10
10.5
11
11.5
12
12.5
13
13.5
14
14.5
15
16
17
18
19
20
21
22
23
```

```
24
25];

%outer loop to count through the snr array

for snrcnt = 1:1:30;

snrdb = snrv(snrcnt);
snr= 10^(snrdb/10);

%noise STDEV out of correlators

sigma= sqrt(1/(2*snr));

%set carrier phase, vco initial phase, loop filter
%integrator variables and phase error

sigphs=0;
vcophs=0;
fltint=0;
phserr=0;
fltlast=0;

%Reset stats for calculating variance

sumerr=0;
sqrerr=0;
maxerr=0;

%Initialize random number generator

rand('seed',650);

%Statistics loop. This loop iterates once for each sample
%used in the variance calculation

for statcnt = 1:1:stattot;

%The loop that sets the number of samples used
%between the statistical samples

for simcnt = 1:1:statsize(snrcnt);

%Fix data

 im=1.0;
 qm=0.0;

%Generate noise

ni=sigma*rand(1);
```

```
nq=sigma*rand(1);

%Calculate correlator outputs

i=im*cos(phserr)+qm*sin(phserr)+ni;
q=-im*sin(phserr)+qm*cos(phserr)+nq;

%Make data estimates

rcvdphs=atan2(q,i);

if (rcvdphs<0.392699082)&(rcvdphs>=-0.392699082),
        ihat=1.0;
        qhat=0.0;
elseif (rcvdphs<1.178097245)&(rcvdphs>=0.392699082),
        ihat=0.707106781;
        qhat=0.707106781;
elseif (rcvdphs<1.963495409)&(rcvdphs>=1.178097245),
        ihat=0.0;
        qhat=1.0;
elseif (rcvdphs<2.748893572)&(rcvdphs>=1.963495409),
        ihat=-0.707106781;
        qhat=0.707106781;
elseif (rcvdphs<-2.748893572)|(rcvdphs>=2.748893572),
        ihat=-1.0;
        qhat=0.0;
elseif (rcvdphs<-1.963495409)&(rcvdphs>=-2.748893572),
        ihat=-0.707106781;
        qhat=-0.707106781;
elseif (rcvdphs<-1.178097245)&(rcvdphs>=-1.963495409),
        ihat=0.0;
        qhat=-1.0;
else,
        ihat=0.707106781;
        qhat=-0.707106781;
end

%Generate error signal

error=i*qhat-q*ihat;

%Calculate filter output

filtout= fltint+error;

%Calculate filter integrator's new value for next time

fltint=fltint+error*c;

%Calculate next value of the vco phase
```

```
vcophs=vcophs+fltlast*k2;

%Set next vco input value;

fltlast=filtout;

%Calculate next value of the phase error

phserr=-vcophs;

%Store max phase encountered

if(abs(phserr)>maxerr),
maxerr=abs(phserr);
end

end

%Iterate statistical parameters

sqrerr=sqrerr+phserr^2;
sumerr=sumerr+phserr;

end

meanphs(snrcnt)=sumerr/stattot;
vp=sqrerr/(stattot-1)-sumerr^2/(stattot*(stattot-1));
varphs(snrcnt)=vp;
maxsave(snrcnt)=maxerr;
end

%check time and save data

t2=clock;
tdiff=t2-t1;

save 8pk1650b wn zeta sr meanphs varphs maxsave
```

The simulation data is tabulated in the following tables for BPSK, QPSK, 8PSK, and 16PSK. The simulations were conducted using three specific high-SNR loop bandwidths (the same three used in the hardware) and a symbol rate of 500 kilo-samples-per-second. The ratios of the three specific bandwidths to the above symbol

rate are listed on the simulation data graphs of Figures 6-6 through 6-17 and at the tops of the following data tables.

The BPSK simulation data are tabulated in Table G-1. The QPSK data is contained in Table G-2 and Table G-3 contains the 8PSK variance data. The 16PSK data are tabulated in Table G-4. All the data are plotted in dB.

Table G-1. The BPSK simulation variance data.

SNR (dB)	High SNR BL/SR=0.19% (variance)	High SNR BL/SR=0.33% (variance)	High SNR BL/SR=0.66% (variance)
25			-49.67
20	-50.31	-50.31	-44.67
15	-45.31	-45.31	-39.67
10	-40.31	-40.31	-34.67
5	-35.74	-35.74	-29.98
4	-34.67	-34.67	-28.99
3	-33.14	-33.14	-27.26
2	-32.06	-32.06	-26.25
1	-30.89	-30.89	-25.39
0	-29.15	-29.15	-24.82

Table G-2. The QPSK simulation variance data.

SNR (dB)	High SNR BL/SR=0.19% (variance)	High SNR BL/SR=0.33% (variance)	High SNR BL/SR=0.66% (variance)
25			-49.67
20	-50.11	-47.98	-44.67
15	-45.31	-42.99	-39.67
10	-40.44	-37.74	-34.74
9	-39.70	-37.12	-33.77
8	-36.88	-35.75	-32.73
7	-35.06	-33.64	-30.76
6	-35.34	-32.74	-30.27
5	-34.45	-30.91	-29.00
4	-31.85	-27.77	-27.31
3	-29.16	-26.13	-22.89
2	-28.88	-26.42	-22.21
1	-24.01	-22.88	-19.11
0	-20.75	-21.14	-16.87

Table G-3. The 8PSK simulation variance data.

SNR (dB)	High SNR BL/SR=0.19% (variance)	High SNR BL/SR=0.33% (variance)	High SNR BL/SR=0.66% (variance)
25		-52.99	-49.521
24		-51.99	-48.52
23		-50.99	-47.521
22		-49.99	-46.521
21		-48.99	-45.521
20	-50.31	-47.99	-44.52
19	-49.31	-46.99	-43.52
18	-48.31	-45.99	-42.52
17	-47.52	-45.04	-41.426
16	-46.32	-44.16	-40.396
15	-45.5	-43.09	-38.695
14.5	-44.83	-42.63	-38.203
14	-43.58	-41.93	-37.962
13.5	-43.35	-41.02	-37.664
13	-43.58	-39.95	-36.233
12.5	-42.54	-39.6	-36.674
12	-41.89	-38.21	-35.111
11.5	-38.9	-37.94	-34.602
11	-38.48	-36.13	-32.811
10.5	-37.76	-35.78	-31.246
10	-35.57	-35.23	-30.566
9.5	-36.39	-34.27	-28.792
9	-34.24	-31.12	-27.952
8.5	-31.6	-30.91	-27.439
8	-30.63	-30.19	-25.411
7.5	-29.66	-28	-22.216
7	-26.91	-23.11	
6.5		-21.28	

Table G-4. The 16PSK simulation variance data.

SNR (dB)	High SNR BL/SR=0.19% (variance)	High SNR BL/SR=0.33% (variance)	High SNR BL/SR=0.66% (variance)
25			-49.67
24			-48.67
23			-47.7
22		-50.3	-46.61
21		-48.87	-45.52
20	-49.93	-46.81	-44.48
19.5	-49.2	-46.63	-44.23
19	-48.43	-46.69	-44
18.5	-47.34	-45.14	-40.66
18	-46.76	-44.7	-39.92
17.5	-45.5	-43.57	-39.76
17	-44.33	-43.37	-38.18
16.5	-44.13	-42.02	-38.15
16	-41.72	-41.3	-37.4
15.5	-41.83	-39.36	-36.81
15	-39.14	-37.39	-33.75
14.5	-37.11	-35.41	-33
14	-35.85	-33.51	-30.71
13.5	-31.57	-30.03	-29.17

Appendix H

THE HARDWARE TEST CONFIGURATION AND RESULTS

As discussed in Chapter 6 an MPSK high-SNR carrier tracking loop was constructed in hardware to verify the variance results. A simulated MPSK transmission was created and used as an input to the loop. In fact, just as was done with the numerical anaylsis and the computer simulations, the MPSK transmission represented the transmission of the same symbol continuously. This made the MPSK signal a continuous wave (CW) carrier signal that could be obtained from a standard frequency synthesizer and it removed the impact of intersymbol interference as a dependent variable in the testing. White noise was added to the CW carrier signal and the result passed to the demodulator front-end of the carrier tracking loop. This demodulator front end is a quadrature structure that power-divides the CW carrier-with-noise signal into two signals that are mixed in quadrature with the "VCO" signal. Actually a numerically controlled oscillator (NCO) was used in place of a VCO since much of the loop was constructed with digital hardware. The outputs of the quadrature mixers are fed through a set of lowpass filters. The use of lowpass filters instead of integrate-and-dump circuits does not cause a problem since the test set-up is calibrated at the output of the filters. Analog-to-digital conversion takes place after the lowpass filters and the generated 8 bits of I channel baseband data and 8 bits of Q

channel baseband data are passed to a set of electronically programmable read only memory (EPROM) chips. These EPROM chips generate the error signal of the high-SNR loop using16 bits. This error signal is processed by a digital filter that creates a second order transfer function for the loop. The output from digital filter, a 16-bit word, is added to a 32-bit word that represents the quiescent frequency of the output sinusoid from the loop NCO. This 32-bit sum is the frequency that the NCO will output during the next symbol period and it is transferred byte-serially to a Stanford Telecomm 1172/1272 NCO/evaluation board that generates both the sine and cosine of the desired output frequency. These two sinusoids are analog when they leave the evaluation board and return to the demodulation front-end where they are mixed in quadrature with the "received" signal. This circuit is shown in Figure H-1.

The I and Q baseband data at the output of the lowpass filters are corrupted by the input noise and thus variance measurements cannot be made using these data. To facilitate making variance measurements the outputs from the NCO are mixed in quadrature with the "clean" CW carrier from the synthesizer. The mixer outputs are lowpass filtered to remove the double frequency term and create I and Q baseband data that are corrupted only with phase jitter from the NCO.

This I and Q data are displayed on a modulation analyzer that can plot the I and Q data in the constellation space. If there is

no noise and if the carrier tracking loop is phaselocked the display will show a single lock point. If there is noise present and therefore jitter on the NCO signals then the lock point will take the shape of an arc. The arc is a plot of past samples of the phase error. It is brightest in the center, at the lock point, indicating that the mean of the phase error is zero. The modulation analyzer samples the I and Q components 4096 times over a period of approximately 30 seconds and calculates the statistical variance of the samples. By taking such a large sample set it was hoped that any correlation between adjacent samples would be averaged out. The results seem to indicate this is indeed the case. All the tabulated data that follows is plotted in dB.

Table H-1 and Table H-2 contain the hardware results for BPSK that were plotted in Figure 6-18. The BPSK data plotted in Figure 6-19, for the second loop bandwidth is tabulated in Table H-3 and H-4. The third bandwidth that was tested for BPSK yielded the data plotted in Figure 6-20 and tabulated in Tables H-5 and H-6.

For QPSK, H-7 and H-8 contain the hardware results for the smallest high-SNR loop bandwidth-to-symbol rate ratio. This is the data shown in Figure 6-21. The data in Figure 6-22 is tabulated in Tables H-9 and H-10, and the data in Figure 6-23 can be found in Tables H-11 and H-12, corresponding to the widest high-SNR loop-to-symbol rate ratio tested.

Table H-13 and Table H-14 contain the hardware results for 8PSK that were plotted in Figure 6-24. Table H-15 is the tabulated data for the results in Figure 6-25 and the data corresponding to the largest high-SNR loop bandwidth-to-symbol rate ratio, plotted in Figure 6-26, is tabulated in Tables H-16 and H-17.

For 16PSK the data shown in Figure 6-27 is tabulated in Table H-18 and the data of Figure 6-28 is contained in Table H-19. The final two tables, Table H-20 and H-21, contain the the data for the largest high-SNR loop bandwidth-to-symbol rate ratio. This is the data shown in Figure 6-29.

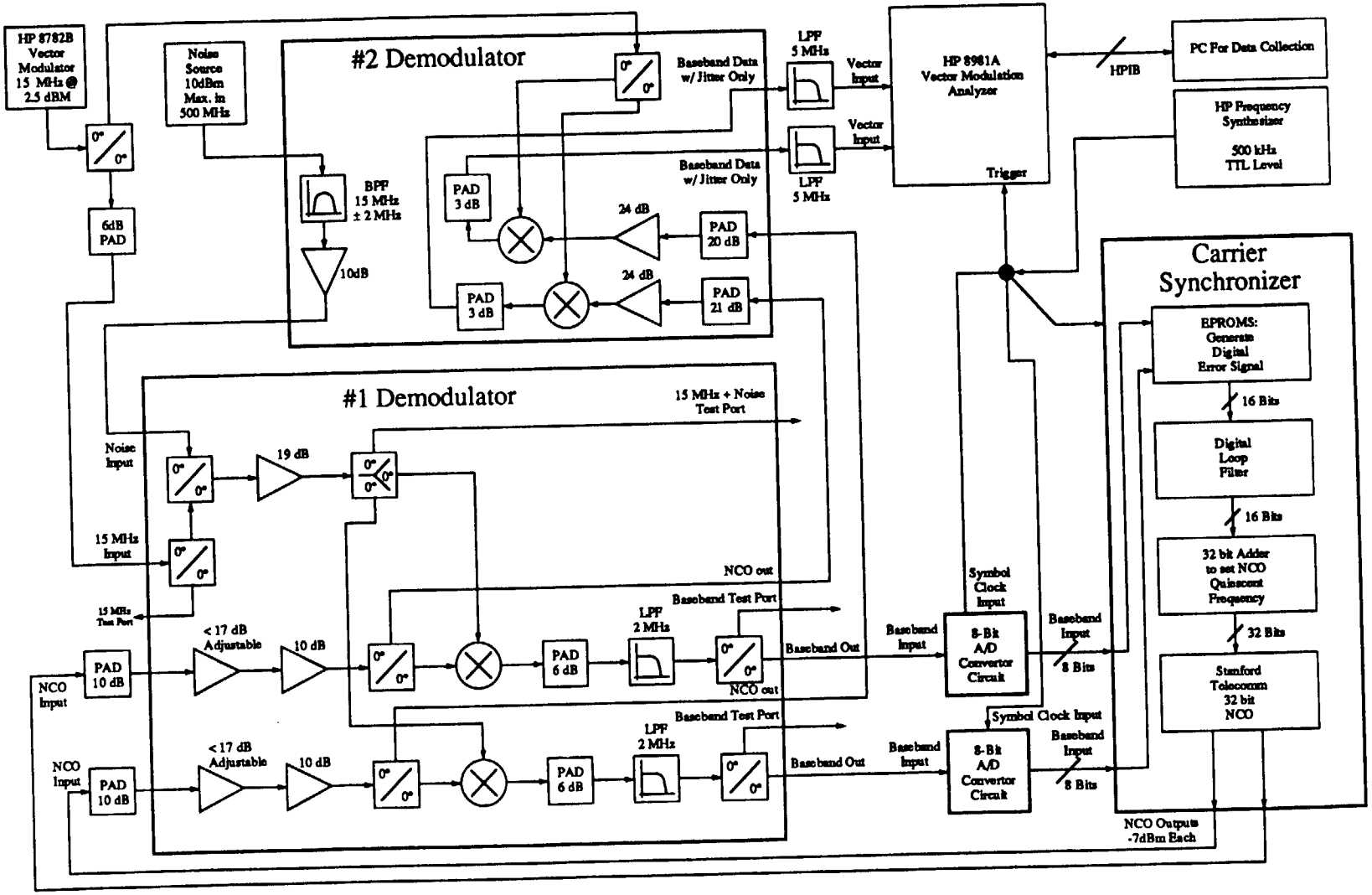

Figure H-1. The MPSK high-SNR carrier tracking hardware test configuration.

Table H-1. The first set of BPSK hardware variance data at 0.19% high-SNR loop bandwidth-to-symbol rate ratio.

LAB SNR (dB)	Measured Variance		SNR for Theoretical Data (dB)	Theoretical variance with added noise floor	Theoretical variance
32.9	-43.775		35		
27.9	-44.223		30	-43.898	-60.232
25.4	-43.736		27.5		
22.9	-43.59		25	-43.685	-55.232
22.4	-43.824		24.5		
21.9	-43.673		24	-43.607	-54.232
21.4	-43.644		23.5		
20.9	-43.623		23	-43.51	-53.232
20.4	-43.004		22.5		
19.9	-43.405		22	-43.392	-52.232
19.4	-42.997		21.5		
18.9	-43.401		21	-43.248	-51.232
18.4	-42.93		20.5		
17.9	-42.679		20	-43.072	-50.232
17.4	-42.519		19.5		
16.9	-42.461		19	-42.861	-49.232
16.4	-42.471		18.5		
15.9	-42.169		18	-42.609	-48.232
15.4	-41.869		17.5		
14.9	-41.604		17	-42.312	-47.232
14.4	-41.538		16.5		
13.9	-41.201		16	-41.964	-46.232
13.4	-40.599		15.5		
12.9	-40.321		15	-41.562	-45.232
12.4	-39.876		14.5	-41.34	-44.732
11.9	-39.865		14	-41.104	-44.232
11.4	-39.644		13.5	-40.853	-43.732
10.9	-39.137		13	-40.589	-43.232
10.4	-38.874		12.5	-40.309	-42.732
9.9	-38.481		12	-40.016	-42.232
9.4	-38.033		11.5	-39.709	-41.732

Table H-2. The second set of BPSK hardware variance data at 0.19% high-SNR loop bandwidth-to-symbol rate ratio.

LAB SNR (dB)	Measured Variance		SNR for Theoretical Data (dB)	Theoretical variance with added noise floor	Theoretical variance
8.9	-37.538		11	-39.389	-41.232
8.4	-37.276		10.5	-39.055	-40.732
7.9	-36.884		10	-38.709	-40.232
7.4	-36.474		9.5	-38.351	-39.732
6.9	-36.047		9	-37.981	-39.231
6.4	-35.92		8.5	-37.601	-38.732
5.9	-35.148		8	-37.209	-38.23
5.4	-34.776		7.5	-36.811	-37.732
4.9	-33.937		7	-36.395	-37.223
4.4	-33.854		6.5	-35.985	-36.732
3.9	-33.308		6	-35.538	-36.206
3.4	-32.568		5.5	-35.128	-35.732
2.9	-31.852		5	-34.632	-35.166
2.4	-31.857		4.5		
1.9	-31.5		4	-33.671	-34.093
1.4	-30.865		3.5		
0.9	-30		3	-32.645	-32.975
0.4	-29.315		2.5		
-0.1	-28.551		2	-31.549	-31.804
-0.6	-28.171		1.5		
-1.1	-27.231		1	-30.381	-30.574
-1.6	-26.453		0.5		
-2.1	-26.101		0	-29.141	-29.285

Table H-3. The first set of BPSK hardware variance data at 0.33% high-SNR loop bandwidth-to-symbol rate ratio.

LAB SNR (dB)	Measured Variance		SNR for Theoretical Data (dB)	Theoretical variance with added noise floor	Theoretical variance
30.4	-43.952		32.5		
27.9	-43.693		30	-43.776	-57.824
25.4	-43.976		27.5		
22.9	-43.878		25	-43.421	-52.824
20.4	-42.771		22.5		
19.4	-42.46		21.5		
18.9	-41.89		21	-42.726	-48.824
18.4	-41.844		20.5	-42.458	-47.824
17.9	-41.376		20		
17.4	-41.262		19.5	-42.143	-46.824
16.9	-40.806		19		
16.4	-40.844		18.5	-41.776	-45.824
15.9	-40.543		18		
15.4	-39.92		17.5	-41.355	-44.824
14.9	-39.651		17		
14.4	-39.419		16.5	-40.876	-43.824
13.9	-39.066		16		
13.4	-38.712		15.5	-40.34	-42.824
12.9	-38.463		15	-40.051	-42.324
12.4	-37.94		14.5	-39.748	-41.824
11.9	-37.376		14	-39.431	-41.324
11.4	-37.271		13.5	-39.101	-40.824
10.9	-36.902		13	-38.759	-40.324
10.4	-36.069		12.5	-38.404	-39.824
9.9	-35.815		12	-38.038	-39.324
9.4	-35.528		11.5	-37.661	-38.824
8.9	-35.014		11	-37.273	-38.324
8.4	-34.561		10.5	-36.876	-37.824
7.9	-34.156		10	-36.47	-37.324
7.4	-33.601		9.5	-36.054	-36.824
6.9	-33.033		9	-35.632	-36.324

Table H-4. The second set of BPSK hardware variance data at 0.33% high-SNR loop bandwidth-to-symbol rate ratio.

LAB SNR (dB)	Measured Variance		SNR for Theoretical Data (dB)	Theoretical variance with added noise floor	Theoretical variance
6.4	-32.483		8.5	-35.201	-35.822
5.9	-32.081		8	-34.766	-35.324
5.4	-31.793		7.5	-34.316	-34.817
4.9	-31.512		7	-33.875	-34.324
4.4	-30.824		6.5	-33.4	-33.801
3.9	-30.217		6	-32.964	-33.324
3.4	-29.643		5.5	-32.446	-32.764
2.9	-29.23		5		
2.4	-29.029		4.5	-31.447	-31.698
1.9	-27.975		4		
1.4	-27.667		3.5	-30.394	-30.59
0.9	-26.965		3		
0.4	-26.345		2.5	-29.283	-29.434
-0.1	-25.66		2		
-0.6	-25.077		1.5	-28.11	-28.225
-1.1	-24.51		1		
-1.6	-23.864		0.5	-26.877	-26.963

Table H-5. The first set of BPSK hardware variance data at 0.66% high-SNR loop bandwidth-to-symbol rate ratio.

SNR (dB)	Theoretical variance with added noise floor	Theoretical variance	Measured variance
30	-43.469	-54.814	-43.464
29			-43.529
28			-43.372
27			-43.193
26			-43.036
25	-42.83	-49.814	-42.849
24.5			-42.711
24	-42.61	-48.814	-42.573
23.5			-42.658
23	-42.349	-47.814	-42.619
22.5			-42.148
22	-42.04	-46.814	-41.995
21.5			-41.988
21	-41.681	-45.814	-41.672
20.5			-41.395
20	-41.267	-44.814	-40.893
19.5			-40.909
19	-40.797	-43.814	-40.456
18.5			-40.325
18	-40.269	-42.814	-40.005
17.5			-39.652
17	-39.684	-41.814	-39.384
16.5			-38.788
16	-39.045	-40.814	-38.664
15.5			-38.093
15	-38.354	-39.814	-37.781
14.5	-37.991	-39.314	-37.435
14	-37.617	-38.814	-37.036
13.5	-37.232	-38.314	-36.779
13	-36.838	-37.814	-36.477
12.5	-36.434	-37.314	-35.788

Table H-6. The second set of BPSK hardware variance data at 0.66% high-SNR loop bandwidth-to-symbol rate ratio.

SNR (dB)	Theoretical variance with added noise floor	Theoretical variance	Measured variance
12	-36.021	-36.814	-35.537
11.5	-35.601	-36.314	-35.061
11	-35.173	-35.814	-34.53
10.5	-34.738	-35.314	-34.015
10	-34.297	-34.814	-33.715
9.5	-33.851	-34.314	-33.163
9	-33.398	-33.813	-32.832
8.5	-32.942	-33.314	-32.384
8	-32.479	-32.812	-31.836
7.5	-32.016	-32.314	-31.341
7	-31.54	-31.806	-30.721
6.5	-31.075	-31.314	-30.628
6	-30.578	-30.79	-29.845
5.5	-30.123	-30.314	-29.298
5	-29.586	-29.754	-28.683
4.5			-28.53
4	-28.556	-28.687	-27.837
3.5			-27.167
3	-27.477	-27.58	-26.747
2.5			-26.076
2	-26.345	-26.424	-25.76
1.5			-25.243
1	-25.155	-25.215	-24.479
0.5			-23.781
0	-23.908	-23.953	-23.279

Table H-7. The first set of QPSK hardware variance data at 0.19% high-SNR loop bandwidth-to-symbol rate ratio.

SNR (dB)	Theoretical variance with added noise floor	Theoretical variance	Measured variance
30	-41.047	-60.232	-41.002
29			-41.101
28			-41.184
27			-41.045
26			-40.962
25	-40.935	-55.232	-40.657
24	-40.894	-54.232	-40.472
23	-40.842	-53.232	-40.504
22.5			-40.83
22	-40.778	-52.232	-40.667
21.5			-40.477
21	-40.698	-51.232	-40.593
20.5			-40.492
20	-40.6	-50.232	-40.478
19.5			-40.342
19	-40.479	-49.232	-40.178
18.5			-40.281
18	-40.332	-48.232	-40.153
17.5			-39.854
17	-40.153	-47.232	-39.925
16.5			-39.922
16	-39.938	-46.232	-39.628
15.5			-39.322
15	-39.682	-45.232	-39.302
14.5			-39.165
14	-39.379	-44.232	-39.104
13.5			-38.726
13	-39.026	-43.23	-38.656
12.5			-38.394
12	-38.616	-42.225	-38.063
11.5			-37.943

Table H-8. The second set of QPSK hardware variance data at 0.19% high-SNR loop bandwidth-to-symbol rate ratio.

SNR (dB)	Theoretical variance with added noise floor	Theoretical variance	Measured variance
11	-38.14	-41.201	-37.666
10.5			-37.381
10	-37.661	-40.129	-36.864
9.5			-36.707
9	-36.894	-38.968	-36.303
8.5			-35.746
8	-36.046	-37.673	-35.393
7.5			-35.095
7	-34.992	-36.212	-34.354
6.5			-33.77
6	-33.701	-34.574	-32.996
5.5			-32.469
5	-32.166	-32.76	-31.553
4.5			-31.134
4	-30.392	-30.778	-30.111
3.5			-29.217
3	-28.398	-28.638	-27.976
2.5			-26.731
2	-26.2	-26.343	-25.37
1.5			-24.211
1	-23.813	-23.895	-23.505
0	-21.243	-21.288	

Table H-9. The first set of QPSK hardware variance data at 0.33% high-SNR loop bandwidth-to-symbol rate ratio.

LAB SNR (dB)	Measured Variance		SNR for Theoretical Data (dB)	Theoretical variance with added noise floor	Theoretical variance
42.9	-41.589		30	-41.107	-57.824
32.9	-41.234		25	-40.911	-52.824
27.9	-41.291		24	-40.839	-51.824
22.9	-41.115		23	-40.751	-50.824
21.9	-40.665		22	-40.641	-49.824
20.9	-40.555		21	-40.508	-48.824
19.9	-40.491		20	-40.345	-47.824
18.9	-40.136		19	-40.149	-46.824
17.9	-39.788		18	-39.913	-45.824
17.4	-39.737		17	-39.634	-44.824
16.9	-39.619		16	-39.307	-43.824
16.4	-39.256		15	-38.926	-42.824
15.9	-39.346		14	-38.491	-41.824
15.4	-38.803		13	-37.997	-40.823
14.9	-38.703		12	-37.444	-39.818
14.4	-38.449		11	-36.823	-38.796
13.9	-38.341		10	-36.169	-37.73
13.4	-38.013		9	-35.295	-36.583
12.9	-37.369		8	-34.319	-35.315
12.4	-37.549		7.5		
11.9	-37		7	-33.157	-33.898
11.4	-36.501		6.5		
10.9	-36.291		6	-31.795	-32.324
10.4	-35.905		5.5		
9.9	-35.418		5	-30.236	-30.599
9.4	-35.243		4.5		
8.9	-34.63		4	-28.491	-28.731
8.4	-34.217		3.5		
7.9	-33.549		3	-26.579	-26.731
7.4	-33.167		2.5		
6.9	-32.637		2	-24.509	-24.603

Table H-10. The second set of QPSK hardware variance data at 0.33% high-SNR loop bandwidth-to-symbol rate ratio.

LAB SNR (dB)	Measured Variance		SNR for Theoretical Data (dB)	Theoretical variance with added noise floor	Theoretical variance
6.4	-32.119		1.5		
5.9	-31.399		1	-22.286	-22.342
5.4	-30.825		0.5		
4.9	-29.933		0	-19.905	-19.938
4.4	-29.435				
3.9	-28.202				
3.4	-27.348				
2.9	-26.246				
2.4	-24.741				
1.9	-23.983				
1.4	-22.603				

Table H-11. The first set of QPSK hardware variance data at 0.66% high-SNR loop bandwidth-to-symbol rate ratio.

SNR (dB)	Theoretical variance with added noise floor	Theoretical variance	Measured variance
30	-40.823	-54.814	-40.821
29.5			-40.909
29			-40.754
28.5			-40.593
28			-40.576
27.5			-40.735
27			-40.703
26.5			-40.51
26			-40.528
25.5			-40.48
25	-40.464	-49.814	-40.118
24.5			-40.548
24	-40.335	-48.814	-40.365
23.5			-40.038
23	-40.178	-47.814	-40.215
22.5			-39.852
22	-39.989	-46.814	-39.989
21.5			-39.826
21	-39.761	-45.814	-39.597
20.5			-39.52
20	-39.491	-44.814	-39.002
19.5			-39.021
19	-39.173	-43.814	-38.84
18.5			-38.631
18	-38.803	-42.814	-38.466
17.5			-38.287
17	-38.378	-41.814	-37.868
16.5			-37.699
16	-37.896	-40.814	-37.459
15.5			-37.39
15	-37.356	-39.814	-36.56

Table H-12. The second set of QPSK hardware variance data at 0.66% high-SNR loop bandwidth-to-symbol rate ratio.

SNR (dB)	Theoretical variance with added noise floor	Theoretical variance	Measured variance
14.5			-36.672
14	-36.76	-38.814	-36.104
13.5			-35.698
13	-36.11	-37.813	-35.61
12.5			-35.101
12	-35.406	-36.808	-34.917
11.5			-34.376
11	-34.643	-35.786	-33.969
10.5			-33.533
10	-33.834	-34.72	-33.24
9.5			-32.782
9	-32.851	-33.573	-32.225
8.5			-31.69
8	-31.755	-32.305	-31.064
7.5			-30.551
7	-30.484	-30.888	-29.88
6.5			-29.554
6	-29.029	-29.314	-28.639
5.5			-27.87
5	-27.395	-27.588	-27.069
4.5			-26.656
4	-25.593	-25.72	-25.52
3.5			-24.494
3	-23.641	-23.721	-23.368
2.5			-22.224
2	-21.543	-21.593	-21.034
1.5			-19.804
1	-19.302	-19.332	
0	-16.91	-16.927	

Table H-13. The first set of 8PSK hardware variance data at 0.19% high-SNR loop bandwidth-to-symbol rate ratio.

LAB SNR (dB)	Measured Variance		SNR for Theoretical Data (dB)	Theoretical variance with added noise floor	Theoretical variance
42.9	-42.266		30	-42.329	-60.232
32.9	-42.532		25	-42.179	-55.232
27.9	-42.383		24	-42.124	-54.232
26.9	-42.293		23	-42.055	-53.232
25.9	-42.085		22	-41.97	-52.232
24.9	-41.556		21	-41.866	-51.232
23.9	-41.973		20	-41.738	-50.232
22.9	-41.486		19	-41.581	-49.232
22.4	-41.068		18	-41.392	-48.228
21.9	-41.668		17	-41.161	-47.213
21.4	-41.632		16	-40.874	-46.156
20.9	-41.943		15	-40.499	-45.002
20.4	-41.42		14.5	-40.263	-44.368
19.9	-41.154		14	-39.984	-43.682
19.4	-41.414		13.5	-39.649	-42.935
18.9	-41.278		13	-39.248	-42.12
18.4	-41.084		12.5	-38.765	-41.229
17.9	-40.961		12	-38.185	-40.253
17.4	-40.827		11.5	-37.493	-39.188
16.9	-40.932		11	-36.673	-38.024
16.4	-40.587		10.5	-35.709	-36.757
15.9	-41.133		10	-34.591	-35.377

Table H-14. The second set of 8PSK hardware variance data at 0.19% high-SNR loop bandwidth-to-symbol rate ratio.

LAB SNR (dB)	Measured Variance		SNR for Theoretical Data (dB)	Theoretical variance with added noise floor	Theoretical variance
15.4	-40.573		9.5	-33.307	-33.878
14.9	-40.313		9	-31.851	-32.252
14.4	-40.038		8.5	-30.222	-30.493
13.9	-39.918		8	-28.419	-28.596
13.4	-39.414		7.5	-26.444	-26.555
12.9	-38.963		7	-24.303	-24.37
12.4	-38.66		6.5	-22.004	-22.044
11.9	-37.924		6	-19.557	-19.579
11.4	-37.293		5.5	-16.973	-16.986
10.9	-35.912				
10.4	-35.193				
9.9	-34.191				
9.4	-33.189				
8.9	-31.169				
8.4	-29.823				
7.9	-27.121				

Table H-15. 8PSK hardware variance data at 0.33% high-SNR loop bandwidth-to-symbol rate ratio.

LAB SNR (dB)	Measured Variance		SNR for Theoretical Data (dB)	Theoretical variance with added noise floor	Theoretical variance
42.9	-44.041		40	-43.982	-67.824
37.9	-43.395		30	-43.824	-57.824
32.9	-43.706		25	-43.465	-52.824
27.9	-43.754		24	-43.337	-51.824
22.9	-43.713		23	-43.337	-51.824
21.9	-42.661		22	-42.991	-49.824
20.9	-42.506		21	-42.764	-48.824
19.9	-42.375		20	-42.494	-47.824
18.9	-41.532		19	-42.176	-46.824
17.9	-41.343		18	-41.806	-45.821
17.4	-41.116		17	-41.374	-44.807
16.9	-40.953		16	-40.865	-43.755
16.4	-40.559		15	-40.242	-42.615
15.9	-40.144		14.5	-39.871	-41.992
15.4	-39.933		14	-39.448	-41.323
14.9	-39.591		13.5	-38.965	-40.599
14.4	-39.38		13	-38.41	-39.813
13.9	-38.847		12.5	-37.776	-38.959
13.4	-38.432		12	-37.051	-38.03
12.9	-37.892		11.5	-36.228	-37.022
12.4	-37.122		11	-35.298	-35.927
11.9	-36.557		10.5	-34.254	-34.74
11.4	-36.17		10	-33.089	-33.456
10.9	-35.095		9.5	-31.798	-32.067
10.4	-34.4		9	-30.373	-30.566
9.9	-33.107		8.5	-28.811	-28.945
9.4	-32.425		8	-27.108	-27.198
8.9	-30.864		7.5	-25.257	-25.315
8.4	-29.812		7	-23.255	-23.292
7.9	-27.931		6.5	-21.103	-21.125
			6	-18.8	-18.814

Table H-16. The first set of 8PSK hardware variance data at 0.66% high-SNR loop bandwidth-to-symbol rate ratio.

SNR (dB)	Theoretical variance with added noise floor	Theoretical variance	Measured variance
30	-40.535	-54.814	-40.56
29			-40.664
28			-40.466
27			-40.27
26			-40.36
25	-40.198	-49.814	-40.153
24.5			-40.106
24	-40.076	-48.814	-40.041
23.5			-39.795
23	-39.929	-47.814	-39.597
22.5			-39.685
22	-39.749	-46.814	-39.48
21.5			-39.375
21	-39.534	-45.814	-39.617
20.5			-38.955
20	-39.277	-44.814	-39.309
19.5			-38.694
19	-38.973	-43.814	-38.632
18.5			-38.436
18	-38.618	-42.811	-38.104
17.5			-38.236
17	-38.203	-41.797	-37.637
16.5			-37.357
16	-37.712	-40.744	-37.306
15.5			-37.063

Table H-17. The second set of 8PSK hardware variance data at 0.66% high-SNR loop bandwidth-to-symbol rate ratio.

SNR (dB)	Theoretical variance with added noise floor	Theoretical variance	Measured variance
15	-37.107	-39.604	-36.568
14.5	-36.746	-38.982	-36.278
14	-36.334	-38.313	-35.785
13.5	-35.861	-37.589	-35.392
13	-35.318	-36.803	-34.756
12.5	-34.695	-35.949	-34.096
12	-33.981	-35.02	-33.474
11.5	-33.168	-34.011	-32.584
11	-32.247	-32.917	-31.882
10.5	-31.212	-31.73	-30.813
10	-30.054	-30.446	-29.454
9.5	-28.769	-29.057	-28.191
9	-27.35	-27.555	
8.5	-25.792	-25.935	
8	-24.091	-24.187	
7.5	-22.242	-22.305	
7	-20.242	-20.281	
6.5	-18.091	-18.115	
6	-15.789	-15.803	

Table H-18. 16PSK hardware variance data at 0.19% high-SNR loop bandwidth-to-symbol rate ratio.

LAB SNR (dB)	Measured Variance		SNR for Theoretical Data (dB)	Theoretical variance with added noise floor	Theoretical variance
42.9	-43.233		30	-43.213	-60.232
32.9	-43.496		25	-43.03	-55.232
27.9	-43.003		24	-42.963	-54.232
26.9	-43.587		23	-42.88	-53.232
25.9	-43.277		22	-42.777	-52.232
24.9	-43.136		21	-42.652	-51.232
23.9	-43.125		20	-42.402	-49.687
22.9	-42.966		19.5	-42.25	-48.933
22.4	-42.898		19	-42.059	-48.103
21.9	-42.776		18.5	-41.812	-47.188
21.4	-42.799		18	-41.494	-46.178
20.9	-42.653		17.5	-41.082	-45.061
20.4	-42.535		17	-40.545	-43.827
19.9	-42.191		16.5	-39.851	-42.462
19.4	-42.313		16	-38.959	-40.952
18.9	-42.125		15.5	-37.829	-39.278
18.4	-41.413		15	-36.422	-37.42
17.9	-41.327		14.5	-34.709	-35.356
17.4	-40.591		14	-32.669	-33.062
16.9	-40.048		13.5	-30.293	-30.516
16.4	-39.216		13	-27.578	-27.696
15.9	-38.354		12.5	-24.531	-24.589
15.4	-37.427		12	-21.16	-21.187
14.9	-35.61		11.5	-17.48	-17.491
14.4	-33.335		11	-13.508	-13.513
13.9	-33.859		10.5	-9.2716	-9.2733
13.4	-30.431				

Table H-19. 16PSK hardware variance data at 0.33% high-SNR loop bandwidth-to-symbol rate ratio.

LAB SNR (dB)	Measured Variance		SNR for Theoretical Data (dB)	Theoretical variance with added noise floor	Theoretical variance
42.9	-43.466		40	-44.231	-67.824
37.9	-43.967		30	-44.063	-57.824
32.9	-44.254		25	-43.685	-52.824
27.9	-44.104		24	-43.55	-51.824
22.9	-43.473		23	-43.386	-50.824
22.4	-43.406		22	-43.188	-49.824
21.9	-43.129		21	-42.95	-48.824
21.4	-42.939		20	-42.512	-47.328
20.9	-43.135		19.5	-42.256	-46.597
20.4	-42.722		19	-41.945	-45.798
19.9	-42.211		18.5	-41.563	-44.923
19.4	-42.081		18	-41.093	-43.962
18.9	-41.888		17.5	-40.517	-42.908
18.4	-41.398		17	-39.812	-41.75
17.9	-41.029		16.5	-38.956	-40.478
17.4	-40.326		16	-37.925	-39.078
16.9	-39.703		15.5	-36.695	-37.533
16.4	-39.023		15	-35.242	-35.825
15.9	-38.276		14.5	-33.544	-33.93
15.4	-37.185		14	-31.579	-31.82
14.9	-36.303		13.5	-29.325	-29.467
14.4	-34.703		13	-26.764	-26.842
13.9	-33.224		12.5	-23.88	-23.92
13.4	-31.945		12	-20.665	-20.684
			11.5	-17.12	-17.128
			11	-13.257	-13.261
			10.5	-9.1027	-9.104

Table H-20. The first set of 16PSK hardware variance data at 0.66% high-SNR loop bandwidth-to-symbol rate ratio.

SNR (dB)	Theoretical variance with added noise floor	Theoretical variance	Measured variance
30	-41.398	-54.814	-41.427
29.5			-41.275
29			-41.256
28.5			-41.377
28			-41.156
27.5			-41.239
27			-41.346
26.5			-41.099
26			-41.222
25.5			-41.033
25	-40.99	-49.814	-40.917
24.5			-40.727
24	-40.845	-48.814	-40.522
23.5			-40.625
23	-40.669	-47.814	-40.247
22.5			-40.341
22	-40.457	-46.814	-40.125
21.5			-39.91
21	-40.204	-45.814	-39.788
20.5			-39.613

Table H-21. The second set of 16PSK hardware variance data at 0.66% high-SNR loop bandwidth-to-symbol rate ratio.

SNR (dB)	Theoretical variance with added noise floor	Theoretical variance	Measured variance
20	-39.739	-44.318	-39.329
19.5	-39.47	-43.587	-39.114
19	-39.143	-42.788	-38.807
18.5	-38.743	-41.912	-38.361
18	-38.254	-40.952	-37.908
17.5	-37.656	-39.898	-37.487
17	-36.928	-38.74	-36.483
16.5	-36.05	-37.468	-36.057
16	-34.996	-36.067	-35.075
15.5	-33.746	-34.523	-33.843
15	-32.275	-32.815	-32.491
14.5	-30.563	-30.919	-31.217
14	-28.587	-28.81	-29.658
13.5	-26.326	-26.457	
13	-23.76	-23.832	
12.5	-20.873	-20.91	
12	-17.656	-17.674	